INFORMATION TO USERS

This manuscript has been reproduced from the microfilm master. UMI films the text directly from the original or copy submitted. Thus, some thesis and dissertation copies are in typewriter face, while others may be from any type of computer printer.

The quality of this reproduction is dependent upon the quality of the copy submitted. Broken or indistinct print, colored or poor quality illustrations and photographs, print bleedthrough, substandard margins, and improper alignment can adversely affect reproduction.

In the unlikely event that the author did not send UMI a complete manuscript and there are missing pages, these will be noted. Also, if unauthorized copyright material had to be removed, a note will indicate the deletion.

Oversize materials (e.g., maps, drawings, charts) are reproduced by sectioning the original, beginning at the upper left-hand corner and continuing from left to right in equal sections with small overlaps.

Photographs included in the original manuscript have been reproduced xerographically in this copy. Higher quality 6" x 9" black and white photographic prints are available for any photographs or illustrations appearing in this copy for an additional charge. Contact UMI directly to order.

Bell & Howell Information and Learning
300 North Zeeb Road, Ann Arbor, MI 48106-1346 USA
800-521-0600

INVESTIGATIONS IN STRUCTURAL OPTIMIZATION OF NONLINEAR PROBLEMS USING THE FINITE ELEMENT METHOD

by

Ramin Sedaghati
B. Sc., Amirkabir University of Technology, Tehran, Iran, 1988
M. Sc., Amirkabir University of Technology, Tehran, Iran, 1990

A Dissertation Submitted in Partial Fulfillment of the
Requirements for the Degree of

DOCTOR OF PHILOSOPHY

in the Department of Mechanical Engineering

We accept this dissertation as conforming
to the required standard

The late Dr. B. Tabarrok, Supervisor (Department of Mechanical Engineering)

Dr. A. Suleman, Supervisor (Department of Mechanical Engineering)

Dr. S. Dost, Co-Supervisor (Department of Mechanical Engineering)

Dr. J. Haddow, Departmental Member (Department of Mechanical Engineering)

Dr. W. S. Lu, Outside Member (Department of Electrical and Computer Engineering)

Dr. M. S. Gadala, External Examiner (Department of Mechanical Engineering,
University of British Columbia, B.C., Canada)

Supervisors: Drs. B. Tabarrok/A. Suleman

ABSTRACT

Structural optimization is an important field in engineering with a strong foundation on continuum mechanics, structural finite element analysis, computational techniques and optimization methods. Research in structural optimization of linear and geometrically nonlinear problems using the force method has not received appropriate attention by the research community.

The present thesis constitutes a comprehensive study in the area of structural optimization. Development of new methodologies for analysis and optimization and their integration in finite element computer programs for analysis and design of linear and nonlinear structural problems are among the most important contributions.

For linear problems, a force method formulation based on the complementary energy is proposed. Using this formulation, the element forces are obtained without the direct generation of the compatibility matrix. Application of the proposed method in structural size optimization under stress, displacement and frequency constraints has been investigated and its efficiency is compared with the conventional displacement formulation. Moreover, an efficient methodology based on the integrated force method is developed for topology optimization of adaptive structures under static and dynamic loads. It has been demonstrated that structural optimization based on the force method is computationally more efficient.

For nonlinear problems, an efficient methodology has been developed for structural optimization of geometrical nonlinear problems under system stability constraints. The technique combines the nonlinear finite element method based on the displacement control technique for analysis and optimality criterion methods for optimization. Application of the proposed methodology has been investigated for shallow structures. The efficiency of the proposed optimization algorithms are compared with the mathematical programming method based on the Sequential Quadratic Programming

technique. It is shown that structural design optimization based on the linear analysis for structures with intrinsic geometric nonlinearites may lead to structural failure.

Finally, application of the group theoretic approach in structural optimization of geometrical nonlinear symmetric structures under system stability constraint has been investigated. It has been demonstrated that structural optimization of nonlinear symmetric structures using the group theoretic approach is computationally efficient and excellent agreement exists between the full space and the reduced subspace optimal solutions.

Examiners:

The late Dr. B. Tabarrok, Supervisor (Department of Mechanical Engineering)

Dr. A. Suleman, Supervisor (Department of Mechanical Engineering)

Dr. S. Dost, Co-supervisor (Department of Mechanical Engineering)

Dr. J. Haddow, Departmental Member (Department of Mechanical Engineering)

Dr. W. S. Lu, Outside Member (Department of Electrical and Computer Engineering)

Dr. M. S. Gadala, External Examiner (Department of Mechanical Engineering, University of British Columbia, B.C., Canada)

TABLE OF CONTENTS

LIST OF TABLES

LIST OF FIGURES

NOMENCLATURE

The principal symbols used in the thesis are listed below.

Roman Letters

A	Cross-sectional area of the element
A_i	Cross-sectional area of the i^{th} element or member
$\mathbf{A}$	Vector of cross-sectional area of the elements
$\overline{\mathbf{A}}$	Lower bound on the vector of cross-sectional area
$\boldsymbol{B}$	Strain-displacement matrix
$\boldsymbol{C}$	Compatibility matrix
$\boldsymbol{D}$	Differential operator
$\mathbf{d}$	Vector of displacement function
$\boldsymbol{E}$	Elasticity matrix
E	Modulus of elasticity
$\mathbf{F}$	Vector of element forces
$\mathbf{F}_d$	Vector of statically determinate element forces
$\mathbf{F}_r$	Vector of redundant element forces
f	General representation of the objective function
$\boldsymbol{G}$	Flexibility matrix
$\mathbf{g}$	Vector of constraints
$\boldsymbol{H}$	Hessian matrix
$\boldsymbol{I}$	Identity matrix
i_s , i_d and i_f	Number of stress, displacement and frequency constraints.
$\boldsymbol{K}$	System tangent stiffness matrix
$\boldsymbol{k}$	Element tangent stiffness matrix
$\boldsymbol{K}_E$	System linear stiffness matrix
$\boldsymbol{K}_G$	System geometric stiffness matrix
$\boldsymbol{k}_E$	Element linear stiffness matrix

$\boldsymbol{k}_G$	Element geometric stiffness matrix
$\boldsymbol{k}_{D1}$	Element displacement geometric stiffness (first order)
$\boldsymbol{k}_{D2}$	Displacement geometric stiffness matrix (second order)
$\boldsymbol{k}_\sigma$	Element stress stiffness matrix
$\boldsymbol{k}_{\sigma c}$	Element classical stress stiffness matrix
$\boldsymbol{k}^g$	Element stiffness matrix in global coordinates
$\boldsymbol{K}_r$	Reduced system tangent stiffness matrix
L_i	Length of the i^{th} element or member
L_{0i}	Unreformed length of the i^{th} element or member
L	Lagrangian
l_x, l_y, l_z	Direction cosines
$\boldsymbol{M}$	System mass matrix
$\boldsymbol{M}_r$	Reduced system mass matrix
$\boldsymbol{m}$	Element mass matrix
m	Number of displacement degrees of freedom
m_r	Reduced number of degrees of freedom
n	Number of force degrees of freedom
n_a	Number of active members in adaptive structures.
$\boldsymbol{N}$	Shape function
$\mathbf{P}$	Vector of external nodal forces
$\mathbf{P}_{ref}$	Reference load vector
$\mathbf{P}'$	Vector of the nodal resultant member forces at time step t
$\Delta\mathbf{P}$	Out-of-balance force vector
$\mathbf{P}_r$	Reduced external nodal load vector
$\boldsymbol{Pr}$	Projection matrix
$\boldsymbol{Q}$	Equilibrium matrix
$\boldsymbol{R}$	Rotation matrix
$\boldsymbol{Rot}$	3×3 rotation matrix
$\boldsymbol{Ref}$	3×3 refelection matrix
r	Number of redundancy

$\boldsymbol{S}$	Combined equilibrium and compatibility matrix
S_G	Symmetric group
$\mathbf{s}^v$	Direction vector in each iteration v
Sf	Scale factor
$\boldsymbol{T}$	Orthogonal representation of the symmetric group on $\Re^{m \times m}$
t	time step in nonlinear analysis
$\mathbf{U}$	Total nodal displacement vector
U_i , $\overline{U}_i$	i^{th} constrained nodal displacement and its allowable limit value
$\Delta\mathbf{U}$	Vector of increment in nodal displacements
$\mathbf{u}$	Element nodal displacement vector
u, v, w	Displacement functions in the x, y, z-directions, respectively
$\mathbf{U}_r$	Total nodal displacement vector in reduced sub-space problem
U	Total potential energy
V	Kinetic energy
W	External work
W^*	Complementary work
$\mathbf{X}$	General representation of the design variable vector
X, Y, Z	Global coordinate system
x,y,z	Element or local coordinate system

Greek Letters

${}^t\alpha$	Load factor parameter at time step t
α_{cr}	critical buckling load factor
β	Step size parameter
δ	Variation
ε	Strain vector
ε_D	Displacement convergence tolerance
ε_F	Out-of-balance convergence tolerance
ε_E	Energy convergence tolerance

η	Adjoint vector
$\varphi_.$	Vector corresponds to the angles of the active members
λ	Lagrange multiplier
ν	Iteration number for optimization
θ	Angle of rotation
ρ	Density
σ	Stress vector
σ_i, $\overline{\sigma}_i$	i^{th} constraint stress and its allowable limit value
τ	Impulse
ω_i , $\overline{\omega}_i$	i^{th} constrained frequency and its allowable limit value.
Δ	Vector of element deformations
Φ	Symmetry modes
Π	Virtual strain energy
Π^*	Complementary virtual potential energy
Θ	Basis eigenvector of the projection matrix
$\Re^{m\times m}$	Space of $m\times m$ dimensional matrices

Acronyms

DM	Displacement Method
FM	Force Method
FUD	Fully Utilized Design
FSD	Fully Stresses Design
FMCE	Force Method based on Complementary Energy
GTA	Group Theoretic Approach
IFM	Integrated Force Method
MP	Mathematical Programming technique
OC	Optimality Criterion technique
SFM	Standard Force Method
SQP	Sequential Quadratic Programming method

ACKNOWLEDGEMENT

I wish to express my highest gratitude to my supervisor, the late Professor Behruz Tabarrok. Professor Tabarrok unfortunately passed away during the course of this research. However, his support, enthusiastic guidance, constructive instruction, consistent encouragement, and energetic spirit paved the way for this work and my understanding of the structural optimization and the finite element method. Professor Afzal Suleman has generously provided his time and effort in the guidance and completion of my thesis research. His broad knowledge, helpful comments, and invaluable advice have made a significant impact in this work.

I am indebted to my co-supervisor, Professor Sadik Dost, who patiently offered warm-hearted support and helpful suggestions during the course of this study. My gratitude is also extended to Professors James Haddow and Wu Sheng Lu who as members of the supervisory committee have offered helpful and constructive comments in this work.

I want to thank all my graduate fellows, especially my colleague Stan Burns who have made my stay at the University of Victoria an enjoyable experience. I would also like to thank the department's faculty and staff for their continuous cooperation. My warmest appreciation is especially directed to Mrs.Winnie Williams, the department's graduate secretary.

The Graduate Teaching Fellowship of the University of Victoria and the Graduate Research Assistantship provided by the Natural Sciences and Engineering Research Council (NSERC) of Canada, are gratefully acknowledged.

Finally, I would like to express my special thanks to my parents, Mr. Arsalan Sedaghati and Mrs. Effat Karimai. Without their love and continuous encouragement, this work would not have been possible.

To my parents, Arsalan Sedaghati and Effat Karimai,
for their support, encouragement and love
and
to the memory of the late Professor Behrouz Tabarrok

Chapter 1

INTRODUCTION

1.1 Problem Statement and Motivation

Structural optimization is an important field in engineering with a strong foundation on continuum mechanics, structural finite element analysis, computational techniques and optimization methods. Research in structural optimization of linear and geometrically nonlinear problems using the force method has not received appropriate attention by the research community. The objective of the present thesis is to present a comprehensive and complete investigation on structural analysis and optimization of linear and nonlinear problems using the finite element method.

1.2 State of the Art

The concept of structural optimization is not new, but the development of structural optimization as a nonlinear, equality or inequality constrained, mathematical programming problem has a relatively short history. Most research in structural optimization has been carried out for linear problems using the displacement method. A few of the excellent published review papers on structural optimization include the articles by Sheu and Prager [1], Niordson and Pierson [2], Venkayya [3], Krishnamoorthy and Mosi [4], Haftka and Prasad [5], Schmit [6,7], Vanderplaatsand [8] and Grandhi [9].

In 1869, Maxwell [10] published a landmark paper on pin-jointed frameworks and this work is considered to be an important contribution to the theory of optimal structures. Michell [11] extended Maxwell's work and investigated the design of minimum weight, stress-constrained, pin-jointed frameworks subjected to a single load condition.

With the advent of the simplex method [12] for solving linear programs, structural optimization advanced in the area of structural systems with the development of the digital computer and the finite element method. In 1960, Schmit [13] posed the structural

optimization problem as a nonlinear, inequality-constrained mathematical programming problem. Mathematical programming algorithms require the evaluation of the objective, constraint functions and their gradients, and in turn this requires a complete structural analysis each time the design variables are modified.

The primary difficulty with the mathematical programming algorithms is the evaluation of large numbers of functions, constraints and constraint gradients that requires a complete finite element analysis each time the design variables are modified. Sander and Flurry [14] pointed out that the number of structural analysis increases with the number of design variables. Since the cost of a single analysis for a large dimension structure is significant, numerical optimization was not computationally feasible. Frind and Wright [15] and Pappas [16] concluded that the mathematical programming methods were not suited to the structural optimization problem because of the heavy computational burden and the large number of structural re-analyses required.

At about the same time, as the mathematical programming approach to structural optimization was looked upon as impractical; the optimality criteria method emerged as a workable alternative. Optimality criteria methods are capable of providing solutions to large-scale problems while requiring fewer structural analyses than the mathematical programming methods. In the optimality criteria approach, a set of conditions are derived which must be satisfied at the optimum. These conditions are used to derive a recursive redesign procedure that derives the current design towards that which satisfies the optimality criterion. The stress ratio method is derived from a very special type of optimality criterion, namely the fully stressed design criterion. Here, the conditions of optimality are such that each member must be fully stressed in at least one load condition. The stress ratio formula is designed to resize the member so that the optimality criterion is satisfied. The method cannot handle constraints on global behavior quantities like displacements, although the fully stressed design can be scaled up uniformly to satisfy any violated displacement constraints. Furthermore, the method does not necessarily converge to the optimum design, especially when materials with different mass densities and stress limits are used, as Fleury [17] pointed out. Also, in some cases, the method diverges. Despite these disadvantages, the method has enjoyed widespread use. Wright et

al [18-20] have used the technique for plane frames to generate a design which is reasonably close to the optimum. Iserb [21] and Svanberg [22] have also used the fully stressed design criterion for the design of three-dimensional beam structures.

A more powerful optimality criterion has been derived by invoking the Karush-Kuhn-Tucker (KKT) conditions of mathematical programming. Optimality criteria methods based on KKT conditions have been developed primarily for structures, which can be modeled with truss, membrane, and shear panel elements. These elements are characterized by element stiffness matrices which are proportional to their transverse dimensions (cross-sectional area for trusses and thickness for membranes and shear panels). Khot. [23] has developed the optimality criterion for these types of structures subjected to stress and displacement constraints. The virtual load technique was used to generate explicit constraint approximations to the actual stress and displacement constraints.

The central problem in the optimality criteria methods involves calculating the Lagrange multipliers. Numerous techniques for calculating the Lagrange multipliers have been presented by Dobbs and Nelson [24], Khan, Willmert, and Thonton [25], Khot, Berke, and Venkayya [26], Allwood and Chung [27], and Tabak and Wright [19]. Templeman [28] has pointed out that the optimality criteria methods indirectly minimize the weight by using a recurrence relation which forces the design towards that which satisfies the optimality criterion, in contrast to the direct approach of mathematical programming methods where the optimum is sought blindly by some pure numerical search.

However, the outlook for the mathematical programming approach did not deter researchers from attempting to improve the situation. Schmit and Farshi [29] and Schmit and Miura [30-32] recognized that the application of mathematical programming techniques to structural optimization presented the following problems: too many independent design variables, too many behavior constraints, and too many structural analyses. In the context of structural optimization, "too many" meant more than necessary to generate a practical optimum design. Instead of condemning the mathematical programming approach, Schmit and Muira [33] contended that it was the blind combination of mathematical programming techniques and finite element structural

analysis programs that led to these difficulties. Schmit and his co-workers sought to alleviate these problems by introducing several approximation concepts such as: design variable linking, constraint deletion, and explicit approximation of constraints. Design variable linking reduced the number of independent design variables by making groups of elements linearly dependent upon a single generalized design variable. Design variable linking can also be used to impose structural symmetry and to reduce the number of design variables when the number of finite elements used to model a structure exceeds the actual number of structural components, which can be independently sized. Constraint deletion procedures can be used to temporarily ignore behavior constraints, which would have no influence in the upcoming design step. Finally, Schmit and his co-workers proposed to reduce the number of structural analyses by employing explicit constraint approximations. These are generated using first order Taylor series expansions in the generalized reciprocal design variable to approximate the behavior constraints. The selection of first order Taylor series approximations in the reciprocal design variables is motivated by the fact that for statically determinate structures modeled with elements in which the element stiffness matrix is proportional to the transverse element size and the element stresses are dependent upon nodal displacements only (for example, trusses, membranes, and shear panels), the stress and displacement constraints are strictly linear in the reciprocal design variables. Thus, stress and displacement constraints will also be linear in reciprocal design variables. For moderately statically indeterminate structures, using the reciprocals of the design variables proved to be a useful device in making the constraints more linear [34,35].

A common disadvantage present in the algorithms discussed so far is their inability to distinguish local and global minima. Many structural design problems have several local minima, and depending on the starting point, these algorithms may converge to one of these local minima. The simplest way to check for a better local solution is to restart the optimization from randomly selected initial points to check if other solutions are possible. However, for problems with a large number of variables, the possibility of missing the global minimum is high unless an impractically large number of optimization runs are performed. Simulated annealing [36] and genetic algorithms [37] have emerged more recently as tools ideally suited for optimization problems where global minimum is

sought. In addition to being able to locate near global solutions, these two algorithms are also powerful tools for problems with discrete-valued design variables. Both algorithms are based on naturally observed phenomena and their implementation calls for the use of a random selection process that is guided by probabilistic decisions. Elperin [38] applied the simulated annealing technique to the design of a ten-bar truss problem where member cross-section dimensions were to be selected from a set of discrete values. Kincaid and Padula [39] used it for minimizing the distortion and internal forces in a truss structure. A 6-story 156-member frame structure with discrete valued variables was considered by Balling and May [40]. Optimal placement of active and passive members in a truss structure was investigated by Chen et al. [41] to maximize the finite-time energy dissipation to achieve increased damping properties. The first application of a genetic algorithm to a structural design problem was presented by Goldberg and Samtani [42] who applied it to the 10-bar truss weight minimization problem. Hajela [43] used genetic search for several structural design problems. Rao et al. [44] addressed the optimal selection of discrete actuator locations in actively controlled structures via genetic algorithms as well.

The more recent works in structural optimization include the homogenization method, pioneered by Bendsoe [45] in 1995, and the evolutionary structural optimization technique proposed by Xie and Steven [46] in 1997. These methods have proved to be successful in generating optimum topologies for continuum structures.

1.3 Structural Optimization and the Finite Element Force Method

The concepts of equilibrium of forces and compatibility of deformations are fundamental to analysis methods for solving problems in structural mechanics. The underlying principle behind the equilibrium equations is force balance. The equilibrium equations, expressed in terms of forces, are sufficient to calculate member forces for statically determinate structures. However, equilibrium equations are not sufficient to solve general structural analysis problems, as they have to be augmented by the compatibility conditions. In other words, equilibrium equations are indeterminate in nature, and

determinacy for a continuum is achieved by adding the compatibility conditions. Two theoretical approaches, the force and the displacement methods, have been developed to analyze indeterminate structures and these are the foundations of the analytical mechanics.

Clebsch [47] noticed that, if the equilibrium equations are written in terms of nodal displacements, the number of equations and the displacement unknowns are identical. With that observation the displacement method was born, but it was not useful because there was no practical way to solve the potentially large number of simultaneous equations by hand, except perhaps by relaxation methods.

A more useful method was introduced by Maxwel [47], who proposed cutting redundant members and introduced unknown redundant forces at the cuts. The remaining determinate structure was solved for both applied and redundant loads in order to obtain the internal forces and the relative displacements at the cuts for all the load systems. Because the equilibrium equations for determinate trusses essentially represent a triangular system of equations, their solution is easily obtained. Next, in order to re-establish compatibility, the analyst sets up simultaneous equations that express the conditions at which the relative displacements due to the external loads are closed by the redundant loads. The solution of these equations yields the redundant force, and superposition of the two sets of internal loads gives the final solution. This method is known as the Standard Force Method (SFM). This method became the analysis method of choice for generations of engineers, as the number of simultaneous equations was usually small for the truss structures studied. With the advent of the digital computer, the displacement method became practical and amenable to computer automation in the form of the stiffness method.

A structure in the force method of analysis can be designated as structure (n, m), where (n, m) are the force and displacement degrees of freedoms (fof,dof), respectively. The n component force vector $\mathbf{F}$ must satisfy the m equilibrium equations along with $r=(n-m)$ compatibility conditions. If $n=m$, the structure is determinate and its analysis is trivial. The emphasis here is on the analysis of indeterminate structure for

which $n > m$. There are at present two force formulations, the Standard (or classic) Force Method (SFM) and the Integrated Force Method (IFM). Both the SFM and IFM use the same equilibrium equations. The elemental equilibrium matrices for bar and beam elements can be obtained from the direct force balance principle [48]. For continuous structures, such as plates or shells, very few equilibrium matrices are reported in the literature [47,49]. The equilibrium matrix is a $(m \times n)$ banded rectangular matrix, which is independent of the material properties and design parameters of the indeterminate structure(n, m). For finite element analysis this matrix is assembled from elemental equilibrium matrices. The equilibrium matrices for the plate flexure problem have been given by Przemieniecki [47] and Robinson [49]. Przemieniecki generated the matrix for a rectangular element in flexure from direct application of the force balance principle at nodes. Robinson utilized the concept of virtual work to derive the matrix for a rectangular plate element in flexure. The generation of the compatibility conditions is the most cumbersome part of the SFM. In SFM first equilibrium equation is satisfied and then using compatibility conditions, the r redundant forces will be obtained.

In the classical force method, the compatibility conditions are generated by splitting the structure (n, m) into a determinate basis structure (m, m) and r redundant members. The compatibility conditions are written in the redundant members by establishing the continuity of deformations between the r redundant members and the basis structure (m, m) for the external loads, thus the redundant members are the primal variables of the compatibility conditions in the SFM. This procedure was originally developed by Navier [50] for the analysis of indeterminate trusses. Prior to the 1960's, the basis structure and redundant members were generated manually. In the post-1960's, several schemes have been devised to automatically generate redundant members and the basis determinate structure [51-56], however with limited success.

Patnaik [57-64] developed the IFM method. In IFM, the compatibility matrix is obtained by extending St. Venant's principle of elasticity strain formulation to discrete structural mechanics [65-68]. Both equilibrium equations and compatibility conditions are satisfied simultaneously. The compatibility conditions are generated without any recourse to redundant members and the basis determinate structure.

Commercial finite element programs are based on the displacement method and very few investigations have been reported in structural optimization using the finite element force method. The displacement method is an efficient approach, however for stress-displacement constraint, it loses its advantages for size optimization when the number of stress constraints are larger than the displacement constraints and for topology optimization when the structural strength is the primary design concern. Additionally, when the structure is not highly redundant i.e. the number of redundant elements is lower than the displacement degrees of freedom ($r < m$), analysis through the force method is more efficient than the displacement method. Application of available force method techniques to structural optimization is limited to size optimization in truss structures under stress and displacement constraints with small design variables.

The application of the integrated force method to structural optimization problems was first proposed by Patnaik [69-72]. However, the automation of the force method is the main obstacle in the application of force method in the structural optimization, nevertheless the IFM has provided automation for simpler structures.

1.4 Nonlinear Finite Element Method in the Structural Optimization

The finite element literature is vast and it is well documented in many text books [73-77]. A number of element and solution methods have been developed for the analysis of structures exhibiting nonlinear behavior. Total Lagrangian and updated Lagrangian have been successfully implemented in many commercial and research codes [78,79], to predict the nonlinear behavior. In the total Lagrangian approach, all variables are referred to the reference configuration while in the updated Lagrangian they are referred to the last known configuration. A co-rotational (or convected coordinates) approach [80-82] has been used to solve large rotation /small strain problems. This approach is based on the simple decomposition of the total displacements into a rigid body and a strain-producing component. The earliest paper on nonlinear finite element analysis appears to be that by Turner et al. [83] which dates from 1960. For genuine geometric non-linearity, 'incremental' procedures were originally adopted by Turner et al. [83] and Argyris

[84,85] using the 'geometric stiffness matrix' in conjunction with an updating of coordinates and, possibly, an initial displacement matrix [86,87]. A similar approach was adopted with material non-linearity [73].

Unfortunately, the incremental approach can lead to an unquantifyable build-up of error. To counter this problem, the Newton-Raphson iteration was used by Mallet and Marcel [86] and Oden [88]. A modified Newton-Raphson procedure was also recommended by Oden [89], Haisler et al. [90] and Zienkiewicz [91]. In contrast to the full Newton-Raphson method, the stiffness matrix was not continuously updated in the modified Newton-Raphson procedure. Acceleration procedures were also considered [91]. The concept of combining incremental (predictor) and iterative (corrector) methods was introduced by Brebbia and Connor [92] and Murray and Wilson [93] who thereby adopted a form of 'continuation method'.

In stability problems, standard finite element procedures allow the nonlinear equilibrium path to be traced until a point just before limit point, but at this stage the iterations will probably fail. Several procedures have been used by different investigators to overcome this difficulty [94-98]. Zienkiewic [96] suggested a form of the displacement control method. Haisler et al. [97]used it by partitioning the stiffness matrix. A simplified displacement control method has been introduced by Batoz and Dhatt [98] where one of the displacement components is incremented at each time step and the solution is iterated. Arc-length methods [99-102] and automatic time stepping procedures [103] are among the more sophisticated techniques available today for post buckling solution.

Rosen and Schmit [104,105] investigated the optimization of truss structures having local and system geometric imperfections. They developed an approximate analysis for imperfect truss elements. Though the analysis procedure considered geometric stiffness effects, it did not allow for large displacements of the nodal points. The optimization was carried out by a Sequence of Unconstrained Minimization Technique (SUMT) algorithm based on the penalty function method. It was shown that small imperfections affect the optimum design considerably and lead to optimum designs with material distributions distinctly different from those obtained when imperfections are ignored.

Teixeira de Freitas [106] presented an interesting and rather general formulation of the structural synthesis problems for elastic truss structures. The formulation considered large displacements and nonlinear force displacement relations to account for the initial imperfections. The problem was posed in the combined space of the design variables as well as the static and kinematics variables. The general mathematical problem was reduced to an incremental one, by using incremental equilibrium and compatibility relations. A perturbation based solution procedure was suggested to solve the resulting mathematical programming problem. The use of the perturbation procedure, with the help of the equality constraints, resulted in eliminating all the variables in the problem except the design variables (member size). This procedure is equivalent to solving a weight minimization problem for each load increment.

Khot [107] described an optimality criterion method for finding the minimum weight design of space trusses subject to system stability constraints. Linear stability analysis was carried out during the optimization process. The resulting optimum designs were analyzed using incremental nonlinear analysis, with the load control technique, to account for geometric nonlinearities. Constraints were specified to ensure that the eigenvalues associated with all critical buckling modes are either equal or separated by a specified factor. The effect of specified geometric imperfections on the optimum design was also studied. It was concluded that a nonlinear analysis should be considered when optimizing structures subject to system stability constraints.

Kamat et al. [108-110] studied optimization of shallow trusses and arches. In the first paper, two special cases were considered, a two-bar shallow truss and a four-bar shallow space truss. An explicit relation for the critical load was obtained in terms of design variables and then maximized subject to a given volume, analytically. It was shown that optimized trusses satisfy the constant-strain energy density criteria and the problem of maximization of the critical load, for a fixed volume, is the dual of the problem of minimization of the weight for a given critical load. Numerically, two different solution strategies were used. The first was a mathematical programming approach in which, the equality constraint was used to eliminate one of the design variables. Powell's conjugate directions algorithm for unconstrained minimization was used to solve the resulting

unconstrained problem. The second approach used an optimality criterion, requiring a uniform strain energy density in all the elements. In the second paper, a simple method based on mathematical programming technique was used to maximize the critical load of an arch subjected to a constant volume constraint. It was demonstrated that for very low-rise arches, which exhibit symmetrical limit point instability, the optimality criterion reduces to that of a uniform strain energy density. Finally, they showed that there is a duality between the minimum weight design for a specified critical load and the volume constrained design for a maximum critical load. In the third paper, the calculation of the sensitivity derivatives of the critical load parameter using the ad joint method was introduced for the arch problem. However, this method is based on the implicit differentiation of equilibrium equations and the Hessian of the total potential energy, making it computationally expensive.

Methods for obtaining optimum designs of truss structures, while guarding against instability and considering geometric nonlinearities, were presented by Khot and Kamat [111] based on the optimality criterion approach. A recurrence relation, based on equal strain energy density in all the members, was used to develop an algorithm. The nonlinear critical load was determined by finding the load level at which the Hessian of the potential energy ceases to be positive definite. Kamat and Raungasilasingha [112] also studied the optimum design of truss structures by addressing the problem of maximizing the critical load of shallow space trusses of given configuration and volume. A sequential quadratic programming method was used to solve the resulting mathematical program. Sensitivity derivatives of the critical load parameters were developed through implicit differentiation of the nonlinear equilibrium equations.

Levy and Perng [113] studied the optimal design of trusses subject to system stability requirements by considering equality constraints in which the lowest buckling load factor was set equal to a specified buckling load factor. A two-phase iterative procedure of analysis and redesign was proposed for the stability optimization problem. Phase one utilizes an incremental technique up to the point of instability and phase two utilizes a recurrence relation based on optimality criteria for redesign. The derivation of the

recurrence relation was made for the linear stability problem. The need for nonlinear type solutions was demonstrated for the problems investigated.

An integrated approach in structural optimization with geometric nonlinearity was introduced by Smaui and Schmit [114,115]. They used this approach to determine the minimum weight design of dome-truss structures with and without geometric imperfections. In the integrated approach, design and response quantities were considered as independent variables and the equilibrium equations for the finite element model were considered as equality constraints. The advantage of this approach is that the nonlinear structural analysis and the optimization are merged in a single process. The resulting integrated problem was solved directly using the generalized gradient projection approach. It was found that the algorithm was able to detect and guard against system as well as element stability, without having to explicitly impose the system stability constraint.

Wu and Arora [116,117] implemented optimization and sensitivity calculations into a nonlinear finite element analysis code. Stress, strain, displacement and buckling constraints were considered. After nonlinear analysis for a specified base load, linear buckling analysis was implemented to estimate the nonlinear buckling load.

Carduso and Arora [118,119] presented a variational approach for calculating design sensitivity information for nonlinear structural analysis using the reference volume and the adjoint structure concept.

Choi and Santos [120,121] presented a design sensitivity analysis procedure based on the virtual work for nonlinear structural systems. The incremental virtual work equations were implicitly differentiated to obtain the sensitivity derivatives.

Haftka [122] used the integrated approach for design optimization of structures that require nonlinear analysis. In his approach, the optimization process begins with a linearized structural response, and the amount of nonlinearity is increased, as one gets closer to the optimum design. The procedure was demonstrated on two truss problems subject to stress and minimum gauge constraints. It was found that the analysis cost required for the design could be reduced close to that of a single nonlinear analysis.

Orozco and Ghattas [123] compared the efficiency of simultaneous (integrated) approach with the traditional approach of nesting the analysis and design phases for geometrically nonlinear structures. It was shown that when projected Lagrangian methods are used, the simultaneous method is computationally more efficient than the nested, when the sparsity of the Jacobian matrix is exploited.

Saka [124] presented optimal design of space trusses beyond the elastic limit. The nonlinear load-deflection relationships of members were used and approximated from the nonlinear stress-strain diagrams of the members both in tension and compression by linear segments. Each segment was used to represent the changes in the axial stiffness of the member. This made it possible to predict the post critical behavior of the members as the load increases. The nonlinear response of the truss was employed by optimality criteria technique to update the variables in every design step. It was noticed from the numerical examples solved that most of the computation time was used in the nonlinear analysis routine.

Saka and Ulker [125] considered optimum design of geometrically nonlinear space trusses with displacement, stress and cross-sectional area constraints. It was shown that the consideration of nonlinear behavior of the space trusses in their optimum design makes it possible to achieve further reduction in the overall weight.

Lin et al. [126] studied weight optimization of nonlinear truss structures with static response under displacement, stress and cross sectional area constraints. The incremental finite element procedure was used for structural analysis and the linear approximation concept, using reciprocal variables, was used for optimization. Both geometric and material nonlinearities were considered. It was concluded that the optimal volume of a structure with geometric nonlinearities can be less than the optimal volume in the absence of geometric nonlinearities. It was found that with a small limitation for displacement constraints, the effect of geometric nonlinearity can be neglected. However if the larger tolerance for displacement constraints is applied, the effect of geometric nonlinearities can become evident.

Levy [127] considered optimization of a two-bar truss structure subject to nonlinear stability constraints analytically. It was shown that the optimal design for nonlinear stability exhibit for both nonshallow and shallow trusses require equal cross-sectional areas for high unsymmetries.

Levy [128] also considered inequality constraints in which the lowest buckling load factor should be equal to or greater than a specified buckling load factor. He considered linear stability constraints for which he defined a generalized eigenvalue problem. Orozco and Ghattas [129] presented a Sequential Quadratic Programming method based on reduced Hessian matrix for simultaneous analysis and design of nonlinearly behaving structures and compared it with the conventional nested analysis and design methods.

The present literature review presents the state of the art in structural analysis and optimization and it provides a platform for further development of a comprehensive study carried out in this thesis where issues, concerns and shortcomings are addressed and solutions are proposed.

1.5 Present Work

The present thesis constitutes a comprehensive study in the area of structural analysis and optimization. Development of new analysis methods, optimization algorithms and their integration into a structural analysis and optimization tool to study linear and nonlinear structural problems are among the most important contributions of this thesis.

Relatively few investigations have been reported in the literature on formulation and application of the finite element force method in structural optimization. Here, a structural analysis technique using the finite element force method based on the complementary strain energy (FMCE) is introduced. Similar to the SFM and the IFM, the FMCE uses the same equilibrium equations. However, the compatibility conditions in the FMCE are satisfied through the complementary energy [130]. The Gauss elimination technique has been employed successfully to automatically generate a basis determinate structure and redundant members for truss and frame type structures. The advantages of

the FMCE and the IFM in optimization of structures with low redundant members have been studied.

The application of the force method to study structures with small redundancies has proved to be computationally more efficient than the displacement method. The formulation is developed for static analysis and is compared to the classical force method and the more recent integrated force method. An efficient approach based on single-value-decomposition technique has been developed to generate the compatibility matrix in the integrated force method for truss and beam structures. Application of the force method in size structural optimization problems (minimizing the weight of the structure with size design variables) with displacement and stress constraints and topology structural optimization problems (maximizing the structural strength with geometry design variables) are considered and are extended to structural problems with frequency constraints. Efficient computer codes have been developed for size and topology structural optimization of linear problems under stress, displacement, frequency and geometric constraints. Furthermore, the application of the integrated force method in topology optimization of adaptive structures under dynamic load is investigated. Also, a new force method based on the complementary Hamilton principle (compatibility dynamic equation) has been formulated for frequency analysis.

In nonlinear analysis, the nonlinear finite element method based on the force and the displacement control techniques is considered. An efficient approach is formulated to account for the effect of element imperfections. A strategy has been formulated and implemented for calculating the limit load and sensitivity of the limit load using the information obtained from nonlinear buckling analysis based on the displacement method. Effect of different geometry stiffness matrices on final optimum solution has been investigated.

In optimization, optimization algorithms based on optimality criterion technique have been developed and their accuracy compared to that of the SQP technique.

In structurally symmetric problems, the introduction of the Group Theoretic Approach (GTA) to the field of structural optimization allows the reduction in the number of

degrees of freedom resulting in considerable computational savings. The GTA is used in conjunction with the nonlinear finite element based on the displacement control method to obtain the limit load, post buckling behavior of structures and optimization of geometrical nonlinear problems under system stability constraints.

1.6 Thesis Organization

The present thesis contains six chapters. Chapter 1 introduces the problem under investigation and the motivation. A historical perspective to the field of structural analysis and optimization is presented with the most important and relevant contributions to the field to date, with an in-depth review on the linear and nonlinear finite element analysis, the displacement and the force methods and their applications in structural optimization. The chapter concludes by identifying the most important and relevant contributions of the present study and the layout of the monogram.

Chapter 2 presents the general formulations for the classical (standard) force and the integrated force methods. Next, the new force method formulation based on the complementary energy is introduced and its merit and limitations are compared with the classical and integrated force methods. Towards the end of the chapter, the extension of the force method to dynamics is addressed and a new impulse method for frequency analysis is introduced.

Chapter 3 introduces the nonlinear finite element analysis. First, a general formulation for the nonlinear structural analysis is introduced. Next, the energy and the perturbation methods are used to obtain the geometric stiffness matrices based on stress or displacement arguments. Then, the solution of the nonlinear finite element equations based on the force control and displacement control techniques are presented. Also, the nonlinear buckling analysis using the finite element analysis based on the displacement control technique and the strategy for capturing the limit load are also introduced and discussed. Finally, the nonlinear finite element analysis of symmetric problems using the Group Theoretic Approach is investigated.

Chapter 4 pertains to the optimization aspects of the research. First, optimization statements are mathematically formulated for size and geometry optimization and the solution procedures are presented and discussed. Finally, the optimization algorithm based on the optimality criterion technique is formulated and applied to nonlinear structural problems.

Chapter 5 contains a large array of numerical benchmark tests and examples to illustrate, evaluate and verify the application of the proposed formulations and methodologies in structural analysis and optimization. The numerical simulations are classified into the following categories: (i) structural size optimization under stress and displacement constraints; (ii) structural size optimization under frequency constraints, (iii) structural size optimization under stability constraints, and (iv) structural geometry optimization. For geometry optimization, the concept of adaptive structures is introduced and a truss structure with active elements is optimized for varying static and dynamic loading conditions.

Finally, Chapter 6 concludes with a synthesis of the most important findings and contributions of the present investigation and various recommendations are put forward for future work.

Chapter 2

FORCE METHOD FORMULATIONS

2.1 Introduction

The force method of analysis is based on the equations of equilibrium expressed in terms of the element forces. For particular and simple structures, these equations are sufficient to determine all the forces and subsequently the element stresses and displacements. Such structures are said to be *statically determinate*. However, for general and complex structures, the number of element forces exceeds the number of available equations of equilibrium, and the structure is said to be *statically indeterminate* (or redundant). For such cases, the equations of equilibrium are insufficient to obtain solutions for the element forces, and therefore additional equations are required. These additional equations are in the form of compatibility conditions on displacements. In Chapter 2, the general formulations of the standard (classical) force and integrated force methods are presented. Next, the development of the formulation for the force method based on the *complementary strain energy* is introduced. The advantages and limitations of the three methods are discussed and a comparison of the force and displacement methods is carried out. At the end of the chapter, the application of the force method in frequency and dynamic problems is studied, and in this context, a new methodology based on the impulse technique is introduced for calculation of the natural frequencies.

2.2 The Standard Force Method (SFM)

The standard (classical) force method is based on the virtual force method and more specifically, on the unit load theorem. For the virtual force method, virtual work is obtained by multiplying *virtual forces by real displacements*. Implementation of virtual work principle based on the virtual forces (complementary virtual work) enables one to calculate deflection (or rotation) of any point on a deformed body. The complementary virtual work can be simply stated as

$$\delta W^* = \delta \Pi^* \tag{2-1}$$

where W^* and Π^* are the complementary virtual work and complementary virtual strain energy, respectively.

Let us assume now that a virtual load $\delta \mathbf{P}$ in the direction of the displacement U is applied in a discrete or discretized structure (n,m), where *structure* denotes a type of structure (truss, frame, plate, shell, or a combination) under the action of a system of forces that induce internal element forces $\mathbf{F}$. The complementary virtual work is then

$$\delta W^* = \mathrm{U}\ \delta \mathbf{P}. \tag{2-2}$$

Now, due to the virtual force $\delta \mathbf{P}$, the virtual complementary energy of total deformation on the i-th element is given by

$$\delta \Pi^{*(i)} = \delta \mathbf{F}^{(i)^T} \Delta^{(i)}, \tag{2-3}$$

and for the complete structure,

$$\delta \Pi^* = \delta \mathbf{F}^T \Delta \tag{2-4}$$

where Δ is the deformation vector and

$$\delta \mathbf{F} = \begin{bmatrix} \delta \mathbf{F}^{(1)} \\ \delta \mathbf{F}^{(2)} \\ \vdots \\ \delta \mathbf{F}^{(i)} \\ \vdots \end{bmatrix} \quad \text{and} \quad \Delta = \begin{bmatrix} \Delta^{(1)} \\ \Delta^{(2)} \\ \vdots \\ \Delta^{(i)} \\ \vdots \end{bmatrix}. \tag{2-5}$$

For linear elasticity, $\delta \mathbf{F}$ in Eq. (2-5) can be expressed as

$$\delta \mathbf{F} = \begin{bmatrix} \hat{\mathbf{F}}^{(1)} \\ \hat{\mathbf{F}}^{(2)} \\ \vdots \\ \hat{\mathbf{F}}^{(i)} \\ \vdots \end{bmatrix} \delta \mathbf{P} = \hat{\mathbf{F}}\, \delta \mathbf{P} \tag{2-6}$$

where $\hat{\mathbf{F}}$ represents the vector of element forces due to $\delta P = 1$. Now, substituting Eq. (2-6) into Eq. (2-4) and subsequently Eqs (2-4) and (2-2) into Eq. (2-1), we obtain

$$U\ \delta P = \hat{\mathbf{F}}^T \Delta\ \delta P \qquad \text{or} \qquad U = \hat{\mathbf{F}}^T \Delta . \tag{2-7}$$

The deformation vector Δ may be related to the element forces using the following relation:

$$\Delta = \boldsymbol{G}\ \mathbf{F} \tag{2-8}$$

where $\boldsymbol{G}$ is the $(n \times n)$ flexibility matrix of the structure. Substituting Eq. (2-8) into Eq. (2-7), we obtain

$$U = \hat{\mathbf{F}}^T \boldsymbol{G}\ \mathbf{F} \tag{2-9}$$

Eq. (2-9) represents the matrix form of the unit-load theorem for a single displacement U.

The unit-load theorem introduced above has been applied to external forces. However, it may be generalized so as to be applicable to internal forces as well. In this case, the resulting displacements represent internal relative displacements which must be equal to zero in order to satisfy continuity of deformations (compatibility conditions). To illustrate this point, consider a two-dimensional redundant truss structure subject to external loads P at nodes 2 and 4, as shown in Fig. 2-1. The relative displacement Δ, on the individual elements due to P are given by Eq. (2-8). Let us assume that a fictitious cut is introduced in the diagonal member 9 near joint 2. The force F_9 (which existed in the member before the cut was introduced) must be supplied by some external means in order to maintain equilibrium with the external loading. It is noted that this particular structure is redundant with degree of redundancy $r = n - m = 10 - 8 = 2$. When introducing the cut in the diagonal member 9, it is reduced to the degree of redundancy $r = n - m = 9 - 8 = 1$.

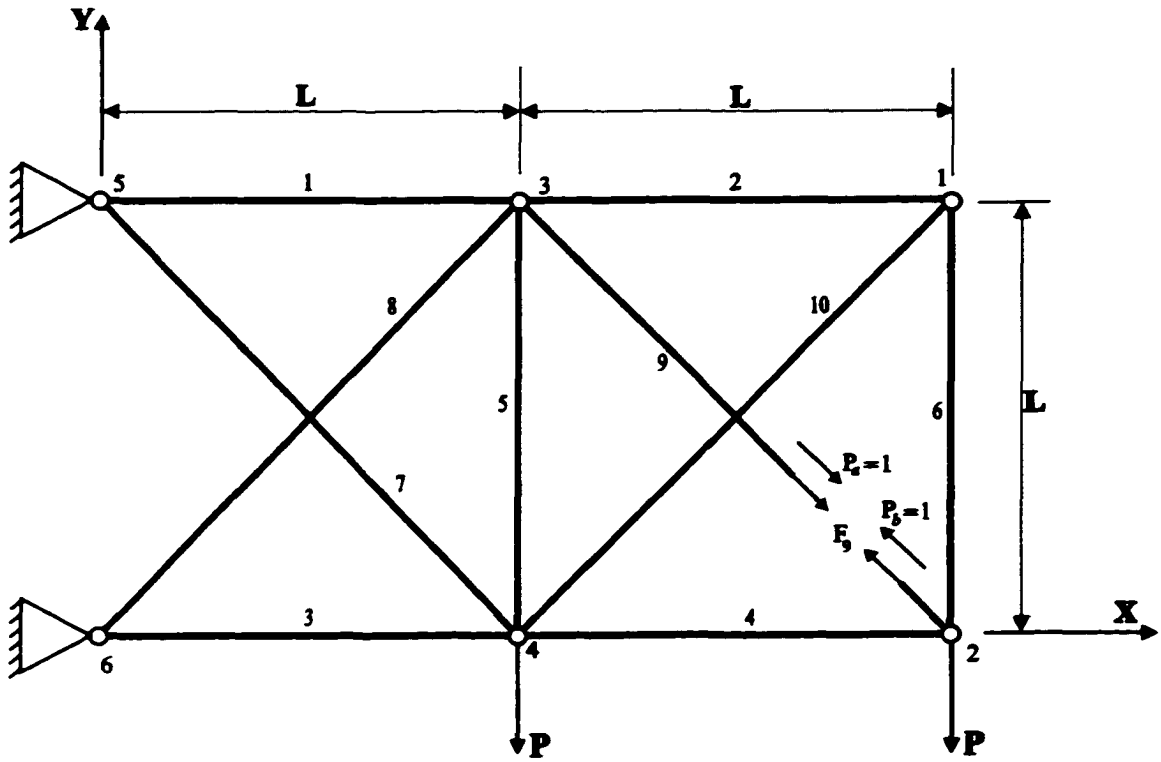

Figure 2-1 Redundant ten-bar truss structure.

If a unit load P_a is applied at the cut in the direction ③ ⇒ ②(from node 3 to node 2), as shown in Fig. 2-1, the unit load theorem gives a deflection U_a, obtained using Eq. (2-9) as

$$U_a = \hat{\mathbf{F}}_a^T \boldsymbol{G}\ \mathbf{F}, \tag{2-10}$$

where $\hat{\mathbf{F}}_a$ represents the vector of statically equivalent element forces due to $P_a = 1$. If instead of P_a, a unit force P_b is applied in the direction ② ⇒ ③, again from Eq. (2-9) it follows that

$$U_b = \hat{\mathbf{F}}_b^T \boldsymbol{G}\ \mathbf{F} \tag{2-11}$$

where $\hat{\mathbf{F}}_b$ represents the vector of statically equivalent element forces for $P_b = 1$. In order to preserve the continuity of deformations at the point of the cut, we must have

$$U_a = -U_b \quad \text{or} \quad U_a + U_b = 0. \tag{2-12}$$

Substituting Eqs. (2-10) and (2-11) into Eq. (2-12) we may have

$$(\hat{\mathbf{F}}_a + \hat{\mathbf{F}}_b)^T \boldsymbol{G}\,\mathbf{F} = \boldsymbol{0} \quad \text{or} \quad \hat{\mathbf{F}}_C{}^T \boldsymbol{G}\,\mathbf{F} = \boldsymbol{0} \tag{2-13}$$

where $\hat{\mathbf{F}}_C = \hat{\mathbf{F}}_a + \hat{\mathbf{F}}_b$. The matrix $\hat{\mathbf{F}}_C$ can be interpreted as an internal-force system representing statically equivalent forces due to a unit force applied across the fictitious cut.

A number of cuts equal to the degree of redundancy can be introduced until the structure is reduced to a statically determinate system. For a structure with $r = n - m$ degree of redundancy, r cuts are required. For each cut, according to Eq. (2-13), the following set of equations is obtained

$$\begin{aligned} &\hat{\mathbf{F}}_{C1}{}^T \boldsymbol{G}\,\mathbf{F} = \boldsymbol{0} \\ &\hat{\mathbf{F}}_{C2}{}^T \boldsymbol{G}\,\mathbf{F} = \boldsymbol{0} \\ &\cdots\cdots\cdots\cdots \\ &\hat{\mathbf{F}}_{Cr}{}^T \boldsymbol{G}\,\mathbf{F} = \boldsymbol{0} \end{aligned} \tag{2-14}$$

The above equations are r compatibility equations, and these can be combined into a single matrix equation:

$$\boldsymbol{C}\ \boldsymbol{G}\ \mathbf{F} = \mathbf{0} \tag{2-15}$$

where $\boldsymbol{C} = \left[\hat{\mathbf{F}}_{C1} \quad \hat{\mathbf{F}}_{C2} \quad \cdots \quad \hat{\mathbf{F}}_{Cr}\right]^T$ is the $(r \times n)$ compatibility matrix.

For derivation of the equilibrium equations, the components of the element forces in the directions of all the displacement degrees of freedom at the nodes of the discrete or discretized structure are algebraically summed up and subsequently equated to the corresponding components of the externally applied loads. The m equilibrium equations can be combined into a single matrix equation as

$$\boldsymbol{Q}\,\mathbf{F} = \mathbf{P} \tag{2-16}$$

where $\boldsymbol{Q}$ is the $(m \times n)$ equilibrium matrix whose coefficients are the direction cosines used in resolving the element forces **F**, and **P** is a vector of external forces applied in the direction of displacement degrees of freedom. If the structure is statically determinate (i.e. $m = n$ and the rank of the matrix $\boldsymbol{Q} = m$), the element forces **F** can be calculated directly from Eq. (2-16). For this special case,

$$\mathbf{F} = \boldsymbol{Q}^{-1}\mathbf{P}. \tag{2-17}$$

For statically indeterminate structures (i.e. $m < n$ and the rank of the matrix $\boldsymbol{Q} = m$), the equations of equilibrium are not sufficient to determine the forces **F**. The required additional equations are supplied by the r compatibility conditions given by Eq. (2-15).

The element forces **F** may be partitioned symbolically into statically determinate forces $\mathbf{F}_d$ and redundant forces $\mathbf{F}_r$, that is

$$\mathbf{F} = \begin{bmatrix} \mathbf{F}_d \\ \mathbf{F}_r \end{bmatrix} \tag{2-18}$$

Also, the equilibrium matrix $\boldsymbol{Q}$ may be consistently partitioned for $\mathbf{F}_d$ and $\mathbf{F}_r$ as

$$\boldsymbol{Q} = [\boldsymbol{Q}_d \quad \boldsymbol{Q}_r] \tag{2-19}$$

Thus, one can re-write the equilibrium equation (2-16) as

$$[\boldsymbol{Q}_d \quad \boldsymbol{Q}_r]\begin{bmatrix} \mathbf{F}_d \\ \mathbf{F}_r \end{bmatrix} = \mathbf{P} \tag{2-20}$$

Solving for $\mathbf{F}_d$,

$$\mathbf{F}_d = [\boldsymbol{Q}_d^{-1} \quad -\boldsymbol{Q}_d^{-1}\boldsymbol{Q}_r]\begin{bmatrix} \mathbf{P} \\ \mathbf{F}_r \end{bmatrix} \tag{2-21}$$

Combining $\mathbf{F}_d$ from Eq. (2-21) and $\mathbf{F}_r$, we obtain

$$\mathbf{F} = \begin{bmatrix} \mathbf{F}_d \\ \mathbf{F}_r \end{bmatrix} = \begin{bmatrix} \boldsymbol{Q}_d^{-1} & -\boldsymbol{Q}_d^{-1}\boldsymbol{Q}_r \\ \mathbf{0} & \boldsymbol{I}_r \end{bmatrix}\begin{bmatrix} \mathbf{P} \\ \mathbf{F}_r \end{bmatrix} \tag{2-22}$$

where I_r is the identity matrix of order r, and

$$\mathbf{F} = A_d \mathbf{P} + A_r \mathbf{F}_r \tag{2-23}$$

where

$$A_d = \begin{bmatrix} Q_d^{-1} \\ 0 \end{bmatrix} \quad \text{and} \quad A_r = \begin{bmatrix} -Q_d^{-1} Q_r \\ I \end{bmatrix}. \tag{2-24}$$

Substituting Eq. (2-23) in the compatibility Eq. (2-15), we obtain

$$C G A_d \mathbf{P} + C G A_r \mathbf{F}_r = \mathbf{0} \tag{2-25}$$

From Eq. (2-25), the redundant forces $\mathbf{F}_r$ are derived from the following equations:

$$(C G A_r)\mathbf{F}_r = -(C G A_d \mathbf{P}). \tag{2-26}$$

The determinate forces $\mathbf{F}_d$ are obtained from Eq. (2-21). It is noted that the matrices Q, C and G are banded and have full-row ranks of m, r and n, respectively. The matrices Q, C depend on the geometry of the structure and are independent of design variables and material properties. For a finite element idealization, the generation of the equilibrium matrix Q and the flexibility matrix G is straightforward and its application is found in Refs.[47-49,131]. However, the automatic generation of the compatibility matrix C is a laborious and difficult task using the standard force method.

It has been noted that the primary variables in the SFM are the redundant forces. A limitation of this method is the difficulty in automatic selection of the consistent redundant elements. Another limitation is the explicit generation of compatibility matrix C. Summarizing, the automatic generation of the compatibility matrix C is cumbersome and difficult in the SFM since it is needed to cut the redundant members and write the unit load theorem for each cut.

2.3 The Integrated Force Method (IFM)

In the integrated force method, the m equilibrium equations in Eq. (2-16) and the r compatibility conditions in Eq. (2-15) are coupled to yield the integrated force formulation, expressed jointly as

$$\begin{bmatrix} \boldsymbol{Q} \\ \cdots\cdots \\ \boldsymbol{C}\,\boldsymbol{G} \end{bmatrix} \mathbf{F} = \begin{bmatrix} \mathbf{P} \\ \cdots \\ \mathbf{0} \end{bmatrix} \quad \text{or} \quad \boldsymbol{S}\,\mathbf{F} = \mathbf{P}^{*} \tag{2-27}$$

where $$\boldsymbol{S} = \begin{bmatrix} \boldsymbol{Q} \\ \cdots\cdots \\ \boldsymbol{C}\,\boldsymbol{G} \end{bmatrix} \quad \text{and} \quad \mathbf{P}^{*} = \begin{bmatrix} \mathbf{P} \\ \cdots \\ \mathbf{0} \end{bmatrix}.$$

The $(n \times n)$ matrix $\boldsymbol{S}$ is banded and has full-row rank of n. In the IFM, the primary variables are the forces in the elements. Eliminating the displacements from the strain-displacement relationships without any recourse to the redundant members and the basis determinate structure generates the compatibility conditions. Following St. Venant's procedure, the compatibility conditions in the IFM are generated by eliminating the displacements from the deformation-displacement relationship of the structure (in discrete analysis, deformations are analogous to strains).

In the IFM, the selection of redundant forces and basis determinate structure is not necessary, however the automatic generation of compatibility equation is not straightforward.

2.3.1 Generation of the Compatibility Equations in the IFM

The compatibility matrix $\boldsymbol{C}$ is obtained by extending St. Venant's principle of elasticity strain formulation [64] to discrete structural mechanics [65,66]. This procedure is illustrated by taking the plane stress elasticity problem as an example. The strain-displacement relations are:

$$\varepsilon_x = \frac{\partial u_x}{\partial x} \quad , \quad \varepsilon_y = \frac{\partial u_y}{\partial y} \quad \text{and} \quad \gamma_{xy} = \frac{\partial u_y}{\partial x} + \frac{\partial u_x}{\partial y} \tag{2-28}$$

In Eq. (2-28), three strains (ε_x, ε_y, and γ_{xy}) are expressed as functions of two displacements (u_x and u_y). The compatibility constraint on strains is obtained by eliminating the two displacements from the three relations in Eq. (2-28), resulting in the single compatibility condition:

$$\frac{\partial^2 \varepsilon_x}{\partial y^2} + \frac{\partial^2 \varepsilon_y}{\partial x^2} - \frac{\partial^2 \gamma_{xy}}{\partial x \partial y} = 0. \tag{2-29}$$

The two-step St. Venant's procedure used to generate compatibility conditions establishes the strain-displacement relations; and subsequently eliminates displacements from the strain-displacement relations to obtain the compatibility conditions.

The equivalent relations of strain-displacement relations in the mechanics of discrete structures are the deformation-displacement relations. Deformations (Δ) of the discrete analysis are analogous to strain (ε) of the elasticity analysis. Thus, the deformation-displacement relations can be obtained using the following energy argument. The equality, relating internal strain energy and external work for a discrete structure (n,m) can be written in the following form:

$$\frac{1}{2}\mathbf{F}^T \Delta = \frac{1}{2}\mathbf{P}^T \mathbf{U} \tag{2-30}$$

where **U** is the nodal displacements vector. Eq. (2-30) can be re-written by eliminating the applied loads vector **P** in lieu of the element force vector **F** using the equilibrium equation (Eq. 2-16), to obtain the following relationship:

$$\frac{1}{2}\mathbf{F}^T \boldsymbol{Q}^T \mathbf{U} = \frac{1}{2}\mathbf{F}^T \Delta \quad \text{or} \quad \frac{1}{2}\mathbf{F}^T (\boldsymbol{Q}^T \mathbf{U} - \Delta) = \mathbf{0}. \tag{2-31}$$

Since the force vector **F** is not a null space, we obtain the following relation between member deformations and nodal displacements:

$$\Delta = \boldsymbol{Q}^T \mathbf{U}. \tag{2-32}$$

The expression given by Eq. (2-32) is the general deformation-displacement relation applicable to the finite element models whose equilibrium equations are given by Eq. (2-16). In the deformation-displacements relation, n deformations are expressed in terms of m displacements. Thus, there are $r = n - m$ constraints on deformations that represent the compatibility conditions of the structure (n,m). The r compatibility conditions, which are obtained by eliminating m displacements from n deformation-displacement relations, can be expressed in matrix form as

$$\boldsymbol{C}\ \Delta = \mathbf{0} \qquad \text{or} \qquad \boldsymbol{C}\ \boldsymbol{G}\mathbf{F} = 0 \tag{2-33}$$

Eq. (2-33) is exactly the Eq. (2-15). The procedure is independent of the redundant members and the basis determinate structure. The indirect generation of the $(r \times n)$ banded compatibility matrix $\boldsymbol{C}$ through selection of independent rows is amenable to computer automation and has been documented in Refs.[65,66].

One of the contributions of the present research has been to develop a new technique to directly generate the compatibility matrix $\boldsymbol{C}$ in the IFM using the deformation-displacement relations (Eq. 2-32) and the Singular Value Decomposition (SVD) method [132]. This enhancement to the IFM method is presented next.

2.3.2 A New Method to Directly Generate the Compatibility Matrix in the IFM

Expressing displacements in terms of deformations using Eq. (2-32), we obtain

$$\mathbf{U} = (\boldsymbol{Q}\ \boldsymbol{Q}^T)^{-1}\boldsymbol{Q}\ \Delta = \left(\boldsymbol{Q}^T\right)^{pinv}\Delta. \tag{2-34}$$

The matrix $\left(\boldsymbol{Q}^T\right)^{pinv}$ denotes the Moore-Penrose pseudo-inverse of $\boldsymbol{Q}^T$. Substituting displacements U (Eq. 2-34) into Eq. (2-32), we obtain

$$\Delta = \boldsymbol{Q}^T\left(\boldsymbol{Q}^T\right)^{pinv}\Delta \ \Rightarrow\ [\boldsymbol{I} - \boldsymbol{Q}^T\left(\boldsymbol{Q}^T\right)^{pinv}]\Delta = \mathbf{0} \tag{2-35}$$

or $$\boldsymbol{A}\Delta = 0 \tag{2-36}$$

where $$\boldsymbol{A} = [\boldsymbol{I}_n - \boldsymbol{Q}^T(\boldsymbol{Q}^T)^{pinv}]. \tag{2-37}$$

The $(n \times n)$ matrix $\boldsymbol{A}$ is of rank r. It is noted that $r < n$. This means that some of the rows of matrix $\boldsymbol{A}$ are dependent on each other. In order to extract the $(r \times n)$ compatibility matrix $\boldsymbol{C}$ from the matrix $\boldsymbol{A}$, i.e. in order to reduce the matrix $\boldsymbol{A}$ to matrix $\boldsymbol{C}$, the singular value decomposition (SVD) method is employed. A basic theory of the SVD method can be found in Ref. [132].

Applying SVD to $\boldsymbol{A}$, we obtain

$$\boldsymbol{A} = \boldsymbol{A}_u \, \boldsymbol{A}_\sigma \, \boldsymbol{A}_v^T \tag{2-38}$$

where $\boldsymbol{A}_u$ and $\boldsymbol{A}_v$ are $(n \times n)$ orthogonal matrices and

$$\boldsymbol{A}_\sigma = \begin{bmatrix} \Lambda & \mathbf{0} \\ \mathbf{0} & \mathbf{0} \end{bmatrix}_{(n \times n)} \tag{2-39}$$

with $\Lambda = \text{diag}\{\Lambda_1 \quad \Lambda_2 \quad \cdots \quad \Lambda_r\}$, and $\Lambda_1 \geq \Lambda_2 \geq \cdots \geq \Lambda_r > 0$. It follows that

$$\boldsymbol{A} = \boldsymbol{A}_u \begin{bmatrix} \boldsymbol{C} \\ \mathbf{0} \end{bmatrix}. \tag{2-40}$$

Subsequently, the $(r \times n)$ compatibility matrix $\boldsymbol{C}$ can be represented as

$$\boldsymbol{C} = \Lambda[\boldsymbol{A}_{v1} \quad \boldsymbol{A}_{v2} \quad \cdots \quad \boldsymbol{A}_{vi} \quad \cdots \quad \boldsymbol{A}_{vr}]^T \tag{2-41}$$

where $\boldsymbol{A}_{vi}$ denotes the i-th column of matrix $\boldsymbol{A}_v$. The compatibility matrix introduced in Eq. (2-41) may not be banded. This does not raise any problem for relatively small size problems, however it may be numerically expensive for very large size problems.

The direct generation of the compatibility matrix proposed and developed here to enhance the IFM method has been implemented successfully for analysis of truss and beam type structures.

2.3.3 Direct Displacement-Force Relations

Although Eq. (2-32) is sufficient to obtain the element deformations using nodal displacements, it is not sufficient to obtain nodal displacements using element deformations or forces because redundant structures are represented by rectangular equilibrium matrix $\boldsymbol{Q}$ with no inverse. This implies that the compatibility equations should be merged with the equilibrium equations. For this reason, using $\boldsymbol{S}$ instead of $\boldsymbol{Q}$ in Eq.(2-32) and solving for nodal displacements **U**, we obtain

$$\mathbf{U} = \boldsymbol{J}\,\Delta \quad \text{or} \quad \mathbf{U} = \boldsymbol{J}\,\boldsymbol{G}\,\mathbf{F} \tag{2-42}$$

where

$$\boldsymbol{J} = \text{m rows of } \boldsymbol{S}^{-T}\ . \tag{2-43}$$

2.4 The Force Method Based on the Complementary Strain Energy

A force method based on the complementary strain energy (FMCE) is proposed here. The m equilibrium equations are satisfied and subsequently the complementary energy is minimized with respect to the r redundant forces to satisfy the r compatibility equations. Similarly to the SFM, it is required to identify the redundant elements and the basis determinate forces. However, the generation of the compatibility matrix $\boldsymbol{C}$ is circumvented, making the proposed method more amenable to automation. Consider Eq. (2-20):

$$\boldsymbol{Q}_r\,\mathbf{F}_r + \boldsymbol{Q}_d\,\mathbf{F}_d = \mathbf{P}, \tag{2-44}$$

and solving for $\boldsymbol{F}_d$, we obtain

$$\mathbf{F}_d = \boldsymbol{H}_1 - \boldsymbol{H}_2\,\mathbf{F}_r \tag{2-45}$$

where $\boldsymbol{H}_1 = \boldsymbol{Q}_d^{-1}\,\mathbf{P}$ and $\boldsymbol{H}_2 = \boldsymbol{Q}_d^{-1}\,\boldsymbol{Q}_r$ (2-46)

The flexibility matrix $\boldsymbol{G}$ may be *consistently* partitioned for $\mathbf{F}_d$ and $\mathbf{F}_r$ as

$$\boldsymbol{G} = \begin{bmatrix} \boldsymbol{G}_d & \mathbf{0} \\ \mathbf{0} & \boldsymbol{G}_r \end{bmatrix} \tag{2-47}$$

where $\boldsymbol{G}_d$ and $\boldsymbol{G}_r$ are $(m \times m)$ and $(r \times r)$ flexibility matrices related to the basis determinate structure and the redundant elements. Thus, the complementary strain energy can be expressed as

$$\Pi^* = \frac{1}{2}\mathbf{F}^T \Delta \quad \text{or} \quad \Pi^* = \frac{1}{2}\mathbf{F}^T \boldsymbol{G}\, \mathbf{F}\,. \tag{2-48}$$

Substituting Eq. (2-18) and Eq. (2-47) into Eq. (2-48), we obtain

$$\Pi^* = \frac{1}{2}\mathbf{F}_d{}^T \boldsymbol{G}_d\, \mathbf{F}_d + \frac{1}{2}\mathbf{F}_r{}^T \boldsymbol{G}_r\, \mathbf{F}_r \tag{2-49}$$

Substituting Eq. (2-45) into Eq. (2-49), it can be obtained

$$\Pi^* = \frac{1}{2}(\boldsymbol{H}_1 - \boldsymbol{H}_2\, \mathbf{F}_r)^T \boldsymbol{G}_d\, (\boldsymbol{H}_1 - \boldsymbol{H}_2\, \mathbf{F}_r) + \frac{1}{2}\mathbf{F}_r{}^T \boldsymbol{G}_r\, \mathbf{F}_r \quad \Rightarrow$$

$$\begin{aligned} \Pi^* = {} & \frac{1}{2}\mathbf{F}_r{}^T \boldsymbol{G}_r\, \mathbf{F}_r + \frac{1}{2}\mathbf{F}_r{}^T (\boldsymbol{H}_2{}^T \boldsymbol{G}_d\, \boldsymbol{H}_2)\mathbf{F}_r - \frac{1}{2}\mathbf{F}_r{}^T (\boldsymbol{H}_2{}^T \boldsymbol{G}_d\, \boldsymbol{H}_1) \\ & - \frac{1}{2}(\boldsymbol{H}_1{}^T \boldsymbol{G}_d\, \boldsymbol{H}_2)\mathbf{F}_r + \frac{1}{2}\boldsymbol{H}_1{}^T \boldsymbol{G}_d\, \boldsymbol{H}_1 \end{aligned} \tag{2-50}$$

The matrix $\boldsymbol{G}_d$ is symmetric, $\mathbf{F}_r{}^T (\boldsymbol{H}_2{}^T \boldsymbol{G}_d\, \boldsymbol{H}_1) = (\boldsymbol{H}_1{}^T \boldsymbol{G}_d\, \boldsymbol{H}_2)\mathbf{F}_r$, and thus Eq. (2-50) can be expressed as

$$\Pi^* = \frac{1}{2}\mathbf{F}_r{}^T \boldsymbol{G}_r\, \mathbf{F}_r + \frac{1}{2}\mathbf{F}_r{}^T (\boldsymbol{H}_2{}^T \boldsymbol{G}_d\, \boldsymbol{H}_2)\mathbf{F}_r - \mathbf{F}_r{}^T (\boldsymbol{H}_2{}^T \boldsymbol{G}_d\, \boldsymbol{H}_1) + \frac{1}{2}\boldsymbol{H}_1{}^T \boldsymbol{G}_d\, \boldsymbol{H}_1. \tag{2-51}$$

Minimization of the Eq. (2-51) with respect to redundant forces $\mathbf{F}_r$ gives the r compatibility equations:

$$\frac{\partial \Pi^*}{\partial \mathbf{F}_r} = 0 \quad \Rightarrow \quad (\boldsymbol{H}_2{}^T \boldsymbol{G}_d\, \boldsymbol{H}_2 + \boldsymbol{G}_r)\mathbf{F}_r = \boldsymbol{H}_2{}^T \boldsymbol{G}_d\, \boldsymbol{H}_1. \tag{2-52}$$

Here, the r redundant forces are obtained and subsequently the m basis determinate forces are determined from Eq. (2-45). It is emphasized that the proposed technique presents a marked advantage over the other force methods since it does not require the explicit generation of the compatibility matrix $\boldsymbol{C}$.

2.4.1 Selection of the Redundant Members and Basis Determinate Structure

The selection of the redundant members is not unique and there are multiple combinations of matrices $\boldsymbol{Q}_d$ and $\boldsymbol{Q}_r$ for an indeterminate structure. For example, a simple structure with $m = 5$ and $n = 20$ can have a maximum of 15504 probable combinations of $\boldsymbol{Q}_d$ and $\boldsymbol{Q}_r$. Redundant forces should be selected so that the remaining determinate structure is not a mechanism. In other worlds, the selection of the consistent set of redundant members and basis determinate structure is such that the rank of the matrix $\boldsymbol{Q}_d$ is equal to m. The violation of this condition makes the matrix $\boldsymbol{Q}_d$ singular. Here, a robust technique based on the Gauss elimination technique is applied to automatically identify the consistent set of redundant members and basis determinate structure. The technique was introduced by Robinson [54] for identifying dependent and independent equations among a system of static equations including external, joint and element equilibrium equations. Here, this technique has been applied to redundant structures to identify the consistent set of redundant members and basis determinate structure. The technique is outlined as follows:

1) Augment the equilibrium matrix $\boldsymbol{Q}$ with the external load $\mathbf{P}$ as $[\boldsymbol{Q}\ \mathbf{P}]$

2) Select one of the non-zero elements in the first row of the augmented matrix and divide all elements in this row by this number.

3) Multiply the first row by the coefficient of the corresponding element in the second row (if it is not zero) and subtracted from the second row.

4) Continue this procedure for each of the remaining rows.

5) The column corresponding to that element has now a one in the first row and zeros in all other rows.

6) Repeat the same process from steps 2 through 4, in turn for the remaining rows until either all of the rows are exhausted or all of the remaining rows have all zeros as elements.

7) All the m unit columns are independent and they correspond to the basis determinate structure. The remaining columns correspond to the consistent redundant members.

8) The consistent redundant members selected are not unique since the redundancy is dependent on the order in which the equations are generated and by the selection of the non-zero element in each row when applying the Gaussian elimination procedure. This point is illustrated next.

2.4.2 Illustrative Example

Consider a 10-bar truss structure shown in the Fig. 2-1. This structure has $r = n - m = 10 - 8 = 2$ redundant members. It is required to identify the redundant members and eliminate them so that the basis determinate structure is stable (the rank of the basis matrix is m). The equilibrium matrix Q for this structure is

$$Q = \begin{bmatrix} 0 & 1 & 0 & 0 & 0 & 0 & 0 & 0 & 0 & \sqrt{2}/2 \\ 0 & 0 & 0 & 0 & 0 & 1 & 0 & 0 & 0 & \sqrt{2}/2 \\ 0 & 0 & 0 & 1 & 0 & 0 & 0 & 0 & \sqrt{2}/2 & 0 \\ 0 & 0 & 0 & 0 & 0 & -1 & 0 & 0 & -\sqrt{2}/2 & 0 \\ 1 & -1 & 0 & 0 & 0 & 0 & 0 & \sqrt{2}/2 & -\sqrt{2}/2 & 0 \\ 0 & 0 & 0 & 0 & 1 & 0 & 0 & \sqrt{2}/2 & \sqrt{2}/2 & 0 \\ 0 & 0 & 1 & -1 & 0 & 0 & \sqrt{2}/2 & 0 & 0 & -\sqrt{2}/2 \\ 0 & 0 & 0 & 0 & -1 & 0 & -\sqrt{2}/2 & 0 & 0 & -\sqrt{2}/2 \end{bmatrix}. \quad \textbf{(2-53)}$$

Now, select the maximum non-zero element in each row. At the end of the Gauss elimination procedure, the matrix Q is transformed into

$$\boldsymbol{Q}=\begin{bmatrix} 0 & \sqrt{2} & 0 & 0 & 0 & 0 & 0 & 0 & 0 & 1 \\ 0 & -1 & 0 & 0 & 0 & 1 & 0 & 0 & 0 & 0 \\ 0 & \sqrt{2} & 0 & 0 & 0 & 0 & 0 & 0 & 1 & 0 \\ 0 & -1 & 0 & 1 & 0 & 0 & 0 & 0 & 0 & 0 \\ \sqrt{2} & 0 & 0 & 0 & 0 & 0 & 0 & 1 & 0 & 0 \\ -1 & -1 & 0 & 0 & 1 & 0 & 0 & 0 & 0 & 0 \\ \sqrt{2} & 0 & 0 & 0 & 0 & 0 & 1 & 0 & 0 & 0 \\ -1 & 0 & 1 & 0 & 0 & 0 & 0 & 0 & 0 & 0 \end{bmatrix}. \tag{2-54}$$

Here, the columns 1 and 2 corresponding to the elements 1 and 2, respectively, represent the consistent redundant members. The columns 3-10 corresponding to the elements 3-10 represent the consistent determinate basis structure. As the columns 3-10 are independent, the rank of the determinate basis structure is m=8.

Now, select the first non-zero element in each row. At the end of the Gauss elimination, the matrix $\boldsymbol{Q}$ is transformed into

$$\boldsymbol{Q}=\begin{bmatrix} 0 & 1 & 0 & 0 & 0 & 0 & 0 & 0 & 0 & \sqrt{2}/2 \\ 0 & 0 & 0 & 0 & 0 & 1 & 0 & 0 & 0 & \sqrt{2}/2 \\ 0 & 0 & 0 & 1 & 0 & 0 & 0 & 0 & 0 & \sqrt{2}/2 \\ 0 & 0 & 0 & 0 & 0 & 0 & 0 & 0 & 1 & -1 \\ 1 & 0 & 0 & 0 & 0 & 0 & 0 & \sqrt{2}/2 & 0 & 0 \\ 0 & 0 & 0 & 0 & 1 & 0 & 0 & \sqrt{2}/2 & 0 & \sqrt{2}/2 \\ 0 & 0 & 1 & 0 & 0 & 0 & 0 & \sqrt{2}/2 & 0 & 0 \\ 0 & 0 & 0 & 0 & 0 & 0 & 1 & -1 & 0 & 0 \end{bmatrix}. \tag{2-55}$$

Here, the columns 8 and 10 corresponding to the elements 8 and 10, respectively, represent the consistent redundant members. The columns 1,2,3,4,5,6,7,9 corresponding to the elements 1,2,3,4,5,6,7,9 represent the consistent determinate basis structure. It is observed that the columns 1,2,3,4,5,6,7,9 are independent. Thus, the rank of the determinate basis structure is m=8 again.

Summarizing, it is possible to identify the consistent redundant elements and basis determinate structure using the Gauss elimination procedure. This method is easily

implemented computationally. The consistent redundant members are not unique and depend on which non-zero element is selected in each row.

2.5 Comparison of the Force Methods

The merits and limitations of the force methods presented and discussed previously are identified in Table 2-1.

Table 2-1 Advantages and Limitations of the Force Methods.

	Advantages	**Limitations**
SFM	*r* equations need to be solved instead of the *m* equations in the displacement method.	Primary variables are redundant members ⇒ consistent set of redundant members need to be selected.
		Generation of compatibility matrix needs cutting the redundant members ⇒ difficult to automate.
IFM	No need to select redundant members	Generation of compatibility matrix.
	Compatibility matrix can be obtained automatically and directly.	*n* equations need to be solved simultaneously in comparison to the *m* equations in the displacement method.
FMCE	No need to generate compatibility matrix	Selection of the consistent redundant members and determinate basis structure
	It can be automated easily by Gaussian elimination procedure.	
	r equations need to be solved simultaneously.	

2.6 Comparison between the Force and Displacement Methods

In the displacement method, the compatibility equations are implicitly satisfied when the nodal equilibrium equations are written. The governing equation in the displacement method (load-nodal displacement relations) may be derived using the force method given by Eqs. (2-8), (2-16) and (2-32) promptly, and the reverse is not true. Substituting deformation Δ from Eq. (2-32) into Eq. (2-8) and solving for the element forces, we obtain

$$\mathbf{F} = \boldsymbol{G}^{-1}\boldsymbol{Q}^{T}\,\mathbf{U}. \tag{2-56}$$

Now substituting Eq. (2-56) into the equilibrium Eq. (2-16):

$$(\boldsymbol{Q}\,\boldsymbol{G}^{-1}\boldsymbol{Q}^{T})\mathbf{U} = \mathbf{P} \quad \Rightarrow \quad \boldsymbol{K}\,\mathbf{U} = \mathbf{P} \tag{2-57}$$

where $$\boldsymbol{K} = \boldsymbol{Q}\,\boldsymbol{G}^{-1}\boldsymbol{Q}^{T}. \tag{2-58}$$

Here, the matrix $\boldsymbol{K}$ is the stiffness matrix used in the displacement method. It is noted that since the equilibrium and the compatibility equations are satisfied explicitly in the force method, it is not possible to derive the governing equation in the force method (Eq. 2-16) from Eq. (2-57), confirming the non-commutative property of the two formulations.

In the force method, the element forces **F** are calculated directly from the loads. On the other hand, in the displacement method, one has to calculate the nodal displacements **U** from the loads using the load-displacement relation (Eq.2-57). In practical design and optimization problems, it is required to obtain element forces in all elements and fewer nodal displacements may be necessary. To illustrate this point, consider structural optimization problems, in general. Here, the number of stress constraints is usually greater than the number of displacement constraints. The computation time is considerably reduced using force method. This is attributed to the following factors:

The displacement method requires a series of transformations and back substitutions (from local to global system to generate displacements and then from global to local

system to calculate the forces). In the force methods, these transformations are not required.

In the displacement method, m equations are solved simultaneously, while only r equations are solved using the force method.

In the force method, the equilibrium matrix $\boldsymbol{Q}$ for the general determinate structure, after some rearrangement of rows and columns can be represented as a triangular matrix. The stiffness matrix in the displacement method is not a triangular matrix for the determinate structure. The triangular system of equations requires insignificant computation, and it can be solved even manually irrespective of the size or complexity of the problem. This feature of the force method made it the popular analysis method in the pre-computer era.

In the force method, the coefficients of the equilibrium matrix $\boldsymbol{Q}$ and the compatibility matrix are dimensionless numbers, making them numerically stable. On the other hand, the coefficients of the stiffness matrix in the displacement method have the dimensions of force per unit length. Since the coefficients depend on material properties and design parameters, an ill conditioned stiffness matrix can result with a numerically unfavourable combination of these properties.

2.7 Extension of the Force Method to Dynamics

The force method can be extended to analyze dynamic problems. In the displacement method, the basic equation in dynamics problems in the absence of damping is

$$\boldsymbol{M}\ddot{\mathbf{U}} + \boldsymbol{K}\mathbf{U} = \mathbf{P} \tag{2-59}$$

where $\boldsymbol{M}$ is the stiffness matrix of system. Using Eq. (2-42) and noting that $\boldsymbol{K}\mathbf{U}$ in the displacement method is equivalent to $\boldsymbol{S}\mathbf{F}$ in the force method, Eq. (2-59) may be written as

$$\boldsymbol{M}^{*}\ddot{\mathbf{F}} + \boldsymbol{S}\mathbf{F} = \mathbf{P}^{*} \tag{2-60}$$

where $$\boldsymbol{M}^{*} = \begin{bmatrix} \boldsymbol{M}\,\boldsymbol{J}\,\boldsymbol{G} \\ \cdots\cdots \\ \mathbf{0} \end{bmatrix}. \tag{2-61}$$

In forced vibration problems , $\mathbf{P}^{*}$ is a function of time. There are a few time integration techniques in the literature [82,83] for solving Eq. (2-60). One of the most powerful techniques is the Newmark direct integration method [133]. It is assumed that the initial values of force vector $\mathbf{F}$ and the vector $\dot{\mathbf{F}}$ at time t=0 is known. The vector $\ddot{\mathbf{F}}$ at t=0 is obtained from Eq. (2-60). Considering a time increment Δt, the predictor parameters, $\bar{\mathbf{F}}_{n+1}$ and $\dot{\bar{\mathbf{F}}}_{n+1}$ at time $(n+1)\Delta t$ in terms of the known vectors at time $n\,\Delta t$ are computed as

$$\begin{aligned} \bar{\mathbf{F}}_{n+1} &= \mathbf{F}_n + \Delta t\,\dot{\mathbf{F}}_n + 0.5\Delta t^2(1-2\beta)\,\ddot{\mathbf{F}}_n \\ \dot{\bar{\mathbf{F}}}_{n+1} &= \dot{\mathbf{F}}_n + \Delta t(1-\gamma)\,\ddot{\mathbf{F}}_n \end{aligned} \tag{2-62}$$

Now, the vector $\ddot{\mathbf{F}}$ at time $(n+1)\,\Delta t$, $\ddot{\mathbf{F}}_{n+1}$ is obtained from the following equation

$$(\boldsymbol{M}^{*} + \beta\Delta t^2\,\boldsymbol{S})\,\ddot{\mathbf{F}}_{n+1} = \mathbf{P}^{*}_{n+1} - \boldsymbol{S}\,\bar{\mathbf{F}}_{n+1}. \tag{2-63}$$

Knowing $\ddot{\mathbf{F}}_{n+1}$, the force vector $\mathbf{F}$ and the vector $\dot{\mathbf{F}}$ at time $(n+1)\Delta t$ are obtained from the following relations

$$\begin{aligned} \mathbf{F}_{n+1} &= \bar{\mathbf{F}}_{n+1} + \beta\Delta t^2\,\ddot{\mathbf{F}}_{n+1} \\ \dot{\mathbf{F}}_{n+1} &= \dot{\bar{\mathbf{F}}}_{n+1} + \gamma\,\Delta t\,\ddot{\mathbf{F}}_{n+1} \end{aligned} \tag{2-64}$$

Constants β and γ in the above equations are the accuracy and stability parameters in the Newmark method. The Newmark method is unconditionally stable if $0.5 \le \gamma \le 2\beta$.

In free vibration, it is assumed that element forces are harmonics in time ($\mathbf{F} = \overline{\mathbf{F}}\sin(\omega t)$) where ω and $\overline{\mathbf{F}}$ are frequency and force mode shape, respectively. Considering Eq. (2-60):

$$\boldsymbol{S}\,\overline{\mathbf{F}} - \omega^2\,\boldsymbol{M}^{*}\,\overline{\mathbf{F}} = \mathbf{0} \tag{2-65}$$

To overcome some computational difficulties during the analysis, the $(n \times n)$ system of equations (2-65) can be reduced to a $(m \times m)$ system by taking advantage of the null matrices. To obtain these matrices, the matrices in Eq. (2-65) are partitioned as the redundant and basis determinate structure as

$$\begin{bmatrix} \boldsymbol{S}_{dd} & \boldsymbol{S}_{dr} \\ \mathbf{S}_{rd} & \boldsymbol{S}_{rr} \end{bmatrix} \begin{bmatrix} \overline{\mathbf{F}}_d \\ \overline{\mathbf{F}}_r \end{bmatrix} - \omega^2 \begin{bmatrix} \tilde{\boldsymbol{M}}_r & \tilde{\boldsymbol{M}}_d \\ \cdots\cdots & \\ \mathbf{0} & \end{bmatrix} \begin{bmatrix} \overline{\mathbf{F}}_d \\ \overline{\mathbf{F}}_r \end{bmatrix} = \mathbf{0} \tag{2-66}$$

or

$$\begin{aligned} &\boldsymbol{S}_{dd}\,\overline{\mathbf{F}}_d + \boldsymbol{S}_{dr}\,\overline{\mathbf{F}}_r - \omega^2(\tilde{\boldsymbol{M}}_d\,\overline{\mathbf{F}}_d + \tilde{\boldsymbol{M}}_r\,\overline{\mathbf{F}}_r) = \mathbf{0} \\ &\boldsymbol{S}_{rd}\,\overline{\mathbf{F}}_d + \boldsymbol{S}_{rr}\,\overline{\mathbf{F}}_r = \mathbf{0} \end{aligned} \tag{2-67}$$

Eliminating $\mathbf{F}_r$ from the $(n \times n)$ system of equations (2-67) results in the reduced $(m \times m)$ subsystem:

$$(\boldsymbol{S}_{dd} - \boldsymbol{S}_{dr}\,\boldsymbol{S}_{rr}^{-1}\,\boldsymbol{S}_{rd})\overline{\mathbf{F}}_d - \omega^2(\tilde{\boldsymbol{M}}_d - \tilde{\boldsymbol{M}}_r\,\boldsymbol{S}_{rr}^{-1}\,\boldsymbol{S}_{rd})\overline{\mathbf{F}}_d = \mathbf{0} \tag{2-68}$$

and

$$\overline{\mathbf{F}}_r = \boldsymbol{S}_{rr}^{-1}\,\boldsymbol{S}_{rd}\,\overline{\mathbf{F}}_d . \tag{2-69}$$

Selection of consistent redundant members ensures the existence of the inverse of $\boldsymbol{S}_{22}$.

The solution of the reduced eigenvalue problem expressed by Eq. (2-68) gives all the eigenvalues, whereas both Eqs. (2-68) and (2-69) are used to calculate the force eigenvectors. Once the force mode shapes are known, the displacement mode shapes can be generated by using Eq. (2-42).

2.8 Development of the Impulse Method in Frequency Analysis

Here, the complementary Hamilton equation is expressed in the form of an impulse and then the frequency equation is derived in the form of impulse for truss element using the finite element technique.

The complementary Hamilton equation may be represented as [130]

$$\delta \int_{t_1}^{t_2} (\Pi^* - V) dt = 0 \tag{2-70}$$

where Π^* and V are complementary energy and kinetic energies [130], respectively. For a one-dimensional element with constant area A, constant density ρ, constant Young's modulus E, length of L and the x-axis along the element axis:

$$\dot{\tau}_x = F = \sigma_x A \tag{2-71}$$

where τ_x, F and σ_x are impulse, force and stress in the element . Using Eq. (2-71) and considering that

$$\sigma_{,x} = \rho \ddot{u}_x \tag{2-72}$$

where u_x is the displacement function along the x-axis, we obtain

$$\frac{\dot{\tau}_{x,x}}{A} = \rho \ddot{u}_x \tag{2-73}$$

or assuming that $\tau_{x,x}\big|_{t=0} = \rho A \dot{u}_x\big|_{t=0}$, we obtain

$$\frac{\tau_{x,x}}{A} = \rho \dot{u}_x. \tag{2-74}$$

In linear elasticity, potential energy is equal to the complementary energy. Considering Eqs. (2-71) and (2-74):

$$V = \frac{1}{2} \int_0^L A \rho \dot{u}_x^2 \, dx = \frac{1}{2\rho A} \int_0^L \tau_{x,x}^2 \, dx \tag{2-75}$$

and

$$\Pi = \Pi^* = \int_0^L \frac{\sigma_x^2}{2E} dx = \frac{1}{2AE} \int_0^L \dot{\tau}_x^2 \, dx. \tag{2-76}$$

Substituting Eqs. (2-75) and (2-76) into Eq. (2-70), we obtain

$$\delta\int_{t_1}^{t_2}\int_0^L\left(\frac{\dot{\tau}_x}{2AE}-\frac{\tau_{x,x}^2}{2\rho A}\right)dx\,dt=0. \tag{2-77}$$

2.8.1 Finite Element Formulation for a Truss Element with Nodal Impulses

Consider a truss element with nodal impulses shown in Figure 2-2:

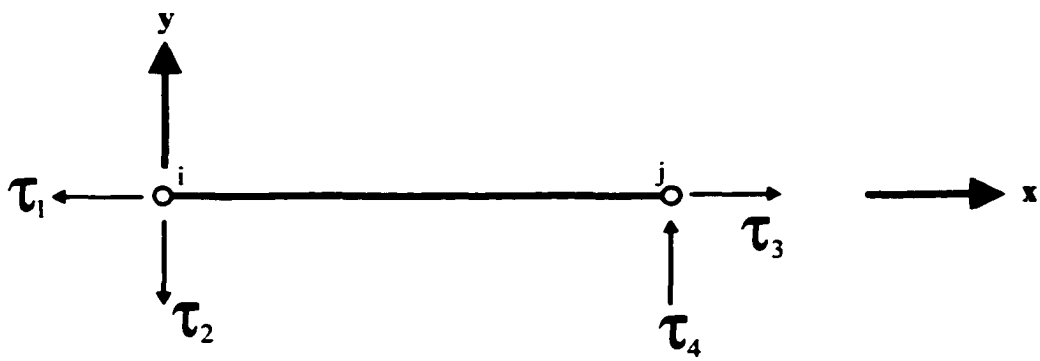

Figure 2-2 Illustration of nodal impulses in the truss element.

Assuming a linear shape function, an impulse can be represented as

$$\tau_x=\begin{bmatrix}1-\frac{x}{L} & \frac{x}{L}\end{bmatrix}\begin{bmatrix}\tau_1\\ \tau_3\end{bmatrix} \tag{2-78}$$

where τ_1 and τ_3 are nodal impulses along the x-axis at node i and j, respectively. From Eq.(2-78):

$$\tau_{x,x}=\begin{bmatrix}-\frac{1}{L} & \frac{1}{L}\end{bmatrix}\begin{bmatrix}\tau_1\\ \tau_3\end{bmatrix}\quad\text{and}\quad\dot{\tau}_x=\begin{bmatrix}1-\frac{x}{L} & \frac{x}{L}\end{bmatrix}\begin{bmatrix}\dot{\tau}_1\\ \dot{\tau}_3\end{bmatrix}. \tag{2-79}$$

Substituting Eq.(2-79) into Eqs. (2-75) and (2-76), we obtain

$$V=\frac{1}{2\rho AL}\begin{bmatrix}\tau_1 & \tau_3\end{bmatrix}\begin{bmatrix}1 & -1\\ -1 & 1\end{bmatrix}\begin{bmatrix}\tau_1\\ \tau_3\end{bmatrix}$$

$$\Pi^*=\frac{L}{2AE}\begin{bmatrix}\dot{\tau}_1 & \dot{\tau}_3\end{bmatrix}\begin{bmatrix}1/3 & 1/6\\ 1/6 & 1/3\end{bmatrix}\begin{bmatrix}\dot{\tau}_1\\ \dot{\tau}_3\end{bmatrix} \tag{2-80}$$

Substituting Eq. (2-80) into Eq. (2-77), performing variation and assuming that $\delta\tau_x = 0$ at $t = t_1$ and $t = t_2$, the following equation for free vibration is obtained:

$$\frac{L}{AE}\begin{bmatrix} 1/3 & 1/6 \\ 1/6 & 1/3 \end{bmatrix}\begin{bmatrix} \ddot{\tau}_1 \\ \ddot{\tau}_3 \end{bmatrix} + \frac{1}{\rho A L}\begin{bmatrix} 1 & -1 \\ -1 & 1 \end{bmatrix}\begin{bmatrix} \tau_1 \\ \tau_3 \end{bmatrix} = \begin{bmatrix} 0 \\ 0 \end{bmatrix}. \tag{2-81}$$

Assuming a sinusoidal impulse in free vibrations, the following is obtained:

$$\tau = \begin{bmatrix} \tau_1 & \tau_3 \end{bmatrix}^T = \bar{\tau}\sin(\omega t) \tag{2-82}$$

where $\bar{\tau}$ is the impulse modes shape. Considering Eqs. (2-81) and (2-82), we have

$$\boldsymbol{m}_{Im}\bar{\tau} - \omega^2 \boldsymbol{k}_{Im}\bar{\tau} = \mathbf{0} \tag{2-83}$$

where

$$\boldsymbol{k}_{Im} = \frac{L}{6AE}\begin{bmatrix} 1 & 2 \\ 2 & 1 \end{bmatrix} \qquad \boldsymbol{m}_{Im} = \frac{1}{\rho A L}\begin{bmatrix} 1 & -1 \\ -1 & 1 \end{bmatrix}. \tag{2-84}$$

Eq. (2-83) is the free vibration equation of linear system in the impulse formulation. This is compared to the equation from the displacement formulation, given by

$$\boldsymbol{k}\bar{\mathbf{u}} - \omega^2 \boldsymbol{m}\bar{\mathbf{u}} = \mathbf{0} \tag{2-85}$$

where $\bar{\mathbf{u}} = \begin{bmatrix} \bar{u}_1 & \bar{u}_2 \end{bmatrix}$ is the displacement mode shape and

$$\boldsymbol{k} = \frac{AE}{L}\begin{bmatrix} 1 & -1 \\ -1 & 1 \end{bmatrix} \qquad \boldsymbol{m} = \frac{\rho AL}{6}\begin{bmatrix} 1 & 2 \\ 2 & 1 \end{bmatrix}. \tag{2-86}$$

It is noted that using the displacement formulation, the mass matrix $\boldsymbol{m}$ is obtained using the kinetic energy. However, in the impulse method, the matrix $\boldsymbol{k}_{Im}$ is obtained using the complementary energy. Similarly, in the displacement formulation, the stiffness matrix $\boldsymbol{k}$ is obtained via the potential energy, and in the impulse formulation, the matrix $\boldsymbol{m}_{Im}$ is obtained via the kinetic energy.

To take into account the degrees of freedom along the element $y-\text{axis}(u_2$ and u_4 for displacement formulation and τ_2 and τ_4 for impulse formulation), the above matrices can be expanded. For example, the expanded form of the mass and stiffness matrices in the displacement formulation can be found in Refs.[74,75,134] and are written here

$$\boldsymbol{k} = \frac{AE}{L}\begin{bmatrix} 1 & 0 & -1 & 0 \\ 0 & 0 & 0 & 0 \\ -1 & 0 & 1 & 0 \\ 0 & 0 & 0 & 0 \end{bmatrix} \quad \text{and} \quad \boldsymbol{m} = \frac{\rho AL}{6}\begin{bmatrix} 1 & 0 & 2 & 0 \\ 0 & 1 & 0 & 2 \\ 2 & 0 & 1 & 0 \\ 0 & 2 & 0 & 1 \end{bmatrix}. \tag{2-87}$$

To develop the mass matrix given in Eq. (2-87), a similar linear shape function has been used for both the x and y - axis . Similarly, for impulse formulation, using the same linear shape function for both x and y - axis , the following is obtained:

$$\boldsymbol{k}_{\text{Im}} = \frac{L}{6AE}\begin{bmatrix} 1 & 0 & 2 & 0 \\ 0 & 0 & 0 & 0 \\ 2 & 0 & 1 & 0 \\ 0 & 0 & 0 & 0 \end{bmatrix} \quad \text{and} \quad \boldsymbol{m}_{\text{Im}} = \frac{1}{\rho AL}\begin{bmatrix} 1 & 0 & -1 & 0 \\ 0 & 1 & 0 & -1 \\ -1 & 0 & 1 & 0 \\ 0 & -1 & 0 & 1 \end{bmatrix}. \tag{2-88}$$

Here, it has been found that frequencies obtained through Eq. (2-83) using $\boldsymbol{k}_{\text{Im}}$ and $\boldsymbol{m}_{\text{Im}}$ in Eq. (2-88) are slightly different from those obtained from displacement formulation. The reason for this discrepancy is found to be in the $\boldsymbol{m}_{\text{Im}}$ in Eq. (2-88). It is found that in the impulse formulation, the correct kinetic energy along the y - axis is different from that in Eq. (2-88).

The kinetic energy along the y - axis for the truss element shown in Figure 2-3, may be written as

$$V = \frac{\tau_y^{\,2}}{2M} + \frac{\tau_\theta^{\,2}}{2I} \tag{2-89}$$

where τ_y and τ_θ are traverse and rotational impulse acting in the center of the truss. $M = \rho A L$ and $I = \rho A L^3 / 12$ are mass and moment of inertia about the center of the

truss, respectively. Considering nodal impulses at nodes i and j equivalent to the τ_y and τ_θ as it is shown in the Fig. (2-3), for equilibrium we may have

$$\tau_y = \tau_4 - \tau_2 \quad \text{and} \quad \tau_\theta = (\tau_4 + \tau_2)L/2. \tag{2-90}$$

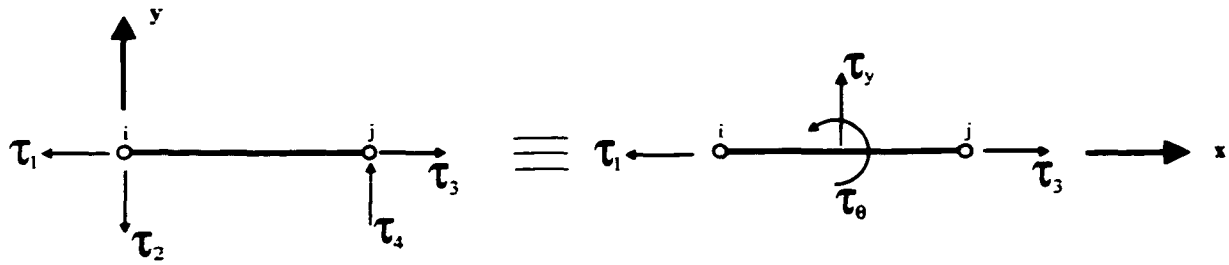

Figure 2-3 Equivalent nodal impulses for the truss element.

Substituting Eq. (2-90) into Eq. (2-89), we obtain

$$V = \frac{1}{2\rho A L}(\tau_4^2 - 2\tau_4\tau_2 + \tau_2^2) + \frac{3}{2\rho A L}(\tau_4^2 + 2\tau_4\tau_2 + \tau_2^2). \tag{2-91}$$

Eq. (2-91) can be cast in matrix form like the Eq. (2-80) as follows

$$V = \frac{1}{2\rho A L}\begin{bmatrix}\tau_2 & \tau_4\end{bmatrix}\begin{bmatrix}4 & 2\\ 2 & 4\end{bmatrix}\begin{bmatrix}\tau_2\\ \tau_4\end{bmatrix} \tag{2-92}$$

From Eq. (2-92), we may say that $\boldsymbol{m}_{lm}$ along the y-axis should be equal to $\frac{1}{\rho AL}\begin{bmatrix}4 & 2\\ 2 & 4\end{bmatrix}$.

Therefore, the matrix $\boldsymbol{m}_{lm}$ in Eq. (2-88), may be modified to

$$\boldsymbol{m}_{lm} = \frac{1}{\rho AL}\begin{bmatrix}1 & 0 & -1 & 0\\ 0 & 4 & 0 & 2\\ -1 & 0 & 1 & 0\\ 0 & 2 & 0 & 4\end{bmatrix}. \tag{2-93}$$

Frequencies obtained using the impulse formulation and using $\boldsymbol{m}_{lm}$ in Eq. (2-93) are exactly equal to those obtained using the displacement formulation.

2.8.2 Illustrative Example

Consider a three-bar planar truss shown in the Figure 2-4. The system has $n = 3$ elements (force degrees of freedom) and $m = 2$ displacement degrees of freedom. Therefore, the number of redundancy is $r = 1$. The area of the elements 1, 2 and 3 are $A_1 = 1\ \text{in}^2$, $A_2 = 1\ \text{in}^2$ and $A_3 = 2\ \text{in}^2$, respectively. The structure has both structural masses with density $\rho = 0.1\ \text{lbm/in}^3 = 0.1/386\ \text{lb-s}^2/\text{in}^4$ and non-structural mass (lumped) $M_0 = 0.68\ \text{lb-s}^2/\text{in}$. The Young modulus for the material is E=30000 ksi.

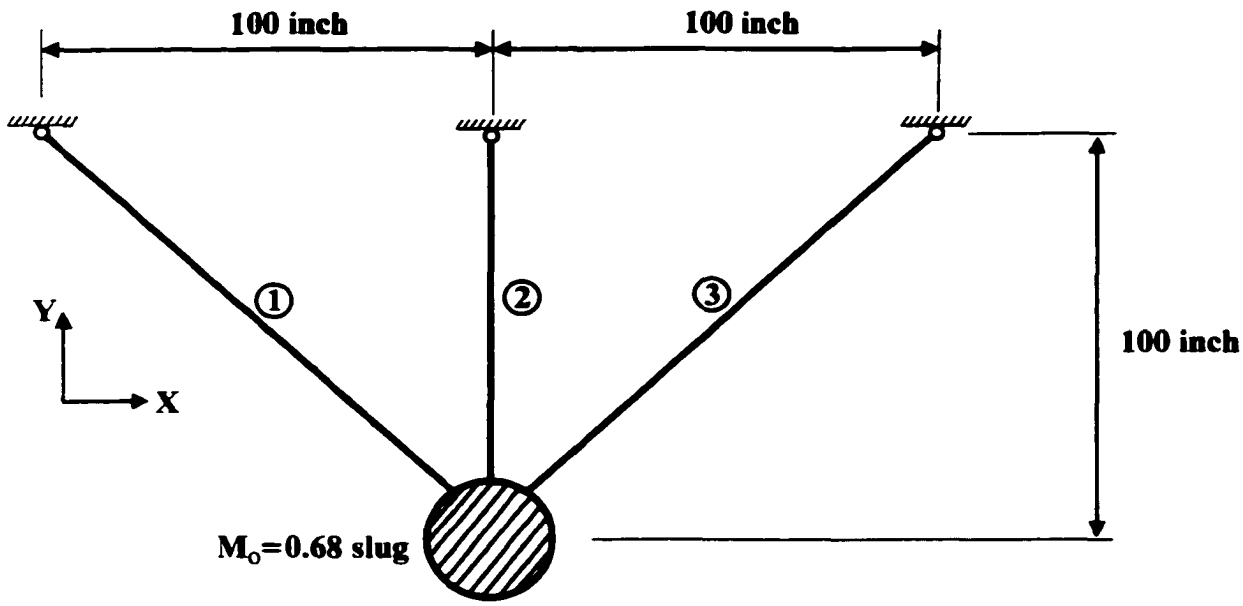

Figure 2-4 The 3-bar planar truss structure.

The system has two natural frequencies for the two displacement degrees of freedom. Using the displacement formulation, (Eq. 2-85), these natural frequencies are found to be: $\omega_1 = 99.6782$ Hz and $\omega_2 = 150.8909$ Hz and the displacement mode shapes are

$$\overline{U}_1 = \begin{Bmatrix} 1.0000 \\ -0.3178 \end{Bmatrix} \quad \text{and} \quad \overline{U}_2 = \begin{Bmatrix} 0.3178 \\ 1.0000 \end{Bmatrix}. \tag{2-94}$$

Using the force method (Eq. 2-65), the natural frequency are found to be $\omega_1 = 99.6782$ Hz $\omega_2 = 150.8909$ Hz, as well. The force mode shapes are

$$\overline{\mathbf{F}}_1 = \begin{Bmatrix} 0.9659 \\ 0.4659 \\ -1.0000 \end{Bmatrix} \text{ and } \overline{\mathbf{F}}_2 = \begin{Bmatrix} 0.2588 \\ 0.7588 \\ 1.0000 \end{Bmatrix}. \tag{2-95}$$

Using Eq. (2-42), we can easily obtain displacement mode shape from force mode shapes in Eq. (2-95). The first displacement mode shape develops a compression force in the element 3 and a tensile force in elements 1 and 2. The second displacement mode shape develops tensile force in all three elements.

Now, since we have three force degrees of freedom, we expect to have three natural frequencies. In fact, if we use the Eq. (2-62), we can obtain three natural frequencies as $\omega_1 = 99.6782$ Hz , $\omega_2 = 150.8909$ Hz and $\omega_3 = \infty$ (large number). Here, the third natural frequency is infinite, implying that the structure is not vibrating and it is in equilibrium. The force mode shape relative to this infinite natural frequency is

$$\overline{\mathbf{F}}_3 = \begin{Bmatrix} 0.7071 \\ -1.0000 \\ 0.7071 \end{Bmatrix}. \tag{2-96}$$

Here, it can be seen that, in this mode, the element forces are in equilibrium, confirming that the structure is in equilibrium.

Using the impulse method, we have considered four impulses (two in each node) for each element, giving 12 impulses for the overall system. Like the force method, we expect to have 12 natural frequencies, but only two of these natural frequencies are meaningful. These two natural frequencies are found to be exactly equal to those obtained using the displacement or force methods. Computationally, the impulse method is more expensive than the other two methods.

Chapter 3

NONLINEAR FINITE ELEMENT ANALYSIS

3.1 Introduction

In the presence of large deflections, geometrical nonlinearity becomes important. In such cases although the strains are small and the material behaves linearly, the response of the structure becomes nonlinear as a result of finite rotations and displacements. It is therefore necessary to write the joint equilibrium in terms of the final geometry of the structure. To accomplish this, an incremental form of the nonlinear finite element equation is used. Since linear approximations are used, the equilibrium at the next step will not be exactly satisfied. Therefore, a load increment (in load control technique) or displacement increment (in displacement control technique) coupled with iterations is used to satisfy equilibrium. In this chapter, using a principle of virtual work a general geometrically nonlinear finite element equation is derived and then cast into a displacement incremental form. In the case of large displacements, the strain-displacement relationships include nonlinear terms. Considering these terms the stress and displacement geometric stiffness matrices have been obtained using energy and perturbation methods. Next the solution of the nonlinear finite element equations based on the load and displacement control techniques is presented. Then linear and nonlinear buckling analyses are discussed. At the end, nonlinear analysis of symmetric structures using Group Theoretic Approach is studied.

3.2 The Geometrically Nonlinear Finite Element

The principle of virtual work applied to a structural element can be expressed as

$$\delta\Pi^{(e)} = \delta W^{(e)} \tag{3-1}$$

where $\delta\Pi^{(e)}$ is the virtual strain energy due to internal stresses, and $\delta W^{(e)}$ is the virtual work due to the external forces applied on the structural element. The internal virtual strain energy can be expressed as

$$\Pi^{(e)} = \int_{v(e)} \delta\boldsymbol{\varepsilon}^T \boldsymbol{\sigma}\, dv. \tag{3-2}$$

The internal strain energy is due to internal stresses $\boldsymbol{\sigma}$ moving through virtual strains $\delta\boldsymbol{\varepsilon}$, while the external virtual work is due to nodal, surface, and body forces. The external virtual work can be expressed as

$$\delta W^{(e)} = \delta\mathbf{u}^{(e)^T}\mathbf{f}_p^{(e)} + \int_{s(e)} \delta\mathbf{d}^T \boldsymbol{\chi}^s\, ds + \int_{v(e)} \delta\mathbf{d}^T(\boldsymbol{\chi}^b - \rho\ddot{\mathbf{d}})\, dv \tag{3-3}$$

where $\delta\mathbf{u}$ is the vector of virtual nodal displacement in local axis, $\mathbf{f}_p$ is the nodal load vector in local axis, $\delta\mathbf{d}$ is the vector of virtual displacement functions δu, δv and δw in local axis , $\boldsymbol{\chi}^s$ is the surface force vector per unit area acted on surface ds and $\boldsymbol{\chi}^b$ is the body force vector per unit volume dv. Substituting Eqs. (3-2) and (3-3) into Eq. (3-1), we obtain

$$\int_{v(e)} \delta\boldsymbol{\varepsilon}^T \boldsymbol{\sigma}\, dv = \delta\mathbf{u}^{(e)^T}\mathbf{f}_p^{(e)} + \int_{s(e)} \delta\mathbf{d}^T \boldsymbol{\chi}^s ds + \int_{v(e)} \delta\mathbf{d}^T(\boldsymbol{\chi}^b - \rho\ddot{\mathbf{d}})\, dv. \tag{3-4}$$

The application of D'Alembert's principle yields effective inertial forces $-\rho\ddot{u}\,dv$, $-\rho\ddot{v}\,dv$ and $-\rho\ddot{w}\,dv$ where the double dot indicates second derivative with respect to time of the displacement translations u, v and w in the x, y and z element-axis directions, respectively.

In order to formulate the finite element, the approximation field must be defined. This may be assumed to be of a Kantorovich-type in which the displacement function vector $\mathbf{d}(\mathbf{x},t)$ at point $\mathbf{x}$ and time t within the ith element can be expressed, in matrix form, as

$$\mathbf{d}(\mathbf{x},t) = \boldsymbol{N}(\mathbf{x})\,\mathbf{u}(t) \tag{3-5}$$

where $\boldsymbol{N}(\mathbf{x})$ is a matrix of the element shape functions. The strain vector $\boldsymbol{\varepsilon}$ can be written as

$$\varepsilon = \boldsymbol{D}\mathbf{d} = (\boldsymbol{D}_L + \boldsymbol{D}_{NL})\mathbf{d} \tag{3-6}$$

where the matrix $\boldsymbol{D}$ is called a differential operator and $\boldsymbol{D}_L$ and $\boldsymbol{D}_{NL}$ are the linear and nonlinear parts of $\mathbf{d}$. Now, using Eqs. (3-5) and (3-6), we have

$$\varepsilon = \boldsymbol{B}\,\mathbf{u} \tag{3-7}$$

where

$$\boldsymbol{B} = \boldsymbol{D}\,\boldsymbol{N} = \boldsymbol{B}_E + \boldsymbol{B}_G\,, \tag{3-8}$$

and $$\boldsymbol{B}_E = \boldsymbol{D}_L\,\boldsymbol{N} \quad , \quad \text{and} \quad \boldsymbol{B}_G = \boldsymbol{D}_{NL}\,\boldsymbol{N} \tag{3-9}$$

where $\boldsymbol{B}$ is the strain-displacement matrix, $\boldsymbol{B}_E$ is its linear part , and $\boldsymbol{B}_G$ is the nonlinear contribution to $\boldsymbol{B}$, written as a function of displacements. Recalling the small strain assumption, the stress vector may be written as

$$\sigma = \boldsymbol{E}\,\varepsilon \tag{3-10}$$

where $\boldsymbol{E}$ is the elasticity matrix. Substituting for the strain,

$$\sigma = \boldsymbol{E}\,\boldsymbol{B}\,\mathbf{u}, \tag{3-11}$$

and substituting for $\mathbf{d}$, ε and σ into Eq. (3-4),

$$\int_{v(e)} \delta\mathbf{u}^T\,\mathbf{B}^T\,\mathbf{D}\,\mathbf{B}\;\mathbf{u}\,dv = \delta\mathbf{u}^{(e)^T}\mathbf{f}_p^{(e)} + \int_{s(e)} \delta\mathbf{u}^T\,\mathbf{N}^T\chi^s\,ds + \int_{v(e)} \delta\mathbf{u}^T\,\mathbf{N}^T(\chi^b - \rho\mathbf{N}\ddot{\mathbf{u}})\,dv. \tag{3-12}$$

Since $\mathbf{u}$ is the vector of nodal displacements independent of integration, Eq. (3-12) is re-written as

$$\delta\mathbf{u}^{(e)^T}\int_{v(e)} \mathbf{B}^T\,\mathbf{D}\,\mathbf{B}\;\mathbf{u}\,dv = -\delta\mathbf{u}^{(e)^T}\mathbf{f}_p^{(e)} - \delta\mathbf{u}^{(e)^T}\int_{s(e)} \mathbf{N}^T\chi^s\,ds - \delta\mathbf{u}^{(e)^T}\int_{v(e)} \mathbf{N}^T(\chi^b - \rho\mathbf{N}\ddot{\mathbf{u}})\,dv. \tag{3-13}$$

The term $\delta\mathbf{u}^{(e)^T}$ is an arbitrary virtual nodal displacement vector common to each term, and it can be cancelled out from both sides of Eq. (3-13). Assembling all elements in the global coordinates (X, Y, Z), the following equations of motion are obtained:

$$\boldsymbol{M}\ddot{\mathbf{U}} + \boldsymbol{K}\mathbf{U} = \mathbf{P}. \tag{3-14}$$

For static problems,

$$\boldsymbol{K}\mathbf{U} = \mathbf{P} \tag{3-15}$$

where

$$\begin{aligned}
&\boldsymbol{M} = \sum_{e=1}^{n} \boldsymbol{m}^{(e)} = \sum_{e=1}^{n} \int_{v(e)} \rho \mathbf{N}^T \mathbf{N}\, dv \\
&\boldsymbol{K} = \sum_{e=1}^{n} \boldsymbol{k}^{(e)} = \sum_{e=1}^{n} (\boldsymbol{k}_E{}^{(e)} + \boldsymbol{k}_G{}^{(e)}) = \sum_{e=1}^{n} \int \boldsymbol{B}^T \boldsymbol{E}\, \boldsymbol{B}\, dv = \boldsymbol{K}_E + \boldsymbol{K}_G \\
&\mathbf{f}_s = \sum_{e=1}^{n} \int_{s(e)} \mathbf{N}^T \chi^s\, ds \qquad \mathbf{f}_b = \sum_{e=1}^{n} \int_{v(e)} \mathbf{N}^T \chi^b\, dv \qquad \mathbf{f}_p = \sum_{e=1}^{n} \mathbf{f}_p{}^{(e)} \\
&\mathbf{P} = \mathbf{f}_p + \mathbf{f}_s + \mathbf{f}_v \qquad \mathbf{U} = \sum_{e=1}^{n} \mathbf{u}^{(e)}
\end{aligned} \tag{3-16}$$

Here, $\mathbf{U}$ is the system nodal displacements; $\boldsymbol{M}$ is system consistent mass matrix; $\boldsymbol{K}$ and $\boldsymbol{k}$ are system and local tangent stiffness matrix, respectively; $\boldsymbol{K}_E$ and $\boldsymbol{K}_G$ are system linear and geometric stiffness matrix, respectively; and $\boldsymbol{k}_E$ and $\boldsymbol{k}_G$ are local linear and geometric stiffness matrices, respectively. $\mathbf{P}$ is the total nodal load vector; $\mathbf{f}_s$ is the vector of equivalent nodal loads due to surface forces; and $\mathbf{f}_b$ is the vector of equivalent nodal loads due to body forces; and n is the total number of elements for the system.

$\boldsymbol{K}_E$ represents the conventional linear elastic stiffness matrix and is given by

$$\boldsymbol{K}_E = \sum_{e=1}^{n} \int_{v(e)} \boldsymbol{B}_E{}^T \boldsymbol{E}\, \boldsymbol{B}_E\, dv. \tag{3-17}$$

The matrix $\boldsymbol{K}_E$ does not depend on the geometry of the structure and can be found in Refs.[82,83]. The matrix $\boldsymbol{K}_G$ in Eq. (3-16) is due to the large displacements and rotations and is called the geometric stiffness matrix. $\boldsymbol{K}_G$ depends on the geometry and initial stress, and is given by:

$$\boldsymbol{K}_G = \sum_{e=1}^{n} \int_{v(e)} (\mathbf{B}_E{}^T \mathbf{E} \mathbf{B}_G + \mathbf{B}_G{}^T \mathbf{E} \mathbf{B}_G + \mathbf{B}_G{}^T \mathbf{E} \mathbf{B}_E)\, dv. \tag{3-18}$$

Using the Green-Lagrange strain [74,75] relation, the complete nonlinear form of the $\mathbf{K}_G$ matrix can be expressed as

$$\boldsymbol{K}_G = \boldsymbol{K}_{D1}(\mathbf{U}) + \boldsymbol{K}_{D2}(\mathbf{U}^2) \tag{3-19}$$

where $\boldsymbol{K}_{D1}$ and $\boldsymbol{K}_{D2}$ are the geometric stiffness matrices, and they are a linear and quadratic functions of the nodal displacement vector **U**, respectively [135]. When considering the nonlinear problem as a sequence of linear steps during the analysis process, the $\boldsymbol{K}_{D2}$ matrix may be neglected. Thus, Eq. (3-15) can be cast into an incremental form as follows:

$$(\boldsymbol{K}_E + \boldsymbol{K}_{D1})\Delta\mathbf{U} = \Delta\mathbf{P}. \tag{3-20}$$

Also, the system stress stiffness matrix $\boldsymbol{K}_\sigma$ can be represented as a function of the stress in the element. Ignoring the quadratic stiffness terms, two forms of incremental equations are obtained:

$$(\boldsymbol{K}_E + \boldsymbol{K}_{D1})\Delta\mathbf{U} = \Delta\mathbf{P} \qquad (\boldsymbol{K}_E + \boldsymbol{K}_\sigma)\Delta\mathbf{U} = \Delta\mathbf{P}. \tag{3-21}$$

Next, the element geometric stiffness matrices ($\boldsymbol{K}_{D1}$ and $\boldsymbol{K}_\sigma$) are derived for truss and beam type elements, using both the energy method and the perturbation technique.

3.2.1 The Geometric Stiffness Matrix – The Energy Method

When applying the energy method, the strain energy is obtained first and subsequently the equilibrium equations are derived using the first Castigliano's theorem (applicable to large deflections). This leads to the consistent linear and nonlinear stiffness matrices.

i) Truss Element:

Consider the two-dimensional pin-jointed truss element as shown in Figure (3-1). The displacements in the local x and y directions of the end i are u_1 and u_2 and at the end j are u_3 and u_4, respectively. The cross-sectional area of the element is A, its length is L, and the Young's modulus of the bar material is E.

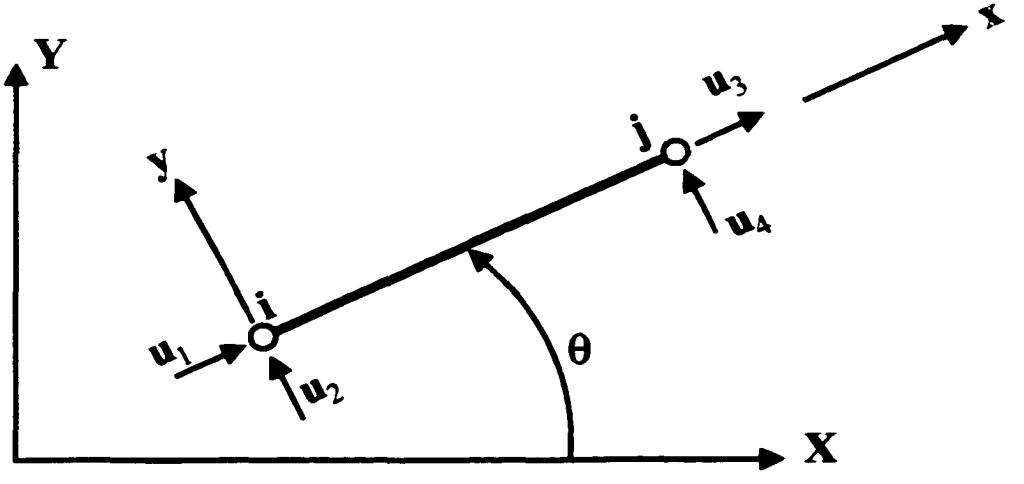

Figure 3-1 Truss element with positive displacements in local axis.

The strain ε_x in the direction of the bar axis is determined from the large-deflection strain-displacement equation (Green-Lagrange Strain) as follows:

$$\varepsilon_x = u_{x,x} + \frac{1}{2}(u_{x,x}^2 + u_{y,x}^2) \tag{3-22}$$

where the second and the third terms are nonlinear. Using a linear shape function, the displacement functions u_x and u_y are obtained as:

$$\mathbf{d} = \begin{bmatrix} u_x \\ u_y \end{bmatrix} = \begin{bmatrix} 1-\zeta & 0 & \zeta & 0 \\ 0 & 1-\zeta & 0 & \zeta \end{bmatrix} \begin{bmatrix} u_1 \\ u_2 \\ u_3 \\ u_4 \end{bmatrix} = \boldsymbol{N}\,\mathbf{u} \tag{3-23}$$

where

$$\zeta = \frac{x}{L},\quad \boldsymbol{N} = \begin{bmatrix} 1-\zeta & 0 & \zeta & 0 \\ 0 & 1-\zeta & 0 & \zeta \end{bmatrix} \quad \text{and} \quad \mathbf{u} = \begin{bmatrix} u_1 \\ u_2 \\ u_3 \\ u_4 \end{bmatrix}. \tag{3-24}$$

It follows that

$$u_{x,x} = \frac{1}{L}(-u_1 + u_3) \qquad \text{and} \qquad u_{y,x} = \frac{1}{L}(-u_2 + u_4). \tag{3-25}$$

The strain energy $\Pi^{(e)}$ stored in the bar (e) for small strain (linear stress-strain) and large rotation can be determined as follows:

$$\Pi^{(e)} = \frac{1}{2}\int_{v(e)} E\varepsilon_x{}^2\, dv = \frac{1}{2} A E \int_0^L \varepsilon_x{}^2\, dx =$$

$$\frac{1}{2} A E \int_0^L (u_{x,x}{}^2 + \frac{1}{4}u_{x,x}{}^4 + \frac{1}{4}u_{y,x}{}^4 + u_{x,x}u_{x,x}{}^2 + u_{x,x}\,u_{y,x}{}^2 + \frac{1}{4}u_{x,x}{}^2\,u_{y,x}{}^2)\, dx. \tag{3-26}$$

The higher-order terms (order four) originates the stiffness matrix $\boldsymbol{k}_{D2}(\mathbf{u}^2)$. Substituting Eq. (3-25) into Eq. (3-26) and then neglecting the higher-order terms,

$$\Pi^{(e)} = \frac{AE}{2L}(u_3 - u_1)^2 + \frac{AE}{2L^2}(u_3 - u_1)(u_3 - u_1)^2 + \frac{AE}{2L^2}(u_3 - u_1)(u_4 - u_2)^2. \tag{3-27}$$

Applying the first Castigliano's theorem (which is applicable to large deflections) to Eq. (3-27), the following element force-displacement relations are obtained:

$$p_1 = \frac{\partial \Pi^{(e)}}{\partial u_1} = \frac{AE}{L}(u_1 - u_3) + \frac{AE}{2L^2}(6u_1u_3 - 3u_3{}^2 - 3u_1{}^2) + \frac{AE}{2L^2}(-u_2{}^2 + 2u_2u_4 - u_4{}^2)$$

$$p_2 = \frac{\partial \Pi^{(e)}}{\partial u_2} = \frac{AE}{L^2}(u_2u_3 - u_3u_4 - u_1u_2 + u_1u_4)$$

$$p_3 = \frac{\partial \Pi^{(e)}}{\partial u_3} = \frac{AE}{L}(u_3 - u_1) + \frac{AE}{2L^2}(-6u_1u_3 + 3u_3{}^2 + 3u_1{}^2) + \frac{AE}{2L^2}(u_2{}^2 - 2u_2u_4 + u_4{}^2)$$

$$p_4 = \frac{\partial \Pi^{(e)}}{\partial u_4} = \frac{AE}{L^2}(-u_2u_3 + u_3u_4 + u_1u_2 - u_1u_4)$$

(3-28)

The incremental form of Eq. (3-28) can be obtained by differentiating both sides of Eq. (3-28). Collecting the incremental forms into a single matrix equation,

$$(\boldsymbol{k}_E + \boldsymbol{k}_{DI})\Delta\mathbf{u} = \Delta\mathbf{p} \tag{3-29}$$

where

$$\boldsymbol{k}_E = \frac{AE}{L}\begin{bmatrix} 1 & 0 & -1 & 0 \\ 0 & 0 & 0 & 0 \\ -1 & 0 & 1 & 0 \\ 0 & 0 & 0 & 0 \end{bmatrix}; \quad \boldsymbol{k}_{DI} = \frac{AE}{L^2}\begin{bmatrix} 3(u_3-u_1) & u_4-u_2 & 3(u_1-u_3) & u_2-u_4 \\ u_4-u_2 & u_3-u_1 & u_2-u_4 & u_1-u_3 \\ 3(u_1-u_3) & u_2-u_4 & 3(u_3-u_1) & u_4-u_2 \\ u_2-u_4 & u_1-u_3 & u_4-u_2 & u_3-u_1 \end{bmatrix} . \tag{3-30}$$

Note that if the higher-order terms (order four) in Eq. (3-26) are not neglected, $\boldsymbol{k}_{D2}$ is obtained in the following form:

$$\boldsymbol{k}_{D2} = \frac{AE}{2L^2}\begin{bmatrix} \tilde{\boldsymbol{k}}_{D2} & -\tilde{\boldsymbol{k}}_{D2} \\ -\tilde{\boldsymbol{k}}_{D2} & \tilde{\boldsymbol{k}}_{D2} \end{bmatrix} \tag{3-31}$$

where

$$\tilde{\boldsymbol{k}}_{D2} = \begin{bmatrix} 3(u_3-u_1)^2+(u_4-u_2)^2 & 2(u_3-u_1)(u_4-u_2) \\ 2(u_3-u_1)(u_4-u_2) & 3(u_3-u_1)^2+(u_4-u_2)^2 \end{bmatrix}. \tag{3-32}$$

The quantity $AE\frac{u_3-u_1}{L}$ in Eq. (3-27) may be treated as a constant equal to the axial force in the bar (for relatively large deflections as well). Introducing

$$F = \frac{AE}{L}(u_3-u_1) \tag{3-33}$$

into Eq. (3-27):

$$\Pi = \frac{AE}{2L}(u_3-u_1)^2 + \frac{F}{2L}(u_3-u_1)^2 + \frac{F}{2L}(u_4-u_2)^2 \ , \tag{3-34}$$

and applying the first Castigliano's theorem to Eq. (3-34), and writing the result in an incremental and single matrix form, we obtain

$$(\boldsymbol{k}_E + \boldsymbol{k}_\sigma)\Delta\mathbf{u} = \Delta\mathbf{p} \tag{3-35}$$

where

$$\boldsymbol{k}_\sigma = \frac{F}{L}\begin{bmatrix} 1 & 0 & -1 & 0 \\ 0 & 1 & 0 & -1 \\ -1 & 0 & 1 & 0 \\ 0 & -1 & 0 & 0 \end{bmatrix}. \tag{3-36}$$

Neglecting the term $u_{x,x}$ in comparison to $u_{y,x}$, the classical form of the stress stiffness matrix for the truss element used in large deformation or buckling analysis [82] is obtained as

$$\boldsymbol{k}_{\sigma c} = \frac{F}{L}\begin{bmatrix} 0 & 0 & 0 & 0 \\ 0 & 1 & 0 & -1 \\ 0 & 0 & 0 & 0 \\ 0 & -1 & 0 & 1 \end{bmatrix}. \tag{3-37}$$

It is noted that $\boldsymbol{k}_\sigma$ is similar to $\boldsymbol{k}_{\sigma c}$. However, it contains four more nonzero terms. The additional nonzero terms occupy the same positions as the nonzero terms in the conventional linear stiffness matrix. Thus, in the total stiffness matrix $\boldsymbol{k}_E + \boldsymbol{k}_\sigma$, the coefficients $(AE + F)/L$ (corresponding to u_1 and u_3) and F/L (corresponding to u_2 and u_4) are present. Since the relation $AE >> F$ is true for any practical large rotation problems, the extra F/L in $\boldsymbol{k}_\sigma$ can be discarded and $\boldsymbol{k}_\sigma$ reduces to $\boldsymbol{k}_{\sigma c}$.

The matrices $\boldsymbol{k}_E$, $\boldsymbol{k}_{DI}$, $\boldsymbol{k}_\sigma$ and $\boldsymbol{k}_{\sigma c}$ have been defined in the local element axis (x,y). These can be transformed to global coordinates (X,Y) using the rotation matrix $\boldsymbol{R}$, such that

$$\boldsymbol{k}^g = \boldsymbol{R}^T \boldsymbol{k} \boldsymbol{R} \tag{3-38}$$

where $\boldsymbol{k}^g$ is the elemental stiffness matrix in global coordinates. The rotation matrix for the truss element is

$$\boldsymbol{R} = \begin{bmatrix} \boldsymbol{Rot} & \mathbf{0} \\ \mathbf{0} & \boldsymbol{Rot} \end{bmatrix}$$

where $$\boldsymbol{Rot} = \begin{bmatrix} l_x & l_y \\ -l_y & l_x \end{bmatrix} \tag{3-39}$$

where

$$l_x = \cos(\theta) = \frac{X_j - X_i}{L} \quad , \; l_y = \sin(\theta) = \frac{Y_j - Y_i}{L} \quad , \tag{3-40}$$

are the direction cosines of a typical element relative to the global X and Y axes, respectively. Using Eqs. (3-38)-(3-40):

$$\boldsymbol{k}_{\sigma}^{g} = \frac{F}{L}\begin{bmatrix} 1 & 0 & -1 & 0 \\ 0 & 1 & 0 & -1 \\ -1 & 0 & 1 & 0 \\ 0 & -1 & 0 & 1 \end{bmatrix}, \; \boldsymbol{k}_{\sigma c}^{g} = \frac{F}{L}\begin{bmatrix} 1-l_x^2 & -l_x l_y & -1+l_x^2 & l_x l_y \\ -l_x l_y & 1-l_y^2 & l_x l_y & -1+l_y^2 \\ -1+l_x^2 & l_x l_y & 1-l_x^2 & -l_x l_y \\ l_x l_y & -1+l_y^2 & -l_x l_y & 1-l_y^2 \end{bmatrix} \tag{3-41}$$

Here, $\boldsymbol{k}_{\sigma}$ does not depend on the element orientation while $\boldsymbol{k}_{\sigma c}$ is dependent on the element orientation. $\boldsymbol{k}_{\sigma}$ is both simpler and more accurate than $\boldsymbol{k}_{\sigma c}$.

Appendix A presents an extension of the truss element formulation to account for imperfections.

ii) Beam Element:

Consider the two-dimensional beam element as shown in Figure (3-2). The displacements along the local x and y axis and the rotation about the local z-axis at the end i are u_1, u_2 and u_3 respectively, while those at the end j are u_3, u_4 and u_6. A linear shape function for axial displacement and cubic shape function for lateral displacement are assumed. Thus, the displacement distribution for a beam element may be given as

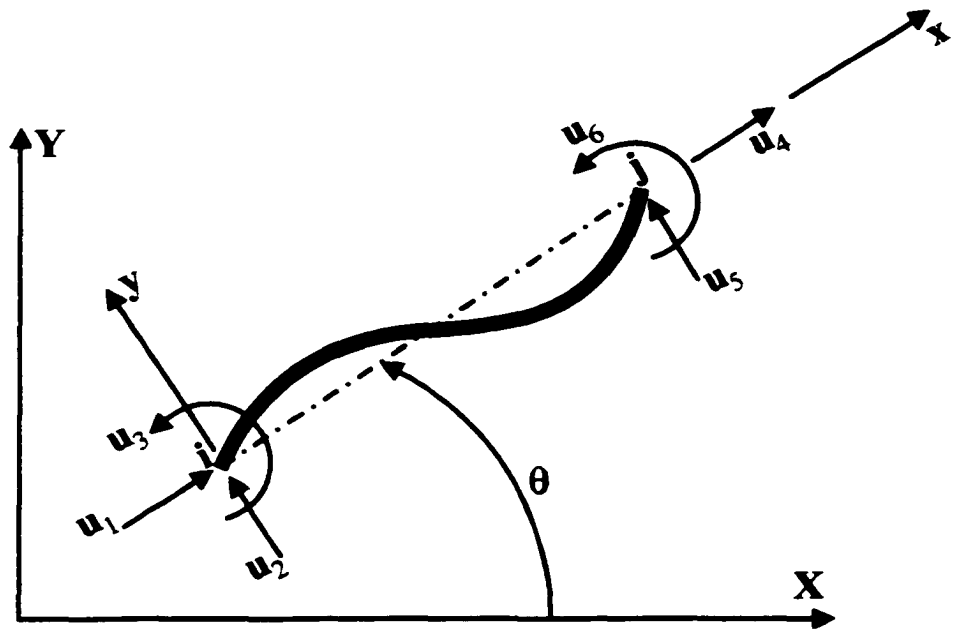

Figure 3-2 Beam element with positive displacements in local axis.

$$\mathbf{d}=\begin{bmatrix}u_x\\u_y\end{bmatrix}=\begin{bmatrix}1-\zeta & 0 & 0 & \zeta & 0 & 0\\ 0 & 1-3\zeta^2+2\zeta^3 & (\zeta-2\zeta^2+\zeta^3)L & 0 & 3\zeta^2-2\zeta^3 & (-\zeta^2+\zeta^3)L\end{bmatrix}\begin{bmatrix}u_1\\u_2\\u_3\\u_4\\u_5\\u_6\end{bmatrix}$$

or $$\mathbf{d} = \boldsymbol{N}\,\mathbf{u} \qquad \textbf{(3-42)}$$

In the expression for the strain energy Π, the contributions from the shearing strains are neglected. Thus, only normal strains ε_x are included. These strains, for a beam with large deflections in bending, are given by:

$$\varepsilon_x = u_{x,x} - y\,u_{y,xx} + \frac{1}{2}(u_{x,x}{}^2 + u_{y,x}{}^2) \qquad \textbf{(3-43)}$$

where y is measured from the neutral axis of the beam.

Considering Eq. (3-43), and neglecting the higher order terms (order 4), the strain energy $\Pi^{(e)}$ stored in the beam for small strains (linear stress-strain law) and large rotations takes the form:

$$\Pi^{(e)} = \frac{1}{2}\int_{v(e)} E\varepsilon_x^{\,2}\, dv = \frac{1}{2}AE\int_0^L \varepsilon_x^{\,2}\, dx =$$

$$\frac{1}{2}E\int_{x=0}^{L}\int_{A}(u_{x,x}^{\,2} + y^2\, u_{y,xx}^{\,2} - 2u_{x,x}\, u_{y,xx} + u_{x,x}\, u_{x,x}^{\,2} + u_{x,x}\, u_{y,x} - u_{y,xx}\, u_{x,x}^{\,2} - u_{y,xx}\, u_{y,x}^{\,2})dx\,dA.$$

(3-44)

Integrating over the cross-sectional area A and noting that y is measured from the neutral axis, all integrals of the form $\int y\, dA$ vanish. Thus,

$$\Pi^{(e)} = \frac{1}{2}EA\int_0^L u_{x,x}^{\,2}\, dx + \frac{1}{2}EI\int_0^L u_{y,xx}^{\,2}\, dx + \frac{1}{2}EA\int_0^L u_{x,x}\, u_{x,x}^{\,2}\, dx + \frac{1}{2}EA\int_0^L u_{x,x}\, u_{y,x}^{\,2}\, dx \quad \textbf{(3-45)}$$

where I denotes the moment of inertia of the cross-section. The first two integrals in Eq. (3-45) represent the linear strain energy while the third and the fourth integrals are the contributions from the nonlinear components of the strain. Additionally, recalling Eq. (3-42),

$$u_{x,x} = \frac{1}{L}(u_4 - u_1)$$

$$u_{y,x} = \frac{1}{L}[6(-\zeta + \zeta^2)u_2 + (1 - 4\zeta + 3\zeta^2)Lu_3 + 6(\zeta - \zeta^2)u_5 + (-2\zeta + 3\zeta^2)Lu_6] \quad \textbf{(3-46)}$$

$$u_{y,xx} = \frac{1}{L^2}[6(-1 + 2\zeta)u_2 + 2(-2 + 3\zeta)Lu_3 + 6(1 - 2\zeta)u_5 + 2(-1 + 3\zeta)Lu_6]$$

Substitution of Eq. (3-46) into (3-45) and subsequent integration leads to

$$\begin{aligned}\Pi^{(e)} = {} & \frac{EA}{2L}(u_1^{\,2} - 2u_1u_4 + u_4^{\,2}) + \frac{2EI}{L^3}(3u_2^{\,2} + L^2u_3^{\,2} + 3u_5^{\,2} + L^2u_6^{\,2} \\ & + 3Lu_2u_3 - 6u_2u_5 + 3Lu_2u_6 - 3Lu_3u_5 + L^2u_3u_6 - 3Lu_5u_6) \\ & + \frac{EA}{2L^2}(u_4 - u_1)(u_1^{\,2} - 2u_1u_4 + u_4^{\,2}) + \frac{EA}{30L^2}(u_4 - u_1)(18u_2^{\,2} + 2L^2u_3^{\,2} \\ & + 18u_5^{\,2} + 2L^2u_6^{\,2} + 3Lu_2u_3 - 36u_2u_5 + 3Lu_2u_6 - 3Lu_3u_5 - L^2u_3u_6 - 3Lu_5u_6)\end{aligned} \quad \textbf{(3-47)}$$

Finally, applying the first Castigliano's theorem to the strain energy expression, the following relations are obtained:

$$p_1 = \frac{\partial \Pi^{(e)}}{\partial u_1} = \frac{L}{EA}(u_1 - u_4) - \frac{3L^2}{2EI}(u_4 - u_1)^2 - \frac{L^2}{30EI}(18u_2^2 + 2L^2 u_3^2 + 18u_5^2 + 2L^2 u_6^2 + 3Lu_2 u_3 - 36u_2 u_5 + 3Lu_2 u_6 - 3Lu_3 u_5 - L^2 u_3 u_6 - 3Lu_5 u_6)$$

$$p_2 = \frac{\partial \Pi^{(e)}}{\partial u_2} = \frac{3L^3}{EI}(2u_2 - 2u_5 + Lu_3 + Lu_6) + \frac{L^2}{30EI}(u_4 - u_1)(36u_2 - 36u_5 + 3Lu_3 + 3Lu_6)$$

$$p_3 = \frac{\partial \Pi^{(e)}}{\partial u_3} = \frac{L^2}{30EI}(u_4 - u_1)(4L^2 u_3 - L^2 u_6 + 3Lu_2 - 3Lu_5) + \frac{L^3}{EI}(2L^2 u_3 + L^2 u_6 + 3Lu_2 - 3Lu_5)$$

$$p_4 = \frac{\partial \Pi^{(e)}}{\partial u_4} = \frac{L}{EA}(u_4 - u_1) + \frac{3L^2}{2EI}(u_4 - u_1)^2 + \frac{L^2}{30EI}(18u_2^2 + 2L^2 u_3^2 + 18u_5^2 + 2L^2 u_6^2 + 3Lu_2 u_3 - 36u_2 u_5 + 3Lu_2 u_6 - 3Lu_3 u_5 - L^2 u_3 u_6 - 3Lu_5 u_6)$$

$$p_5 = \frac{\partial \Pi^{(e)}}{\partial u_5} = \frac{3L^3}{EI}(2u_5 - 2u_2 - Lu_3 - Lu_6) + \frac{L^2}{30EI}(u_4 - u_1)(36u_5 - 36u_2 - 3Lu_3 - 3Lu_6)$$

$$p_6 = \frac{\partial \Pi^{(e)}}{\partial u_6} = \frac{L^2}{30EI}(u_4 - u_1)(4L^2 u_6 - L^2 u_3 + 3Lu_2 - 3Lu_5) + \frac{L^3}{EI}(2L^2 u_6 + L^2 u_3 + 3Lu_2 - 3Lu_5)$$

(3-48)

Analogous to the truss element formulation, the incremental form of Eq. (3-48) can be obtained by forming expressions for Δp_1, Δp_2, Δp_3 ,Δp_4,Δp_5 and Δp_6. Collecting these

incremental forms into a single matrix equation, the stiffness matrices are obtained in the form:

$$\boldsymbol{k}_E = \frac{EI}{L^3}\begin{bmatrix} AL^2/I & & & & & \\ 0 & 12 & & & \text{SYM} & \\ 0 & 6L & 4L^2 & & & \\ -AL^2/I & 0 & 0 & AL^2/I & & \\ 0 & -12 & -6 & 0 & 12 & \\ 0 & 6L & 2L^2 & 0 & -6L & 4L^2 \end{bmatrix},$$

and

$$\boldsymbol{k}_{DI} = (AE/L^2) =$$

$$\begin{bmatrix} 3(u_4-u_1) & & & \text{SYM} \\ \frac{-6(u_2-u_5)}{5} - \frac{L(u_3+u_6)}{10} & \frac{6(u_4-u_1)}{5} & & \\ \frac{-L(u_2-u_5)}{10} - \frac{L^2(4u_3-u_6)}{30} & \frac{L(u_4-u_1)}{10} & \frac{2L^2(u_4-u_1)}{15} & \\ -3(u_4-u_1) & \frac{6(u_2-u_5)}{5} + \frac{L(u_3+u_6)}{10} & \frac{L(u_2-u_5)}{10} + L^2(4u_3-u_6) & \\ \frac{6(u_2-u_5)}{5} + \frac{L(u_3+u_6)}{10} & \frac{-6(u_4-u_1)}{5} & \frac{-L(u_4-u_1)}{10} & \\ -\frac{L(u_2-u_5)}{10} + \frac{L^2(u_3-4u_6)}{30} & \frac{L(u_4-u_1)}{10} & \frac{-L^2(u_4-u_1)}{30} & \end{bmatrix}$$

$$\begin{bmatrix} & & \text{SYM} & \\ 3(u_4-u_1) & & & \\ \frac{-6(u_2-u_5)}{5} - \frac{L(u_3+u_6)}{10} & \frac{6(u_4-u_1)}{5} & & \\ \frac{L(u_2-u_5)}{10} - \frac{L^2(u_3-4u_6)}{30} & \frac{-L(u_4-u_1)}{10} & \frac{2L^2(u_4-u_1)}{15} & \end{bmatrix}. \quad \textbf{(3-49)}$$

Introducing the variable F:

$$F = \frac{EA}{L}(u_4 - u_1) \approx \text{ constant }, \tag{3-50}$$

and substituting into Eq. (3-47), the strain energy expression becomes:

$$\Pi^{(e)} = F^2/2 + \frac{2EI}{L^3}(3u_2^{\,2} + L^2u_3^{\,2} + 3u_5^{\,2} + L^2u_6^{\,2} + 3Lu_2u_3 - 6u_2u_5 + 3Lu_2u_6 -$$
$$3Lu_3u_5 + L^2u_3u_6 - 3Lu_5u_6) + \frac{F^3}{2L} + \frac{F}{30L}(18u_2^{\,2} + 2L^2u_3^{\,2} + 18u_5^{\,2} + 2L^2u_6^{\,2} + \tag{3-51}$$
$$3Lu_2u_3 - 36u_2u_5 + 3Lu_2u_6 - 3Lu_3u_5 - L^2u_3u_6 - 3Lu_5u_6)$$

Applying the first Castigliano's theorem to Eq. (3-51), the geometric stiffness for the beam element takes the form:

$$\boldsymbol{k}_\sigma = \frac{F}{30L}\begin{bmatrix} 30 & & & & & \\ 0 & 36 & & & \text{SYM} & \\ 0 & 3L & 4L^2 & & & \\ -30 & 0 & 0 & 30 & & \\ 0 & -36 & -3L & 0 & 36 & \\ 0 & 3L & -L^2 & 0 & -3L & 4L^2 \end{bmatrix}. \tag{3-52}$$

Neglecting the term $u_{x,x}$ in comparison to $u_{y,x}$ in Eq. (3-45), the classical form of the stress stiffness matrix for the beam element is obtained. This is the matrix used for structures with large deformations and in buckling analyses [82]. It has the form:

$$\boldsymbol{k}_{\sigma c} = \frac{F}{30L}\begin{bmatrix} 0 & & & & & \\ 0 & 36 & & & \text{SYM} & \\ 0 & 3L & 4L^2 & & & \\ 0 & 0 & 0 & 0 & & \\ 0 & -36 & -3L & 0 & 36 & \\ 0 & 3L & -L^2 & 0 & -3L & 4L^2 \end{bmatrix}. \tag{3-53}$$

The matrix $\boldsymbol{k}_\sigma$ is similar to $\boldsymbol{k}_{\sigma c}$, however it contains four more nonzero terms. These nonzero terms occupy the same position as the nonzero terms in the conventional linear

stiffness matrix. In the total stiffness matrix $\boldsymbol{k}_E + \boldsymbol{k}_\sigma$, coefficients $(AE+F)/L$ (corresponding to d.o.f. u_1 and u_4) and F/L (corresponding to d.o.f. u_2 and $u_5$and u_3 and u_6) are observed. Since $AE >> F$ in most practical large rotation problems, the extra F/L in $\boldsymbol{k}_\sigma$ can be discarded, and $\boldsymbol{k}_\sigma$ reduces to $\boldsymbol{k}_{\sigma c}$.

To transform the locally defined matrices to the global coordinates, Eq. (3-38) is recalled. For the beam element, the rotation matrix is

$$\boldsymbol{R} = \begin{bmatrix} \boldsymbol{Rot} & \boldsymbol{0} \\ \boldsymbol{0} & \boldsymbol{Rot} \end{bmatrix} \quad \text{and} \quad \boldsymbol{Rot} = \begin{bmatrix} l_x & l_y & 0 \\ -l_y & l_x & 0 \\ 0 & 0 & 1 \end{bmatrix}, \tag{3-54}$$

and l_x and l_y are direction cosines which are defined in (3-41). For example

$$\boldsymbol{k}_\sigma^g = \frac{F}{30L} \begin{bmatrix} 30l_x^2+36l_y^2 & 0 & 0 & 0 & 0 & 0 \\ -6l_x l_y & 30l_y^2+36l_x^2 & 0 & 0 & \text{SYM} & 0 \\ -3l_y L & 3l_x L & 4L^2 & 0 & 0 & 0 \\ -30l_x^2-36l_y^2 & 6l_x l_y & 3l_y L & 30l_x^2+36l_y^2 & 0 & 0 \\ 6l_x l_y & -30l_y^2-36l_x^2 & -3l_x L & -6l_x l_y & 30l_y^2+36l_x^2 & 0 \\ -3l_y L & -3l_x L & -L^2 & 3l_y L & -3l_x L & 4L^2 \end{bmatrix}. \tag{3-55}$$

3.2.2 Perturbation Technique

The perturbation method is based on differentiating the equilibrium equation. The method consists of applying a perturbation load to a structure in equilibrium and linearizing the equations of equilibrium [77,136-138].

i) Truss Element

Let us assume that Eq. (2-16) describes the equation of equilibrium in the deformed configuration. In the presence of a perturbation, the equation takes the form

$$\Delta \boldsymbol{Q}\ \mathbf{F} + \boldsymbol{Q}\ \Delta \mathbf{F} = \Delta \mathbf{P} \tag{3-56}$$

Here, the term $\boldsymbol{Q}\ \Delta \mathbf{F}$ describes the change in the member forces while keeping the equilibrium matrix $\boldsymbol{Q}$ fixed, implying a simple linear elastic analysis. The term $\Delta \boldsymbol{Q}\ \mathbf{F}$ describes the effect of varying the structural geometry while keeping the member force fixed, implying that $\Delta \boldsymbol{Q}\ \mathbf{F}$ represents the geometric stiffness.

$$\Delta(\boldsymbol{Q}\mathbf{F})\big|_{\text{F fixed}} = \boldsymbol{K}_{\sigma}\ \Delta \mathbf{U} \tag{3-57}$$

Since the geometric stiffness matrix depends on the force in the elements, the stress stiffness matrix is given by Eq. (3-57). The equilibrium matrix $\boldsymbol{Q}$ has n columns, corresponding to the number of elements. These can be obtained through the balance of forces at each node. Now consider the term $(\boldsymbol{Q}\mathbf{F})^{(e)}$ of Eq. (3-57), which is the contribution of element e to the equilibrium equations. For a typical space truss with the direction cosines vector $\boldsymbol{l}$ and element force F as shown in the Figure 3-3, this term can be written as

$$(\boldsymbol{Q}\mathbf{F})^{(e)} = \begin{bmatrix} \cdots & -l_x & -l_y & -l_z & \cdots & l_x & l_y & l_z & \cdots \end{bmatrix}^T \mathrm{F} \tag{3-58}$$

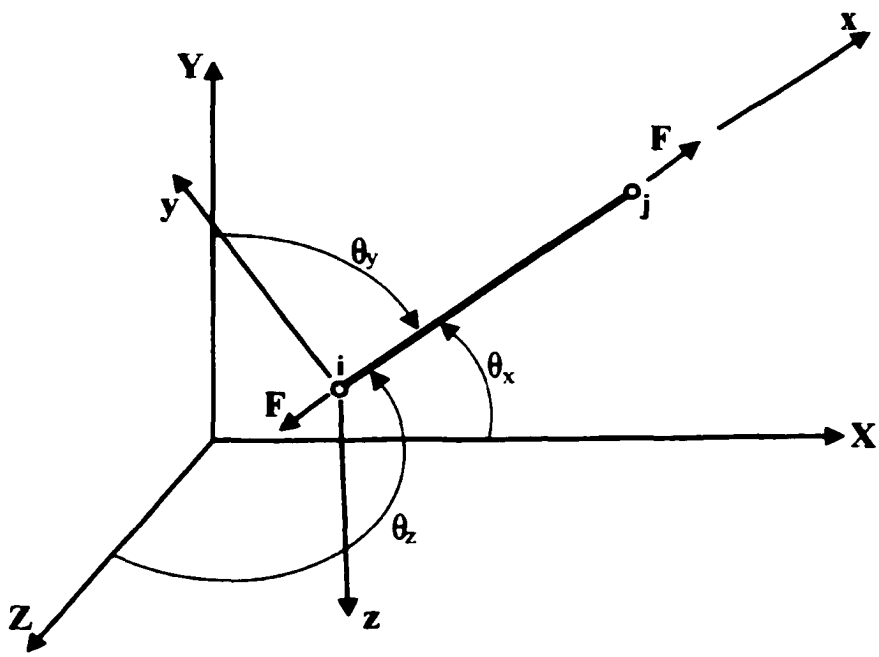

Figure 3-3 Typical truss element with element force F.

where l_x , l_y and l_z are the direction cosines of the element with respect to the global X , Y, and Z directions, respectively. F is the force in the element. Since $\boldsymbol{Q}^{(e)}$ is a function of the coordinates X_i, Y_i, Z_i in node i and X_j, Y_j, Z_j in node j, the chain rule of differentiation yields:

$$\Delta(\boldsymbol{Q}\mathbf{F})^{(e)}\Big|_{\text{F fixed}} = [(\nabla \boldsymbol{Q})^{(e)}\Delta\mathbf{X}]\mathbf{F}$$
$$= \left(\frac{\partial \boldsymbol{Q}}{\partial X_i}\Delta X_i + \frac{\partial \boldsymbol{Q}}{\partial Y_i}\Delta Y_i + \frac{\partial \boldsymbol{Q}}{\partial Z_i}\Delta Z_i + \frac{\partial \boldsymbol{Q}}{\partial X_j}\Delta X_j + \frac{\partial \boldsymbol{Q}}{\partial Y_j}\Delta Y_j + \frac{\partial \boldsymbol{Q}}{\partial Z_j}\Delta Z_j\right)^{(e)} \mathbf{F} \tag{3-59}$$

where $\nabla \boldsymbol{Q}$ is the gradient of the $\boldsymbol{Q}$. The perturbed coordinates $\Delta X_i, \Delta Y_i, \Delta Z_i$ are interpreted as perturbed nodal displacements and substituting the expression $(\boldsymbol{Q}\mathbf{F})^{(e)}$ from Eq. (3-58) into Eq. (3-59), the element geometric stiffness matrix in global coordinates ($\boldsymbol{k}_\sigma{}^g$) can be written as:

$$\boldsymbol{k}_\sigma^g = \frac{\mathrm{F}}{\mathrm{L}}\begin{bmatrix} \tilde{\boldsymbol{k}}_\sigma & -\tilde{\boldsymbol{k}}_\sigma \\ -\tilde{\boldsymbol{k}}_\sigma & \tilde{\boldsymbol{k}}_\sigma \end{bmatrix} \tag{3-60}$$

where

$$\tilde{\boldsymbol{k}}_\sigma = \begin{bmatrix} 1-l_x^2 & -l_x l_y & -l_x l_y \\ -l_x l_y & 1-l_x^2 & -l_x l_y \\ -l_x l_y & -l_x l_y & 1-l_x^2 \end{bmatrix}, \tag{3-61}$$

and for a for two-dimensional case

$$\boldsymbol{k}_\sigma^g = \begin{bmatrix} 1-l_x^2 & -l_x l_y & -1+l_x^2 & l_x l_y \\ -l_x l_y & 1-l_y^2 & l_x l_y & -1+l_y^2 \\ -1+l_x^2 & l_x l_y & 1-l_x^2 & -l_x l_y \\ l_x l_y & -1+l_y^2 & -l_x l_y & 1-l_y^2 \end{bmatrix}. \tag{3-62}$$

Eq. (3-60) follows directly from the differentiation of the direction cosines of the element. For example, l_x can be written in terms of nodal coordinates as:

$$l_x = \cos(\theta) = \frac{X_j - X_i}{L} = \frac{X_j - X_i}{\sqrt{(X_j - X_i)^2 + (Y_j - Y_i)^2 + (Z_j - Z_i)^2}}. \quad \textbf{(3-63)}$$

The differentiation of l_x with respect to X_j, Y_j and Z_j yields

$$\frac{\partial l_x}{\partial X_j} = \frac{1 - l_x^2}{L} \quad , \quad \frac{\partial l_x}{\partial Y_j} = -\frac{l_x l_y}{L} \quad , \quad \frac{\partial l_x}{\partial Z_j} = -\frac{l_x l_z}{L}. \quad \textbf{(3-64)}$$

The derivatives of l_y and l_z with respect to X_j, Y_j and Z_j follow in a similar fashion. The derivatives with respect to the coordinates at the end i are the negative of the derivatives with respect to the coordinates at the end j.

Comparing Eq. (3-62) with Eq. (3-41), calculated using the energy method, it is observed that the geometric matrix obtained using the perturbation method is the classical stress stiffness matrix, obtained previously using the energy method with a few assumptions. Thus, it is concluded that the energy method provides a more accurate and a simpler form of the stress stiffness matrix.

ii) Beam Element

To derive the geometric stiffness matrix for plane beams using the perturbation technique, the contribution of member *i* to the equilibrium equations is formulated first and subsequently the gradient of the contributions is used to generate the element geometric stiffness matrix.

Figure (3-4) describes a typical member of plane frame in local axis. At each end there is a shear force, a moment and an axial force.

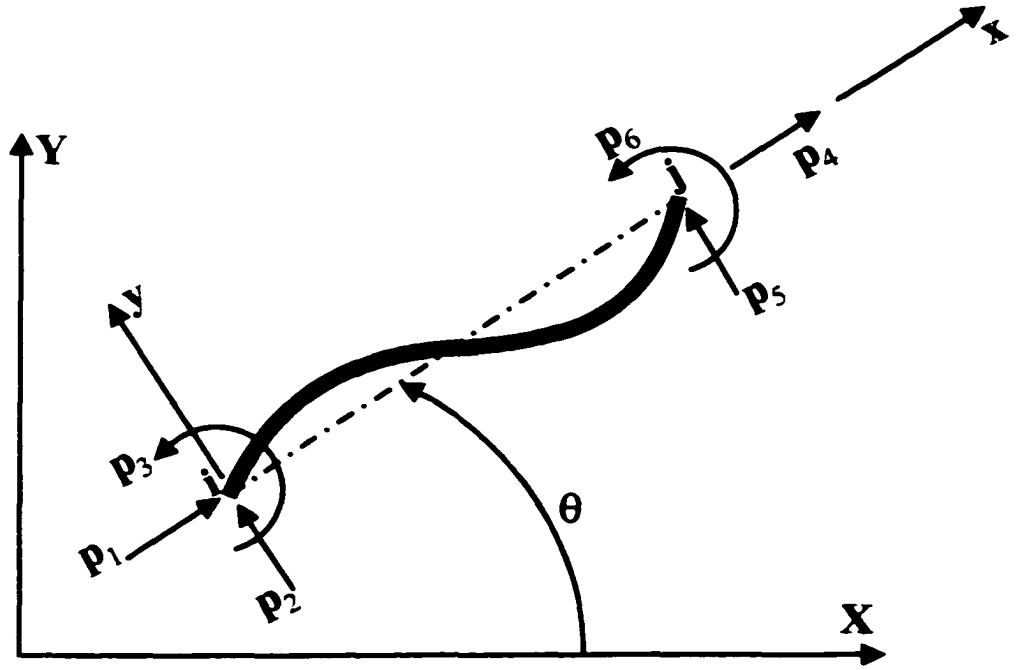

Figure 3-4 Typical Beam element with positive element forces in local axis.

The equilibrium equations for this typical member have the form:

$$\begin{aligned} p_3 + p_6 + p_5 L &= 0 \\ p_2 + p_5 &= 0 \\ p_1 + p_4 &= 0 \end{aligned} \tag{3-65}$$

According to Eq. (3-65), three member forces can be considered as independent. The choice of independent member forces is arbitrary. Here the two end moments (p_3 and p_6) and the axial force of the end j (p_4) are selected as the independent element forces, i.e.:

$$m^- = p_3 \quad , \quad m^+ = p_6 \quad \text{and} \quad F = p_4 . \tag{3-66}$$

The other three quantities i.e. the two end-shear forces and the axial force at the end i are related to the first three quantities via Eq. (3-65). Therefore, the element force vector can be written as

$$\mathbf{F} = \begin{bmatrix} F & m^+ & m^- \end{bmatrix}^T . \tag{3-67}$$

The nodal force vectors at both ends of the beam can be expressed as:

$$\mathbf{p}^{+} = [p_4 \quad p_5 \quad p_6] \quad \text{and} \quad \mathbf{p}^{-} = [p_1 \quad p_2 \quad p_3]. \tag{3-68}$$

Considering Eqs. (3-65)-(3-68), the following relations are obtained:

$$\mathbf{p}^{+} = \boldsymbol{Q}^{+}\mathbf{F} \qquad \text{and} \qquad \mathbf{p}^{-} = \boldsymbol{Q}^{-}\mathbf{F} \tag{3-69}$$

where

$$\boldsymbol{Q}^{+} = \begin{bmatrix} 1 & 0 & 0 \\ 0 & -1/L & -1/L \\ 0 & 1 & 0 \end{bmatrix} \quad \text{and} \quad \boldsymbol{Q}^{-} = \begin{bmatrix} -1 & 0 & 0 \\ 0 & 1/L & 1/L \\ 0 & 0 & 1 \end{bmatrix}. \tag{3-70}$$

In order to express end nodal forces in the global coordinate system, a rotation matrix given by Eq. (3-54) is required. The transformation takes from a local to a global system (X, Y) whereas the rotation matrix ***Rot*** takes vectors from the global to a local system. The inverse rotation is performed using the transpose of ***Rot*** to yield $\boldsymbol{Rot}^{T}\boldsymbol{N}^{+^{T}}\mathbf{F}$ and $\boldsymbol{Rot}^{T}\boldsymbol{N}^{-^{T}}\mathbf{F}$. Therefore, the term $(\boldsymbol{Q}\mathbf{F})^{(e)}$ for the plane frame is given by

$$(\boldsymbol{Q}\mathbf{F})^{(e)} = \left[\cdots \quad \boldsymbol{Rot}^{T}\boldsymbol{Q}^{-}\mathbf{F} \quad \cdots \quad \boldsymbol{Rot}^{T}\boldsymbol{Q}^{+}\mathbf{F} \quad \cdots\right]^{T}. \tag{3-71}$$

Expanding out the terms:

$$(\boldsymbol{Q}\mathbf{F})^{(e)} = \begin{bmatrix} \vdots \\ -l_x F - l_y \dfrac{m^{+} + m^{-}}{L} \\ -l_y F + l_x \dfrac{m^{+} + m^{-}}{L} \\ m^{-} \\ \vdots \\ l_x F + l_y \dfrac{m^{+} + m^{-}}{L} \\ l_y F - l_x \dfrac{m^{+} + m^{-}}{L} \\ m^{+} \\ \vdots \end{bmatrix} \tag{3-72}$$

Since $(\boldsymbol{Q}\mathbf{F})^{(e)}$ is a function of the nodal coordinates, the chain rule of differentiation yields:

$$\Delta(\boldsymbol{Q}\mathbf{F})^{(e)} = \nabla(\boldsymbol{Q}\mathbf{F})^{(e)}\,\Delta\mathbf{X}. \tag{3-73}$$

Substituting $(\boldsymbol{Q}\mathbf{F})^{(e)}$ from Eq. (3-72) into Eq. (3-73) and calculating the gradient, the geometric stiffness matrix can be computed directly as done for the truss element as

$$\boldsymbol{k}_{\sigma}^{g} = \begin{bmatrix} \widetilde{\boldsymbol{k}}_{\sigma} & -\widetilde{\boldsymbol{k}}_{\sigma} \\ -\widetilde{\boldsymbol{k}}_{\sigma} & \widetilde{\boldsymbol{k}}_{\sigma} \end{bmatrix} \tag{3-74}$$

where

$$\widetilde{\boldsymbol{k}}_{\sigma} = \begin{bmatrix} a & b & 0 \\ b & c & 0 \\ 0 & 0 & 0 \end{bmatrix}, \tag{3-75}$$

and

$$\begin{aligned} a &= \mathrm{F}\frac{1-l_x^2}{\mathrm{L}} - (\mathrm{m}^{-} + \mathrm{m}^{-})\frac{2l_x\,l_y}{\mathrm{L}^2} \\ b &= -\mathrm{F}\frac{l_x\,l_y}{\mathrm{L}} + (\mathrm{m}^{-} + \mathrm{m}^{-})\frac{1-2l_y^2}{\mathrm{L}^2} \\ c &= \mathrm{F}\frac{1-l_y^2}{\mathrm{L}} + (\mathrm{m}^{-} + \mathrm{m}^{-})\frac{2l_x\,l_y}{\mathrm{L}^2}. \end{aligned} \tag{3-76}$$

Eq. (3-74) follows directly from the differentiation of the direction cosines of the element given by Eq. (3-64). Note the geometric stiffness matrix is obtained in the form of stress stiffness matrix using the perturbation technique and unlike the truss element, it is not similar to $\boldsymbol{k}_{\sigma c}$.

The stress stiffness matrix obtained using the energy method, (Eq. 3-55), accounts for the axial force F only, while in the perturbation approach to calculate the stress stiffness matrix (Eq. 3-74), the axial force and two end moments must be considered. Therefore,

from this point of view, Eq. (3-55) is simpler than Eq. (3-75). The accuracy of these two solutions is discussed in Chapter 5.

3.3 The Solutions of Nonlinear Finite Element Equations

For a linear finite element analysis, the solution procedure is independent of the problem at hand. However, for nonlinear finite element analysis, the solution procedure is problem dependent. Various techniques are available to solve the system of nonlinear finite element equations. All the techniques are iterative in nature. With regard to the solution scheme used for the iterations, the methods can be classified either as Newton-Raphson or quasi-Newton methods. From the point of view of the controlling parameter used in the iterative process, they can be classified as load control technique, displacement control technique and arc-length method. The displacement control techniques and the arc-length techniques are well suited to study post-buckling behavior.

For the sake of completeness, the Newton-Raphson methods are briefly described in the context of load and displacement control techniques. The modifications made in the basic displacement control technique to obtain the limit load factor are also described in this section.

3.3.1 Incremental Finite Element Equations - Load Control Technique

When solving the incremental finite element equations using load control, it is assumed that the equilibrium equations at a load level are known and the configuration at a slightly higher load level is to be determined. As linear approximations are used, the equilibrium at the next step is not exactly satisfied. Therefore, an iteration process is used at each load increment to satisfy the equilibrium. The incremental solution of Eq. (3-21) is conventionally represented as an evolution in time with time step t :

$$
\begin{aligned}
&{}^{t}\boldsymbol{K}\ \Delta\mathbf{U} = \Delta\boldsymbol{P} = {}^{t+\Delta t}\mathbf{P} - {}^{t}\mathbf{P} \\
&{}^{t+\Delta t}\mathbf{U} = {}^{t}\mathbf{U} + \Delta\mathbf{U}
\end{aligned}
\qquad \text{(3-77)}
$$

with

$$^{t+\Delta t}\mathbf{U}^{(0)} = {}^{t}\mathbf{U}\,, \qquad ^{t+\Delta t}\boldsymbol{K}^{(0)} = {}^{t}\boldsymbol{K}\,, \qquad ^{t+\Delta t}\mathbf{P}'^{(0)} = {}^{t}\mathbf{P}' \tag{3-78}$$

where $^{t+\Delta t}\boldsymbol{K} = {}^{t+\Delta t}\boldsymbol{K}_{E} + {}^{t+\Delta t}\boldsymbol{K}_{DI}$ is the tangent stiffness matrix at time step $t+\Delta t$, $^{t+\Delta t}\mathbf{P}'^{(k-1)}$ is the vector of the nodal resultant member forces at time step $t+\Delta t$, and $^{t+\Delta t}\mathbf{P}$ is the vector of externally applied nodal loads at time step $t+\Delta t$. The load vector is assumed to be independent of the deformations and is known at each time step. The vector $\Delta\mathbf{P}$ is the out-of-balance force, $\Delta\mathbf{U}$ is the vector of increments in nodal displacements and $^{t+\Delta t}\mathbf{U}$ is the vector of nodal displacement at time $t+\Delta t$. It is noted that the problem is static and t simply denotes incremental steps during the solution process.

To obtain the vector $^{t+\Delta t}\mathbf{P}'^{(k-1)}$, it is required to obtain the element forces, which depend on the strain-producing component of the displacement vector. To accomplish this, the co-rotational formulation has been employed. According to this formulation, the total displacement is decomposed into a rigid body component and a strain-producing component. In other words, at each iteration step, the rigid body displacements and rotations have to be calculated and subsequently subtracted from the total displacement vector.

Having evaluated an approximation to the displacements corresponding to time $t+\Delta t$, one can now solve for an approximation to the stresses and corresponding nodal forces at time $t+\Delta t$, and then proceed to the next time increment calculations. However, because of the assumption in Eq. (3-77), such a solution may be prone to significant errors and, in some cases, depending on the time or load step sizes used, may indeed be unstable. In practice, it is therefore necessary to iterate until the solution of Eq. (3-77) is obtained with sufficient accuracy.

The widely used iteration methods are based on the classical Newton-Raphson technique. This method is an extension of the simple incremental technique given by Eq. (3-77). After calculating an increment in the nodal displacements, which defines a new total nodal displacement vector, one can repeat the incremental solution presented above using the currently known total displacements instead of the displacements at time t. The equations used for the Newton-Raphson iteration are:

$$
\begin{aligned}
{}^{t+\Delta t}\boldsymbol{K}^{(k-1)}\,\Delta\mathbf{U}^{(k)} &= \Delta\mathbf{P}^{(k-1)} = {}^{t+\Delta t}\mathbf{P} - {}^{t+\Delta t}\mathbf{P}'^{(k-1)} \\
{}^{t+\Delta t}\mathbf{U}^{(k)} &= {}^{t+\Delta t}\mathbf{U}^{(k-1)} + \Delta\mathbf{U}^{(k)}
\end{aligned}
\qquad \textbf{(3-79)}
$$

with the initial conditions defined as follows:

$$
{}^{t+\Delta t}\mathbf{U}^{(0)} = {}^{t}\mathbf{U}\,, \qquad {}^{t+\Delta t}\mathbf{K}^{(0)} = {}^{t}\mathbf{K}\,, \qquad {}^{t+\Delta t}\mathbf{P}'^{(0)} = {}^{t}\mathbf{P}'. \qquad \textbf{(3-80)}
$$

Note that in the first iteration, the relations in Eq. (3-79) reduce to the Eq. (3-77). In subsequent iterations, the latest estimates for the nodal displacements are used to evaluate the corresponding element stresses, nodal forces ${}^{t+\Delta t}\mathbf{P}'^{(k-1)}$, and the tangent stiffness matrix ${}^{t+\Delta t}\boldsymbol{K}^{(k-1)}$. The out-of-balance load vector $\Delta\mathbf{P}^{(k-1)}$ corresponds to a load vector that is not yet balanced by element stresses, and hence an increment in the nodal displacements is required. This updating of the nodal displacements during the iteration is continued until the out-of-balance loads and the incremental displacements are small. An important point to consider is that the correct calculation of ${}^{t+\Delta t}\mathbf{P}'^{(k-1)}$ from ${}^{t+\Delta t}\mathbf{U}^{(k-1)}$ is crucial. Any errors in this calculation will, in general, result in an incorrect response prediction. The correct evaluation of the proper tangent stiffness matrix ${}^{t+\Delta t}\boldsymbol{K}^{(k-1)}$ is also important. The use of the proper tangent stiffness matrix may be necessary for convergence and, in general, will result in fewer iterations until convergence is reached. A characteristic of this iteration is that a new tangent stiffness matrix is calculated in each iteration, hence the adoption of the term 'fully Newton-Raphson' method.

The bulk of the computational effort in the fully Newton-Raphson method lies in the calculation and factorization of the tangential stiffness matrix. For large finite element systems, most of the computational effort is spent in the formation and factorization of the stiffness matrix. Therefore, the solution cost becomes prohibitive since the computational cost in the fully Newton-Raphson method is directly proportional to the number of iterations performed. To reduce the computational effort involved in the iteration process, a variation of the Newton-Raphson method is proposed. Here, the stiffness matrix is updated only at the beginning of the time step. During the iterations, the stiffness matrix is not updated, thus avoiding the calculation of the stiffness matrix at each iteration. Instead, the out-of-balance loads are calculated using the total displacements up to the current iteration. The displacement increment $\Delta\mathbf{U}^{(k)}$ for the next

iteration is obtained using the same stiffness matrix that was generated at the beginning of the current time step.

The out-of-balance load may increase during the iteration process using the modified Newton-Raphson method, if the time step is large. This usually signals a diverging solution that implies displacements increase without bound. To avoid divergence when using the modified Newton-Raphson procedure, smaller steps are required. However, this increases the solution cost. Various investigators [139,140] have suggested schemes to detect and avoid divergence during the solution procedure. In general, the regular or fully Newton-Raphson method exhibits a quadratic convergence and the modified Newton-Raphson method converges more slowly. Various acceleration procedures have been suggested in the literature [141] to accelerate the rate of convergence of the modified Newton-Raphson method. The discussion of these schemas is beyond the scope of this work

In the context of this thesis, the fully Newton-Raphson method has been used in all nonlinear analysis problems.

3.3.2 Incremental Finite Element Equations – Displacement Control Technique

The classical load control procedures, wherein the load is incremented in small steps during the solution, are not suitable for problems with limit points. From a physical point of view, such problems are characterized by load-deflection curves that exhibit a softening effect. At some stage of the iteration process the tangential stiffness becomes indefinite. Several procedures have been used by different investigators to overcome this difficulty (see Chapter 1). The displacement control technique proposed by Batoz and Dhatt [98] is described here.

In the displacement control method, the external load during iteration of a particular time step does not remain constant. During the analysis, the load is assumed to vary so that it is proportional to a given reference load $\mathbf{P}_{ref}$. A load factor parameter $'\alpha$ is used to denote the load at time t. Using the fully Newton-Raphson iterative method described by

Eq. (3-79), the basic equation to be solved within the framework of the iterative process is

$$
\begin{aligned}
&{}^{t+\Delta t}\mathbf{K}^{(k-1)}\,\Delta\mathbf{U}^{(k)} = \Delta\mathbf{P}^{(k-1)} = {}^{t+\Delta t}\alpha^{(k)}\,\mathbf{P}_{ref} - {}^{t+\Delta t}\mathbf{P}'^{(k-1)} \\
&{}^{t+\Delta t}\mathbf{U}^{(k)} = {}^{t+\Delta t}\mathbf{U}^{(k-1)} + \Delta\mathbf{U}^{(k)}
\end{aligned}
\qquad \textbf{(3-81)}
$$

with the initial conditions given by Eq. (3-80).

In this method, instead of varying the load parameter as we do in load control method, a nodal displacement component (for example the qth component of ${}^{t}\mathbf{U}$) is incremented by ΔU_q at each time step. Also, during each time step, this component is constrained to be fixed. In other words,

$$
{}^{t+\Delta t}U_q = {}^{t}U_q + \Delta U_q \qquad \textbf{(3-82)}
$$

and

$$
\Delta U_q^{(k)} = 0 \qquad \textbf{(3-83)}
$$

The constraint Eq. (3-83) may be directly incorporated into the original system of equations given by Eq. (3-81). However, this results in a modified stiffness matrix, which is not symmetric and banded any more. In order to overcome this problem, Eq. (3-81) is rewritten as

$$
{}^{t+\Delta t}\mathbf{K}^{(k-1)}\left[\Delta\mathbf{U}^{I(k)} \middle|\, \Delta\mathbf{U}^{II(k)}\right] = \Delta\mathbf{P}^{(k-1)} = {}^{t+\Delta t}\alpha^{(k)}\,\mathbf{P}_{ref} - {}^{t+\Delta t}\mathbf{P}'^{(k-1)} \qquad \textbf{(3-84)}
$$

where $\Delta\mathbf{U}^{I(k)}$ and $\Delta\mathbf{U}^{II(k)}$ can be obtained relative to $\mathbf{P}_{ref}$ and ${}^{t+\Delta t}\mathbf{P}'^{(k-1)}$ using the following equations:

$$
{}^{t+\Delta t}\mathbf{K}^{(k-1)}\,\Delta\mathbf{U}^{I(k)} = \mathbf{P}_{ref} \qquad {}^{t+\Delta t}\mathbf{K}^{(k-1)}\,\Delta\mathbf{U}^{II(k)} = -{}^{t+\Delta t}\mathbf{P}'^{(k-1)}. \qquad \textbf{(3-85)}
$$

Now, $\Delta\mathbf{U}^{(k)}$ may be expressed as

$$
\Delta\mathbf{U}^{(k)} = {}^{t+\Delta t}\alpha^{(k)}\Delta\mathbf{U}^{I(k)} + \Delta\mathbf{U}^{II(k)} \qquad \textbf{(3-86)}
$$

Writing Eq. (3-86) for the q^{th} component of ${}^{t}\mathbf{U}$, we obtain

$$\Delta U_q^{(k)} = {}^{t+\Delta t}\alpha^{(k)} \Delta U_q^{I(k)} + \Delta U_q^{II(k)} \tag{3-87}$$

Substituting Eq. (3-83) into (3-87) gives

$${}^{t+\Delta t}\alpha^{(k)} = -\frac{\Delta U_q^{I(k)}}{\Delta U_q^{II(k)}}. \tag{3-88}$$

Having obtained the load parameter from Eq. (3-88), other nodal displacement components can be updated using Eq. (3-86). The iterative process described by Eqs. (3-85)-(3-88) is continued until convergence criteria is met (i.e. the new equilibrium position is found). Then, the qth component of ${}^{t}\boldsymbol{U}$ is incremented and the new time step is started. The above technique has been used in this research for optimization of structures with limit stability constraints.

Here, it is implicitly assumed that the tangent matrix $\boldsymbol{K}$ remains non-singular at any solution level. Theoretically, if a solution corresponds to a critical or singular point, the matrix $\boldsymbol{K}$ will be singular. However, in practice, it is impossible to obtain a solution vector exactly corresponding to a singular point, due to possible numerical rounding errors.

3.3.3 The Limit Load

The displacement control method is useful to trace the post-buckling path. However, it does not yield the peak load factor. To obtain the optimum design of a structure for limit load one needs to obtain the exact value of the limit load. Taking very small increments in the controlling displacement component, the peak load factor can be approximated by the largest load parameter obtained. However, the solution obtained is sensitive to the displacement increment employed and the cost of the solution is prohibitive.

In this thesis, the peak load parameter is obtained by performing a quadratic fit to the load displacement curve near the critical load. The procedure is outlined as follows:

1) Increment the displacement until a decrease in the load parameter is observed. Save the three points that trap the maximum point, the points *a*, *b* and *c* in Figure (3-5).

2) Specify the largest load as the approximate limit load and its relative displacement.

3) Fit a quadratic function through the three points and find the new approximate limit load as the maximum of the function and its relative displacement.

4) Modify the displacement increment to make it equal to the difference between the approximation obtained in step 2 and step 3. Apply this incremental displacement and iterate for the new set of points.

5) Repeat steps 2 through 4 until the increment obtained in step 4 is within a desired tolerance. In this case, the maximum load obtained in step 4 is the limit load.

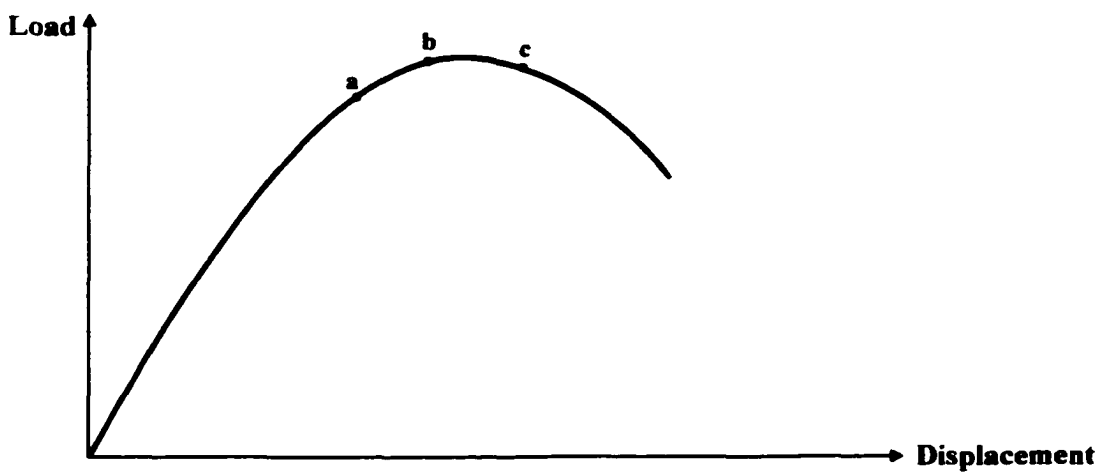

Figure 3-5 Load-deflection curve and the points trapping the pick load.

The foregoing procedure has been successfully implemented and the peak load parameter has been obtained with minimum computational effort.

3.3.4 Convergence Criteria

If an incremental solution strategy based on iterative methods is to be effective, realistic criteria should be used for the termination of the iteration. At the completion of an iteration, the solution obtained should be checked to see whether it has converged within

preset tolerances or whether the iteration is diverging. If the convergence tolerances are too loose, inaccurate results are obtained, and if the tolerances are too tight, most computational effort is spent to obtain needless accuracy. Similarly, an ineffective divergence check can terminate the iteration when the solution is not actually diverging or force the iteration to search for an unattainable solution. In most nonlinear problems, the convergence criterion is based on the nodal displacement or out-of-balance force vector.

For a convergence criterion based on the nodal displacement vector, the norm of nodal displacement increment vector at the end of each iteration may be required to be within a certain tolerance of the norm of the true nodal displacement vector solution. Hence, a realistic convergence criterion may be expressed as:

$$\left\|\Delta \mathbf{U}^{(k)}\right\|_2 \leq \varepsilon_D \left\|{}^{t+\Delta t}\mathbf{U}\right\|_2 \tag{3-89}$$

where ε_D is a displacement convergence tolerance. The vector ${}^{t+\Delta t}\mathbf{U}$ is not known and must be approximated. Frequently, it is appropriate to use the last calculated value ${}^{t+\Delta t}\mathbf{U}^{(k)}$ as an approximation to ${}^{t+\Delta t}\mathbf{U}$ and a sufficiently small value ε_D. However, in some analyses the actual solution may still be far from the value obtained when convergence is measured using Eq. (3-89) with ${}^{t+\Delta t}\mathbf{U}^{(k)}$. This is the case when the calculated displacements change only slightly in each iteration but continue to change for many iterations.

For a convergence criterion based on the out-of-balance force vector, the norm of the out-of-balance force vector at the end of each iteration may be required to be within a certain tolerance of the norm of the initial out-of-balance force vector, such that

$$\left\|{}^{t+\Delta t}\mathbf{P} - {}^{t+\Delta t}\mathbf{P}'^{(k)}\right\|_2 \leq \varepsilon_F \left\|{}^{t+\Delta t}\mathbf{P} - {}^{t}\mathbf{P}'\right\|_2 \tag{3-90}$$

where ε_F is a out-of-balance convergence tolerance. A difficulty with this approach is that the displacement solution does not enter into the termination criterion. In this case, the out-of-balance forces may be very small while the displacements may still be much in

error and far from true solution. Hence, the convergence criteria in Eqs. (3-89) and (3-90) may have to be used with very small values of ε_D and ε_F. Also, the expressions must be scaled appropriately when quantities of different units are measured (such as displacements, rotations, pressures, and so on).

In this research, in order to provide some quantifiable measure or indication of when both the displacements and the forces are near their equilibrium values, a convergence criterion based on the energy of the system is employed. Here, the increment in internal energy during each iteration (i.e., the amount of work done by the out-of-balance forces on the nodal displacement increments) may be required to be within a certain tolerance of the initial internal energy increment, i.e.

$$\Delta \mathbf{U}^{(k)^T}\left({}^{t+\Delta t}\mathbf{P} - {}^{t+\Delta t}\mathbf{P}'^{(k-1)}\right) \le \varepsilon_E \, \Delta \mathbf{U}^{(1)^T}\left({}^{t+\Delta t}\mathbf{P} - {}^{t}\mathbf{P}'\right) \tag{3-91}$$

where ε_E is a energy convergence tolerance. The proposed convergence criterion contains both the displacement and force information, it is practical and effective measure. Bathe and Cimento [139] provided studies on the proposed convergence measures. For the simulations carried out in this thesis, the following ε_E is selected:

$$\varepsilon_E = 10^{-6} \tag{3-92}$$

3.3.5 Illustrative Examples

Two numerical examples are considered to illustrate the application and performance of the nonlinear finite element formulation for the analysis of large-displacement and large-rotation problems. The first example depicts a cantilever beam with a concentrated end moment. The second example consists of a 45° circular bend cantilever beam subjected to a concentrated end load. Both examples exhibit the characteristics of geometrical nonlinearity due to large displacement and rotation. The problems were solved using the fully Newton-Raphson iterative method based on the load control technique.

i) Cantilever beam subjected to a concentrated end moment.

This structure exhibits inextensional bending. Under the action of an end moment M, the vertical and horizontal displacements and rotation at the end of the beam are assumed to be V, U and ϕ, respectively, and these are shown in Fig. 3-6. The beam has a modulus of elasticity E=10000 psi, length of L=100 in, cross-sectional area of A=0.5 in^2 and moment of inertia I=0.01042 in^4. The objective of this simulation is to demonstrate the accuracy of the finite element formulation and its implementation. The results are compared to the numerical solution available in the literature.

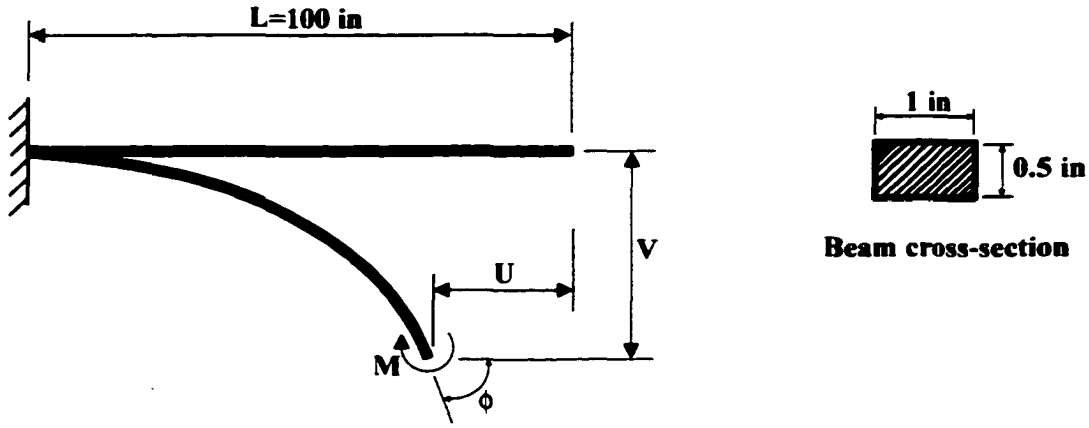

Figure 3-6 Cantilevered beam with an end moment.

The results are summarized as follows. Figure 3-7 shows the vertical displacement versus the moment. With 5 beam elements and 20 load steps, this problem was solved using the stress stiffness matrix $\boldsymbol{k}_\sigma$ based on the energy method, given by Eq. (3-55), and was also solved using the stress stiffness method based on the perturbation method (Eq. 3-74). The results obtained from these methods are in excellent agreement with the exact solution. Both matrices predict the vertical displacement with an accuracy of less than 1%. In the extreme case of $M_u = M L / (2\pi EI) = 1$, one end of the beam reaches the other end and produce a circular beam. The application of the energy convergence criteria and 20 load steps resulted in convergence in three iterations or less. Bathe and Bolurchi [78] also solved this problem with 5 elements using the updated Lagrangian formulation and the method produced inaccurate results beyond $M_u = 0.3$.

The plots for the horizontal and vertical displacements and rotations at the end of the beam are shown in Figure 3-8. When $M_u = 1$, U must be equal to the length of the beam, L for the exact analysis. Using 5 elements and 20 load steps, U/L=1 for $M_u = 1$ which confirms the correct formulation and computer implementation of the geometrically nonlinear analysis.

Figure 3-9 compares the 5-beam and 10-beam element discretization. The vertical displacement results obtained show that there is a 1% difference in the two solutions and the 10-beam solution matches the exact solution. The effect of the number of load steps (5, 10 and 20) is shown in Figure 3-10. The results show that the solutions are not very dependent on the number of load steps and the 5 time-step solution produces accurate results.

The difference between the linear and nonlinear solutions is depicted in Figure 3-11. It is observed that there is good agreement between the two solutions up to a value of $M_u=ML/(2\pi EI)=0.1$. Past this value, the two solutions become substantially distinct.

Figure 3-12 shows the configuration of the beam with 20 elements for different end moments. It is interesting to note that for $M_u=1$, the straight beam changes into a circular shape, exactly predicting the analytical solution. Figure 3-13 shows the final configuration of the beam at $M_u = 1$, for 5, 10 and 20 elements. As the number of elements is increased, the circular shape becomes better defined, as expected.

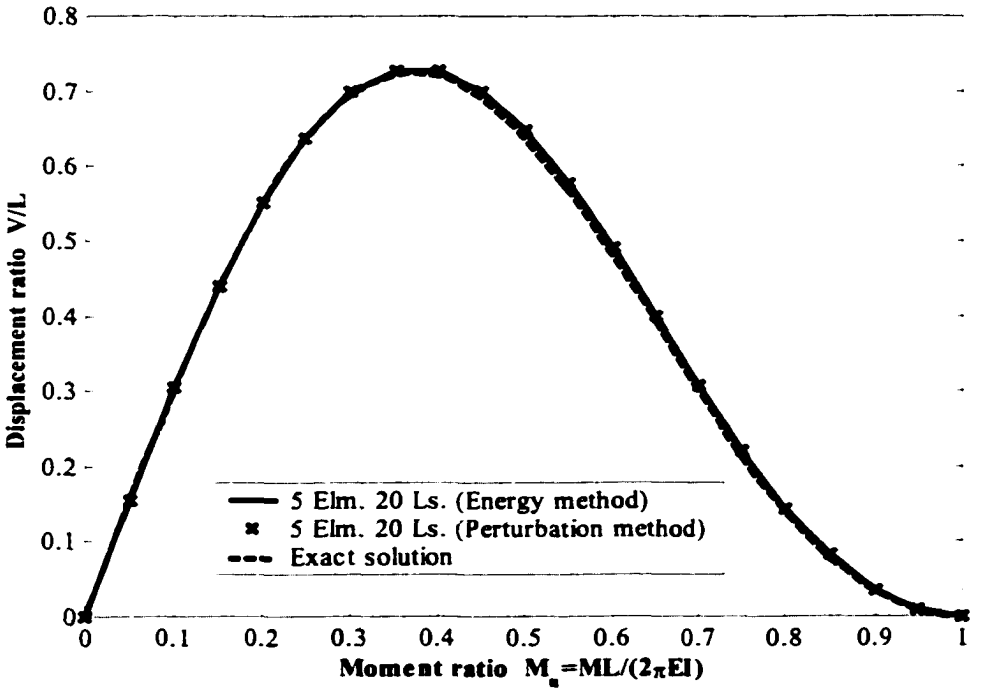

Figure 3-7 Moment-vertical displacement curve for the cantilevered beam.

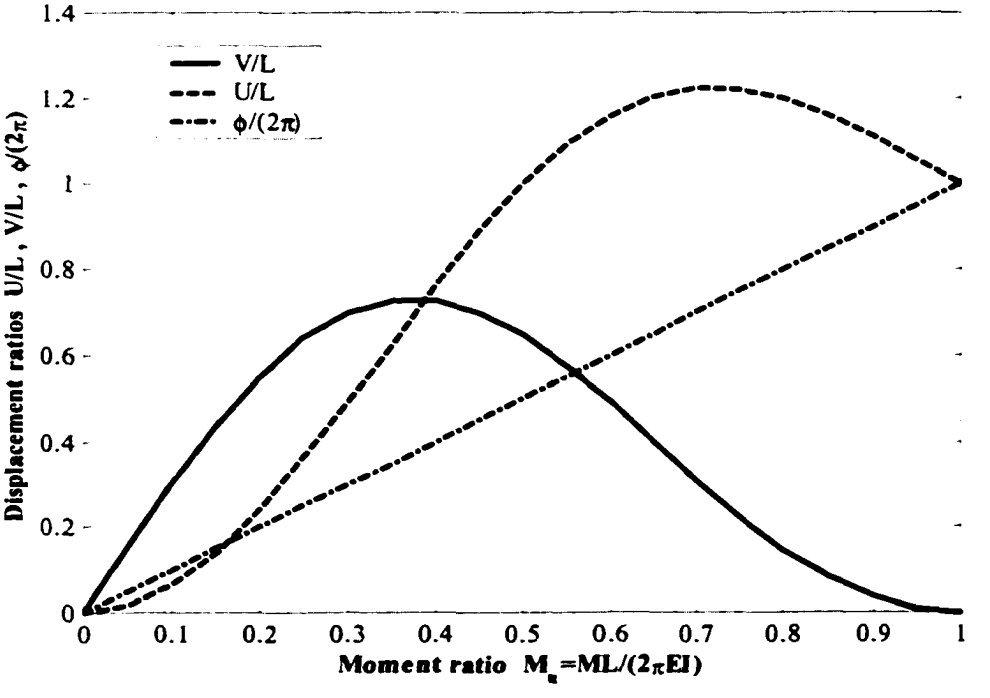

Figure 3-8 Moment- displacements curve for the cantilevered beam.

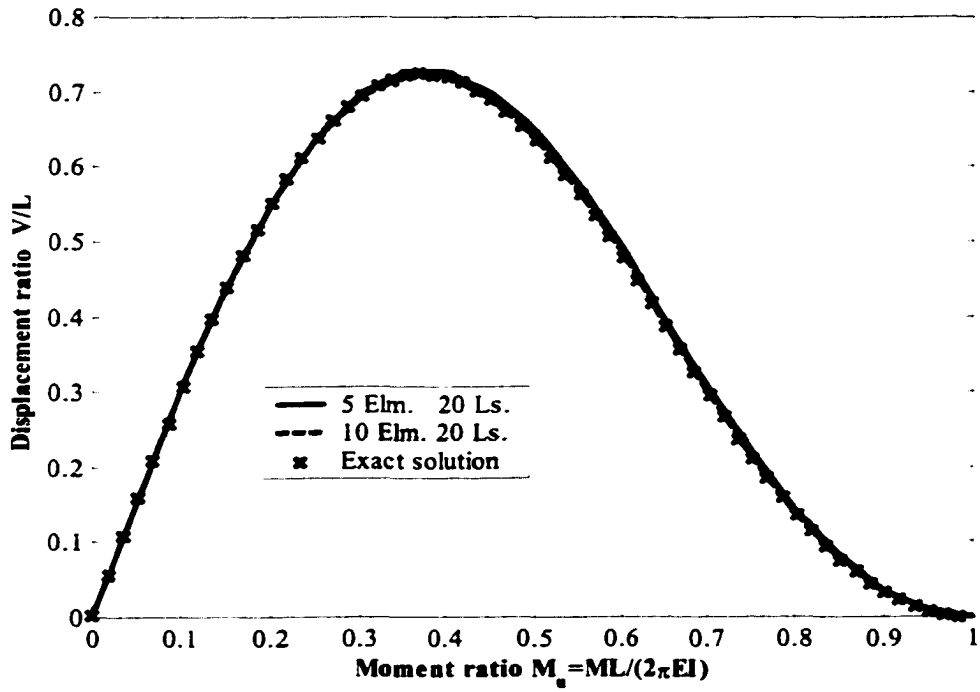

Figure 3-9 Moment-displacement curve of the cantilevered beam for various meshes.

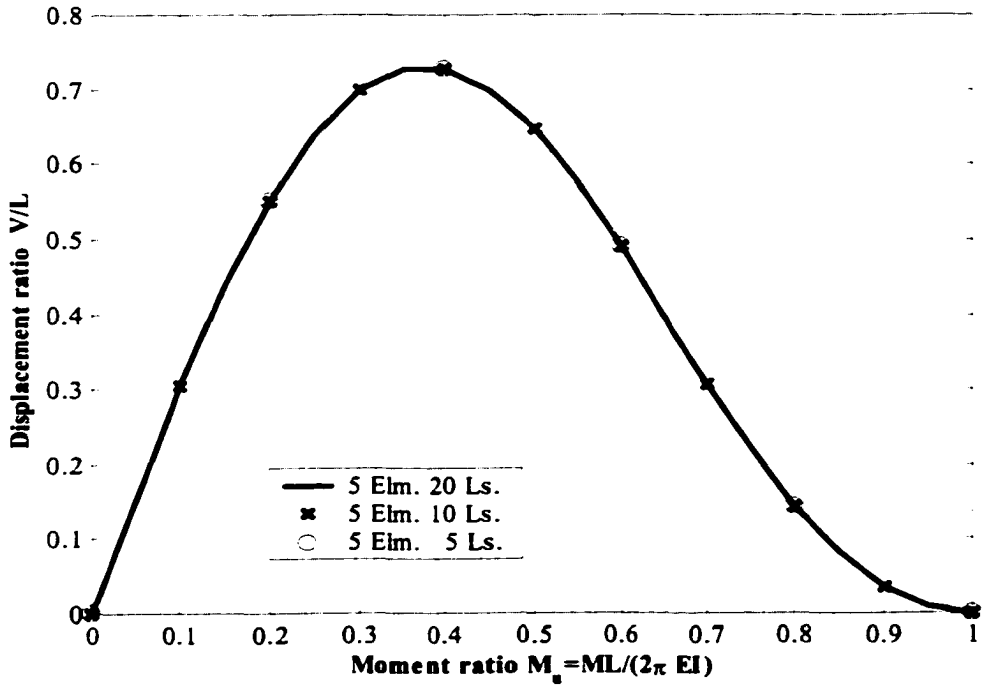

Figure 3-10 Moment- vertical displacement curve of the cantilevered beam for various load steps.

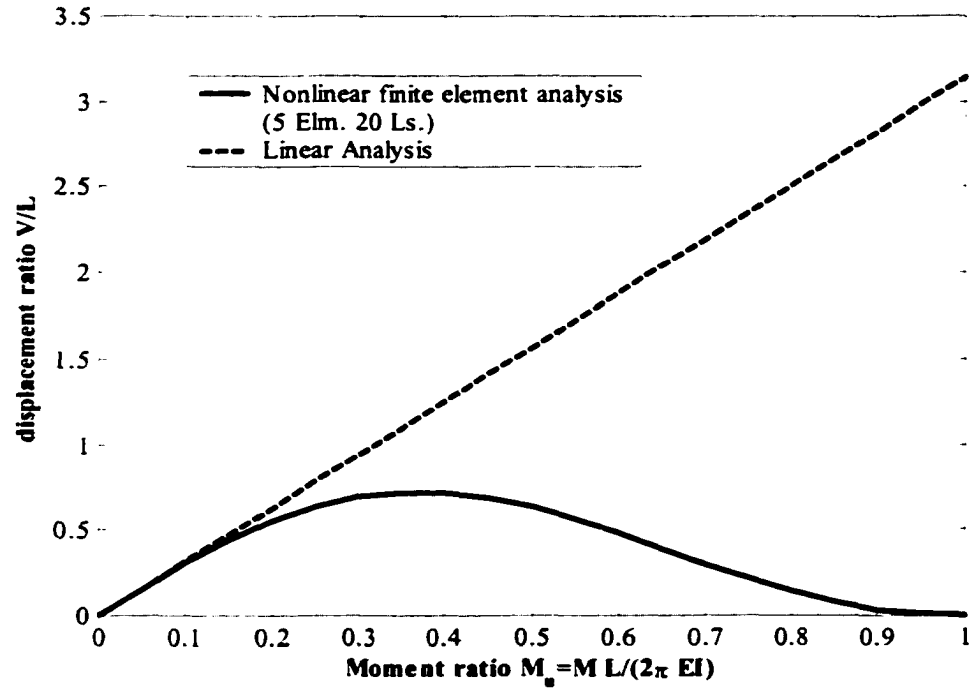

Figure 3-11 Moment-vertical displacement curve of the cantilever beam for linear and nonlinear analysis.

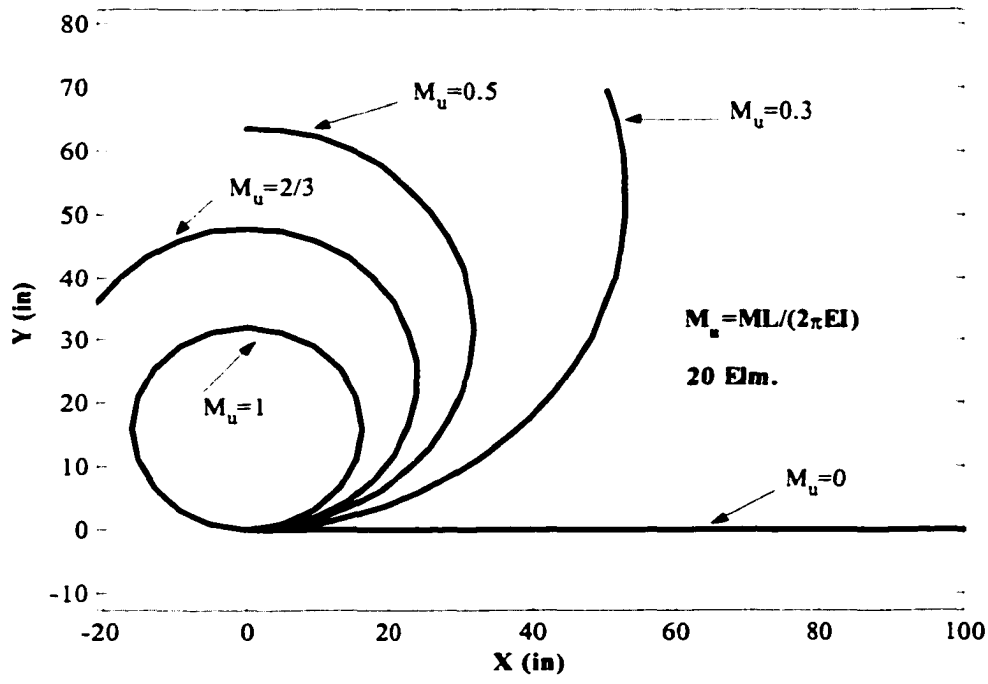

Figure 3-12 Successive configurations for the cantilevered beam.

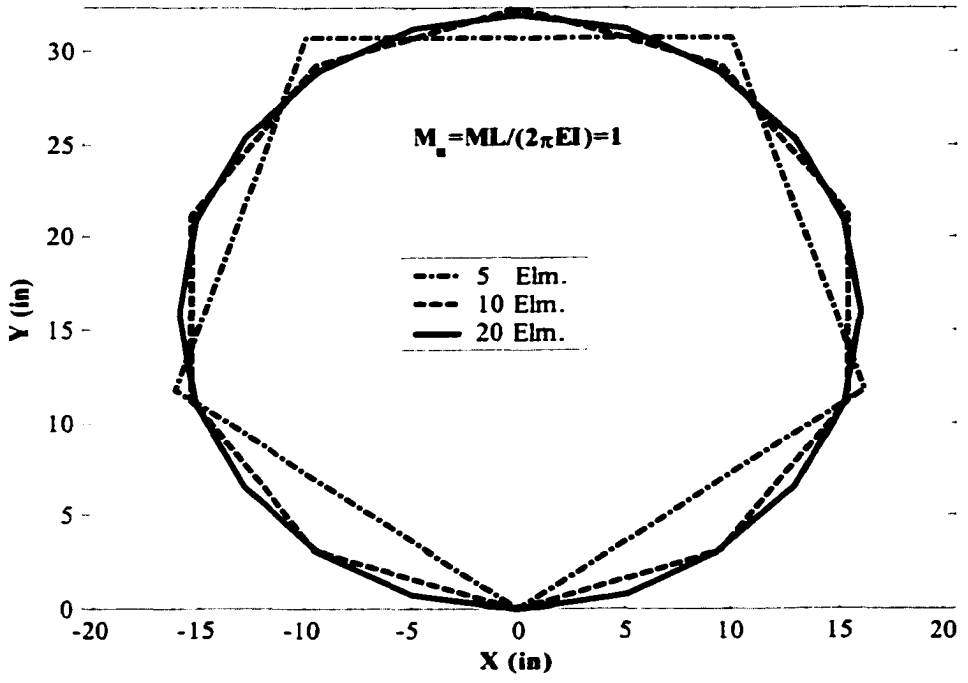

Figure 3-13 Final configuration of the cantilever beam under the end moment (M_u =1) for three different discretizations.

ii) 45° circular bend cantilever beam subjected to a concentrated end load.

In this example, an initially cantilevered beam undergoes large displacements and rotations to describe a transition from a bent position, through a straightened geometry, and finally curving in the opposite direction. The beam is made of aluminum (E=10^7 psi) with a 1 *in* square cross-section, 45° circular bend and a radius of 100 *in*. Under the action of an end load P, the vertical and horizontal displacements and rotation of the end of the beam are assumed to be V, U and ϕ, as shown in Figure 3-14. The structure was idealized using 8 equal straight beam elements and it is subjected to 600 lb end load at different load steps.

Figure 3-15 shows the vertical and horizontal displacements, and rotation at the end of the circular cantilever beam versus the applied end load. As expected, the solutions obtained using both the energy and perturbation methods are exactly identical.

Figure 3-16 shows the result of vertical displacement of the end of the beam for different load steps. The results confirm the proper formulation and computer implementation for the simulation analysis. The results obtained using 5, 10 and 20 load steps are in excellent agreement. Using a 20 load-step simulation with the energy convergence criteria, convergence was achieved in 4 or less iterations at each load step. The 5 and 10 load-step solutions also provided good results in 4 iterations.

The linear and nonlinear analysis provide comparable solutions until about P_u= 1.5 (Figure 3-17). Past this value, the difference between the two solutions becomes significant. Finally, Figure 3-18 shows the configuration of the beam with different end loads, showing clearly the full spectrum of the motion.

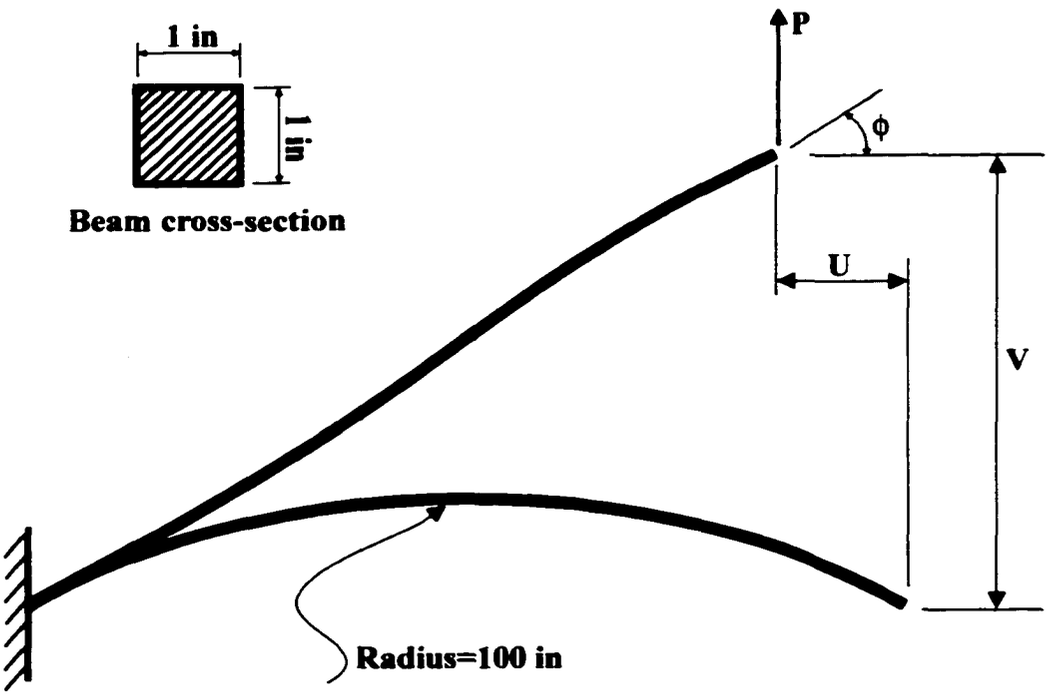

Figure 3-14 45° circular bend cantilever beam subjected to an end load.

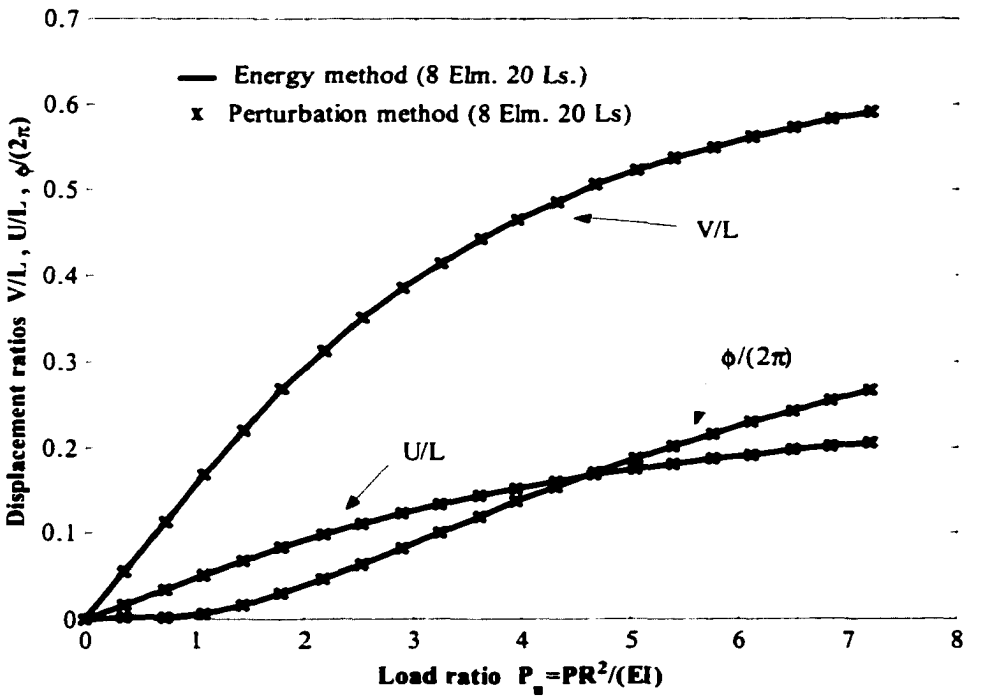

Figure 3-15 Load-displacements curve of the circular cantilever beam.

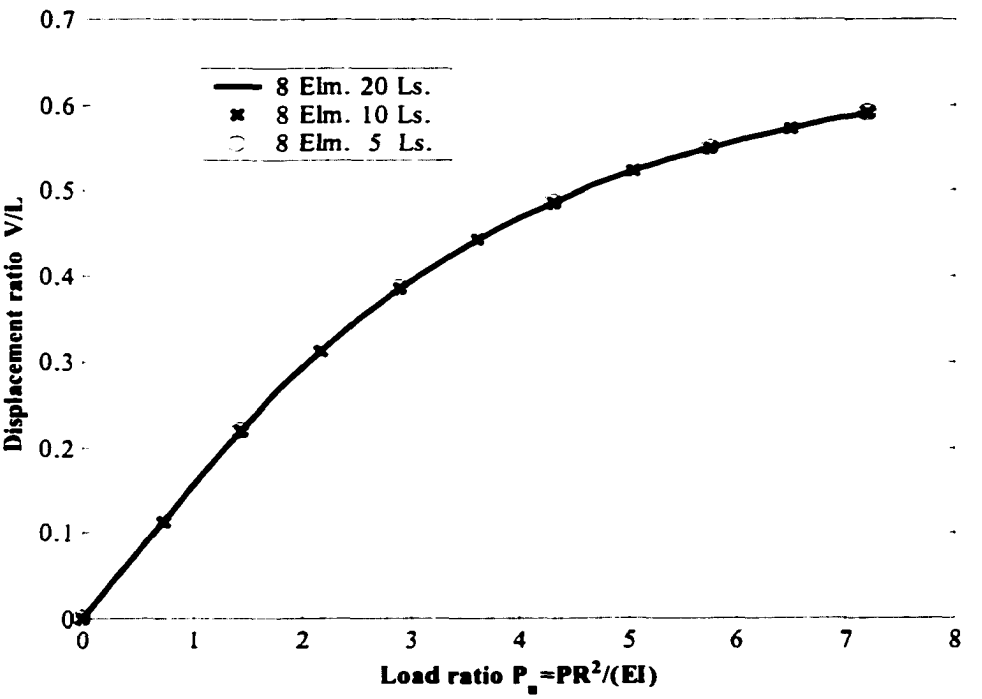

Figure 3-16 Load-vertical displacement curve of the circular cantilever beam for different load steps.

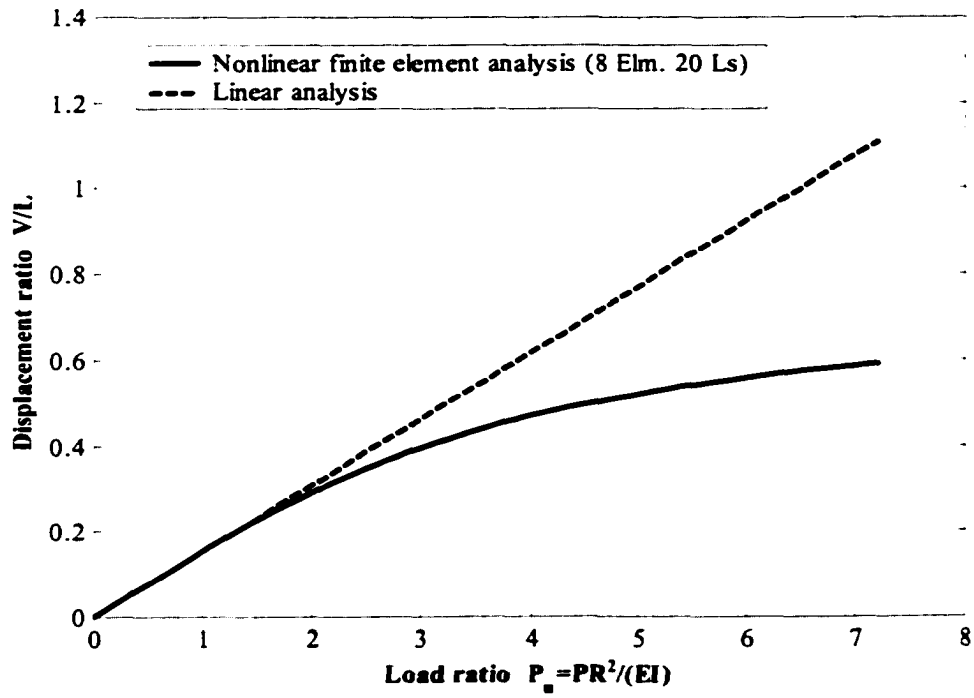

Figure 3-17 Moment-vertical displacement curve of the circular cantilever beam for linear and nonlinear analysis.

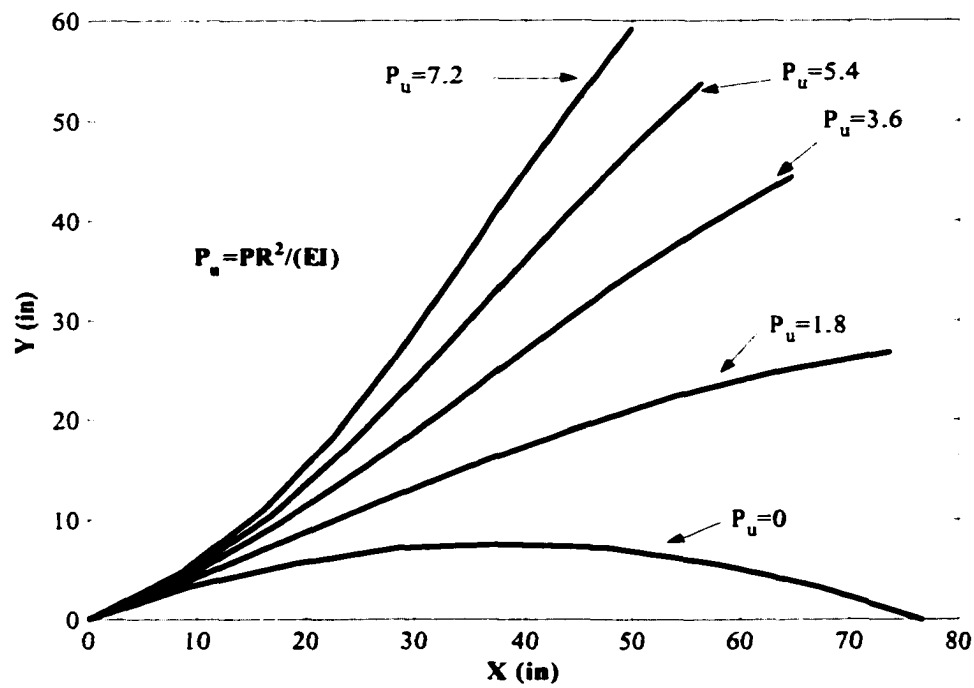

Figure 3-18 Different configurations of the circular cantilever beam.

3.4 Buckling Analysis

In structural optimization problems with system stability constraints, the accuracy of the predicted buckling load is important to ensure the structural integrity. In most previous studies reported in the literature, the system stability requirement has been posed as a linear buckling analysis problem. Such analysis is restricted to small rotations and to equilibrium in the initial state. A linear buckling analysis reduces to the solution of a generalized eigenvalue problem for the buckling loads (bifurcation point). This approach to system stability for nonlinear structures may not be conservative enough since the nonlinear behavior of the structure results in large changes in the geometry of the structure. Furthermore, the presence of geometric imperfections may affect the nonlinear structural response more significantly. For this reason, a nonlinear buckling analysis is warranted to find accurate estimates of buckling loads for nonlinear structural problems (limit point).

3.4.1 Linear Buckling Analysis (Bifurcation Point)

A basic assumption of linear buckling analysis is that the structure behaves linearly before the critical load is reached. In other words, assuming that a reference load vector $\mathbf{P}_{ref}$ is applied, the displacement vector $\mathbf{U}_{ref}$ is calculated carrying out a standard linear static analysis. Subsequently, for a different load level with a positive constant load factor α ($\alpha \mathbf{P}_{ref}$), the new stiffness matrices become

$$\boldsymbol{K}_{\sigma} = \alpha\, \boldsymbol{K}_{\sigma\, ref} \quad \text{and} \quad \boldsymbol{K}_{DI}(\mathbf{U}_{ref}) = \alpha\, \boldsymbol{K}_{DI\, ref}. \tag{3-93}$$

Multiplying all loads by α implies that the intensity of the displacement and stress field are multiplied by α , however the relative distribution of displacements and stresses does not change. Thus, a scale factor α_{cr} corresponding to that of the critical buckling load is defined as

$$\mathbf{P}_{cr} = \alpha_{cr}\, \mathbf{P}_{ref}. \tag{3-94}$$

Since external loads do not change during an infinitesimal buckling displacement $\Delta\mathbf{U}$, then from Eq. (3-21),

$$(\boldsymbol{K}_E + \alpha_{cr}\boldsymbol{K}_{D1\,ref})\Delta\mathbf{U} = 0 \quad \text{or} \quad (\boldsymbol{K}_E + \alpha_{cr}\boldsymbol{K}_{\sigma\,ref})\Delta\mathbf{U} = 0 \qquad \textbf{(3-95)}$$

Eq. (3-95) defines an eigenvalue problem whose lowest eigenvalue α_{cr} is associated with the value of the buckling load and the corresponding eigenvector $\Delta\mathbf{U}$ associated with α_{cr} represents the buckling mode shape.

When using Eqs. (3-95) for linear buckling analysis, $\boldsymbol{K}_{D1}$ implies that prebuckling rotations are small but are not to be ignored, whereas use of $\boldsymbol{K}_\sigma$ implies that prebuckling rotations are either ignored or are zero. The latter is termed the classical buckling analysis. The buckling load found using the linear buckling analysis based on $\boldsymbol{K}_{D1}$ is not the same as that found using classical buckling analysis in the presence of traverse displacements and rotations prior to buckling. In practical problems where the prebuckling rotations are not negligible (geometric nonlinear problems), use of $\boldsymbol{K}_{D1}$ yields a more conservative buckling load with respect to the actual stability limits (limit points).

3.4.2 Combined Buckling Analysis (Bifurcation Point)

A linear buckling analysis alone does not provide an accurate estimate of the actual critical load of the structure. In classical linear buckling analysis (function of $\boldsymbol{K}_\sigma$), the pre-buckling rotations are ignored. In the linear buckling analysis based on $\boldsymbol{K}_{D1}$, the pre-buckling rotations are small and $\boldsymbol{K}_{D1}$ depends on very small deformations. One way to account for the structural non-linearity is to calculate $\boldsymbol{K}_E$ and $\boldsymbol{K}_\sigma$ or $\boldsymbol{K}_{D1}$ based on the configuration just before buckling[135]. To that end, a certain load level $\mathbf{P}_{base}$ is applied and a nonlinear static analysis is performed to calculate the tangent stiffness matrix $\boldsymbol{K}$ in its current deformed configuration. At the subsequent step, a trial load increment $\Delta\mathbf{P}$ is applied, and the resulting displacements produced by $\boldsymbol{K}$ and $\Delta\mathbf{P}$ are used to compute the element forces. This establishes $\boldsymbol{K}_{\sigma\,base}$ or $\boldsymbol{K}_{D1\,base}$ for this base current configuration.

The objective now is to find the proper load level beyond the fundamental state $\mathbf{P}_{base}$ such that the tangent stiffness matrix $\boldsymbol{K}$ becomes completely degraded by subsequent increments of $\boldsymbol{K}_{\sigma}$ or $\boldsymbol{K}_{D1}$. To find this additional load level, the linear eigenvalue problem

$$(\boldsymbol{K} + \Delta\alpha_{cr}\boldsymbol{K}_{\sigma\, base})\Delta\mathbf{U} = 0 \quad \text{or} \quad (\boldsymbol{K} + \Delta\alpha_{cr}\boldsymbol{K}_{D1\, base})\Delta\mathbf{U} = 0 \qquad \textbf{(3-96)}$$

is solved, where $\Delta\alpha_{cr}$ is the critical load factor based on the fundamental base load level. This reduces the total stiffness to zero with respect to the buckling mode to give the predicted buckling load as

$$\mathbf{P}_{cr} = \mathbf{P}_{base} + \Delta\alpha_{cr}\,\Delta\mathbf{P}. \qquad \textbf{(3-97)}$$

Eq. (3-97) assumes that the displacements and forces change in intensity but not in relative distribution when the load is increased by an amount $\Delta\alpha_{cr}\,\Delta\mathbf{P}$. This assumption becomes nearly true as $\mathbf{P}_{base}$ approaches $\mathbf{P}_{cr}$. By using a sequence of increasing loads $\mathbf{P}_{base}$, the solution approaches the correct buckling load. At convergence, $\Delta\alpha_{cr} = 0$ and $\mathbf{P}_{cr} = \mathbf{P}_{base}$.

3.4.3 Nonlinear Buckling Analysis (Limit Point)

In nonlinear buckling analysis, the incremental nonlinear analysis may use either the force or the displacement control technique. Mathematically, when the tangent stiffness matrix $\boldsymbol{K}$ becomes singular, the limit point has been reached. In structural optimization problems under system stability constraints, it is important to obtain precisely the load level that initiates the snap-through. The following example illustrates this point.

3.4.4 Illustrative Example

A Williams toggle frame with a concentrated apex load has been selected to illustrate the theory presented. This example has been solved analytically and experimentally by Williams [142], and also by Meek and Loganathan [143] using the finite element force control technique based on the arc-length technique. Here, the problem is solved using

the fully Newton-Raphson iterative method based on the displacement control technique. The vertical displacement at the apex has been selected as the displacement control. The Williams Toggle frame geometry and the coordinate system are shown in the Figure 3-19. The span length of the frame is L=25.886 in, the height of the beam is H=0.386 in and the width and depth of the cross-section are a=0.753 in and b=0.243 in, respectively. The Young's Modulus is $E=10.3\times10^{6}$ psi. Under the action of the load, the frame exhibits a displacement V at its apex. The frame is discretized into 4, 8 and 16 elements to determine the effect of discretization on the solution. The controlled displacement is incremented 0.01 in per displacement step.

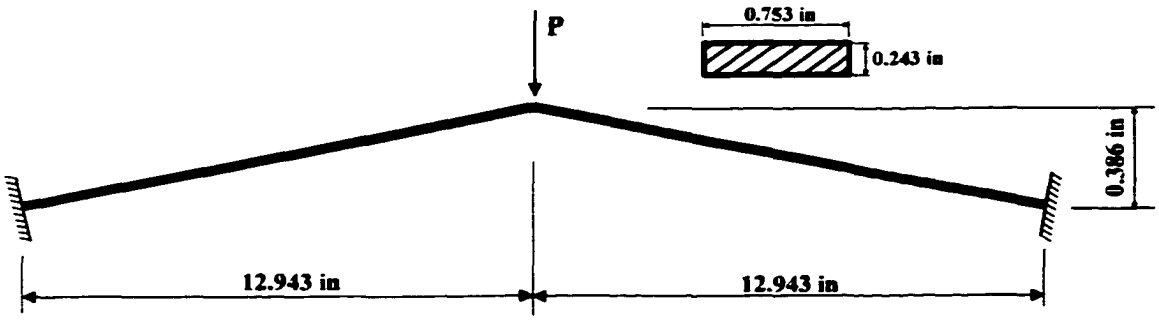

Figure 3-19 The Williams toggle frame.

Figure 3-20 shows pre-buckling and post-buckling path of the Williams toggle frame. The predicted response compares well with the analytical solution. Also, as the number of elements increases, the numerically predicted response improves significantly. The response obtained using 18 elements is in excellent agreement with the analytical solution and especially with the experimental data reported by Williams [142]. The results confirm the validity of the formulation and the accuracy of the solutions for snap-through problems. The convergence was achieved in 4 or less iterations at each displacement step.

Fig. 3-21 shows the load-deflection curve up to the limit load for the Williams toggle frame using 18 elements to discretize the structure. The formulation to find the limit point has been implemented successfully. There is an excellent agreement between the buckling analysis solutions obtained using the energy and perturbation methods. The analytical solution for the limit point is P_{cr}=34.0392 lb; using the energy method is P_{cr}=34.3205 lb; and using the perturbation method is P_{cr}=34.3206 lb. The vertical

displacement for the apex at the limit point has the following solutions: analytical solution is V= 0.231 in; using the energy method is V= 0.236 in; and using the perturbation method is V= 0.235 in.

Figure 3-22 shows the configuration of the frame modeled using 8 and 16 elements with apex load P=30 lb and the deformed structure is compared to the initial configuration.

Figure 3-23 shows the deformed configuration of the frame modeled using 16 elements with apex loads P=20 lb and 30 lb.

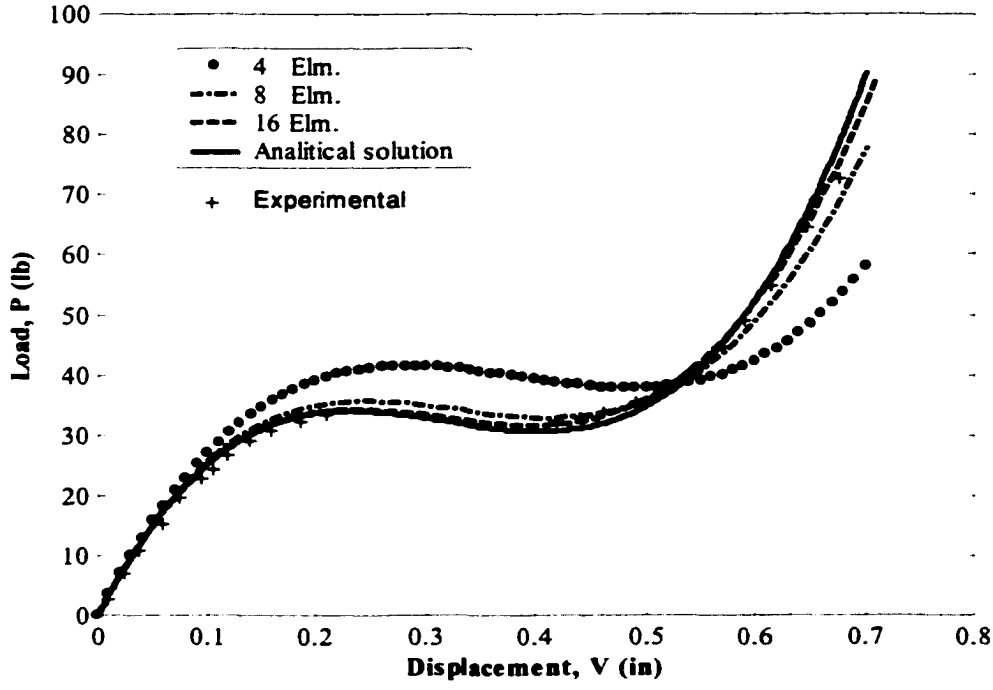

Figure 3-20 Load-displacement curves for the Williams toggle frame.

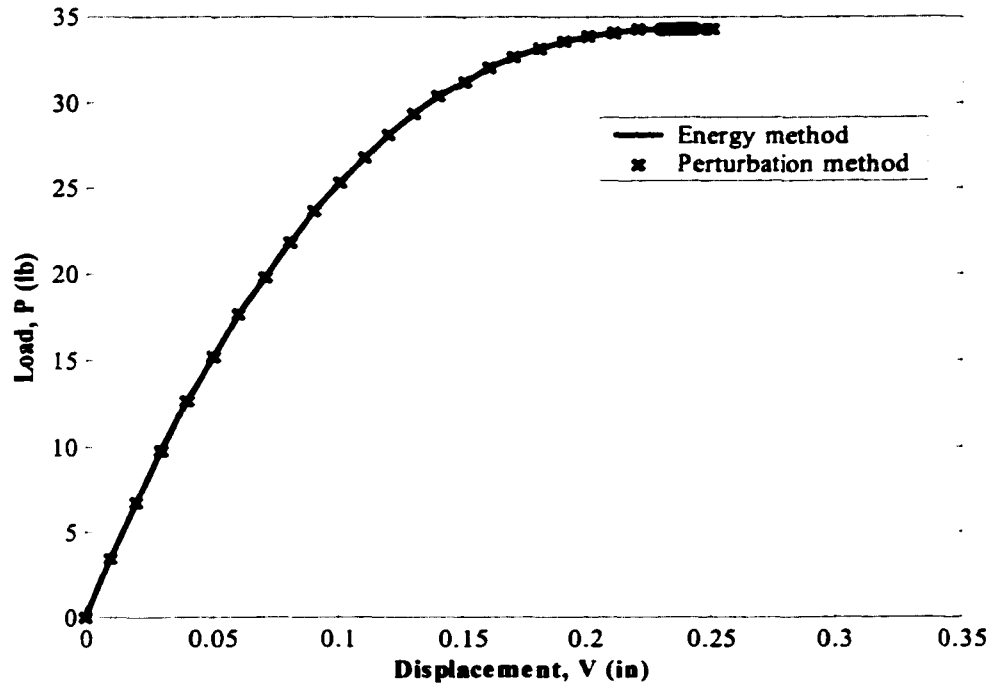

Figure 3-21 Load-displacement curve for the Williams toggle frame until limit load.

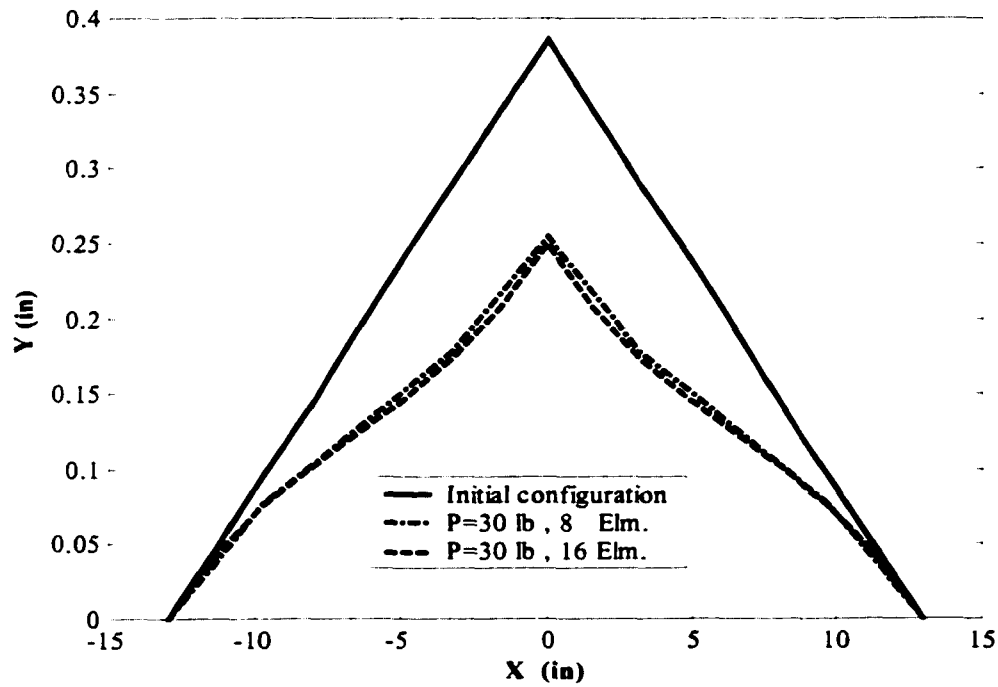

Figure 3-22 Configuration of the Williams toggle frame for various element numbers.

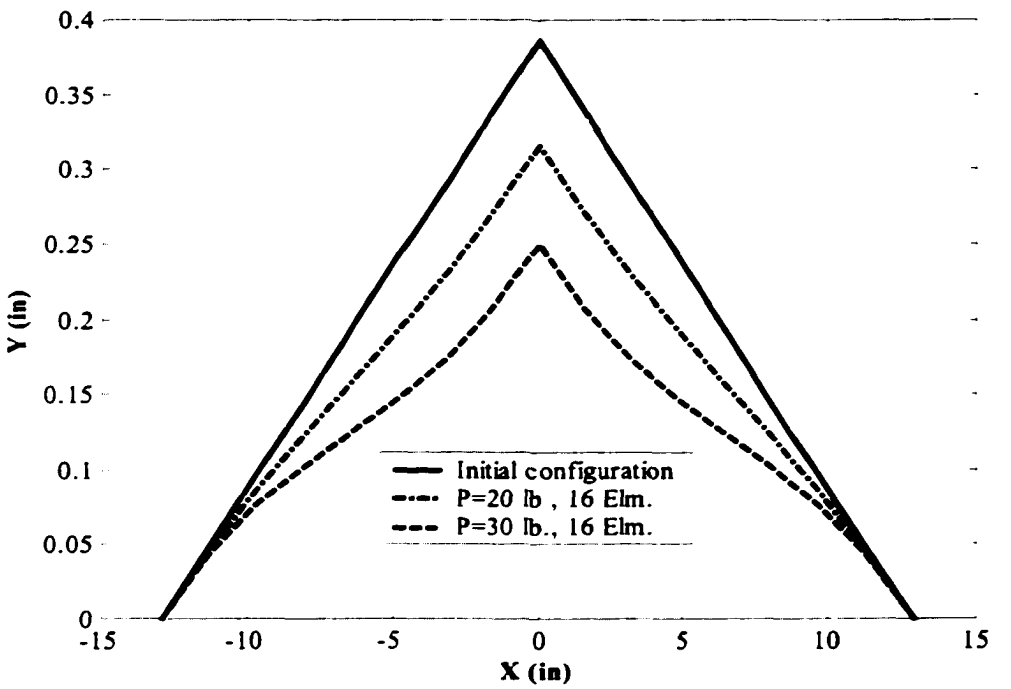

Figure 3-23 Different configurations for the Williams toggle frame.

3.5 Nonlinear Analysis of Symmetric Structures

Most methods used to solve static nonlinear problems are based on Newton's method or quasi-Newton methods. For a m-degree-of-freedom system, these methods require the solution of m simultaneous equations, repetitively. When the number of degrees of freedom is large, the cost of the solution becomes prohibitive. Researchers have proposed many schemes in an attempt to make the solution of nonlinear problems more efficient. For the special case of systems with structural symmetry, it has recently been shown that nonlinear solutions can be computed *exactly* with a reduced number of degrees of freedom based on the symmetry modes using a technique called the Group Theoretic Approach (GTA). The essence of the approach rests on reducing the number of degrees of freedom of the initial configuration by transformation of a large system to a similar much smaller subsystem. In general, the number of displacement degrees of freedom for a large system (m) is much larger than the dof of the reduced system, say m_r. The response **U** of the large system can be obtained by a combination of a few subspace

modes or basis vectors. This is done by expressing **U** as a product of a transformation matrix Φ and the response $\mathbf{U}_r$ of the reduced problem.

In the last decade, there has been a growing interest in the application of the GTA to the solution of nonlinear problems. The group theoretic foundations of the reduction method have been introduced by Healy [144-146]. Using a projection operator of group theory [147], Healey described, within the general setting of symmetric problems in structural mechanics, how to form a dimensionally reduced problem, which can lead to significant computational savings. This technique has been applied to elasto-statics and bifurcation problems. Subsequently, Chang and Healey [148] used the GTA to analyze geometrically nonlinear systems with symmetry. Recently, Li [149] solved static and dynamic analysis of nonlinear problems with symmetries using GTA. However, the nonlinear buckling analysis and post-buckling using GTA have not been reported in the literature.

In structural optimization of nonlinear problems, besides the nonlinear analysis, the optimization procedure has an iterative nature as well. Here, the GTA has been applied to nonlinear analysis of symmetric nonlinear structures, with particular emphasis on the nonlinear buckling analysis and post-buckling behaviour. The detailed theory on the GTA is documented in Refs.[144-148]. For the sake of completeness, a summary of the mathematical procedure is presented next.

3.5.1 Mathematical Formulation

The governing equation of motion (Eq. 3-14) may be expressed in a more compact form as

$$\mathbf{h}(\ddot{\mathbf{U}}, \mathbf{U}, \mathbf{P}) = \mathbf{h}_1(\ddot{\mathbf{U}}) + \mathbf{h}_2(\mathbf{U}) - \mathbf{P} = \mathbf{0} \qquad \textbf{(3-98)}$$

where $\mathbf{h}_1$ and $\mathbf{h}_2$ are functions of $\ddot{\mathbf{U}}$ and **U**, respectively and **h** is the function of $\ddot{\mathbf{U}}$, **U** and **P**.

Suppose Eq. (3-98) models a structure with m degrees of freedom. The undeformed geometry (shape), material properties and geometric boundary conditions have common nontrivial symmetry. Symmetry is characterized mathematically by an isometric (strain-

free) transformation of the undeformed structure into a completely equivalent configuration. The set of all such isometries, $S_G \equiv \{G_1, G_2, \cdots, G_N\}$; $G_i \in \Re^{3\times3}$ is called the symmetry group of the structure. It is noted that, for structural systems of finite dimensions, the relevant isometries are all 3×3 orthogonal matrices corresponding to rotations, reflections and inversion [147,150]. An orthogonal representation of a symmetry group of S_G on m-dimensional space is $T \equiv \{T_1, T_2, \cdots, T_N\}$; $T_i \in \Re^{m\times m}$ called rep of S_G on $\Re^{m\times m}$ and satisfies the following properties:

$T(G_1)T(G_2) = T(G_1G_2)$ for all G_1, $G_2 \in S_G$

$T^T(G_1) = T(G_1^T)$, $T^{-1}(G_1) = T(G_1^{-1})$ for all $G_1 \in S_G$

$T(I) = I$, where I is the $(m\times m)$ identity matrix.

Here, N is the number of reps. The equilibrium equations of symmetry models such as Eq. (3-98) reflect the symmetry of the mechanical or physical system through a property called the equivariance [145] . Eq. (3-98) is said to be equivariant under the action of T if

$$\mathbf{h}(T\ddot{\mathbf{U}}, T\mathbf{U}, \mathbf{P}) = T\mathbf{h}(\ddot{\mathbf{U}}, \mathbf{U}, \mathbf{P}). \tag{3-99}$$

The equivariance condition in Eq. (3-99) follows from the fact that the loading, material properties and the boundary conditions agree with the geometric symmetry of the structure. If any of these has less symmetry than the purely geometric symmetry, then an appropriate subgroup must be employed.

A symmetry solution to Eq. (3-99) consists of a nodal displacement vector $\mathbf{U}$ and a load magnitude $\mathbf{P}$ satisfying equilibrium such that $T\mathbf{U} = \mathbf{U}$. It can be shown [147] that the following average matrix,

$$Pr = \frac{1}{N}\sum_{i=1}^{N} T_i \tag{3-100}$$

is a symmetric ($\boldsymbol{Pr}^{\mathrm{T}} = \boldsymbol{Pr}$)projection ($\boldsymbol{Pr}\,\boldsymbol{Pr} = \boldsymbol{Pr}$)onto the subspace $\boldsymbol{U}_s \subseteq \Re^m$ of all symmetric displacement fields, which is called the symmetry subspace. If the m-vector Θ is in $\boldsymbol{U}_s$, then

$$\boldsymbol{Pr}\,\Theta = \Theta \tag{3-101}$$

i.e. Θ is an eigenvector of $\boldsymbol{Pr}$ corresponding to the unit eigenvalue. It can also be shown [147] that the dimension of $\boldsymbol{U}_s$ is given by

$$m_r = trace(\boldsymbol{Pr}) = \frac{1}{N}\sum_{i=1}^{N} trace(\boldsymbol{T}_i). \tag{3-102}$$

Hence, the multiplicity of the unit eigenvalue in Eq. (3-101) is equal to m_r.

The most useful way to construct a reduced problem is to define the basis for $\boldsymbol{U}_s$ as

$$\Phi = \{\Theta_1, \Theta_2, \cdots, \Theta_{m_r}\}, \text{ where } \Theta_i^{\,T}\Theta_j = \delta_{ij}. \tag{3-103}$$

These basis vectors Θ_i, $i = 1,2,\cdots,m_r$, which are solutions to Eq. (3-101), are called the symmetry modes. The matrix Φ, including the symmetry modes, is a $m \times m_r$ matrix. If the displacement vector $\mathbf{U}$ is in $\boldsymbol{U}_s$ (symmetry solution), then

$$\mathbf{U}_r = \Phi^T \mathbf{U} \tag{3-104}$$

is an m_r-vector with entries corresponding to the components of $\mathbf{U}$ relative to the basis $\{\Theta_1, \Theta_2, \cdots, \Theta_{m_r}\}$, i.e. $\mathbf{U}_{ri} = \Theta_i^{\,T}\mathbf{U}$, $i = 1,2,\ldots,m_r$. From Eq. (104)

$$\mathbf{U} = \Phi\,\mathbf{U}_r. \tag{3-105}$$

Considering Eqs. (3-105) and (3-98) and multiplying both sides by Φ^T the reduced problem may be given explicitly by

$$\Phi^T \mathbf{h}(\Phi\,\ddot{\mathbf{U}}_r, \Phi\,\mathbf{U}_r, \mathbf{P}) = \Phi^T \mathbf{h}_1(\Phi\,\ddot{\mathbf{U}}_r) + \Phi^T \mathbf{h}_2(\Phi\,\mathbf{U}_r) - \Phi^T \mathbf{P} = \mathbf{0} \tag{3-106}$$

and considering Eqs. (3-105) and Eq. (3-14), the equation becomes

$$\boldsymbol{M}_r\,\ddot{\mathbf{U}}_r + \boldsymbol{K}_r\,\mathbf{U}_r = \mathbf{P}_r \tag{3-107}$$

where

$$\boldsymbol{M}_r = \boldsymbol{\Phi}^T \boldsymbol{M} \boldsymbol{\Phi} \ , \quad \boldsymbol{K}_r = \boldsymbol{\Phi}^T \boldsymbol{K} \boldsymbol{\Phi} \ , \text{ and } \quad \mathbf{P}_r = \boldsymbol{\Phi}^T \mathbf{P}. \tag{3-108}$$

It should be noted that not all solutions of Eq. (3-14) are necessarily solutions of Eq. (3-107). Rather, the reduced problem captures only the symmetric solution points of Eq. (3-14). For example, in the nonlinear buckling analysis of symmetric structures, all symmetric solutions appear before the bifurcation point. Therefore, the reduced problem catches all solutions in the full space. After bifurcation, there may be symmetric and unsymmetric solutions in full space. In this case, the reduced problem only catches the symmetric solutions of the full space. In limit point problems, there are solely symmetric solutions before and after the limit point. In this case, the reduced space problems catch all solutions of full space following the limit point, as well.

In the nonlinear problems considered by Li [149], the GTA has been applied to nonlinear problem however the solutions did not reach the limit point. In this work, the GTA has been applied to nonlinear buckling analysis of symmetric problems. It is shown that, using GTA, it is possible to trace the post buckling path in limit point problems and the computation time can be reduced significantly compared to solutions obtained using the full space.

3.5.2 The Solution Procedure using GTA

The steps for obtaining the static response of symmetric nonlinear problems using GTA are as follows:

1) Compute the out-of-balance load vector $\Delta\mathbf{P}$.
2) Set up the reduced symmetry subspace, the basis vector $\boldsymbol{\Phi}$. The reduced stiffness matrix and the reduced out-of-balance force vector become $\boldsymbol{K}_r = \boldsymbol{\Phi}^T \boldsymbol{K} \boldsymbol{\Phi}$ and $\Delta\mathbf{P}_r = \boldsymbol{\Phi}^T \Delta\mathbf{P}$, respectively.
3) Solve the incremental displacements under the subspace. This computation involves solving the reduced system $\boldsymbol{K}_r \Delta\mathbf{U}_r = \Delta\mathbf{P}_r$, for the generalized incremental displacement vector $\Delta\mathbf{U}_r$ using the force or displacement control techniques.

4) Obtain the original full space incremental nodal displacement vector using $\Delta \mathbf{U} = \Phi \ \Delta \mathbf{U}_r$.
5) Update the nodal coordinates.
6) Compute new member forces.
7) Repeat step 1 through 6. The computation stops when the energy convergence criteria, Eq. (3-92), is satisfied.

3.5.3 Illustrative Example

Two numerical examples are considered to illustrate the application of the GTA. The first example depicts a three-member space truss. This simple symmetric structure has been selected to illustrate the construction of the projection operator, the calculation of the symmetry modes and subsequent analysis of the static response. The second example is selected to illustrate the accuracy of the GTA method and search for symmetry modes for complex structures.

i) The 3-bar Space Truss Structure

A three-member space truss, shown in Figure 3-24, with one free node (three translation degrees of freedom) is considered. The space truss has the following equivalent positions: (1) Rotation of the structure by 0° about the global Z axis, (2) Rotation of the structure by 120° about the global Z axis, (3) Rotation of the structure by 240° about the global Z axis, (4) Reflection of the structure across the plane through the Z and X axes. (5) Reflection of the structure across the plane through the Z axes and the line through the origin in the X-Y plane that makes a counterclockwise angle of 60° with the X axes. (6) Reflection of the structure across the plane through the Z axes and the line through the origin in the X-Y plane that makes a counterclockwise angle of 120° with the X axes.

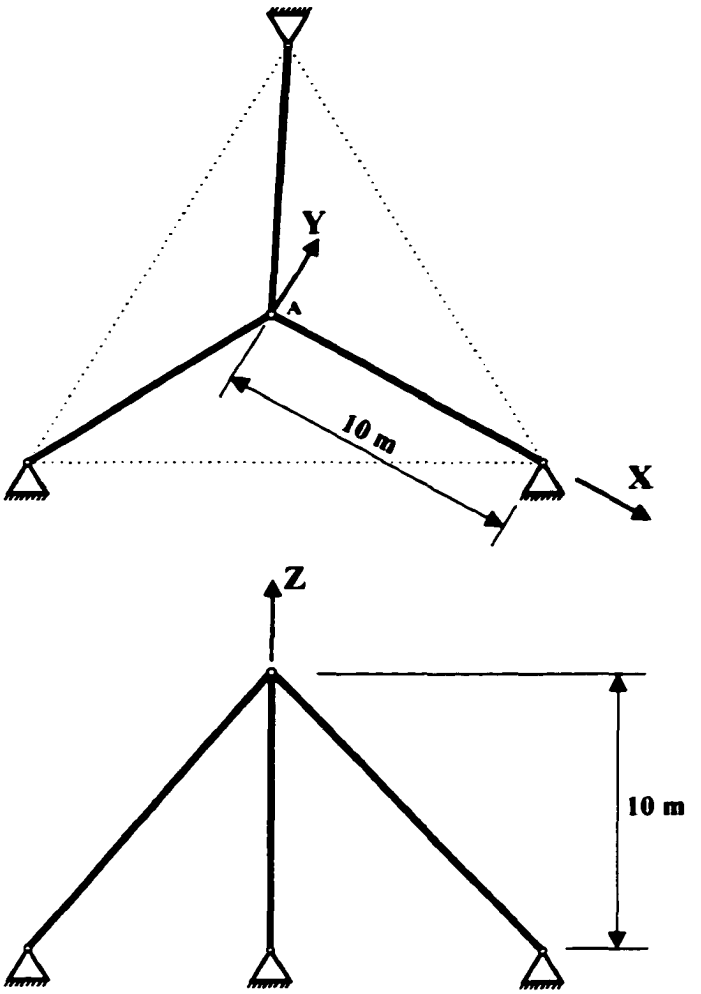

Figure 3-24 The 3-bar space truss structure.

In the Cartesian coordinate system, each of the above actions can be represented by a 3×3 orthogonal rotation or reflection matrix. The rotation about the Z axis through the counterclockwise angle θ is from the global coordinate system to the local axis of the members and therefore it is the transpose of the rotation matrix given by Eq. (3-54)

$$\boldsymbol{Rot}^{T} = \begin{bmatrix} \cos\theta & -\sin\theta & 0 \\ \sin\theta & \cos\theta & 0 \\ 0 & 0 & 1 \end{bmatrix}. \tag{3-109}$$

The reflection across a plane perpendicular to the X-Y plane that makes a counter clockwise angle of $\theta/2$ with the X-Z plane, is given by

$$\boldsymbol{Ref} = \begin{bmatrix} \cos\theta & \sin\theta & 0 \\ \sin\theta & -\cos\theta & 0 \\ 0 & 0 & 1 \end{bmatrix}. \tag{3-110}$$

The complete symmetry group of the structural configuration is the set of all orthogonal transformations that map the system into an equivalent configuration, expressed as

$$\boldsymbol{T}_1 = \boldsymbol{Rot}^T(0^\circ) = \begin{bmatrix} 1 & 0 & 0 \\ 0 & 1 & 0 \\ 0 & 0 & 1 \end{bmatrix}, \qquad \boldsymbol{T}_2 = \boldsymbol{Rot}^T(120^\circ) = \begin{bmatrix} -1/2 & -\sqrt{3}/2 & 0 \\ \sqrt{3}/2 & -1/2 & 0 \\ 0 & 0 & 1 \end{bmatrix},$$

$$\boldsymbol{T}_3 = \boldsymbol{Rot}^T(240^\circ) = \begin{bmatrix} -1/2 & \sqrt{3}/2 & 0 \\ \sqrt{3}/2 & -1/2 & 0 \\ 0 & 0 & 1 \end{bmatrix}, \quad \boldsymbol{T}_4 = \boldsymbol{Ref}(0^\circ) = \begin{bmatrix} 1 & 0 & 0 \\ 0 & -1 & 0 \\ 0 & 0 & 1 \end{bmatrix}$$

$$\boldsymbol{T}_5 = \boldsymbol{Ref}(120^\circ) = \begin{bmatrix} -1/2 & \sqrt{3}/2 & 0 \\ \sqrt{3}/2 & 1/2 & 0 \\ 0 & 0 & 1 \end{bmatrix}, \quad \boldsymbol{T}_6 = \boldsymbol{Ref}(240^\circ) = \begin{bmatrix} -1/2 & -\sqrt{3}/2 & 0 \\ -\sqrt{3}/2 & 1/2 & 0 \\ 0 & 0 & 1 \end{bmatrix} \tag{3-111}$$

The dimension of the symmetry sub-space $\boldsymbol{U}_s$, by virtue of Eq. (3-102) is:

$$\begin{aligned} m_r = \frac{1}{6}[&(1+1+1)+(-1/2-1/2+1)+(-1/2-1/2+1)+(1-1+1) \\ &+(-1/2+1/2+1)+(-1/2+1/2+1)] = 1 \end{aligned} \tag{3-112}$$

This means that the deformation of the space truss can be characterized by one single basis matrix. Using Eq. (3-100), the projection operator is given by

$$\boldsymbol{Pr} = \begin{bmatrix} 0 & 0 & 0 \\ 0 & 0 & 0 \\ 0 & 0 & 1 \end{bmatrix}. \tag{3-113}$$

Eigenvectors with unit eigenvalue can be extracted from Eq. (3-113). $\Theta_1 = [0 \quad 0 \quad 1]^T$ is the only basis eigenvector (symmetry mode) which is a solution of Eq. (3-113). Thus, the transformation matrix Φ becomes

$$\Phi = \Theta_1. \tag{3-114}$$

Using this subspace, the GTA is developed for the analysis of the geometrically nonlinear three-bar truss structure. Two cases are studied to demonstrate the performance of the GTA.

First, the truss is loaded vertically downwards at its central node with P=100 N. The length of each member is L=14.14 m , the cross-sectional area of each member is A = 1 m^2; and the height is H=10 m. The Young's modulus is E=10000 N/m^2.

An energy convergence criteria of $\varepsilon_E = 10^{-7}$ was used here. Using the force control technique, the nonlinear analysis of both the full space and the reduced subspace are performed to obtain the displacement vector at the central node 4.

Table 3-1 The displacement vector at the central node 4 for the 3-bar space truss (m).

Full space	**Reduced Subspace**	**Ref.[149]**
[0 0 -0 .0949604329] ^{T}	[0 0 -0 .0949604329]^T	[0 0 -0 .0942809038]^T

Table 3-1 shows that the results computed using the finite element force control method with full space and reduced subspace match exactly. The number of iterations for nonlinear analysis using both the full space and reduced subspace is 3. The computational effort in the full space was 1.5 times higher than the reduce subspace solution. Also, the results almost match the solution reported in Ref. [149].

Next, the nonlinear buckling analysis of the structure is carried out. Here we assume that H=1. This example illustrates the application of GTA to nonlinear buckling analysis using the displacement control method. The vertical displacement at the apex (W) of the structure (node 4) is considered the controlling displacement and it is incremented in steps of 0.1 m per displacement step.

Figure 3-25 shows the nonlinear buckling analysis until the limit load is reached using both the full space and the reduced subspace for the three-bar space truss. There is

excellent agreement between the two solution spaces. The limit load is obtained with an accuracy of the order of 10^{-6}. When the solution process reaches close to the limit point, the controlling displacement is automatically incremented in steps smaller than the assigned (0.1 m per time steps.). This reduction in step size continues until the limit point is found with the desired accuracy. The solution using both spaces revealed a limit load of 2811.049 N. The number of time steps needed to catch the limit point using the full space and the subspace were 145 and 136, respectively. The computational effort for the full space was 2.5 times higher than the reduced space solution. Convergence was achieved at each displacement step in one or two iterations for both solution spaces.

Figure 3-26 shows the post-buckling solution path. There is perfect agreement between the full space and the reduced subspace in post-buckling path solution. The number of time steps in both the full space and the reduced subspace is 80 and the computational effort in full space was 2 times higher than the reduced subspace solution.

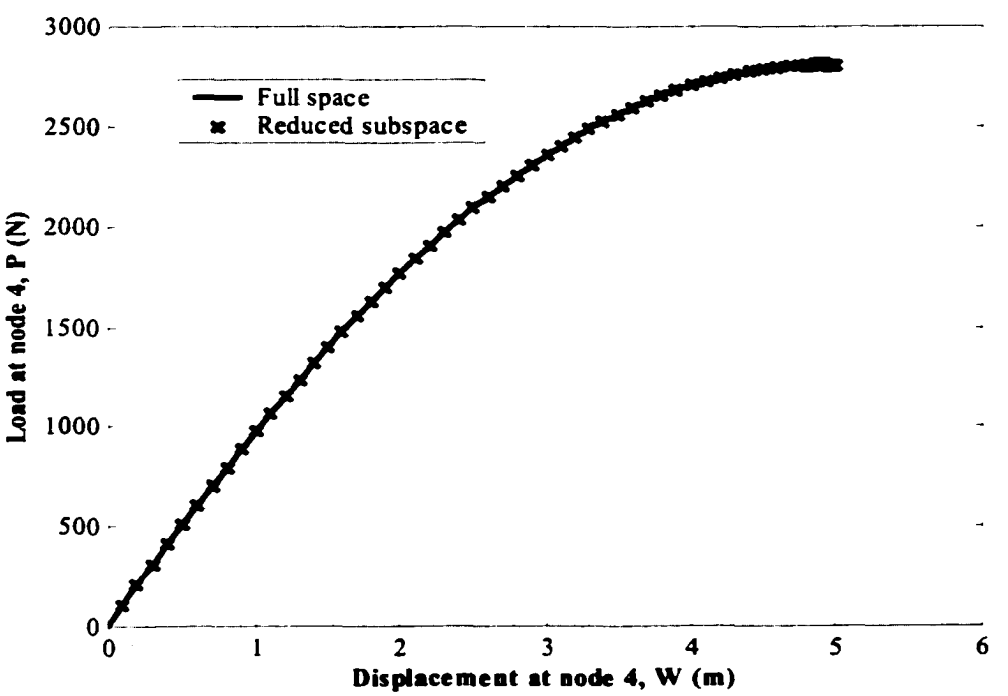

Figure 3-25 Load-Deflection curve for 3-bar space truss until limit load.

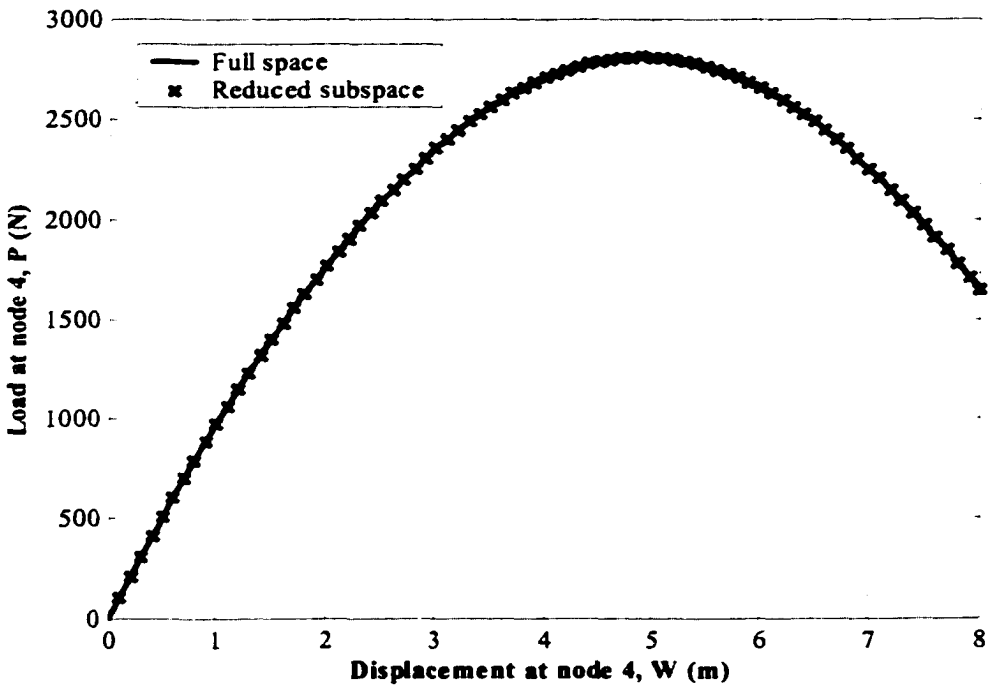

Figure 3-26 Load-Deflection curve for 3-bar space truss (post-buckling)

In all cases above, it can be observed that there is significant computation reduction in reduced subspace in comparison to full space.

ii) The 24-Bar Dome Space Truss

This complex structure is shown in Fig. (3-27). It is made of twenty-four bars and the six vertices are fixed so that there are seven nodes free to move with a total of 21 degrees of freedom. This structure has six equivalent configurations corresponding to rotating the structure through angles of $n\pi/3$; $n = 0,1,\ldots,5$, and six equivalent configurations corresponding to reflection of the structure across the plane through the Z-axis and the line through the origin in the X-Y plane that makes a counterclockwise angle of $n\pi/6$; $n = 0,1,\ldots,5$ with the X-axis. Using the rotation and reflection matrices as defined in the previous example, these 12 equivalent configurations can be described by the following matrices:

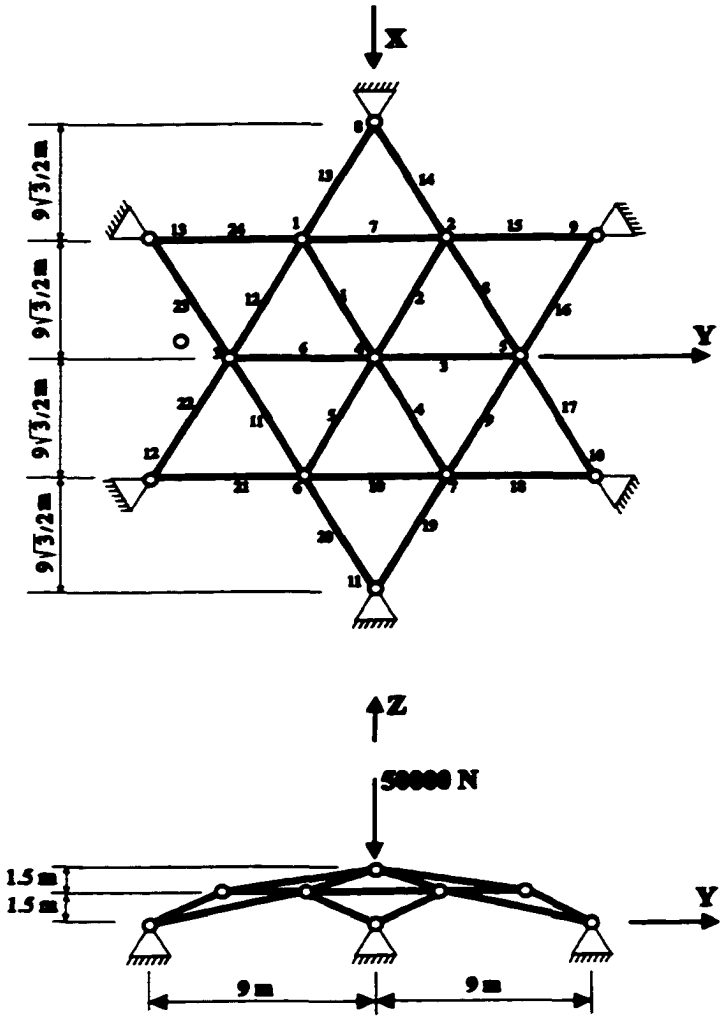

Figure 3-27 The 24-bar space dome truss structure.

$$T_1 = Rot^T(0)(U_1, U_2, U_3, U_4, U_5, U_6, U_7)$$

$$= \begin{bmatrix} Rot^T(0) & 0 & 0 & 0 & 0 & 0 & 0 \\ 0 & Rot^T(0) & 0 & 0 & 0 & 0 & 0 \\ 0 & 0 & Rot^T(0) & 0 & 0 & 0 & 0 \\ 0 & 0 & 0 & Rot^T(0) & 0 & 0 & 0 \\ 0 & 0 & 0 & 0 & Rot^T(0) & 0 & 0 \\ 0 & 0 & 0 & 0 & 0 & Rot^T(0) & 0 \\ 0 & 0 & 0 & 0 & 0 & 0 & Rot^T(0) \end{bmatrix}$$

$$T_2 = \boldsymbol{Rot}^T(60)(\mathbf{U}_2,\mathbf{U}_5,\mathbf{U}_1,\mathbf{U}_4,\mathbf{U}_7,\mathbf{U}_3,\mathbf{U}_6)$$

$$= \begin{bmatrix} 0 & \boldsymbol{Rot}^T(60) & 0 & 0 & 0 & 0 & 0 \\ 0 & 0 & 0 & 0 & \boldsymbol{Rot}^T(60) & 0 & 0 \\ \boldsymbol{Rot}^T(60) & 0 & 0 & 0 & 0 & 0 & 0 \\ 0 & 0 & 0 & \boldsymbol{Rot}^T(60) & 0 & 0 & 0 \\ 0 & 0 & 0 & 0 & 0 & 0 & \boldsymbol{Rot}^T(60) \\ 0 & 0 & \boldsymbol{Rot}^T(60) & 0 & 0 & 0 & 0 \\ 0 & 0 & 0 & 0 & 0 & \boldsymbol{Rot}^T(60) & 0 \end{bmatrix}$$

$$T_3 = \boldsymbol{Rot}^T(120)(\mathbf{U}_5,\mathbf{U}_7,\mathbf{U}_2,\mathbf{U}_4,\mathbf{U}_6,\mathbf{U}_1,\mathbf{U}_3)$$

$$= \begin{bmatrix} 0 & 0 & 0 & 0 & \boldsymbol{Rot}^T(120) & 0 & 0 \\ 0 & 0 & 0 & 0 & 0 & 0 & \boldsymbol{Rot}^T(120) \\ 0 & \boldsymbol{Rot}^T(120) & 0 & 0 & 0 & 0 & 0 \\ 0 & 0 & 0 & \boldsymbol{Rot}^T(120) & 0 & 0 & 0 \\ 0 & 0 & 0 & 0 & 0 & \boldsymbol{Rot}^T(120) & 0 \\ \boldsymbol{Rot}^T(120) & 0 & 0 & 0 & 0 & 0 & 0 \\ 0 & 0 & \boldsymbol{Rot}^T(120) & 0 & 0 & 0 & 0 \end{bmatrix}$$

$$T_4 = \boldsymbol{Rot}^T(180)(\mathbf{U}_7,\mathbf{U}_6,\mathbf{U}_5,\mathbf{U}_4,\mathbf{U}_3,\mathbf{U}_2,\mathbf{U}_1)$$

$$= \begin{bmatrix} 0 & 0 & 0 & 0 & 0 & 0 & \boldsymbol{Rot}^T(180) \\ 0 & 0 & 0 & 0 & 0 & \boldsymbol{Rot}^T(180) & 0 \\ 0 & 0 & 0 & 0 & \boldsymbol{Rot}^T(180) & 0 & 0 \\ 0 & 0 & 0 & \boldsymbol{Rot}^T(180) & 0 & 0 & 0 \\ 0 & 0 & \boldsymbol{Rot}^T(180) & 0 & 0 & 0 & 0 \\ 0 & \boldsymbol{Rot}^T(180) & 0 & 0 & 0 & 0 & 0 \\ \boldsymbol{Rot}^T(180) & 0 & 0 & 0 & 0 & 0 & 0 \end{bmatrix}$$

$$T_5 = \mathbf{Rot}^T(240)(\mathbf{U}_6,\mathbf{U}_3,\mathbf{U}_7,\mathbf{U}_4,\mathbf{U}_1,\mathbf{U}_5,\mathbf{U}_2)$$

$$= \begin{bmatrix} 0 & 0 & 0 & 0 & 0 & \mathbf{Rot}^T(240) & 0 \\ 0 & 0 & \mathbf{Rot}^T(240) & 0 & 0 & 0 & 0 \\ 0 & 0 & 0 & 0 & 0 & 0 & \mathbf{Rot}^T(240) \\ 0 & 0 & 0 & \mathbf{Rot}^T(240) & 0 & 0 & 0 \\ \mathbf{Rot}^T(240) & 0 & 0 & 0 & 0 & 0 & 0 \\ 0 & 0 & 0 & 0 & \mathbf{Rot}^T(240) & 0 & 0 \\ 0 & \mathbf{Rot}^T(240) & 0 & 0 & 0 & 0 & 0 \end{bmatrix}$$

$$T_6 = \mathbf{Rot}^T(300(\mathbf{U}_3,\mathbf{U}_1,\mathbf{U}_6,\mathbf{U}_4,\mathbf{U}_2,\mathbf{U}_7,\mathbf{U}_5)$$

$$= \begin{bmatrix} 0 & 0 & \mathbf{Rot}^T(300) & 0 & 0 & 0 & 0 \\ \mathbf{Rot}^T(300) & 0 & 0 & 0 & 0 & 0 & 0 \\ 0 & 0 & 0 & 0 & 0 & \mathbf{Rot}^T(300) & 0 \\ 0 & 0 & 0 & \mathbf{Rot}^T(300) & 0 & 0 & 0 \\ 0 & \mathbf{Rot}^T(300) & 0 & 0 & 0 & 0 & 0 \\ 0 & 0 & 0 & 0 & 0 & 0 & \mathbf{Rot}^T(300) \\ 0 & 0 & 0 & 0 & \mathbf{Rot}^T(300) & 0 & 0 \end{bmatrix}$$

$$T_7 = \mathbf{Ref}(0)(\mathbf{U}_2,\mathbf{U}_1,\mathbf{U}_5,\mathbf{U}_4,\mathbf{U}_3,\mathbf{U}_7,\mathbf{U}_6)$$

$$= \begin{bmatrix} 0 & \mathbf{Ref}(0) & 0 & 0 & 0 & 0 & 0 \\ \mathbf{Ref}(0) & 0 & 0 & 0 & 0 & 0 & 0 \\ 0 & 0 & 0 & 0 & \mathbf{Ref}(0) & 0 & 0 \\ 0 & 0 & 0 & \mathbf{Ref}(0) & 0 & 0 & 0 \\ 0 & 0 & \mathbf{Ref}(0) & 0 & 0 & 0 & 0 \\ 0 & 0 & 0 & 0 & 0 & 0 & \mathbf{Ref}(0) \\ 0 & 0 & 0 & 0 & 0 & \mathbf{Ref}(0) & 0 \end{bmatrix}$$

$$T_8 = \mathit{Ref}(60)(\mathbf{U}_1, \mathbf{U}_3, \mathbf{U}_2, \mathbf{U}_4, \mathbf{U}_6, \mathbf{U}_5, \mathbf{U}_7)$$

$$= \begin{bmatrix} \mathit{Ref}(60) & 0 & 0 & 0 & 0 & 0 & 0 \\ 0 & 0 & \mathit{Ref}(60) & 0 & 0 & 0 & 0 \\ 0 & \mathit{Ref}(60) & 0 & 0 & 0 & 0 & 0 \\ 0 & 0 & 0 & \mathit{Ref}(60) & 0 & 0 & 0 \\ 0 & 0 & 0 & 0 & 0 & \mathit{Ref}(60) & 0 \\ 0 & 0 & 0 & 0 & \mathit{Ref}(60) & 0 & 0 \\ 0 & 0 & 0 & 0 & 0 & 0 & \mathit{Ref}(60) \end{bmatrix}$$

$$T_9 = \mathit{Ref}(120)(\mathbf{U}_3, \mathbf{U}_6, \mathbf{U}_1, \mathbf{U}_4, \mathbf{U}_7, \mathbf{U}_2, \mathbf{U}_5)$$

$$= \begin{bmatrix} 0 & 0 & \mathit{Ref}(120) & 0 & 0 & 0 & 0 \\ 0 & 0 & 0 & 0 & 0 & \mathit{Ref}(120) & 0 \\ \mathit{Ref}(120) & 0 & 0 & 0 & 0 & 0 & 0 \\ 0 & 0 & 0 & \mathit{Ref}(120) & 0 & 0 & 0 \\ 0 & 0 & 0 & 0 & 0 & 0 & \mathit{Ref}(120) \\ 0 & \mathit{Ref}(120) & 0 & 0 & 0 & 0 & 0 \\ 0 & 0 & 0 & 0 & \mathit{Ref}(120) & 0 & 0 \end{bmatrix}$$

$$T_{10} = \mathit{Ref}(180)(\mathbf{U}_6, \mathbf{U}_7, \mathbf{U}_3, \mathbf{U}_4, \mathbf{U}_5, \mathbf{U}_1, \mathbf{U}_2)$$

$$= \begin{bmatrix} 0 & 0 & 0 & 0 & 0 & \mathit{Ref}(180) & 0 \\ 0 & 0 & 0 & 0 & 0 & 0 & \mathit{Ref}(180) \\ 0 & 0 & \mathit{Ref}(180) & 0 & 0 & 0 & 0 \\ 0 & 0 & 0 & \mathit{Ref}(180) & 0 & 0 & 0 \\ 0 & 0 & 0 & 0 & \mathit{Ref}(180) & 0 & 0 \\ \mathit{Ref}(180) & 0 & 0 & 0 & 0 & 0 & 0 \\ 0 & \mathit{Ref}(180) & 0 & 0 & 0 & 0 & 0 \end{bmatrix}$$

$$T_{11} = \mathbf{Ref}(240)(\mathbf{U}_7,\mathbf{U}_5,\mathbf{U}_6,\mathbf{U}_4,\mathbf{U}_2,\mathbf{U}_3,\mathbf{U}_1)$$

$$= \begin{bmatrix} \mathbf{0} & \mathbf{0} & \mathbf{0} & \mathbf{0} & \mathbf{0} & \mathbf{0} & \mathbf{Ref}(240) \\ \mathbf{0} & \mathbf{0} & \mathbf{0} & \mathbf{0} & \mathbf{Ref}(240) & \mathbf{0} & \mathbf{0} \\ \mathbf{0} & \mathbf{0} & \mathbf{0} & \mathbf{0} & \mathbf{0} & \mathbf{Ref}(240) & \mathbf{0} \\ \mathbf{0} & \mathbf{0} & \mathbf{0} & \mathbf{Ref}(240) & \mathbf{0} & \mathbf{0} & \mathbf{0} \\ \mathbf{0} & \mathbf{Ref}(240) & \mathbf{0} & \mathbf{0} & \mathbf{0} & \mathbf{0} & \mathbf{0} \\ \mathbf{0} & \mathbf{0} & \mathbf{Ref}(240) & \mathbf{0} & \mathbf{0} & \mathbf{0} & \mathbf{0} \\ \mathbf{Ref}(240) & \mathbf{0} & \mathbf{0} & \mathbf{0} & \mathbf{0} & \mathbf{0} & \mathbf{0} \end{bmatrix}$$

$$T_{12} = \mathbf{Ref}(300)(\mathbf{U}_5,\mathbf{U}_2,\mathbf{U}_7,\mathbf{U}_4,\mathbf{U}_1,\mathbf{U}_6,\mathbf{U}_3)$$

$$= \begin{bmatrix} \mathbf{0} & \mathbf{0} & \mathbf{0} & \mathbf{0} & \mathbf{Ref}(300) & \mathbf{0} & \mathbf{0} \\ \mathbf{0} & \mathbf{Ref}(300) & \mathbf{0} & \mathbf{0} & \mathbf{0} & \mathbf{0} & \mathbf{0} \\ \mathbf{0} & \mathbf{0} & \mathbf{0} & \mathbf{0} & \mathbf{0} & \mathbf{0} & \mathbf{Ref}(300) \\ \mathbf{0} & \mathbf{0} & \mathbf{0} & \mathbf{Ref}(300) & \mathbf{0} & \mathbf{0} & \mathbf{0} \\ \mathbf{Ref}(300) & \mathbf{0} & \mathbf{0} & \mathbf{0} & \mathbf{0} & \mathbf{0} & \mathbf{0} \\ \mathbf{0} & \mathbf{0} & \mathbf{0} & \mathbf{0} & \mathbf{0} & \mathbf{Ref}(300) & \mathbf{0} \\ \mathbf{0} & \mathbf{0} & \mathbf{Ref}(300) & \mathbf{0} & \mathbf{0} & \mathbf{0} & \mathbf{0} \end{bmatrix}$$

(3-115)

Here, $\mathbf{Rot}(\theta)$ and $\mathbf{Ref}(\theta)$ are defined by Eqs. (3-109) and (3-110), respectively; $\mathbf{0}$ is a 3×3 zero matrix, and $\mathbf{U}_i$ is the displacement vector of the i^{th} node.

Using Eq. (3-102), the dimension of the symmetry reduced subspace for the twenty-four bar space dome structure is

$$m_r = \frac{1}{12}(21+2+0-1+0+2+3+1+3+1+3+1) = 3. \qquad \textbf{(3-116)}$$

Using Eq. (3-100), the projection operator becomes

$$Pr = \begin{bmatrix} A1 & B1 & C1 & 0 & D1 & E1 & F1 \\ \cdot & B2 & C2 & 0 & D2 & E2 & F2 \\ \cdot & \cdot & C3 & 0 & D3 & E3 & F3 \\ \cdot & \cdot & \cdot & G & 0 & 0 & 0 \\ \cdot & \cdot & \cdot & \cdot & C3 & B3 & A3 \\ S & Y & M & \cdot & \cdot & B2 & A2 \\ \cdot & \cdot & \cdot & \cdot & \cdot & \cdot & A1 \end{bmatrix} \tag{3-117}$$

where

$$A1 = \begin{bmatrix} 0.1250 & 0.0722 & 0 \\ 0.0722 & 0.0417 & 0 \\ 0 & 0 & 0.1667 \end{bmatrix}, \quad B1 = \begin{bmatrix} 0.1250 & -0.0722 & 0 \\ 0.0722 & -0.0417 & 0 \\ 0 & 0 & 0.1667 \end{bmatrix} = A2^T$$

$$B2 = \begin{bmatrix} 0.1250 & -0.0722 & 0 \\ -0.0722 & 0.0417 & 0 \\ 0 & 0 & 0.1667 \end{bmatrix}, \quad C1 = \begin{bmatrix} 0 & 0.1443 & 0 \\ 0 & 0.0833 & 0 \\ 0 & 0 & 0.1667 \end{bmatrix} = A3^T$$

$$C2 = \begin{bmatrix} 0 & 0.1443 & 0 \\ 0 & -0.0833 & 0 \\ 0 & 0 & 0.1667 \end{bmatrix} = B3^T, \quad C3 = \begin{bmatrix} 0 & 0 & 0 \\ 0 & 0.1667 & 0 \\ 0 & 0 & 0.1667 \end{bmatrix}$$

$$D1 = \begin{bmatrix} 0 & -0.1443 & 0 \\ 0 & -0.0833 & 0 \\ 0 & 0 & 0.1667 \end{bmatrix}, \quad D2 = \begin{bmatrix} 0 & -0.1443 & 0 \\ 0 & 0.0833 & 0 \\ 0 & 0 & 0.1667 \end{bmatrix}$$

$$D3 = \begin{bmatrix} 0 & 0 & 0 \\ 0 & -0.1667 & 0 \\ 0 & 0 & 0.1667 \end{bmatrix}, \quad E1 = \begin{bmatrix} -0.1250 & 0.0722 & 0 \\ -0.0722 & 0.0417 & 0 \\ 0 & 0 & 0.1667 \end{bmatrix}$$

$$E2 = \begin{bmatrix} -0.1250 & 0.0722 & 0 \\ 0.0722 & -0.0417 & 0 \\ 0 & 0 & 0.1667 \end{bmatrix}, \quad E3 = \begin{bmatrix} 0 & 0 & 0 \\ -0.1443 & 0.0833 & 0 \\ 0 & 0 & 0.1667 \end{bmatrix}$$

$$F1 = \begin{bmatrix} -0.1250 & -0.0722 & 0 \\ -0.0722 & -0.0417 & 0 \\ 0 & 0 & 0.1667 \end{bmatrix}, \quad F2 = \begin{bmatrix} -0.1250 & -0.0722 & 0 \\ 0.0722 & 0.0417 & 0 \\ 0 & 0 & 0.1667 \end{bmatrix}$$

$$F3 = \begin{bmatrix} 0 & 0 & 0 \\ -0.1443 & -0.0833 & 0 \\ 0 & 0 & 0.1667 \end{bmatrix}, \qquad G = \begin{bmatrix} 0 & 0 & 0 \\ 0 & 0 & 0 \\ 0 & 0 & 1 \end{bmatrix}$$

The eigenvectors of **Pr**, corresponding to an eigenvalue of unity according to Eq. (117), can now be obtained. Since $m_r = 3$, we have three eigenvectors as

$$\Phi = [\Theta_1 \quad \Theta_2 \quad \Theta_3]. \tag{3-118}$$

These eigenvectors represent the basis vectors that span the symmetry subspace, and they are listed in Table 3-2. Note that the twenty-one degrees of freedom in the original full space are now reduced to three dimensional symmetry subspace

Table 3-2 The basis vectors spanning the subspace of the 24-bar space dome truss.

Θ_1	Θ_2	Θ_3
0.000000	0.000000	0.353553
0.000000	0.000000	0.204124
0.000000	0.408248	0.000000
0.000000	0.000000	0.353553
0.000000	0.000000	-0.204124
0.000000	0.408248	0.000000
0.000000	0.000000	0.000000
0.000000	0.000000	0.408248
0.000000	0.408248	0.000000
0.000000	0.000000	0.000000
0.000000	0.000000	0.000000
1.000000	0.000000	0.000000
0.000000	0.000000	0.000000
0.000000	0.000000	-0.408248
0.000000	0.408248	0.000000
0.000000	0.000000	-0.353553
0.000000	0.000000	0.204124
0.000000	0.408248	0.000000
0.000000	0.000000	-0.353553
0.000000	0.000000	-0.204124
0.000000	0.408248	0.000000

The Young's modulus and cross-sectional areas of all members are assumed to be $E=73\times10^{11}$ N/m^2 and A=5 cm^2, respectively.

Using the displacement control technique, the nonlinear buckling analysis using both the full space and reduced subspace are performed to obtain the limit load. The application of GTA to nonlinear buckling analysis using the displacement control method is illustrated. The vertical displacement at the apex (W) of the structure (node 4) is considered to be the controlling displacement and it is incremented in steps of 0.01 m per displacement step.

Figure 3-28 shows the nonlinear buckling response until the limit load is reached using both the full space and the reduced subspace. There is excellent agreement between the full and reduced solutions. The limit load was obtained with accuracy of the order of 10^{-5}. The limit load was found to be 111,729.2 N. The number of time steps needed to catch limit point was 85. The computational time using the full space was 5 times higher than the reduced space solution.

Figure 3-29 shows the post-buckling solution path. There is a perfect match between the two solutions. The number of time steps for both spaces was 100 and the computational time required for the analysis was 4 times higher using the full space.

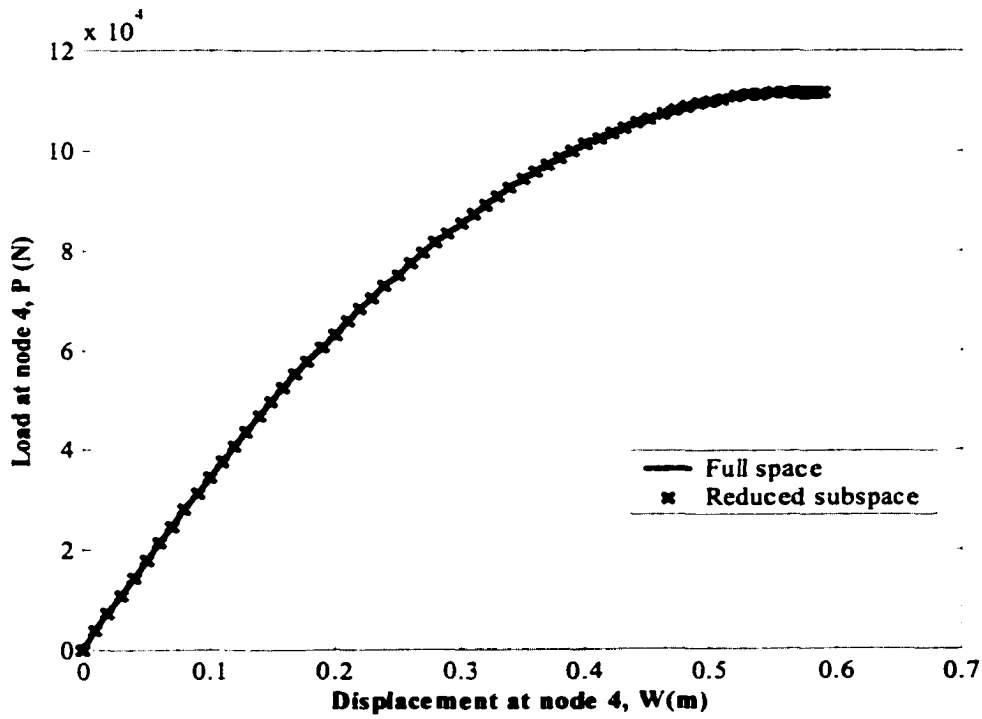

Figure 3-28 Load-deflection curve for the 24-bar space dome truss until limit load.

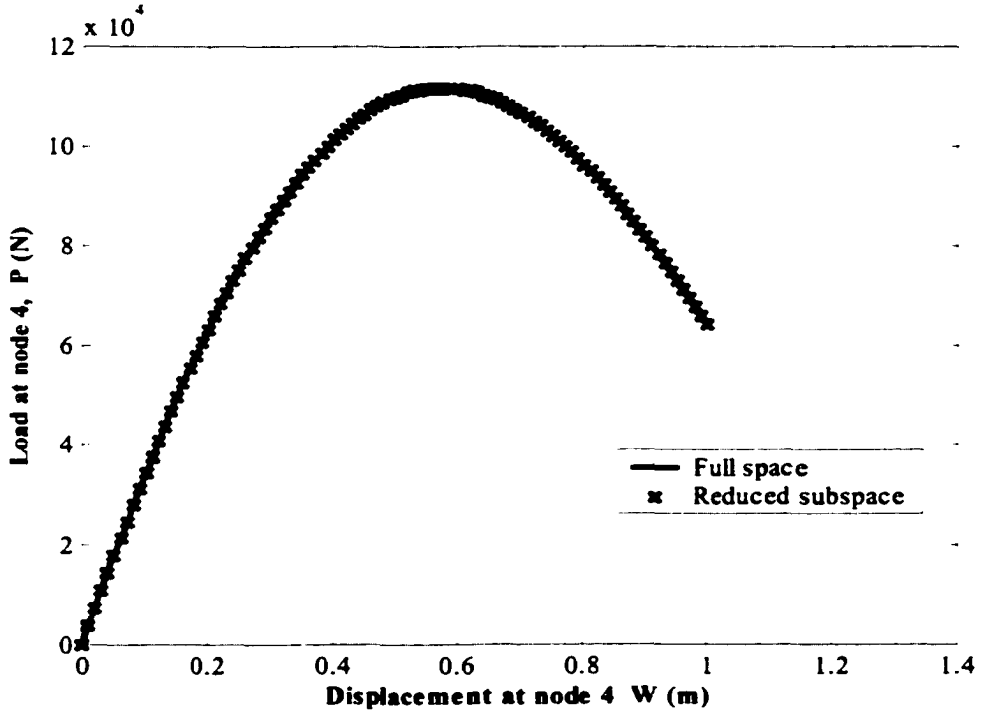

Figure 3-29 Load-deflection curve for the 24-bar space dome truss (post-buckling).

Chapter 4

STRUCTURAL DESIGN OPTIMIZATION

4.1 Introduction

A structural optimization process consists of two steps: analysis and optimization. Appropriate analysis techniques for linear and nonlinear structural problems have been presented in the preceding chapters. Here, the techniques and algorithms developed and used during the optimization step are presented.

A general constrained optimization problem may be described as

$$\begin{aligned} &\text{minimize} && f(\mathbf{X}) \\ &\text{subject to} && \mathbf{g}_i(\mathbf{X}) = 0 \quad i = 1,2,\cdots,n_e \\ &&& \mathbf{g}_i(\mathbf{X}) \le 0 \quad i = n_e+1, n_e+2,\cdots,n_i \\ &&& \mathbf{X}_l \le \mathbf{X} \le \mathbf{X}_u \end{aligned} \tag{4-1}$$

where $\mathbf{X}$ ($\mathbf{X} \in \Re^{n_d}$) is the design variable vector, $f(\mathbf{X})$ is the objective function that returns a scalar value ($f(\mathbf{X}) : \Re^{n_d} \rightarrow \Re$), and the vector function $\mathbf{g}(\mathbf{X}) = [g_1, g_2, \ldots, g_{n_c}]^T$ returns the values of the equality and inequality constraints evaluated at $\mathbf{X}$ ($\mathbf{g}(\mathbf{X}) : \Re^{n_d} \rightarrow \Re^{n_c}$). $\mathbf{X}_l$ and $\mathbf{X}_u$ are lower and upper bounds of the design variable vector. Constraints such as $\mathbf{g}_i(\mathbf{X})$ are usually called behavior constraints and the constraints on the design variables are called side constraints. The values n_d, n_e, n_i are the number of the design variables, number of equality and inequality constraints, respectively and $n_c = n_e + n_i + n_d$ is the total number of constraints, respectively.

For optimum structural design, the design variables are selected so as to minimize or maximize the objective function while satisfying all the constraints. The objective function may be, for example, the weight in size optimization problems, or the structural strength in topology optimization problems. The constraints may be the maximum allowable stresses in the elements, the displacement limits at the joints, the geometry

limitations, the frequency specifications, the system stability, etc. Depending on the nature of the applied loads, the structure and its geometry, one or more of the constraints can be active and control the design process. The design variables of the structure will generally be controlled by the dominant constraints.

Here, two types of optimization problems are studied: the size optimization of linear and nonlinear structures and the topology optimization of adaptive structures. In the size optimization problems, the weight of structure is the objective function and the design variables are the cross-sectional area of the elements. Topology optimization problems are applied to adaptive truss structures with the objective of maximizing the structural strength (objective function) and the design variables are the active members angle.

Two types of constraints are considered: behavior and side constraints. Behavior constraints include stress, displacement, frequency and system stability constraints. Side constraints are lower or/and upper bounds on design variables.

In this chapter, first the problems in size and geometry optimization are stated. Next, the solution procedures of the optimum design problem are explained. The sensitivity of the behaviour constraints is formulated in both displacement and force formulation. In the end, two algorithms based on optimality criterion techniques are developed for structural optimization under system stability constraint.

4.2 Problem Statement in Size Optimization

Three types of problems, classified by the type of constraints, have been optimized for size:

Type 1. Size optimization with stress and/or displacement constraints;

Type 2. Size optimization with frequency constraints;

Type 3. Size optimization with system stability constraints;

For Type 1 problems, both linear and nonlinear (force control technique) analyses have been performed to show the effect of geometric nonlinearity in structural optimization problems with stress and displacement constraints. For Type 3 problems, both linear and nonlinear (displacement control technique) buckling analyses have been carried out to demonstrate the effect of geometric nonlinearity on structural optimization with system stability constraints. Furthermore, for Types 1 and 2 (linear problems), both the displacement and the force methods have been used to demonstrate the application and computational efficiency of the force method in structural optimization problems.

Generally, a structural optimization problem consists in finding the vector of design variables **A** such that

$$\text{minimize} \qquad f(\mathbf{A}) = M = \rho\, \mathbf{A}^T \mathbf{L} \tag{4-2}$$

subject to

$$\textbf{Type 1} \qquad \begin{aligned} & g_i(\mathbf{A}) = |\sigma_i| - |\overline{\sigma}_i| \le 0 \qquad i = 1,2,\cdots,i_s \\ & g_i(\mathbf{A}) = |U_i| - |\overline{U}_i| \le 0 \qquad i = 1,2,\cdots,i_d \\ & \overline{\mathbf{A}} \le \mathbf{A} \end{aligned} \tag{4-3}$$

$$\textbf{Type 2} \qquad \begin{aligned} & g_i(\mathbf{A}) = |\overline{\omega}_i| - |\omega_i| \le 0 \qquad i = 1,2,\cdots,i_f \\ & \overline{\mathbf{A}} \le \mathbf{A} \end{aligned} \tag{4-4}$$

$$\textbf{Type 3} \qquad \begin{aligned} & g(\mathbf{A}) = 1 - \alpha_{cr} \le 0 \\ & \overline{\mathbf{A}} \le \mathbf{A} \end{aligned} \tag{4-5}$$

where M is the total mass of the structure; $\mathbf{A}$ and $\overline{\mathbf{A}}$ denote the vector of cross-sectional areas of the elements and its lower bound; $\mathbf{L}$ is the vector of elemental length; ρ is the density of the element material, σ_i and $\overline{\sigma}_i$ are the i^{th} constrained stress and its allowable limit value, U_i and $\overline{U}_i$ are the i^{th} constrained displacement and its allowable limit value, ω_i and $\overline{\omega}_i$ are i^{th} constrained frequency and its allowable limit value, α_{cr} is the critical load factor; and i_s, i_d and i_f are the number of stress, displacement and frequency constraints, respectively.

The constraints given by Eqs.(4-2)-(4-5) are highly nonlinear functions of **A** , implying therefore a nonlinear optimization problem at hand.

4.3 Problem Statement in Geometry Optimization

The objective is to maximize the structural strength [151-154] of an adaptive truss structure by changing the length of the active members. Thus, the length, angle or some other geometric parameters corresponding to the active members may be considered as design variables. Here, let us assume that the adaptive truss structure is composed of n members, including n_a active members. The vector of design variables $\varphi = \{\varphi_1, \varphi_2, \ldots, \varphi_{n_a}\}$ corresponds to the angles of the n_a active members.

For a given position and direction of the applied load **P**, the element force vector **F** depends on the vectors φ, and also on ψ which includes the directions of nonzero load components of **P**. Thus, for a uniform applied load **P**, **F** can be obtained using the relation

$$\mathbf{F} = \boldsymbol{P}_f \, \mathbf{F}_u \tag{4-6}$$

where $\mathbf{F}_u$ is the vector of element forces due to unit load in the position and direction of the applied load **P**, and the $(n \times n)$ diagonal matrix $\boldsymbol{P}_m$ contains the load factors corresponding to the relative element. The allowable load factors can be obtained from

$$|\mathbf{F}_a| = \boldsymbol{P}_{fa} \, |\mathbf{F}_u| \tag{4-7}$$

where $\mathbf{F}_a$ are the allowable element forces and the diagonal matrix $\boldsymbol{P}_{fa}$ contains the allowable load factors corresponding to the relative elements, i.e. $\boldsymbol{P}_{fa}{}^{(i)}$ is the allowable load factor corresponding to the i^{th} element. The structural strength may be defined as the allowable load factor for the complete structure and is given as

$$S_{st} = \text{Min } \boldsymbol{P}_{fa}. \tag{4-8}$$

Finally, to optimize the topology of the adaptive truss in the presence of a varying applied load, requires finding the vector of geometrical design variables φ such that

$$\text{Max } S_{st}(\varphi, \psi) \tag{4-9}$$

subject to

$$g_i(\varphi) \le 0, \quad i = 1,2,\cdots,i_g \tag{4-10}$$

where i_g is the number of geometrical constraints.

4.4 Solution Procedures of the Optimum Design Problem

In constrained optimization problems, the objective is to project the complete problem into a sub-problem that can then be solved and used as the basis of an iterative process. The early methods translate the constrained problem to a basic unconstrained problem using a penalty function for the constraints, which are near or beyond the constraint boundary. Thus, the constrained problem is solved using a sequence of parameterized unconstrained optimizations, which in the limit (of the sequence) converge to the constrained problem. These methods are now considered relatively inefficient and have been replaced by methods that have focused on the solution of the Karush-Kuhn-Tucker (KKT) equations. The KKT equations are necessary conditions for optimality to solve a constrained optimization problem. If the objective function and the constraints are convex functions, then the KKT equations are both necessary and sufficient to ensure a global solution point.

Recalling Eq. (4-1), the KKT equations can be stated [155] as

$$\begin{aligned} &\nabla f(\mathbf{X}^*) + \sum_{i=1}^{n_c} \lambda^*_i . \nabla g_i(\mathbf{X}^*) = \mathbf{0} \\ &g_i(\mathbf{X}^*) = 0 \qquad 1 \le i \le n_e \\ &\lambda^*_i \, g_i(\mathbf{X}^*) = 0 \qquad n_e + 1 \le i \le n_c \\ &\lambda^*_i \ge 0 \qquad n_e + 1 \le i \le n_c \end{aligned} \tag{4-11}$$

The first equation in Eq. (4-11) reflects a canceling of the gradients between the objective function and the active constraints at the solution point $\mathbf{X}^*$. For the gradients to be

canceled, Lagrange multipliers λ_i are necessary to balance the derivatives in magnitude of the objective function and constraint gradients. Since only *active* constraints are included in this cancellation process, constraints that are not active must not be included in this operation and so the given Lagrange multipliers equal to zero. This is stated implicitly in the last three equations of Eq. (4-11).

Three computationally efficient optimization algorithms are applied here: (1) the Fully Utilized Design (FUD), (2) the Optimality Criterion method (OC); and (3) the Mathematical Programming techniques (MP).

The Fully Stresses Design method [69,156] (FSD), which is based on a simple stress-ratio approach, is an elegant design tool that has been popular across the civil, mechanical, and aerospace engineering industries. However, the FSD is useful only for designs with stress constraints. It cannot properly handle the displacement constraints. However, the FSD method can be extended to handle situations with both stress and displacement constraints. This results in the Fully Utilized Design. Two steps are required to obtain the FUD: (i) generate the FSD for stress constraints only, and then (ii) uniformly prorate it to obtain the FUD. The constant prorating factor is obtained to satisfy the single-most infeasible displacement constraint. Although the FUD obtained is feasible, it can result in an over design. This is the primary limitation of the FUD method. To alleviate deficiencies associated with the FUD method, structural design problems were formulated and solved as non-linear mathematical programming optimization problems. The structural mass was used as the typical objective function and the failure modes were defined as the constraints. Non-linear Mathematical Programming techniques are based on the direct solution of the KKT conditions given by Eq. (4-11). The optimal design resulting from the mathematical programming technique is obtained iteratively from an initial design. At each iteration, the design is updated by calculating two quantities, a direction and a step length. Also, a relatively simpler design technique, termed the optimality criteria method and based on solution of the KKT conditions has been introduced to solve certain types of structural optimization problems.

To finalize, the selection of an efficient optimization procedure depends on the geometry of the structure, applied loads and constraints and is totally problem dependent.

4.4.1 Nonlinear Mathematical Programming Technique

Here, the Sequential Quadratic Programming (SQP) method has been used to solve the Type 1 and Type 2 problems in size optimization and geometry optimization. The computer implementation has been done using MATLAB [157].

Based on the works by Biggs [158], Han [159], and Powell [160,161], the method allows you to closely mimic Newton's method for constrained optimization just as is done for unconstrained optimization. At each major iteration, an approximation is made of the Hessian of the Lagrangian function using a quasi-Newton updating method. This is then used to form a search direction for a line search procedure. An overview of the SQP technique is found in Fletcher [162], Gill et al. [163] and Lu [155]. SQP is indirectly based on the solution of KKT conditions. Given the problem description in Eq. (4-1) the principal idea is the formulation of a QP sub-problem based on a quadratic approximation of the Lagrangian function

$$L(\mathbf{X},\lambda) = f(\mathbf{X}) + \sum_{i=1}^{n_c} \lambda_i . g_i(\mathbf{X}) . \qquad \textbf{(4-12)}$$

It is assumed that bound constraints have been expressed as inequality constraints in Eq. (4-1). The SQP implementation in MATLAB consists of three main steps: (i) a quadratic programming problem solution; (ii) a line search and merit function calculation; and (iii) updating of the Hessian matrix of the Lagrangian function given by Eq. (4-12).

At each major iteration, a QP sub-problem is solved. The solution to the QP sub-problem produces an estimate of the Lagrange multiplier vector, λ, and a search direction vector $\mathbf{s}^{\nu}$ in each iteration ν, which is used to form a new iteration as

$$\mathbf{X}^{\nu+1} = \mathbf{X}^{\nu} + l^{\nu}\mathbf{s}^{\nu}. \qquad \textbf{(4-13)}$$

The step length parameter l^{ν} is determined through a one-dimensional minimization in order to produce a sufficient decrease in the merit function.

At the end of the one-dimensional minimization, the Hessian of the Lagrangian, required for the solution of the next positive definite quadratic programming problem, is updated using the BFGS [160,161] update formula

$$\boldsymbol{H}^{(v+1)} = \boldsymbol{H}^{(v)} + \frac{\mathbf{q}^{(v)}\,\mathbf{q}^{T(v)}}{\mathbf{q}^{T(v)}\,\delta^{v}} - \frac{\boldsymbol{H}^{T(v)}\,\delta^{(v)}\,\delta^{T(v)}\,\boldsymbol{H}^{(v)}}{\mathbf{s}^{T(v)}\,\boldsymbol{H}^{(v)}\,\mathbf{s}^{(v)}} \tag{4-14}$$

where

$$\delta^{v} = \mathbf{X}^{v+1} - \mathbf{X}^{v} \tag{4-15}$$

$$\mathbf{q}^{v} = \nabla L(\mathbf{X}^{v+1}, \lambda^{v+1}) - \nabla L(\mathbf{X}^{v}, \lambda^{v}) \tag{4-16}$$

and $\boldsymbol{H}$ is the approximation of the Hessian of L at $\mathbf{X}^{v+1}$.

Powell recommends keeping the Hessian positive definite even though it may be positive indefinite at the solution point. If $\boldsymbol{H}^{v}$ is positive definite, then $\boldsymbol{H}^{v+1}$, obtained using Eq. (4-14) is also positive definite if and only if $\mathbf{q}^{T(v)}\,\delta^{(v)}$ is positive at each iteration. However, when the Lagrangian has a negative curvature at $(\mathbf{X}^{v+1}, \lambda^{v+1})$, $\mathbf{q}^{T(v)}\,\delta^{(v)}$ is not anymore positive. To guarantee that the updated Hessian matrix $\boldsymbol{H}^{v+1}$ remains positive definite, Powell suggests replacing $\mathbf{q}^{v}$ by

$$\hbar\,\mathbf{q}^{v} + (1-\hbar)\,\boldsymbol{H}^{v}\,\delta^{v} \tag{4-17}$$

where $\mathbf{q}^{v}$ is given by Eq. (4-16), and $\hbar$ is determined by

$$\hbar = \begin{cases} 1 & \text{if } \delta^{T v}\,\mathbf{q}^{v} \geq 0.2\,\delta^{T v}\,\boldsymbol{H}\,\delta^{v} \\ \dfrac{0.8\,\delta^{T v}\,\boldsymbol{H}\,\delta^{v}}{0.8\,\delta^{T v}\,\boldsymbol{H}\,\delta^{v} - \delta^{T v}\,\mathbf{q}^{v}} & \text{if } \delta^{T v}\,\mathbf{q}^{v} < 0.2\,\delta^{T v}\,\boldsymbol{H}\,\delta^{v} \end{cases} \tag{4-18}$$

Additional details of the algorithm may be found in Ref. [160,161]. As it is obvious, the required gradient of the Lagrangian function involves the gradient of the objective function and the constraints with respect to the design variables. Providing this information to the optimizer may result in an efficient and accurate optimum solution.

Here, the gradient of the objective functions and side constraints are relatively straightforward because they depend explicitly on the design variables.

4.4.2 Optimality Criteria Techniques

The optimality criteria method is an alternative design tool for solving the optimization problems given by Eq. (4-1). Unlike the mathematical programming technique which is based on the direct solution of the KKT conditions, the optimality criteria method circumvents the direct solution of the KKT conditions while exploiting the intrinsic nature of the design problem. Thus, this method is problem dependent. The optimality criteria method provides several procedures to iteratively update both the design variables and the Lagrange multipliers [26]. The recurrence relations for the Lagrange multipliers can be formulated using the *active* constraints given by Eq. (4-11). The active constraints can be expressed in the form

$$g_i(\mathbf{X}) = C_i - \overline{C}_i = 0 \quad \text{or} \quad C_i = \overline{C}_i \tag{4-19}$$

where C_i is the actual value of the i^{th} constraint which may be stress, displacement, and $\overline{C}_i$ is its limit or desired value. Multiplying both sides of Eq. (4-19) by λ_i^{β} and taking the β^{th} root, gives the exponential form of the recurrence relation for the Lagrange multipliers, in the form

$$\lambda_i^{\nu+1} = \lambda_i^{\nu}\left(\frac{C_i}{\overline{C}_i}\right)^{1/\xi} \tag{4-20}$$

where ν and $\nu+1$ are the iteration numbers and the parameter ξ determines the step size. The selection of ξ is problem dependent. Only the Lagrange multipliers associated with active constraints are updated. The active constraints set is estimated using a constraint thickness parameter that defines a finite interval within which all constraints are considered active. This constraint thickness becomes progressively tighter at each successive iteration, ultimately reducing to zero. Initial values for the Lagrange multipliers are required in order to start the iteration process.

The recurrence relations for the design variables can be formulated using the first equation in Eq (4-11). Dividing the both sides of the first equation in Eq. (4-11) by the gradient of the objective function $\nabla f(\mathbf{X})$, results in the following optimality criteria

$$OC_i = -\frac{\sum_{i=1}^{nc} \lambda_i . \nabla g_i(\mathbf{X})}{\nabla f(\mathbf{X})} = 1. \qquad \textbf{(4-21)}$$

The exponential form of the recurrence relation for the design variables, can be obtained by multiplying both sides of Eq. (4-21) by $(\mathbf{X}_i)^{\beta}$ and taking the β^{th} root as

$$\mathbf{X}_i^{v+1} = \mathbf{X}_i^{v} (OC_i)_v^{1/\beta} \qquad \textbf{(4-22)}$$

where $\mathbf{X}_i^{v}$ is the i^{th} design variable at the v^{th} iteration and β determines the step size. Only active constraints and their relative Lagrange multipliers are used in Eq. (4-22). Eqs. (4-20) and (4-22) are the most commonly used recurrence relations for the Lagrange multipliers and design variables, respectively, and are reported in Refs. [26]. Other forms of the recurrence relation for Lagrange multipliers and design variables, such as linear forms, can be found in Refs. [26,70].

4.4.3 The Fully Utilized Design

The Fully Utilized Design (FUD) method is an optimization design tool which has been specifically developed for application in size structural optimization problems. The FUD method can be used in two steps: (i) generation of a Fully Stressed Design (FSD); and (ii) the uniform prorating of the FSD to obtain FUD.

A FSD, for stress constraints only, is generated iteratively by using a stress-ratio technique that can be written as

$$\mathbf{A}_i^{v+1} = \mathbf{A}_i^{v} \left(\frac{\max|\sigma_i|}{\overline{\sigma}_i} \right) \qquad \textbf{(4-23)}$$

where A_i^v is the area of the i^{th} member at the v^{th} iteration. The converged solution of Eq. (4-23) is the FSD, designated as the vector of cross-sectional areas of the element $\mathbf{A}^{fsd}$. The FSD technique produces very fast convergence regardless of problem size. By prorating the FSD to satisfy the maximum violated displacement constraint yields the FUD for simultaneous stress and displacement constraints,

$$\mathbf{A}^{fud} = \mathbf{A}^{fsd}\left(\frac{U_{max}}{\overline{U}}\right) \qquad \textbf{(4-24)}$$

where $\mathbf{A}^{fud}$ is the vector of member areas, U_{max} and $\overline{U}$ are the most violated and the allowable displacement values, respectively. The uniform prorating factor $U_{max}/\overline{U}$ in Eq. (4-24) produces a feasible design. The FUD is likely to be over-designed because all member areas are increased by the same amount, while it has only one active displacement constraint.

4.5 Sensitivity of the Behaviour Constraints

Here, the calculation of the gradients of the behavior constraints are presented using both the displacement and the force methods. In the displacement method, the nodal displacements are obtained first and subsequently the element forces are calculated using back substitution. Therefore, the primary variables are the nodal displacements. On the other hand, in the force method, the element forces are obtained first and then the nodal displacements are obtained using back substitution, making the force in the elements the primary variables.

4.5.1 Sensitivity of the Stress-Displacement Constraints using the Displacement Method

(i) Linear Analysis

The linear equations of the equilibrium in terms of the nodal displacement vector **U** are generated using a finite element model in the form

$$\boldsymbol{K}_E \mathbf{U} = \mathbf{P} \tag{4-25}$$

where $\boldsymbol{K}_E$ is the linear elastic stiffness matrix and $\mathbf{P}$ is the external load vector. Constraints, involving a limit on displacement or stress components (Type 1) may be generally written as

$$\mathbf{g}(\mathbf{U}, \mathbf{X}) \leq \mathbf{0}. \tag{4-26}$$

Using the chain rule of differentiation, we obtain

$$\frac{d\mathbf{g}}{d\mathbf{X}} = \frac{\partial \mathbf{g}}{\partial \mathbf{X}} + \boldsymbol{Z}^T \nabla \mathbf{U} \tag{4-27}$$

and

$$\begin{aligned}
&\mathbf{g} = \begin{bmatrix} g_1 & g_2 & \cdots & g_j & \cdots & g_{nc} \end{bmatrix} \quad , \quad \frac{\partial \mathbf{g}}{\partial \mathbf{X}} = \begin{bmatrix} \nabla g_1 & \nabla g_2 & \cdots \end{bmatrix} \\
&\boldsymbol{Z} = \frac{\partial \mathbf{g}}{\partial \mathbf{U}} = \begin{bmatrix} \mathbf{Z}_1 & \mathbf{Z}_2 & \cdots & \mathbf{Z}_j & \cdots & \mathbf{Z}_{nc} \end{bmatrix}^T \quad , \quad \mathbf{Z}_j = \partial g_j / \partial \mathbf{U} \\
&\nabla \mathbf{U} = \begin{bmatrix} \dfrac{\partial \mathbf{U}}{\partial X_1} & \dfrac{\partial \mathbf{U}}{\partial X_2} & \cdots & \dfrac{\partial \mathbf{U}}{\partial X_i} & \cdots & \dfrac{\partial \mathbf{U}}{\partial X_{nd}} \end{bmatrix} , \\
&\nabla = \begin{bmatrix} \partial / \partial X_1 & \partial / \partial X_2 & \cdots & \partial / \partial X_i & \cdots & \partial / \partial X_{nd} \end{bmatrix}^T
\end{aligned} \tag{4-28}$$

The notation $d\mathbf{g}/d\mathbf{X}$ denotes the total derivative of $\mathbf{g}$ with respect to the design variable vector $\mathbf{X}$. This total derivative includes the explicit part $\nabla \mathbf{g}$ plus the implicit part through dependence on $\mathbf{U}$. The explicit part of the derivative is usually zero or easy to obtain. To compute the implicit part, two approaches [164] are usually used in the literature, namely the direct method and the adjoint technique. The direct method consists of solving for $\partial \mathbf{U}/\partial X_i$ and then taking the vector product with the vector $\boldsymbol{Z}_j$ for every typical constraint j. The sensitivity of the nodal displacements vector with respect to the typical design variable vector, X_i, can be obtained by differentiation of the Eq. (4-25) with respect to $\mathbf{X}$ as

$$\boldsymbol{K}_E \frac{\partial \mathbf{U}}{\partial X_i} = \frac{\partial \mathbf{P}}{\partial X_i} - \frac{\partial \boldsymbol{K}_E}{\partial X_i} \mathbf{U}. \tag{4-29}$$

For a typical structural problem analyzed here, the external load vector **P** is a dead load, making its derivative with respect to X_i zero. Therefore, considering Eq. (4-29), the implicit part for a typical constraint j can be expressed as

$$\mathbf{Z}_j^T \frac{\partial \mathbf{U}}{\partial X_i} = \mathbf{Z}_j^T \boldsymbol{K}_E^{-1} \frac{\partial \boldsymbol{K}_E}{\partial X_i} \mathbf{U} \tag{4-30}$$

In the adjoint technique, an adjoint vector η, which is the solution of the following system, is defined as

$$\boldsymbol{K}_E \eta = \mathbf{Z}_j. \tag{4-31}$$

Now, the implicit part can be obtained for every typical constraint j as

$$\mathbf{Z}_j^T \frac{\partial \mathbf{U}}{\partial X_i} = -\eta^T \frac{\partial \boldsymbol{K}_E}{\partial X_i} \mathbf{U}. \tag{4-32}$$

The solution of Eq. (4-31) for η is similar to a solution for nodal displacements in Eq. (4-25), under load vector $\mathbf{Z}_j$. The adjoint method is also known as the dummy-load method because $\mathbf{Z}_j$ is often described as a dummy load. The computational effort associated with the direct and the adjoint methods is a function of the relative number of constraints and design variables. The direct method requires the solution of Eq. (4-29), once for each design variable, while the adjoint method requires the solution of Eq. (4-31), once for each constraint. Thus, the direct method is more efficient when the number of design variables is smaller than the number of displacement and stress constraints that need to be differentiated. On the other hand, the adjoint method is more efficient when the number of design variables is larger than the number of displacement and stress constraints. The explicit part and matrix $\boldsymbol{Z}$ can be found analytically using the displacement method for truss and frame structures (Appendix B).

Both the direct and adjoint methods require the derivative of the stiffness matrix, with respect to the design variables. This derivative can be calculated analytically at the element level for truss and beam elements with cross-sectional area of the elements as the

design variables, or it can be obtained by the first-order forward finite difference approximation given by

$$\frac{\partial \boldsymbol{K}_E}{\partial X_i} \approx \frac{\boldsymbol{K}_E(X_i + \Delta X_i) - \boldsymbol{K}_E(X_i)}{\Delta X_i}. \tag{4-33}$$

The stiffness matrix $\boldsymbol{K}_E$ is usually available at a typical design variable X_i, from the solution of Eq. (4-25). Thus, Eq. (4-33) only requires the computation of the stiffness matrix at the perturbed design variable, $X_i + \Delta X_i$.

(ii) Nonlinear analysis using the force control method

For a nonlinear analysis, the equations of equilibrium may be expressed as

$$\alpha \mathbf{P}_{ref} - \mathbf{P}'(\mathbf{U}, \mathbf{X}) = 0 \tag{4-34}$$

where $\mathbf{P}_{ref}$ and $\mathbf{P}'$ are the nodal reference load vector and the vector of nodal internal forces generated by the deformation of the structure, respectively. For simplicity in notation, the references to time step t and iteration k are dropped here. Differentiating Eq. (4-34) with respect to the typical design variable X_i, and using the chain rule, we obtain

$$\frac{\partial \mathbf{P}'}{\partial \mathbf{U}} \frac{\partial \mathbf{U}}{\partial X_i} = \alpha \frac{d\mathbf{P}_{ref}}{dX_i} - \frac{\partial \mathbf{P}'}{\partial X_i}. \tag{4-35}$$

Considering that the rate of change of the nodal internal forces, $\mathbf{P}'$, with respect to the nodal displacements, is equal to the tangential stiffness matrix, $\boldsymbol{K}$, and $\mathbf{P}_{ref}$ is a dead load (conservative load), Eq. (4-35) can be expressed as

$$\boldsymbol{K} \frac{d\mathbf{U}}{dX_i} = -\frac{\partial \mathbf{P}'}{\partial X_i}. \tag{4-36}$$

Thus, in the direct method, the implicit part for every typical constraint j in Eq. (4-27), can be written as

$$\mathbf{Z}_j^T \frac{d\mathbf{U}}{d\mathbf{X}_i} = -\mathbf{Z}_j^T \boldsymbol{K}^{-1} \frac{\partial \mathbf{P}'}{\partial \mathbf{X}_i} . \tag{4-37}$$

Alternatively, in the adjoint method, introducing the adjoint vector η, which is a solution of Eq. (4-31), and replacing $\boldsymbol{K}_E$ by $\boldsymbol{K}$, the implicit part can be written as

$$\mathbf{Z}_j^T \frac{d\mathbf{U}}{d\mathbf{X}_i} = -\eta^T \frac{\partial \mathbf{P}'}{\partial \mathbf{X}_i}. \tag{4-38}$$

Both the direct and adjoint methods require the derivative of the nodal internal force, $\mathbf{P}'$. These derivatives can be calculated analytically for simple truss and beam type structures

4.5.2 Sensitivity of the Eigenvalue Problems using the Displacement Method

Eigenvalue problems are commonly encountered in structural linear stability and vibration analysis. When the forces are conservative, and no damping is considered, these problems lead to real eigenvalues, which represent buckling (bifurcation) loads or vibration frequencies. In other words, undamped vibration and linear buckling analysis can be expressed as an eigenvalue problem in the form

$$(\boldsymbol{K}_E - \mu \boldsymbol{M})\overline{\mathbf{U}} = \mathbf{0} \tag{4-39}$$

where $\boldsymbol{M}$ is the mass matrix for a vibration analysis, or alternatively the geometric stiffness matrix $\boldsymbol{K}_G$ for a linear buckling analysis, and $\overline{\mathbf{U}}$ is the mode shape. Also, for vibration analysis, $\mu = \omega^2$ is the square of the frequency of the free vibration, and for linear buckling problems, it is the linear buckling load factor. Pre-multiplying Eq. (4-39) by $\overline{\mathbf{U}}^T$, gives

$$\overline{\mathbf{U}}^T (\boldsymbol{K}_E - \mu \boldsymbol{M})\overline{\mathbf{U}} = \mathbf{0}. \tag{4-40}$$

Differentiating Eq. (4-40) with respect to the design variable X yields

$$\overline{\mathbf{U}}^T \left(\frac{d\boldsymbol{K}_E}{d\mathbf{X}_i} - \mu \frac{d\boldsymbol{M}}{d\mathbf{X}_i} - \boldsymbol{M} \frac{d\mu}{d\mathbf{X}_i} \right) \overline{\mathbf{U}} + \frac{d\overline{\mathbf{U}}^T}{d\mathbf{X}_i} (\boldsymbol{K}_E - \mu \boldsymbol{M})\overline{\mathbf{U}} + \overline{\mathbf{U}}^T (\boldsymbol{K}_E - \mu \boldsymbol{M}) \frac{d\overline{\mathbf{U}}}{d\mathbf{X}_i} = 0. \tag{4-41}$$

Considering that matrices $\boldsymbol{K}_E$ and $\boldsymbol{M}$ are symmetric, and recalling Eq. (4-39), we obtain the sensitivity of μ with respect to the typical design variable X_i as

$$\frac{d\mu}{dX_i} = \frac{\overline{\mathbf{U}}^T \left(\frac{d\boldsymbol{K}_E}{dX_i} - \mu \frac{d\boldsymbol{M}}{dX_i} \right) \overline{\mathbf{U}}}{\overline{\mathbf{U}}^T \boldsymbol{M} \overline{\mathbf{U}}}. \tag{4-42}$$

The mode shape is often normalized with respect to the symmetric positive definite matrix $\boldsymbol{M}$ such that

$$\overline{\mathbf{U}}^T \boldsymbol{M} \overline{\mathbf{U}} = 1 \tag{4-43}$$

Using Eq. (4-43), Eq. (4-42) can be simplified in the form

$$\frac{d\mu}{dX_i} = \overline{\mathbf{U}}^T \left(\frac{d\boldsymbol{K}_E}{dX_i} - \mu \frac{d\boldsymbol{M}}{dX_i} \right) \overline{\mathbf{U}}. \tag{4-44}$$

Here, $d\boldsymbol{M}/dX_i$ can be calculated analytically for truss and beam elements (Appendix B).

4.5.3 Sensitivity of the Stress-Displacement Constraints using the Force Method

The governing equations using the force formulation are given by Eq. (2-27). Also, in the force method, the constraints involving a limit on a displacement or stress component (Type I problem) may be generally expressed as

$$\mathbf{g}(\mathbf{F}, \mathbf{X}) \leq \mathbf{0}. \tag{4-45}$$

Using the chain rule of differentiation, we obtain

$$\frac{d\mathbf{g}}{d\mathbf{X}} = \nabla \mathbf{g} + \boldsymbol{Z}^T \nabla \mathbf{F} \tag{4-46}$$

where $\mathbf{Z}_j = \partial g_j / \partial \mathbf{F}$ for every typical constraint j. The direct method consists of solving for $d\mathbf{F}/dX_i$ and then taking the scalar product with the vector $\mathbf{Z}_j$. The sensitivity of the

nodal displacements vector with respect to the typical design variable vector, X_i, can be obtained by differentiating Eq. (2-27) with respect to X as

$$\boldsymbol{S}\frac{d\mathbf{F}}{d\mathrm{X}_i} = \frac{d\mathbf{P}^*}{d\mathrm{X}_i} - \frac{d\boldsymbol{S}}{d\mathrm{X}_i}\mathbf{F}. \tag{4-47}$$

Using Eq. (4-46), and considering that the external load is conservative, the implicit part can be obtained for a typical constraint j as

$$\mathbf{Z}_j^T \frac{d\mathbf{F}}{d\mathrm{X}_i} = -\mathbf{Z}_j^T \boldsymbol{S}^{-1} \frac{d\boldsymbol{S}}{d\mathrm{X}_i}\mathbf{F}. \tag{4-48}$$

Similarly, using the adjoint method, results in

$$\boldsymbol{S}\,\eta = \mathbf{Z}_j \tag{4-49}$$

Now, the implicit part for every typical constraint j can be obtained as

$$\mathbf{Z}_j^T \frac{d\mathbf{F}}{d\mathrm{X}_i} = -\eta^T \frac{d\boldsymbol{S}}{d\mathrm{X}_i}\mathbf{F}. \tag{4-50}$$

The solution of Eq. (4-49) for η is similar to a solution for element forces using Eq. (2-27) under the load vector $\mathbf{Z}_j$. The explicit part and the vector $\mathbf{Z}_j$ are calculated analytically for truss and frame beam elements in Appendix B.

Both the direct and adjoint methods require the derivative of the matrix $d\boldsymbol{S}/d\mathrm{X}_i$. These derivatives are calculated analytically at the element level for truss and beam elements with the cross-sectional area of the elements as the design variables (Appendix B). When it is not possible to calculate analytically, the gradients can be obtained using the first-order forward finite difference approximation.

4.5.4 Sensitivity of the Eigenvalue Problems using the Force Method

Using the force formulation, an eigenvalue problem can be expressed as

$$(\boldsymbol{S} - \mu \boldsymbol{M}^*)\overline{\mathbf{F}} = \mathbf{0} \tag{4-51}$$

where $\mu = \omega^2$. However, the matrix $\boldsymbol{S}$ is not symmetric. Thus, the approach described in section 4.5.3 to obtain derivative of the eigenvalue μ with respect to the design variables is not applicable. To overcome this problem, we introduce the left-hand eigenvector, defined as

$$\overline{\mathbf{F}}^{L^T}\left(\boldsymbol{S}-\mu\boldsymbol{M}^*\right)=\mathbf{0}. \tag{4-52}$$

Pre-multiplying Eq. (4-51) by the transpose of the left-hand eigenvector, $\overline{\mathbf{F}}^{L^T}$, gives

$$\overline{\mathbf{F}}^{L^T}\left(\boldsymbol{S}-\mu\boldsymbol{M}^*\right)\overline{\mathbf{F}}=0 \tag{4-53}$$

Differentiating Eq. (4-53) with respect to the design variable X_i yields

$$\mathbf{F}^{L^T}\left(\frac{d\boldsymbol{S}}{dX_i}-\mu\frac{d\boldsymbol{M}^*}{dX_i}-\boldsymbol{M}^*\frac{d\mu}{dX_i}\right)\overline{\mathbf{F}}+\frac{d\mathbf{F}^{L^T}}{dX_i}\left(\boldsymbol{S}-\mu\boldsymbol{M}^*\right)\overline{\mathbf{F}}+\overline{\mathbf{F}}^{L^T}\left(\boldsymbol{S}-\mu\boldsymbol{M}^*\right)\frac{d\overline{\mathbf{F}}}{dX_i}=0. \tag{4-54}$$

Considering Eqs. (4-51) and (4-52), we obtain the sensitivity of the μ with respect to the design variable X_i:

$$\frac{d\mu}{dX_i}=\frac{\overline{\mathbf{F}}^{L^T}\left(\frac{d\boldsymbol{S}}{dX_i}-\mu\frac{d\boldsymbol{M}^*}{dX_i}\right)\overline{\mathbf{F}}}{\overline{\mathbf{F}}^{L^T}\boldsymbol{M}^*\overline{\mathbf{F}}} \tag{4-55}$$

where $d\boldsymbol{M}^*/dX_i$ can be easily computed using the finite-difference method.

4.6 Optimality Criterion Algorithms

The optimum solution of the nonlinear buckling problems under system stability constraint using general mathematical programming algorithms is computationally inefficient because of the many analyses and sensitivity calculations required. This difficulty can be alleviated by introducing the optimality criterion method. Here, two optimality criterion algorithms have been developed for size optimization of Type III problems.

The first optimality criterion algorithm (Algorithm I) is based on the total potential energy. This algorithm is similar to the algorithm proposed by Khot [111], where a nonlinear analysis based on force control is used and the critical point is characterized by the value of the load, which causes a loss of positive definiteness of the Hessian of the total potential energy evaluated at the equilibrium configuration. Also, the Lagrange multiplier is assumed to be one at each iteration. Here, in algorithm I, the critical point is calculated using the displacement control method with a quadratic fit in the region near the critical point, and the Lagrange multiplier is obtained explicitly.

The second proposed algorithm (Algorithm II) is based on the sensitivity of the critical load factor. A sensitivity analysis establishes the rates of change of the response quantities and the design constraints with respect to the design variables. Since the sensitivity of the nonlinear critical load factor is used in constructing an optimality criterion at the current design, it is important to use a method that produces the sensitivity information accurately. In this work, the sensitivity of the critical load factor is obtained using the displacement control technique and the adjoint method is used to make it computationally efficient.

4.6.1 The Optimality Criterion based on the Potential Energy- Algorithm I

Let us define the optimization problem as:

Minimize the mass

$$M = \sum_{i=1}^{n} \rho_i A_i L_i \tag{4-56}$$

subject to

$$g = U - \overline{U} = 0 \tag{4-57}$$

where ρ_i, A_i, L_i and n are the material density of the i^{th} element, the cross-sectional area of the i^{th} element (design variable), the deformed length of the i^{th} element and the

number of elements, respectively. U is the total potential energy and $\overline{U}$ is the target total potential energy associated with the optimum design at the limit load.

It is noted that the effect of nonlinear buckling constraint is considered implicitly in the equality constraint given by Eq. (4-57). In other words, at the end of the nonlinear buckling analysis for each optimization iteration, the total potential energy is obtained. This total potential energy represents the potential energy of the system at limit point. Thus, it may be said that the constraint on the limit load is equivalent to the constraint on the total potential energy of the system at the limit load.

The total potential energy of a structure made up of n elements may be expressed as

$$U = \sum_{i=1}^{n} \Pi_i - \mathbf{U}^T \boldsymbol{P} = \Pi - \mathbf{U}^T \mathbf{P} \tag{4-58}$$

where **U** is the global displacement vector, **P** is the vector of the externally applied forces , Π is the total strain energy and Π_i is the strain energy of a typical ith element. For one-dimensional elements, it can be expressed as

$$\Pi_i = \frac{1}{2} \mathrm{E}_i \, \varepsilon_i^2 \, \mathrm{A}_i \, \mathrm{L}_i \tag{4-59}$$

where E_i is the modulus of elasticity of the i^{th} element and ε_i is the strain in the i^{th} element expressed as

$$\varepsilon_i = (\mathrm{L}_i - \mathrm{L}_{0i})/\mathrm{L}_{0i} \tag{4-60}$$

where L_{0i} is the undeformed length of the i^{th} element. Using the principle of stationary total potential energy, we obtain

$$\frac{\partial U}{\partial \mathbf{U}} = \frac{\partial \Pi}{\partial \mathbf{U}} - \mathbf{P} = \mathbf{0}. \tag{4-61}$$

Using Eqs. (4-56) and (4-57), the Lagrangian may be written as

$$L = \sum_{i=1}^{n} \rho_i \, \mathrm{A}_i \, \mathrm{L}_i - \lambda (U - \overline{U}) \tag{4-62}$$

where λ is a Lagrange multiplier. The Karush-Kuhn-Tucker conditions for minimization of the Lagrangian with respect to A_i and λ, according to Eq. (4-11), become

$$\rho_i L_i - \lambda\left(\frac{\partial U}{\partial A_i} + \sum_{j=1}^{m} \frac{\partial U}{\partial U_j}\frac{\partial U_j}{\partial A_i}\right) = 0 \qquad \textbf{(4-63)}$$

$$(U - \overline{U}) = 0$$

where m is the number of displacement degrees of freedom. By virtue of Eq. (4-61), corresponding to every nodal displacement U_j, $\frac{\partial U}{\partial U_j}$ vanishes and, hence Eq. (4-63) becomes

$$\rho_i L_i - \lambda\frac{\partial U}{\partial A_i} = 0. \qquad \textbf{(4-64)}$$

Using Eqs. (4-58) and (4-59),

$$\frac{\partial U}{\partial A_i} = \frac{\Pi_i}{A_i} \qquad \textbf{(4-65)}$$

Substitution of Eq. (4-65) into Eq. (4-64) gives

$$\rho_i L_i - \lambda\frac{\Pi_i}{A_i} = 0 \qquad \textbf{(4-66)}$$

or

$$\lambda\hat{\Pi}_i = 1 \qquad \textbf{(4-67)}$$

where $\hat{\Pi}_i = \dfrac{\Pi_i}{\rho_i L_i A_i}$ is the strain energy of the i^{th} element.

Eq. (4-67) is an optimality criterion similar to Eq. (4-16), and it states that in an optimum structure, the strain energy density is the same for all elements.

4.6.1.1 The Recurrence Relation

To obtain a design satisfying the optimality criterion given by Eq. (4-67), an iterative scheme is used. This consists of updating the design variables using a recurrence relation or the design variable update formulas after determining the nonlinear critical point and the associated deformed shape of the structure. A simple and efficient form of the recurrence relation may be expressed by multiplying both sides of Eq. (4-67) by $(A_i)^\beta$ and taking its βth root as

$$A_i^{v+1} = A_i^v \left(\lambda \hat{\Pi}_i\right)_v^{1/\beta} \tag{4-68}$$

where $v+1$ and v are the iteration numbers. The step size parameter β controls the convergence rate and can be changed by assigning appropriate values. Using the recurrence relation in Eq. (4-68), in each optimization iteration the design variables are updated until the relative convergence criteria is satisfied. It is noted that the final optimum design is not influenced by the step size parameter, since $\lambda \hat{U}$ is equal to unity in the final optimum design. Selecting large step size parameter results in a slow and smooth convergence and a large number of optimization iterations before satisfying the convergence criteria. Conversely, choosing a small step-size parameter results in a fast and oscillating convergence so that the required convergence criteria may never be reached. It is recommended that the step size parameter is set to a small number (4 has been selected for the present design), and then increased gradually as the optimization process evolves.

4.6.1.2 Closed-form Solution for the Lagrange Multiplier

To use Eq. (4-68), the Lagrange multiplier λ needs to be calculated. At the optimal design, λ satisfies Eq. (4-67). For non-optimal design, it is desired to obtain a value for λ that most closely satisfies Eq. (4-67). Thus, for non-optimal design, consider a residual Res defined as

$$\text{Res}_i = 1 - \lambda \hat{\Pi}_i. \tag{4-69}$$

Now, λ is taken as the value that minimizes the sum of the squares of the residuals, i.e., the value for which

$$\frac{d}{d\lambda}\left[\sum_{i=1}^{n} \mathrm{Res}_i^2\right] = 0. \tag{4-70}$$

Equation (4-70) results in the following closed-form solution for the value of λ:

$$\lambda = \sum_{i=1}^{n} \hat{\Pi}_i \Big/ \sum_{i=1}^{n} \hat{\Pi}_i^2 \tag{4-71}$$

Substituting Eq. (4-71) into Eq. (4-68), the following recurrence relation for updating the design variables is obtained

$$\mathrm{A}_i^{v+1} = \mathrm{A}_i^{v} \left(\left[\sum_{i=1}^{n} \hat{\Pi}_i \Big/ \sum_{i=1}^{n} \hat{\Pi}_i^2 \right] \hat{\Pi}_i \right)_{v}^{1/\beta}. \tag{4-72}$$

4.6.1.3 Design Scaling

After finding the limit load using the nonlinear buckling analysis at each optimization iteration, the design variables are scaled to the feasible region to satisfy the design constraint. In other words, the design limit load ($\mathbf{P}_{design}$) of the structure must be equal to the limit load ($\mathbf{P}_{cr}$) of the structure after the analysis phase in the iteration cycle.

For truss elements, the strain energy is a linear function of the design variables . For truss elements, the strain energy is a linear function of the design variables; therefore scaling the areas of all the members of the structure by a factor *Sf* has the effect of scaling the limit load $\mathbf{P}_{cr}$ by the same scale factor *Sf*, with no change in the displacement pattern. The scale factor for truss elements may be given by

$$\mathbf{P}_{design} = Sf\ \mathbf{P}_{cr}. \tag{4-73}$$

For beam elements, the strain energy is not a linear function of design variables. Here the scaling process is done iteratively. Illustrative examples to demonstrate the application of these concepts are presented in Chapter 5.

4.6.2 Optimality Criterion based on the Limit Load Sensitivity-Algorithm II

The objective function is similar to Eq. (4-56), however the constraint is defined as

$$g = \mathbf{P}_{Cr} \geq \mathbf{P}_{design} \text{ or } \alpha_{cr} - 1 \geq 0 \tag{4-74}$$

where $\mathbf{P}_{cr} = \alpha_{cr}\ \mathbf{P}_{design}$.

Eq. (4-74) says that, at the optimum point specified, the design load should be equal or less than the limit load of the structure. Now, the Lagrangian may be written as

$$L = \sum_{i=1}^{n} \rho_i\, A_i\, L_i - \lambda(\alpha_{cr} - 1). \tag{4-75}$$

The Karush-Kuhn-Tucker conditions for minimization of the Lagrangian with respect to A_i and λ are

$$\begin{aligned} &\rho_i\, L_i - \lambda \frac{d\alpha_{cr}}{dA_i} = 0 \\ &\alpha_{cr} - 1 = 0 \end{aligned} \tag{4-76}$$

Here, the sensitivity of the load factor α with respect to the design variables needs to be obtained, i.e. $\frac{d\alpha_{cr}}{dA_i}$. Calculation of the derivatives of the critical load factor with respect to the design variables can be done using finite difference approximations, however with high computational cost. For instance, to calculate the derivatives of the critical load factor with respect to *n* design variables using the forward-difference approximation requires n additional analyses, the central-difference approximation requires 2*n* additional analyses, and the higher order approximations are more expensive. On the other hand, the calculation of the limit load factor is usually difficult and not very accurate. Thus, calculation of the derivatives of the critical load factor with respect to the design variable by finite differencing inaccurate critical loads for slight changes in the design variables may result in gross errors for the derivatives. The sensitivity of the critical load factor has been obtained by Kamat et al.[108-110] however, this method is based on the implicit differentiation of equilibrium equations and the Hessian of the total potential energy,

making it computationally expensive. For these reasons, an efficient approach for the calculation of the sensitivity derivatives is deemed necessary. Here, the sensitivity of the critical load factor is obtained using a nonlinear finite element analysis based on the displacement control method.

4.6.2.1 Sensitivity of the Nonlinear Critical Load Factor

Le us assume that the peak load factor has been obtained at the current design after completing the nonlinear structural analysis using displacement control method. The equations of equilibrium of the structure at the peak load are given by

$$\alpha_{cr}\,\mathbf{P}_{ref} - \mathbf{P}' = 0 \tag{4-77}$$

where α_{cr} is the nonlinear critical load factor. It is noted that the reference to time step t and iteration k are dropped here, since only the final converged solution of the nonlinear finite element equations is of concern. Differentiating Eq. (4-77) with respect to a typical design variable A_i, we obtain

$$\frac{d\alpha_{cr}}{dA_i}\mathbf{P}_{ref} + \alpha_{cr}\frac{d\mathbf{P}_{ref}}{dA_i} - \frac{d\mathbf{P}'}{dA_i} = 0. \tag{4-78}$$

In this work, the reference load, $\mathbf{P}_{ref}$, does not depend on the deformation and the design variables (conservative or dead load). Therefore, its differentiation with respect to the design variables is zero. Using the chain rule, we write

$$\frac{d\mathbf{P}'}{dA_i} = \frac{\partial \mathbf{P}'}{\partial A_i} + \frac{\partial \mathbf{P}'}{\partial \mathbf{U}}\frac{d\mathbf{U}}{dA_i} \tag{4-79}$$

Substituting Eq. (4-79) into Eq.(4-78), and rearranging the terms yields

$$\frac{\partial \mathbf{P}'}{\partial \mathbf{U}}\frac{d\mathbf{U}}{dA_i} = \frac{d\alpha_{cr}}{dA_i}\mathbf{P}_{ref} - \frac{\partial \mathbf{P}'}{\partial A_i}. \tag{4-80}$$

Considering that the rate of change of the nodal internal forces with respect to the nodal displacements is equal to the tangential stiffness matrix, $\boldsymbol{K}$, the Eq. (4-80) can be written as

$$\boldsymbol{K}\frac{d\mathbf{U}}{d\mathrm{A}_i} = \frac{d\alpha_{cr}}{d\mathrm{A}_i}\mathbf{P}_{ref} - \frac{\partial \mathbf{P}'}{\partial \mathrm{A}_i}. \tag{4-81}$$

Eq. (4-81) involves more unknowns than equations; therefore it cannot be solved directly to obtain the sensitivity of the load factor. To overcome this problem, it is assumed that the derivatives of one of the displacement components are zero in each time step. This assumption is justified if the selected displacement component is the controlling displacement in the nonlinear buckling analysis using the displacement control method (q^{th} component of **U**). Recalling the nonlinear analysis through displacement control technique, it is possible to express $\frac{d\mathbf{U}}{d\mathrm{A}_i}$ as the sum of the two vectors given by

$$\frac{d\mathbf{U}}{d\mathrm{A}_i} = \frac{d\alpha_{cr}}{d\mathrm{A}_i}\frac{d\mathbf{U}^{I}}{d\mathrm{A}_i} + \frac{d\mathbf{U}^{II}}{d\mathrm{A}_i}. \tag{4-82}$$

Writing Eq. (4-82) for the q^{th} component of **U**, the following relation is obtained:

$$\frac{d\mathrm{U}_q}{d\mathrm{A}_i} = \frac{d\alpha_{cr}}{d\mathrm{A}_i}\frac{d\mathrm{U}_q^{I}}{d\mathrm{A}_i} + \frac{d\mathrm{U}_q^{II}}{d\mathrm{A}_i} \tag{4-83}$$

Now considering that $\mathrm{U}_q = 0$, and using Eq. (4-83), we obtain the sensitivity of the load factor:

$$\frac{d\alpha_{cr}}{d\mathrm{A}_i} = -\frac{d\mathrm{U}_q^{II}}{d\mathrm{A}_i} \Big/ \frac{d\mathrm{U}_q^{I}}{d\mathrm{A}_i} \tag{4-84}$$

where $\frac{d\mathrm{U}_q^{I}}{d\mathrm{A}_i}$ and $\frac{d\mathrm{U}_q^{II}}{d\mathrm{A}_i}$ can be obtained using the following equations:

$$\boldsymbol{K}\frac{d\mathbf{U}^{I}}{d\mathrm{A}_i} = \mathbf{P}_{ref} \qquad \text{and} \qquad \boldsymbol{K}\frac{d\mathbf{U}^{II}}{d\mathrm{A}_i} = -\frac{\partial \mathbf{P}'}{\partial \mathrm{A}_i}. \tag{4-85}$$

In order to obtain $\frac{d\mathrm{U}_q^{I}}{d\mathrm{A}_i}$ and $\frac{d\mathrm{U}_q^{II}}{d\mathrm{A}_i}$ efficiently, with less computational effort, the adjoint method is used. To this end, define an adjoint vector η such that

$$\boldsymbol{K}\,\eta = \mathbf{Z} \tag{4-86}$$

where the vector $\mathbf{Z}$ is the dummy load with its q^{th} component equal to unity. Now, using Eq. (4-86), Eq. (4-85) can be expressed as

$$\frac{dU_q^I}{dA_i} = \eta^T \mathbf{P}_{ref} \qquad \text{and} \qquad \frac{dU_q^{II}}{dA_i} = -\eta^T \frac{\partial \mathbf{P}'}{\partial A_i}. \tag{4-87}$$

It should be mentioned that in Eq. (4-87), there is no need to obtain the tangent stiffness matrix $\boldsymbol{K}$, because it is available at the end of the nonlinear analysis. The Eq. (4-87) requires only calculation of $\partial \mathbf{P}'/\partial A_i$ which can be easily obtained. For truss elements, $\partial \mathbf{P}'/\partial A_i$ can be obtained by dividing the nodal internal forces at each element by its relative area A_i. For plane beam elements, with moment of inertia I, with $I = a A^b$, $\partial \mathbf{P}'/\partial A_i$ may be obtained by dividing the nodal internal forces at each element by its relative area A_i and multiplying the nodal internal moments at each element by b/A_i.

Thus, all the requisites are available to obtain the sensitivity of the load factor according to Eq. (4-84). Knowing the sensitivity of the load factor, Eq. (4-76) can be written as

$$\lambda \frac{(d\alpha_{cr}/dA_i)}{\rho_i L_i} = 1. \tag{4-88}$$

Eq. (4-88) can be cast into a recursive relation similar to Eq. (4-68) in the form:

$$A_i^{v+1} = A_i^v \left(\lambda \frac{(d\alpha_{cr}/dA_i)}{\rho_i L_i} \right)_v^{1/\beta} \tag{4-89}$$

In the same form as in algorithm I, the Lagrange multiplier λ in Eq. (4-89) can be calculated in a closed form (similar to Eq. 4-71):

$$\lambda = \sum_{i=1}^{n} \left[\frac{(d\alpha_{cr}/dA_i)}{\rho_i L_i} \right] \Big/ \sum_{i=1}^{n} \left[\frac{(d\alpha_{cr}/dA_i)}{\rho_i L_i} \right]^2 \tag{4-90}$$

Chapter 5

CASE STUDIES

5.1 Introduction

The analysis methods described in Chapters 2 and 3 and the optimization algorithms presented in Chapter 4 have been integrated and implemented into an efficient computational structural analysis and optimization design tool. The structural optimization problems considered are based on two design objectives: size and topology optimization. In all size optimization problems, the objective is to minimize the weight of the structure and the design variables are the cross-sectional areas of the elements. In topology optimization, the objective is to maximize the structural strength and the design variables represent the relative orientation of the active members.

The test cases results demonstrate the efficiency of the finite element analysis technique based on the force method. The effect of geometrical nonlinearities and element imperfections has been studied as well. The optimization constraints considered during the structural design process include stress-displacement, frequency and system stability.

A brief description of the test cases and respective objectives are outlined in the following tables:

Structural Size Optimization under Stress and Displacement Constraints		
Test Case	**Objectives**	**Analysis and Optimization Procedure**
1. 10-bar planar truss 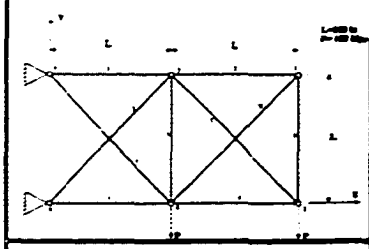	▪ Nonlinear vs. linear analysis ▪ Effect of geometric nonlinearity ▪ FSD vs. optimum design ▪ Current results vs. benchmark	▪ Linear finite element analysis based on FMCE and DM ▪ Nonlinear finite element analysis based on force control technique ▪ Optimization: SQP
2. 25-bar space truss 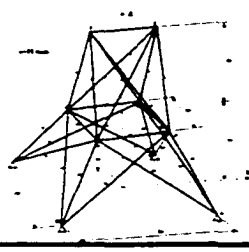	▪ Application of FMCE in size opt. ▪ Nonlinear vs. linear analysis ▪ Effect of geometric nonlinearity ▪ FM vs. DM ▪ Current results vs. benchmark	▪ Linear finite element analysis based on FMCE and DM ▪ Nonlinear finite element analysis based on force control technique ▪ Optimization: SQP
3. 72-bar space truss 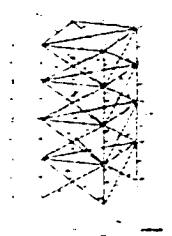	▪ Application of FMCE in size opt. ▪ Nonlinear vs. linear analysis ▪ Effect of geometric nonlinearity ▪ FM vs. DM ▪ Current results vs. benchmark	▪ Linear finite element analysis based on FMCE and displacement method ▪ Nonlinear finite element analysis based on force control technique ▪ Optimization: SQP
4. 10-member frame 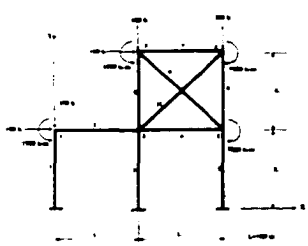	▪ Application of FMCE in size opt. ▪ Nonlinear vs. linear analysis ▪ Effect of geometric nonlinearity ▪ FM vs. DM ▪ Current results vs. benchmark	▪ Linear finite element analysis based on FMCE and DM ▪ Nonlinear finite element analysis based on force control technique ▪ Optimization: SQP
5. 25-member frame 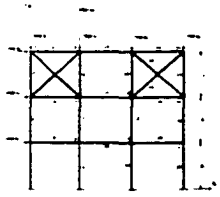	▪ Application of FMCE in size opt. ▪ Nonlinear vs. linear analysis ▪ Effect of geometric nonlinearity ▪ FM vs. DM ▪ Current results vs. benchmark	▪ Linear finite element analysis based on FMCE and DM ▪ Nonlinear finite element analysis based on force control technique ▪ Optimization: SQP

Structural Size Optimization under Frequency Constraints		
Test Case	**Objective**	**Analysis and Optimization Procedure**
6. 10-bar planar truss 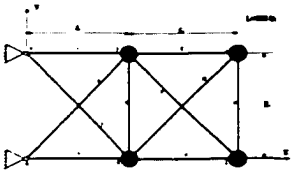	▪ Application of IFM in size opt. ▪ FM vs. DM ▪ Fundamental frequency constraint ▪ Multiple Frequency constraint ▪ Current results vs. benchmark	▪ Frequency finite element analysis based on IFM and DM ▪ Optimization: SQP
7. 72-bar space truss 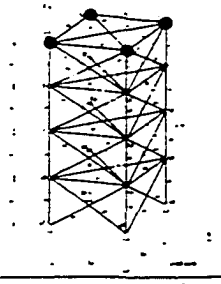	▪ Application of IFM in size opt. ▪ FM vs. DM ▪ Fundamental frequency constraint ▪ Multiple Frequency constraint ▪ Current results vs. benchmark	▪ Frequency finite element analysis based on IFM and DM ▪ Optimization: SQP
8. 6-member frame truss 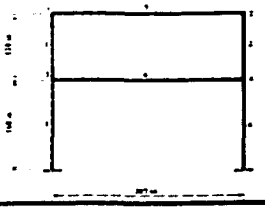	▪ Application of IFM in size opt. ▪ FM vs. DM ▪ Fundamental frequency constraint ▪ Multiple Frequency constraint ▪ Current results vs. benchmark	▪ Frequency finite element analysis based on IFM and DM ▪ Optimization: SQP

Structural Size Optimization under Stability Constraints		
Test Case	**Objective**	**Analysis and Optimization Procedure**
9. 2-bar symmetric truss 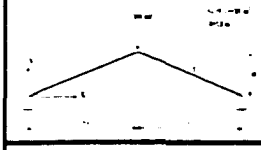	▪ Linear vs. nonlinear buckling ▪ Effect of geometric nonlinearity and element imperfection ▪ Effect of stress and displacement geometry stiffness matrices ▪ Efficiency of the Algorithm I ▪ Current results vs. literature	▪ Linear buckling analysis ▪ Nonlinear buckling analysis (based on displacement control) ▪ Optimization: OC (Algorithm I)
10. 2-bar truss (asymmetric) 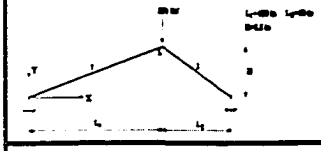	▪ Linear vs. nonlinear buckling ▪ Effect of geometric nonlinearity and element imperfection ▪ Effect of stress and displacement geometry stiffness matrices ▪ Efficiency of the Algorithm I ▪ Current results vs. literature	▪ Linear buckling analysis ▪ Nonlinear buckling analysis (based on displacement control) ▪ Optimization: OC (Algorithm I)
11. 4-Bar Space Truss 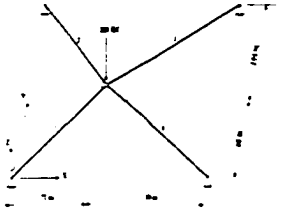	▪ Linear vs. nonlinear buckling ▪ Effect of geometric nonlinearity and element imperfection ▪ Effect of stress and displacement geometry stiffness matrices ▪ Efficiency of the Algorithm I ▪ Current results vs. literature	▪ Linear buckling analysis ▪ Nonlinear buckling analysis (based on displacement control) ▪ Optimization: OC (Algorithm I)
12. 46-Bar Planar Truss 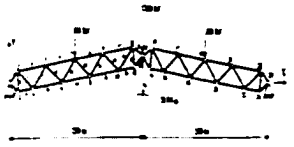	▪ Linear vs. nonlinear buckling ▪ Effect of geometric nonlinearity and element imperfection ▪ Effect of stress and displacement geometry stiffness matrices ▪ Efficiency of the Algorithm I ▪ Current results vs. literature	▪ Linear buckling analysis ▪ Nonlinear buckling analysis (based on displacement control) ▪ Optimization: OC (Algorithm I)
13. 30-Bar Dome Space Truss 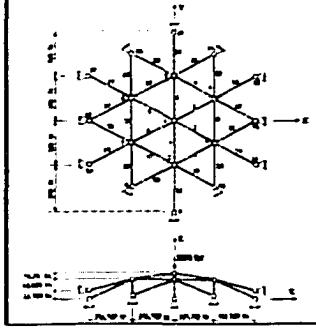	▪ Linear vs. nonlinear buckling ▪ Effect of geometric nonlinearity and element imperfection ▪ Effect of stress and displacement geometry stiffness matrices ▪ Comparison of the Algorithm I and Algorithm II ▪ Efficiency of Algorithm II ▪ Insensitivity of the limit load to the time step incrementation. ▪ Current results vs. literature	▪ Linear buckling analysis ▪ Nonlinear buckling analysis (based on displacement control) ▪ Optimization: OC (Algorithm I,II)

14. 24-Bar Dome Space Truss 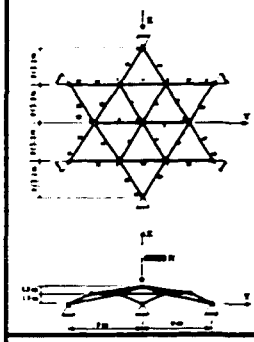	▪ Linear vs. nonlinear buckling ▪ Effect of geometric nonlinearity and element imperfection ▪ Effect of stress and displacement geometry stiffness matrices ▪ Application of GTA ▪ Comparison of the OC and SQP ▪ Current results vs. literature	▪ Linear buckling analysis ▪ Nonlinear buckling analysis (based on displacement control) ▪ Optimization: OC and SQP
15. Frame Shallow Arch 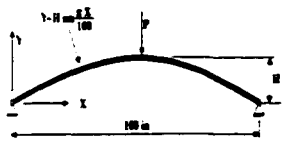	▪ Linear vs. nonlinear buckling ▪ Effect of geometric nonlinearity ▪ Effect of stress and displacement geometry stiffness matrices ▪ Comparison of the OC and SQP ▪ Current results vs. literature	▪ Linear buckling analysis ▪ Nonlinear buckling analysis (based on displacement control) ▪ Optimization: OC and SQP
16. Williams Toggle Frame 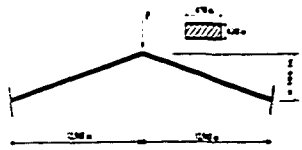	▪ Linear vs. nonlinear buckling ▪ Effect of geometric nonlinearity ▪ Effect of stress and displacement geometry stiffness matrices	▪ Linear buckling analysis ▪ Nonlinear buckling analysis (based on displacement control) ▪ Optimization: OC and SQP

Structural Geometry Optimization		
Example	**Objective**	**Analysis and Optimization Procedure**
17. 24-bar adaptive Truss 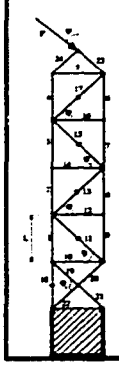	▪ Force vs. displacement method ▪ Application of FMCE and IFM in geometry optimization of adaptive structure	▪ Linear finite element analysis based on FMCE, and IFM and displacement method under static and dynamic load ▪ Optimization: SQP

5.2 Size Optimization - Displacement and Stress Constraints

5.2.1 The 10-Bar Planar Truss

The 10-bar planar truss is shown in the Figure 5-1. This structural design problem is a classical example in the literature and has been extensively investigated using linear analysis based on the displacement method. The material is aluminum with Young's modulus $E=10^7$ psi and density $\rho=0.1$ lbm/in^3. The allowable stress is ±25000 psi for all members. Stress constraints are imposed on all elements. Vertical displacement constraints of ±2 in are imposed on nodes 1-4. The minimum area for all elements was set at 0.1 in^2. The number of displacement degrees of freedom is $m=8$ and the number of force degrees of freedom $n=10$. Thus, the number of redundancy is $r=2$.

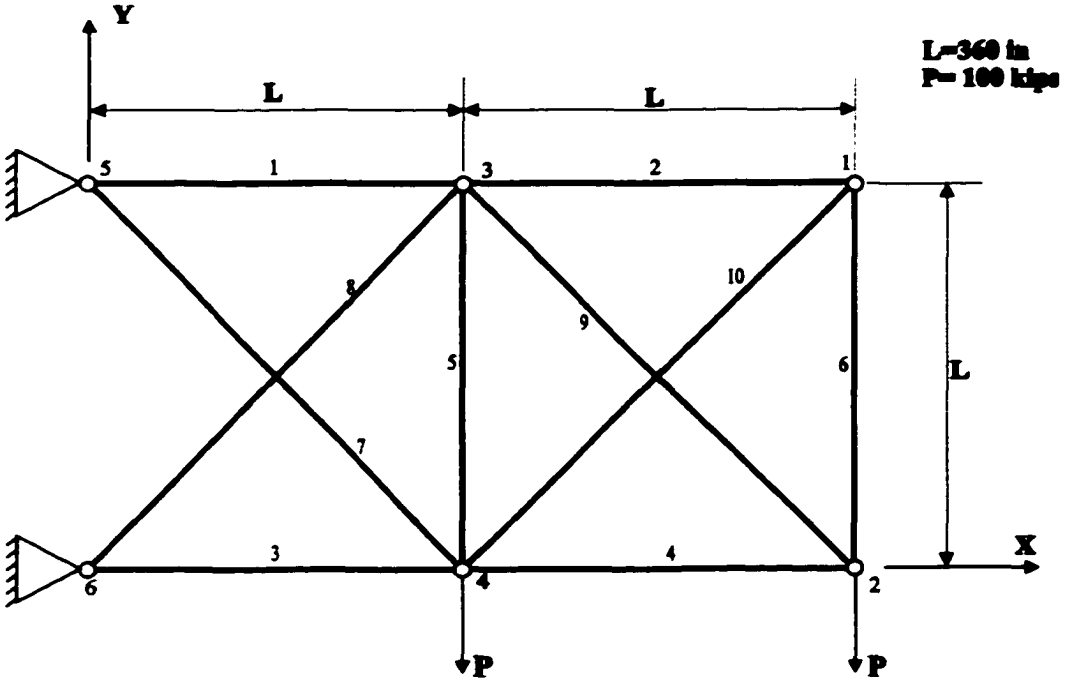

Figure 5-1 The 10-bar planar truss structure.

For linear analysis, a minimum mass of 5069.85 lbm was obtained using both the displacement method (DM) and the force method (FM). The 10-bar planar truss was also optimized using nonlinear analysis and the minimum mass obtained was 5055.56 lbm.

The initial cross sectional area for all the elements is 15 in^2, which is an infeasible guess. In both the linear and the nonlinear analysis, the horizontal negative displacement constraint at node 1 and the tension stress constraint in element 5 are active The final results for both the linear and the nonlinear analyses are tabulated in Table 5-1. The iteration history is shown in Figure 5-2. The nonlinear analysis steps required to obtain the response was 3 in all optimization iterations. The CPU time required by the FM was significantly lower than the DM, thus confirming the efficiency of the FM. The cross-sectional areas in elements 2, 5 and 10 reached to their minimums in both analyses. It is interesting to note that both the stress constraint and the cross-sectional area are active in element 5. The results obtained using the linear analysis match exactly the results reported by Fleury and Schmit [165], and Haftka and Gurdal [164], who solved the problem using the dual method and approximation concepts in linear analysis based on the displacement method. Table 5-1 reveals that the final results using the nonlinear analysis are very close to those of linear analysis, thus indicating that the effect of geometric nonlinearity is not significant.

To confirm the validity of the linear analysis results; a nonlinear analysis was carried out using the optimal cross-sectional areas obtained from the linear analysis. It was observed that the stress in element 5 (25262 psi) exhibited values beyond the limit stress, thus implying a violation of the stress constraint. Thus, it can be inferred that an analysis that does not account for the geometric nonlinear effects may result in structural failure.

The problem was also solved using different initial cross-sectional areas for the elements. The results obtained were exactly the same as in the previous case. The iteration history for three different initial cross sectional areas (using the force method) is shown in the Figure 5-3.

Next, the application of the Fully Stress Design (FSD) to demonstrate its capabilities as an optimizer was examined. It was found that the FSD optimization algorithm produced exactly the same optimal results obtained using the mathematical programming technique. However, it was noticed that when the stress limit was increased in one of the members (member 9 above the 37500 psi limit), the FSD did not produce the expected optimal results, as shown in Table 5-2.

By increasing the stress limit in member 9, it was expected that the ability of the member to sustain higher stresses leads to a lighter structure. However, the results reveal that this is not the case when using the FSD approach. In order to further understand this problem, the member area was tracked for a range of allowable stresses in member 9. When using the FSD method, the area of member 9 decreases as the allowable stress in member 9 increases. When the allowable stress in member 9 reaches beyond 37500 psi, the area of member 9 reaches its minimum size. Thus, the stress in member 9 can not reach its allowable limit, i.e. the structure does not direct sufficient load to this bar to make its stress go any higher. The plot of optimum mass and the final mass in FSD versus allowable stress in member 9 is shown in the Figure 5-4. It can be observed that until the 37500 psi level, the optimum design and FSD solutions totally match, however the solutions diverge after the 37000 level. Using the FSD method, the final mass goes up suddenly as the area of member 9 goes down towards its minimum size and the load finds other paths different from the optimal paths.

It is noted that the number of active constraints in both the optimum design and the FSD methods is equal to 10, which is precisely the number of the design variables. This means that the set of 10 constraint equations alone is sufficient to generate the 10 design variables and the objective function does not participate in the calculation of the design. Naturally, the FSD approach, which is based on the stress-ratio technique without using the objective function, should lead to the same solution as the optimum design [70, 164]. However, as explained above, this is not the case if the stress limit in member 9 reaches beyond the 37000 psi level. A probable explanation is that the 10 constraint equations are not functionally active in FSD after the stress limit, implying that a design based solely on the constraints is not sufficient. From Tables 5-1 and 5-2, it can be observed that the imposition of the displacement constraints results in a substantial increase in structural weight.

Table 5-1 The Final design solution for the cross-sectional areas (in^2) for the 10-bar planar truss structure

Member	Linear Analysis		Nonlinear Analysis
	DM	FM	
1	30.5218	30.5218	30.4707
2	0.1000	0.1000	0.1000
3	23.1999	23.1999	23.1519
4	15.2229	15.2229	15.1619
5	0.1000	0.1000	0.1000
6	0.5514	0.5514	0.5527
7	7.4572	7.4572	7.5117
8	21.0364	21.0364	21.0129
9	21.5284	21.5284	21.5076
10	0.1000	0.1000	0.1000
Mass (lbm)	5060.85	5060.85	5055.66
No. of Iterations	237	237	258
No. of A.C.*	5	5	5
CPU time (sec)	11.24	4.34	40.18

* A. C.: Active Constraints

Table 5-2 Final design of cross-sectional areas (in^2) for various stress limits in member 9.

Stress limit (psi)	25000		35000		37500		40000		75000	
Member	FSD	Opt	FSD	Opt	FSD	Opt	FSD	Opt	FSD	Opt
1	7.938	7.938	7.910	7.9100	6.721	7.900	4.106	7.900	4.106	7.900
2	0.100	0.100	0.100	0.100	1.279	0.100	3.894	0.100	3.894	0.100
3	8.062	8.062	8.090	8.090	9.279	8.100	11.894	8.100	11.894	8.100
4	3.938	3.938	3.910	3.910	2.721	3.900	0.106	3.900	0.106	3.900
5	0.100	0.100	0.100	0.100	0.100	0.100	0.100	0.100	0.100	0.100
6	0.100	0.100	0.100	0.100	1.279	0.100	3.894	0.100	3.894	0.100
7	5.745	5.745	5.784	5.784	7.465	5.798	11.164	5.798	11.164	5.798
8	5.569	5.569	5.530	5.530	3.849	5.515	0.150	5.515	0.150	5.515
9	5.569	5.569	3.950	3.950	2.566	3.677	0.100	3.677	0.100	3.677
10	0.100	0.100	0.127	0.127	1.808	0.141	5.507	0.141	5.507	0.141
Mass(lbm)	1593.2	1593.2	1511.1	1511.1	1568.3	1497.6	1725.2	1497.6	1725.2	1497.6
No. of Iterations	19	81	79	92	10	93	149	93	36	93
No. of A.C.	10	10	10	10	10	10	10	10	10	10

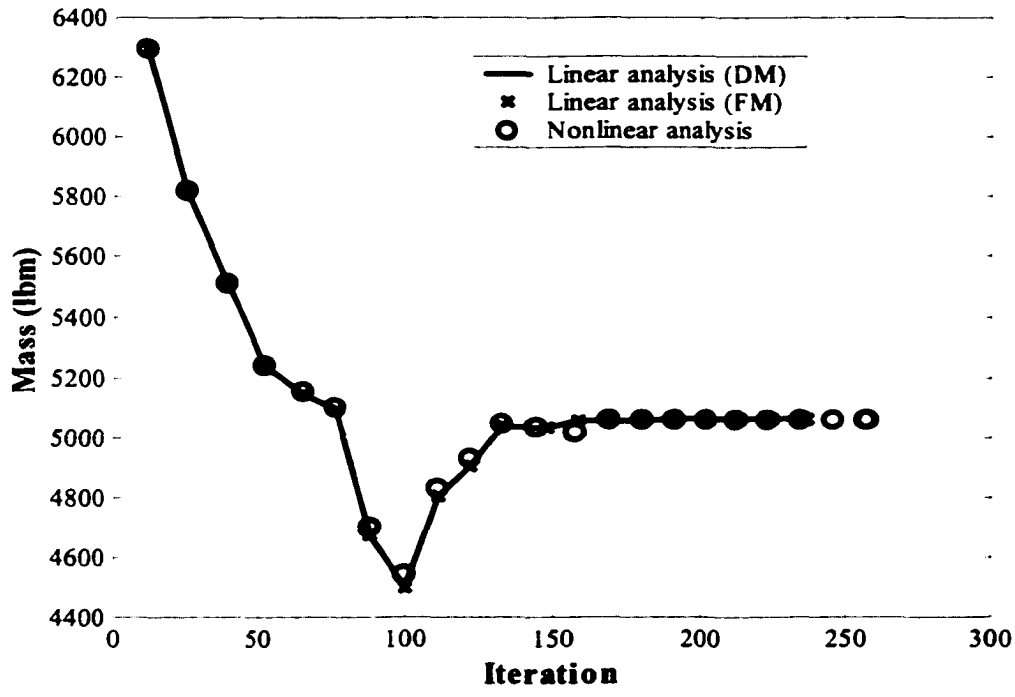

Figure 5-2 Iteration history for the 10-bar planar truss for the linear and nonlinear analysis solutions.

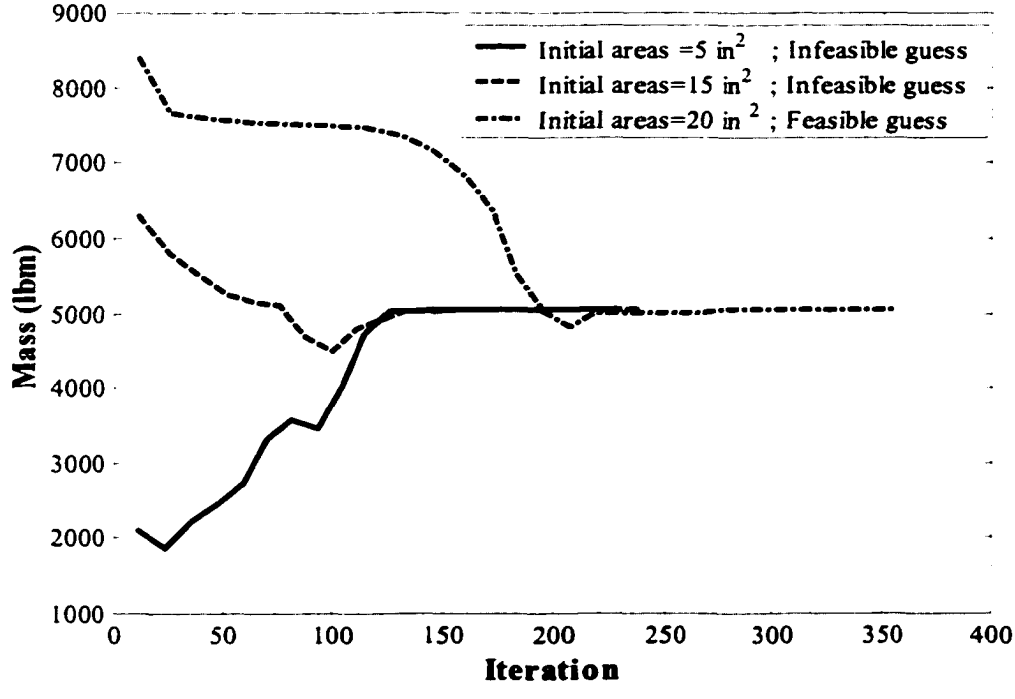

Figure 5-3 Iteration history for different initial areas for the10-bar planar truss.

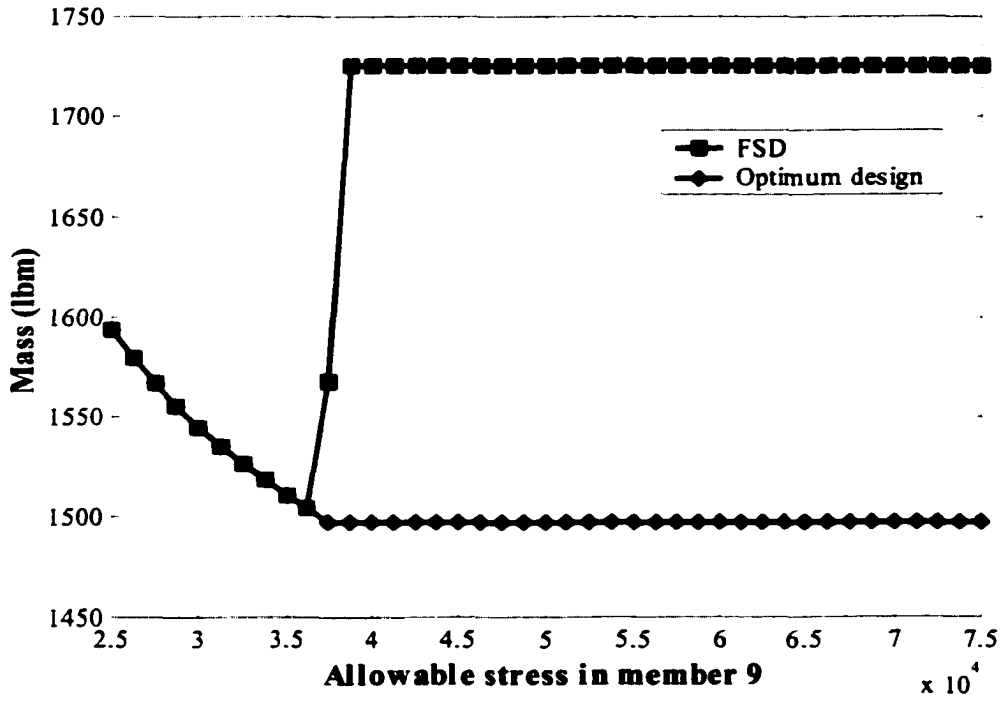

Figure 5-4 Optimum mass and final mass using the FSD method for the 10-bar truss versus allowable stress in member 9.

5.2.2 The 25-Bar Space Truss

The 25-bar space truss is shown in Figure 5-5. This problem has been investigated by Saka using both linear [166] and geometrically nonlinear analyses [125] together with the optimality criterion approach.

The material is steel with E=207 KN/mm^2 and ρ=7830 kg/m^3. The structure has identical symmetries about the X-Z and Y-Z planes, so design variable linking is used to impose symmetry on the structure. Thus, only 8 design variables are required. The structure is subjected to one load case, shown in Table 5-3. The tension allowable stress for all elements is $\sigma_{at} = 240\ \mathrm{N/mm^2}$, however allowable compression stress is obtained according to AISC [167] which are: For $S_R > C_c$; $\sigma_{ac} = \pi^2 E / S_R^2$ and for $S_R < C_c$ $\sigma_{ac} = \sigma_{at}(1 - 0.5 S_R^2 / C_c^2)$. S_R is the slender ratio of each member ($S_R = L/R_G$, where L is the length and R_G is the radius of gyration for each member) and $C_c = \sqrt{2\pi^2 E / \sigma_{at}}$.

Therefore, the allowable compression stress varies during the optimization process. Stress constraints have been imposed on all elements. Displacement constraints of ±10 mm are imposed on nodes 1 and 2 in X and Y directions. The minimum area for all elements was set at 200 mm^2. The members have pipe-type sections [166] with $S_R=aA^b$, where a and b are 0.4993 and 0.6777, respectively. A is the area in square centimeters. The number of displacement degrees of freedom is m=18 and the number of force degrees of freedom is n=25. Therefore, the number of redundancy is r=7. Without linking the design variables, the number of design variables is 25 and the number of the constraints is 56. With linking the design-variables into 8 groups, the number of design variables becomes 8, and the number of the constraints reduces to 22.

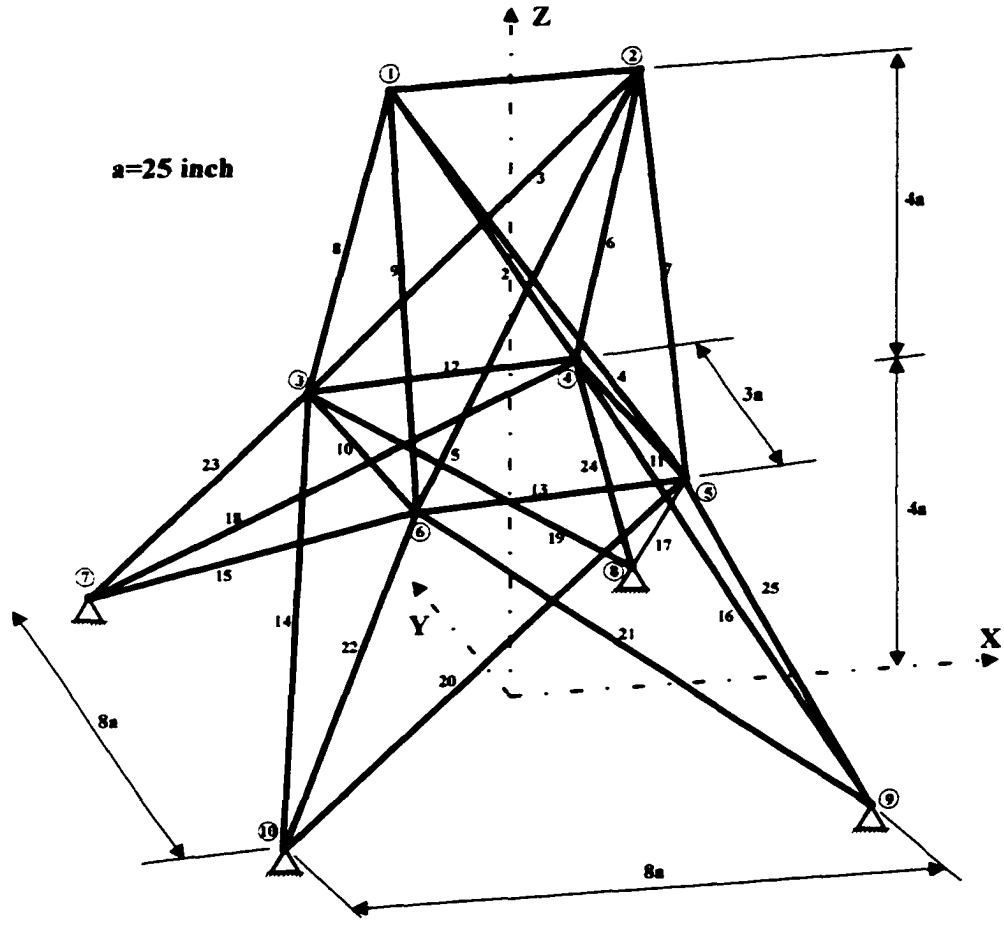

Figure 5-5 The 25-bar space truss structure.

For linear analysis, a minimum mass of 649.7 kg was obtained using both the DM and the FM. The nonlinear analysis produced a minimum mass of 650.9 kg. The final results for

both the linear and the nonlinear analysis is given in Table 5-4 and the iteration history is shown in Figure 5-6. The initial cross sectional area for all the elements is 2000 mm^2. The CPU time required for the FM is significantly lower than the DM, pointing out again the efficiency of the FM. For both the linear and the nonlinear analysis, the compression stress constraint in elements 1, 2, 6, 10, 13, 16, 18 and 24 (one member from each group) are active. According to Table 5-4, there is a slight, however insignificant, difference between the optimum results obtained from the linear and geometrically nonlinear analysis. Nevertheless, to confirm the feasibility of the linear results, the structure was also analyzed using nonlinear analysis based on the optimum cross-sectional areas obtained from linear analysis. It was found that the stress violations were accrued in the elements 10,13,16 and 18. Since these members are under compression, the optimum results obtained using a linear analysis may result in structural failure.

The problem was solved using different initial areas for all elements. The results were exactly the same as for the previous case. The iteration history for two different initial cross sectional areas using the force method is shown in the Figure 5-7.

A minimum weight of 921 kg was obtained by Saka using the linear analysis and 507 kg using the nonlinear analysis. Saka used the optimality criterion based only on satisfying the displacement constraints. The stress constraints were satisfied through stress-ratio technique in linear analysis. In nonlinear analysis, Saka satisfied the stress constraints during the steps of nonlinear analysis, so that when a member force exceeds its allowable limit, then this limit value is used in the computation of the compensating load. According to the Saka, as a result of such redistribution, truss members do not have a force, which is more than their critical force.

Fleury and Schmit [165] also solved the problem using the dual methods and approximation concepts considering just the linear analysis based on the displacement method. This structure was also analyzed using the data provided by Fleury and Schmit and identical results were obtained.

Table 5-3 Nodal load components (N) for the 25-bar space truss structure.

Node	Coordinate directions		
	X	Y	Z
1	80000	120000	30000
2	60000	100000	30000
3	30000	0	0
6	30000	0	0

Table 5-4 Final design of cross-sectional areas (mm^2) for the 25-bar space.

Design variables	Member	Linear Analysis		Nonlinear Analysis
		DM	FM	
1	1	232.7	232.7	233.0
2	2-5	1150.6	1150.6	1149.8
3	6-9	895.1	895.1	894.0
4	10,11	230.4	230.4	235.2
5	12,13	223.3	223.3	227.1
6	14-17	1018.4	1018.4	1023.8
7	18-21	950.2	950.2	954.4
8	22-25	1443.5	1443.5	1440.4
Mass (kg)		649.7	649.7	650.9
No. of Iterations		316	424	380
No. of A.C.*		8	8	8
CPU time (sec)		50.64	16.31	209.77

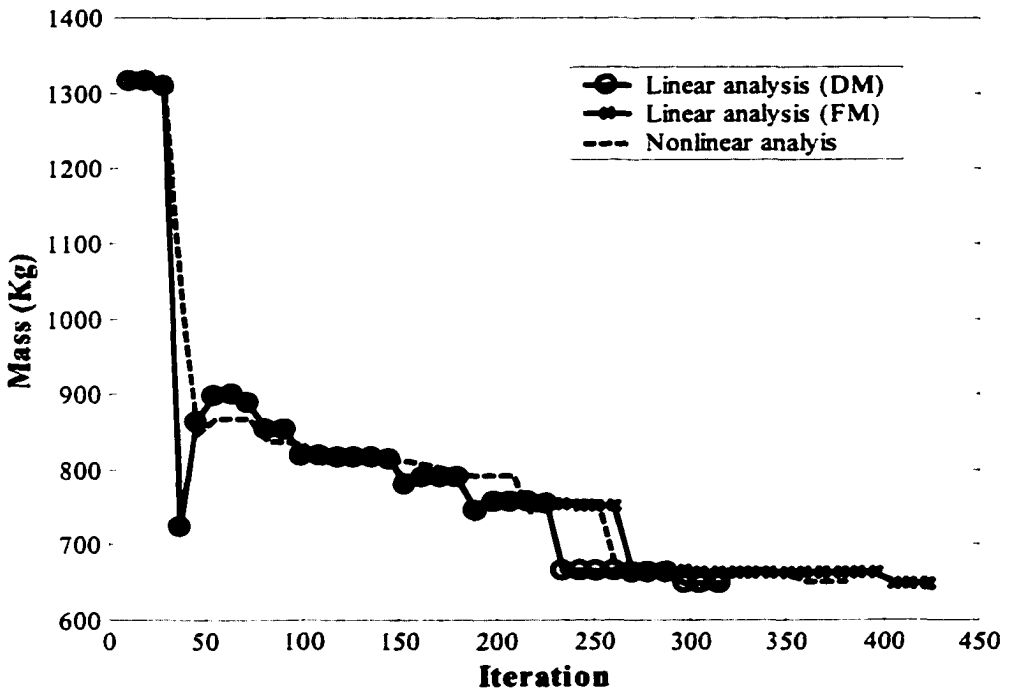

Figure 5-6 Iteration history for the 25-bar space truss for the linear and nonlinear analysis solutions.

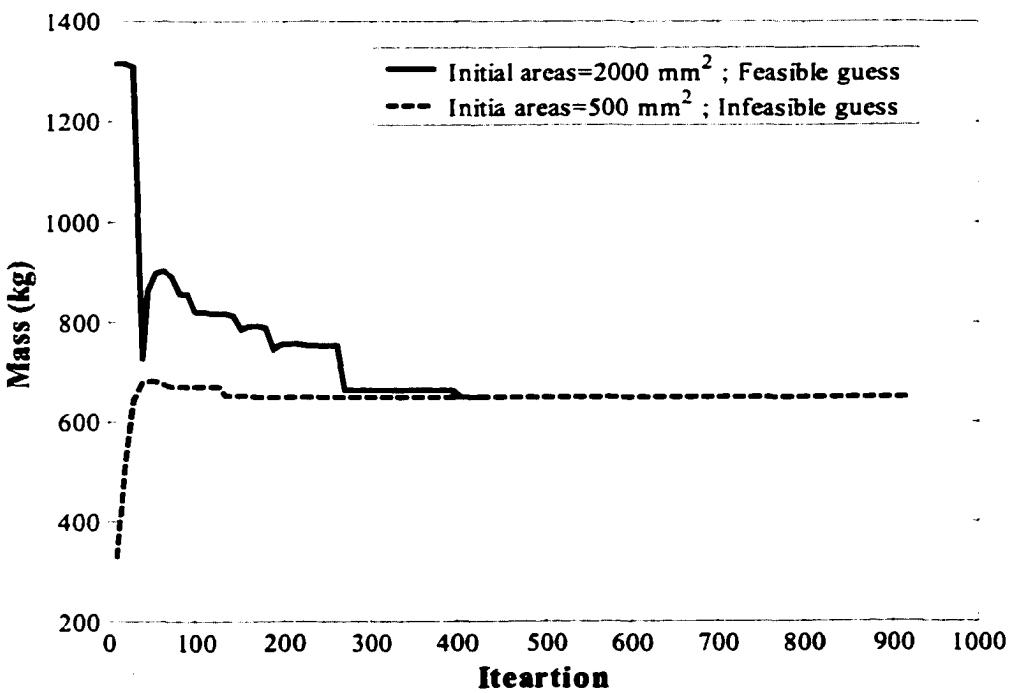

Figure 5-7 Iteration history for different initial areas for the 25-bar space truss.

5.2.3 The 72-Bar Space Truss

The 72-bar space truss is shown in Figure 5-8. This is a relatively large size problem. The material is aluminum with Young's modulus $E=10^7$ psi and density $\rho=0.1$ lbm/in^3. The allowable stress is ±25000 psi for all members. Stress constraints have been imposed on all elements. Displacement constraints of ±0.25 in are imposed on the X and Y directions for nodes 1 to 4. The minimum area for all elements was set at 0.1 in^2.

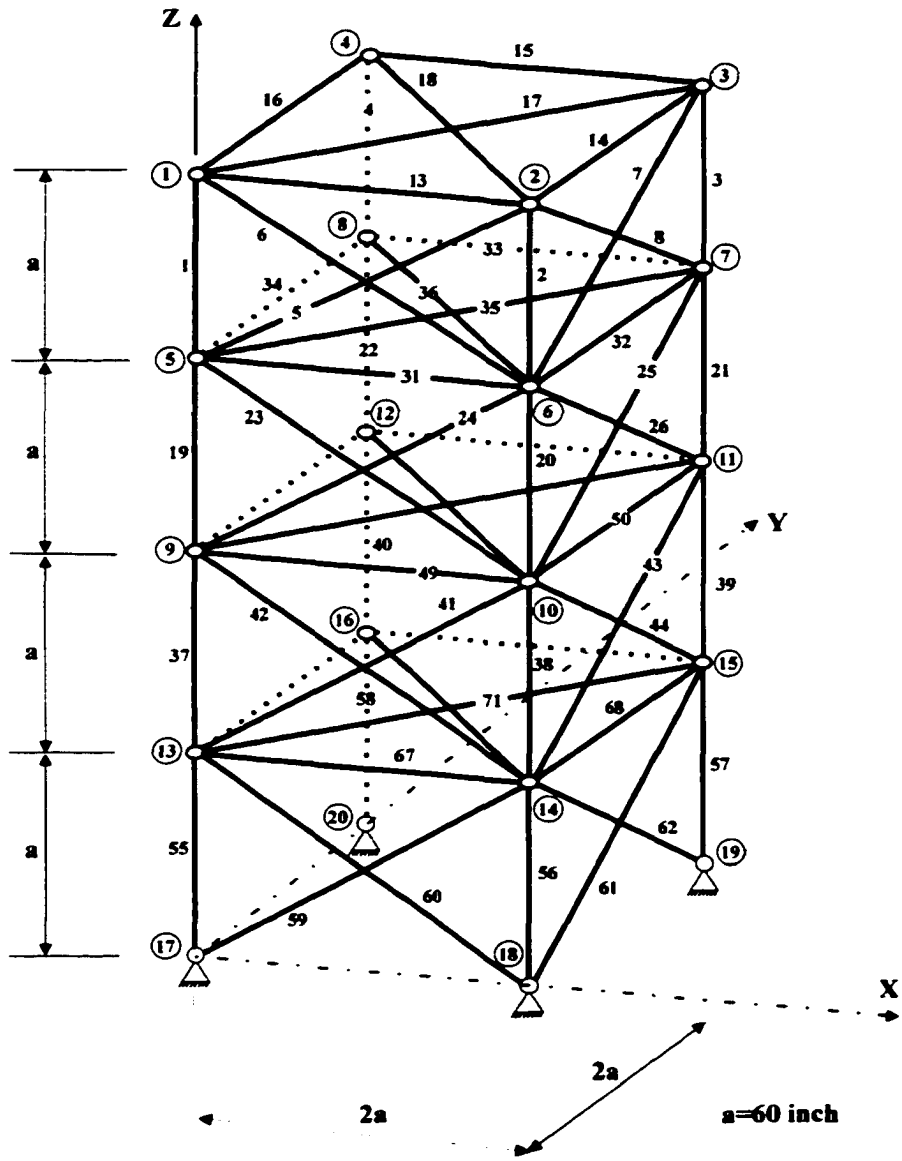

Figure 5-8 The 72-bar space truss structure.

The structure is subjected to two load cases. In the first case, node 1 is subjected to a load of 5000 lbf in the X and Y-directions and a load of –5000 lbf in the Z-direction. In the second case, nodes 1 to 4 are subjected to a load of –5000 lbf in the Z-direction. The number of displacement degrees of freedom is m=48 and the number of force degrees of freedom is n=72. Therefore, the number of redundancy is r=24. Without linking the design variables, the number of design variables is 72 and the number of the constraints is 232. When linking the design-variables into 16 groups, the number of design variables becomes 16, and the number of the constraints reduces to 64.

When using the linear analysis, a minimum mass of 379.615 lbm was obtained for both the DM and the FM. The same problem was analyzed using the nonlinear analysis and the minimum mass increased slightly to 380.079 lbm. The final results for both the linear and the nonlinear analysis is given in Table 5-5 and the iteration history is shown in Figure 5-9. The nonlinear analysis steps required to obtain the response was 2 for load case 1 and 3 steps were required to obtain the solution for load case 2 in all iterations. The computational time required for the FM is significantly lower than the DM, illustrating the efficiency of the FM over the DM for the analysis of large size problems. A closer examination of the results reveals that the in both the linear and the nonlinear analysis the nodal displacement constraints at node 1 in both X and Y directions in the first load case, and the stress constraints in elements 1 to 4 in the second load case are active. The cross-sectional areas in groups 7, 8, 11, 12, 15 and 16 reached their minima in both analyses solutions. The linear analysis solution matches exactly the solution reported by Fleury and Schmit [165], who solved the problem using the dual method and approximation concepts and a linear analysis based on the displacement method.

Note that there is a very slight difference between the optimum results from both the linear and the nonlinear analysis, however insignificant. To confirm the validity of the linear solution, the structure was analyzed considering nonlinear geometrically based on optimum cross-sectional areas obtained from the linear analysis. Surprisingly, both the displacement constraints at node 1 and the stress constraints in elements 1 to 4 for load case 2 were violated, pointing out that structural failure may result when using linear analysis.

Next, the problem was solved without linking the design variables. The results using the FM and the DM were exactly identical and the computational time for the FM was approximately one half of that required by the DM. The number of iterations using the DM and the FM were 3976 and 4707, respectively. The optimum mass reduced to 288.8 lbm, demonstrating that when not imposing symmetry to the structure results in a significantly lower mass in the final design. The number of active constraints in this case was 47. The displacement constraints at node 1 in both X and Y-directions in the first load case, and the stress constraints in members 1, 2, 4 and 19 in the second load case were active. The cross-sectional areas in elements 5, 8, 9, 12-16, 18, 24, 25, 28, 29, 31-36, 38, 40, 41, 48-54 and 56 reached their minima. This iteration history for this case is shown in the Figure 5-10.

Finally, to better illustrate the effect of geometric nonlinearity, the load in all directions and in both load cases was multiplied by 100 and the displacement constraints were increased to ±4 in. The final results are shown in Table 5-6 and the iteration history is shown in Figure 5-11. Note that the effect of geometrically nonlinearity is more pronounced at the final optimum design. At the optimum design, the constraint displacements are very far from the limit value, implying that the design is driven by the stress constraints. Note that when using a linear analysis, the stress constraints in members 6, 11,13,16,17, 23, 30, 39, 42, 47, 57, 59 and 66 in load case 1 and the members 1-4 and 19-22 in the load case 2 are active. However, in the nonlinear analysis for the load case 1, the situation is similar to the linear analysis. However for load case 2, the stress constraints in members 3 and 21 are active.

Summarizing, it may be inferred that for practical truss design problems optimized for size under stress and displacement constraints, the effect of geometrical nonlinearity is not significant and the linear analysis can provide acceptable solutions. Also it is noted that for the test cases presented, the nonlinear analysis based on geometrical nonlinearity does not necessarily produce better optimal solutions (lighter structures) when compared to the linear analysis solution. Nevertheless, a structure optimized based on a linear solution may fail when the stresses at some members reach beyond the allowable design limit, as observed in some of the test cases presented.

Table 5-5 The final design solutions for the cross-sectional areas (in^2) for the 72-bar space truss structure.

Design variable	Members	Linear Analysis		Nonlinear Analysis
		DM	FM	
1	1-4	0.1565	0.1565	0.1570
2	5-12	0.5456	0.5456	0.5462
3	13-16	0.4104	0.4104	0.4114
4	17,18	0.5697	0.5697	0.5713
5	19-22	0.5237	0.5237	0.5246
6	23-30	0.5171	0.5171	0.5178
7	31-34	0.1000	0.1000	0.1000
8	35,36	0.1000	0.1000	0.1000
9	37-40	1.2684	1.2684	1.2705
10	41-48	0.5117	0.5117	0.5120
11	49-52	0.1000	0.1000	0.1000
12	53,54	0.1000	0.1000	0.1000
13	55-58	1.8862	1.8862	1.8890
14	59-66	0.5123	0.5123	0.5126
15	67-70	0.1000	0.1000	0.1000
16	71,72	0.1000	0.1000	0.1000
Mass (lbm)		379.615	379.615	380.079
No. of Iterations		556	557	561
No. of A. C.		9	9	9
CPU time (sec)		274.23	107.10	1427.6

Table 5-6 The final design solution for the cross-sectional areas (in^2) for the 72-bar space truss with increasing load and displacement constraints.

Design variable	Members	Linear Analysis		Nonlinear Analysis
		DM	FM	
1	1-4	19.7262	19.7262	19.8204
2	5-12	7.7727	7.7727	7.8563
3	13-16	6.8390	6.8390	6.9448
4	17,18	8.7806	8.7806	8.8345
5	19-22	20.0118	20.0118	20.4108
6	23-30	7.0918	7.0918	7.1360
7	31-34	0.1000	0.1000	0.1000
8	35,36	0.8321	0.8321	0.9680
9	37-40	21.4901	21.4901	21.6968
10	41-48	6.9959	6.9959	7.0039
11	49-52	0.1000	0.1000	0.1000
12	53,54	0.1000	0.1000	0.1000
13	55-58	29.6865	29.6865	29.9487
14	59-66	6.9505	6.9505	6.9887
15	67-70	0.1000	0.1000	0.1000
16	71,72	0.1000	0.1000	0.1000
Mass (lbm)		5949.99	5949.99	6003.26
No. of Iterations		223	223	257
No. of A. C.		15	15	15
CPU time (sec)		100.92	46.67	1103.6

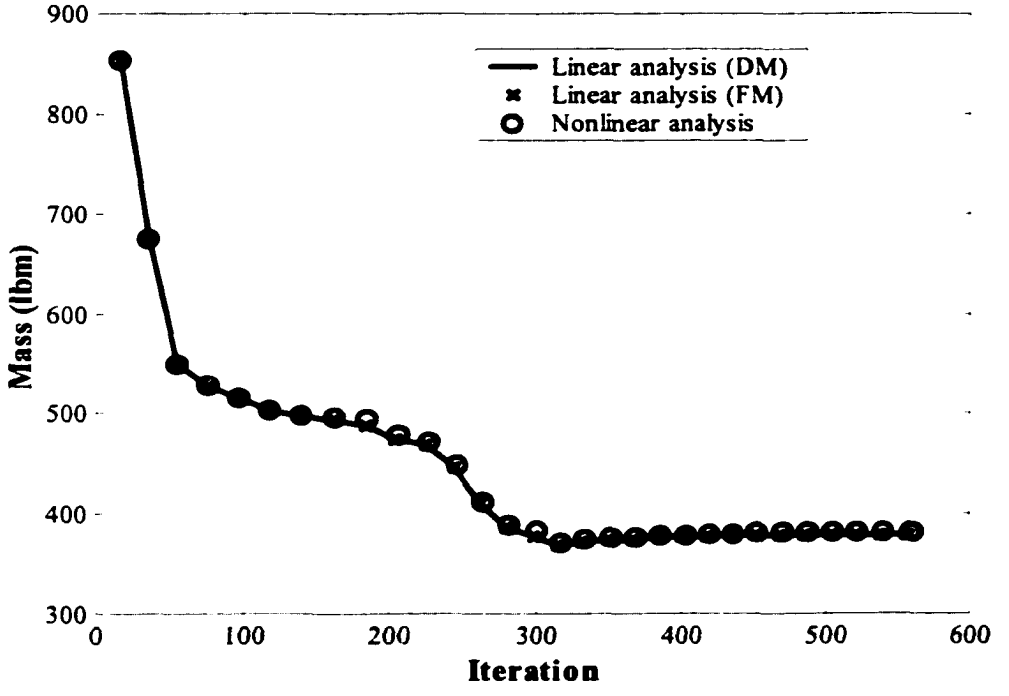

Figure 5-9 Iteration history for the 72-bar space truss for both the linear and nonlinear solutions.

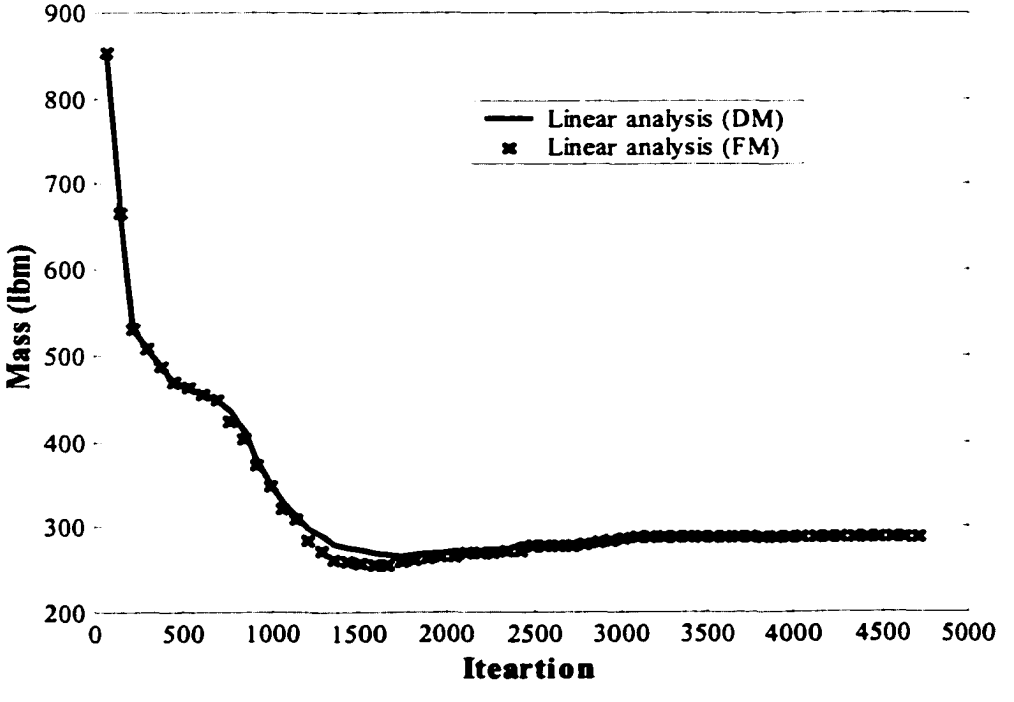

Figure 5-10 Iteration history for the 72-bar space truss with no variables linking

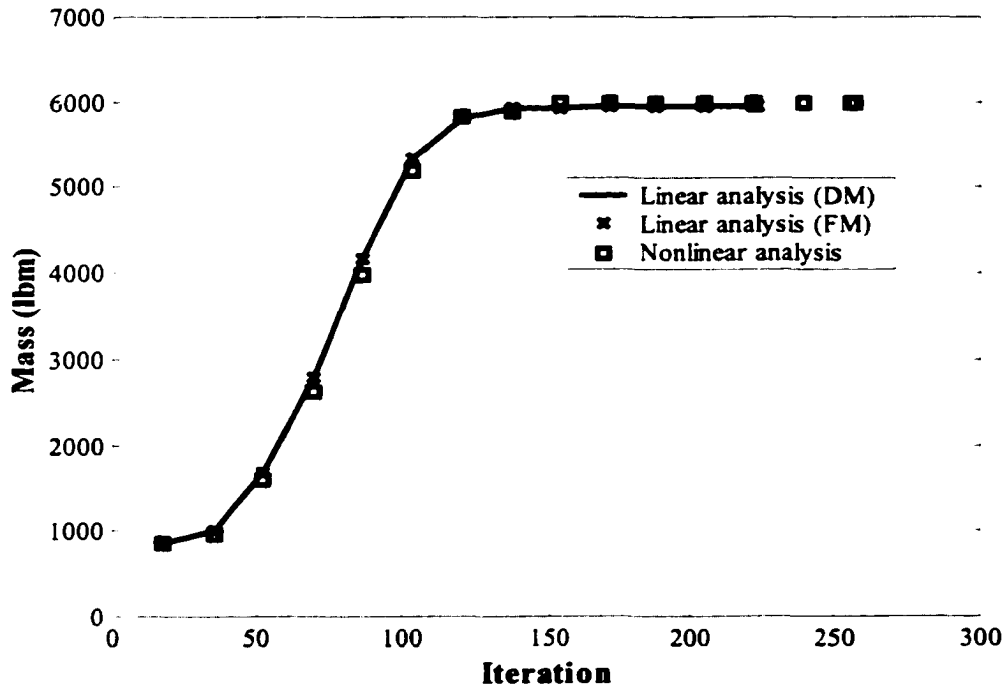

Figure 5-11 Iteration history for the 72-bar space truss with increasing load and displacement constraints.

5.2.4 The 10-Member Frame (Three-Story and Two-Bay)

The 10-member frame structure is illustrated in Figure 5-12. The material is steel with E=206,842,710 Mpa (30,000,000 psi) and ρ=7,833.412 kg/m^3 (0.283 lbm/in^3). The stress limit for all members is 165.474 Mpa (24000 psi). The horizontal displacements for all joints were limited to 0.0254 cm (0.01 in). A minimum area limit of 32.26 cm^2 (5 in^2) and maximum area limit of 645.16 cm^2 (100 in^2) were used. The initial cross-section is 161.29 cm^2 (25 in^2) and is the same for all elements. The following relationships, proposed in Ref. [168],were used for area A, section modulus S and moment of inertia I.

$$\begin{cases} S = 1.6634\,A^{1.511} \\ I = 4.592\,A^{2} \end{cases} \qquad 0 \le A \le 15$$

$$\begin{cases} S = \left(281.077\,A^{2} + 84100\right)^{0.5} - 290 \\ I = 4.638\,A^{2} \end{cases} \qquad 15 < A \le 44$$

$$\begin{cases} S = 13.761\,A - 103.906 \\ I = 256.229\,A - 2300 \end{cases} \qquad 44 < A \le 100$$

where A is the area in square inches. The above relationship is for a steel section according to the AISC code.

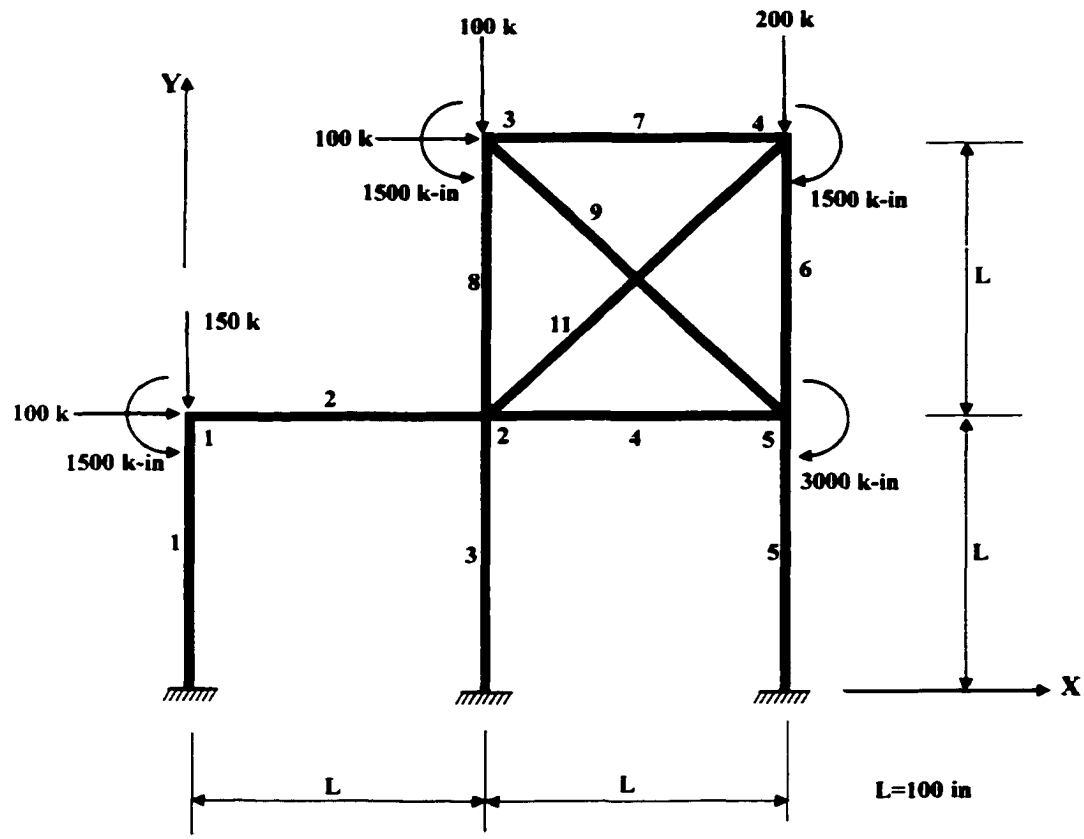

Figure 5-12 The 10-member frame structure.

A minimum weight of 3307.23 kg was obtained when using a linear analysis and 3309.9 kg when using a nonlinear analysis. The horizontal displacement constraint at node 4 and the stress constraints on element 6 are identified as active. The horizontal displacement at node 3 is close to active. The cross-sectional areas on elements 3,4 and 10 reached their

minimum size. The results were compared with research documented in the literature. For instance, Khan et al. [25,168] used a displacement based linear analysis with the optimality criterion technique and obtained a minimum weight of 3391.87 kg with the horizontal displacement of nodes 3 and 4 as active constraints (no active stress constraint). This problem was also solved using the CONMIN code [169] and a minimum weight of 3969.97 kg was reported.

The computational time for the force method was significantly lower than the time required by displacement method, again pointing out the efficiency of the force method, this time when applying the method to frame-type structures. There is a very small discrepancy between the linear and nonlinear solutions, however insignificant. Nevertheless, to confirm the validity of the linear analysis results, the structure was simulated by a nonlinear analysis using the optimum cross-sectional areas obtained via linear analysis. It was observed that the stress constraint in element 6 is a little over active, pointing out the linear analysis have produced acceptable results. The results are tabulated in Table 5-7.

Table 5-7 The final design solutions for the cross-sectional areas (cm^2) for the 10-member frame structure.

Members	Linear Analysis		Nonlinear Analysis
	DM	FM	
1	283.87	283.87	283.87
2	236.82	236.82	237.20
3	32.26	32.26	32.26
4	32.26	32.26	32.26
5	462.55	462.55	462.71
6	102.41	102.41	102.38
7	72.36	72.36	72.51
8	164.33	164.33	164.67
9	162.43	162.43	162.66
10	32.26	32.26	32.26
Mass (kg)	3307.23	3307.23	3309.9
No. of Iterations	620	608	741
No. of A. C.	5	5	5
CPU time (sec)	63.52	20.60	144.39

5.2.5 The 25-Member Frame (Three-Story and Three-Bay)

The 25-member frame is shown in Figure 5-13. The material, stress limit and the relation between area, section modulus and moment of inertia are all the same as in the previous example. The horizontal displacements for nodes 1,2,3,10,11 and 12 are limited to 0.0127 cm (0.005 in). A minimum area limit of 32.26 cm^2 (5 in^2) and maximum area limit of 6451.6 cm^2 (100 in^2) have been set.

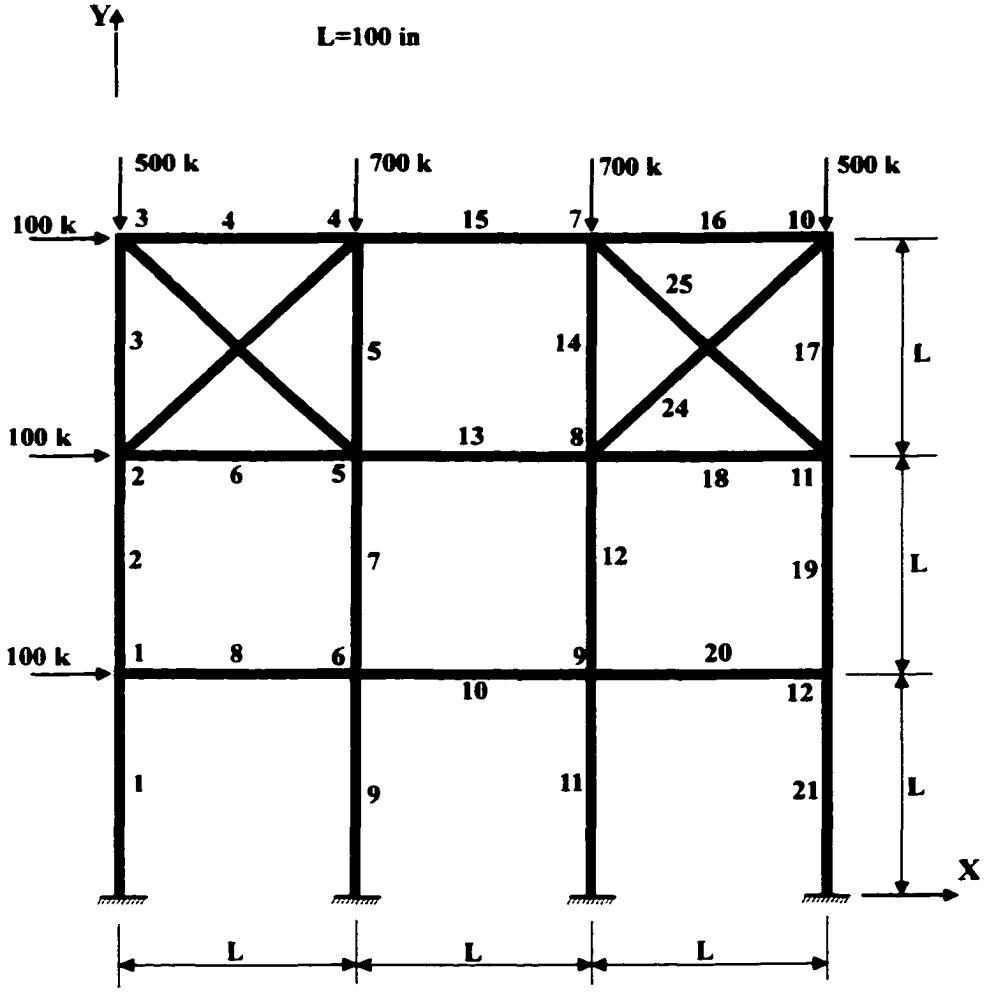

Figure 5-13 The 25-member frame structure.

The minimum weight obtained using linear and nonlinear analysis is 9508.32 kg and 9487.26 kg, respectively. The horizontal displacement constraints at nodes 2 and 10, as well as the stress constraints on elements 1,2,3,5,9,12,14 and 17, are active both in linear and nonlinear analysis. The cross-sectional areas for frame elements 6,11,13,15,18,20,24

and 25 reached their minimum size. This problem was also solved by Khan [168] using displacement based linear analysis and the optimality criterion technique, having obtained a minimum weight of 10049.77 kg with just the horizontal displacement at nodes 2 and 11 being active (no active stress constraint). Once again the finite element force method performed considerably better than the displacement method. The final results are tabulated in Table 5-8.

Table 5-8 The final design results for the cross-sectional areas (cm^2) for the 25-member frame structure.

Members	Linear Analysis		Nonlinear Analysis
	DM	FM	
1	100.07	100.07	94.83
2	71.46	71.47	69.16
3	42.33	42.33	39.52
4	162.10	162.10	167.30
5	202.47	202.46	203.07
6	32.26	32.26	32.26
7	517.57	517.49	522.80
8	148.78	148.85	141.55
9	314.29	314.29	318.78
10	538.70	538.62	532.37
11	645.16	645.16	645.16
12	205.81	205.81	204.43
13	32.26	32.26	32.26
14	195.81	195.81	195.14
15	32.26	32.26	37.47
16	48.26	48.32	50.67
17	131.53	131.54	128.98
18	32.26	32.26	32.26
19	161.65	161.68	150.72
20	32.26	32.26	32.26
21	187.51	187.54	172.97
22	135.46	135.56	137.65
23	467.54	467.39	479.67
24	32.26	32.26	32.26
25	32.26	32.26	32.26
Mass (kg)	9508.32	9508.32	9487.26
No. of Iterations	1849	1665	2757
No. of A. C.	18	18	17
CPU time (sec)	479.93	299.50	1687.90

5.3 Size Optimization - Frequency Constraints

5.3.1 The 10-Bar Planar Truss

This is the same structure as the one discussed in sub-section 5.2.1, with one exception. At each of the four free nodes, a nonstructural lumped mass of 1000 lbm (2.588 lb-s^2/in) is added. At the initial design stage, all the cross-sectional areas are set at 20 in^2 and the initial mass is 8392.94 lbm.

This problem has been investigated by Venkayya and Tischler [170], as well as by Grandhi and Venkayya [171] using the displacement based analysis with the optimality criterion technique. First, the structure was optimized for a fundamental frequency of 14 Hz alone, using both the displacement and force methods. A minimum weight of 5810.24 lbm was obtained. The number of iterations required for the force method was lower than that required for the displacement method resulting in a lower computational cost. The final results for the cross-sectional areas and the fundamental frequency are given in Tables 5-9 and 5-10, respectively. Venkayya and Tischler [170] report a minimum mass of 6665.577 lbm. The structure was analyzed for its fundamental natural frequency using the optimum cross-sectional areas obtained by Venkayya and Tischler. Here, a fundamental natural frequency of 14.47 Hz instead of 14 Hz was obtained. A solution was also attempted using the optimum solution provided by Venkayya and Tischler as the initial design. The final design resulted in a lighter structure (5810.24 lbm) than the one obtained previously. The design was based on the consistent mass matrix. When using a lumped mass matrix representation, the optimization resulted in a minimum mass of 6377.82 lbm, suggesting that a lumped mass representation may have been used in Ref. [170].

Next, the structure was designed for a second natural frequency of 25 Hz. A minimum mass of 1920.52 lbm was obtained. The force method again performed better than the displacement method. Grandhi and Venkayya [171] report a minimum mass of 2243.8 lbm. The optimum design reported by Grandhi and Venkayya was provided as input resulting in a second natural frequency of 25.37 Hz.

Finally, the structure was designed for multiple natural frequency constraints of ω_1=7, $\omega_2 \geq 15$ and $\omega_3 \geq 20$. Here, a minimum mass of 1182.85 lbm was obtained. Upon a closer inspection of the results, it was found that the optimum cross-sectional areas for elements 9 and 10 obtained using the force method (FM) are different than that obtained using the displacement method (DM). It is noted that the optimum mass for both the FM and the DM is exactly the same and so are the final natural frequencies. It is inferred that the optimizer may be very sensitive to the output results from the FM and the DM, so that a slight discrepancy in the intermediate results may cause the optimizer to select a different path. It is noted that for this particular case, the number of iterations required by the DM is lower than that for the FM. However, the computational time required for the FM is still lower than that for the DM. For comparison with the literature, it is noted that Ref. [171] reports a minimum weight of 1308.4 lbm. The final cross-sectional areas and natural frequencies are given in the Tables 5-9 and 5-10. The variation of the optimum mass with the first and second natural frequency limits is shown in Figure 5-14. It is obvious that by increasing the fundamental natural frequency limit, the optimum mass increases drastically from 347.91 lbm for a fundamental natural frequency limit of 4 Hz to 25216.7 lbm for a fundamental natural frequency limit of 22 Hz. However, this is not the case for the second natural frequency limit. The optimum mass increases from 46.83 lbm for a second natural frequency limit of 4 Hz to 1410.14 lbm for a second natural frequency limit of 22 Hz.

Table 5-9 The final design solution for the cross-sectional areas (in^2) for different frequency constraints (Hz) for the10-bar planar truss.

Element No.	DM			FM		
	ω_1=14	ω_2=25	ω_1=7 $\omega_2\geq$15 $\omega_3\geq$20	ω_1=14	ω_2=25	ω_1=7 $\omega_2\geq$15 $\omega_3\geq$20
1	34.086	7.466	5.986	34.085	7.459	5.928
2	7.427	5.557	2.827	7.427	5.554	1.537
3	34.086	7.470	5.929	34.085	7.471	5.986
4	7.427	5.557	1.536	7.427	5.562	2.826
5	0.100	2.294	0.685	0.100	2.298	0.685
6	0.100	1.183	0.651	0.100	1.183	0.650
7	19.162	6.376	3.737	19.162	6.371	3.115
8	19.162	6.377	3.113	19.162	6.383	3.735
9	8.475	2.046	1.775	8.475	2.046	2.153
10	8.475	2.0451	2.154	8.475	2.044	1.775
Mass (lbm)	5810.24	1920.52	1182.85	5810.24	1920.52	1182.85
No. of Iterations	256	1035	637	237	973	705
No. of A.C.	3	1	2	3	1	2
CPU time (sec)	10.54	40.81	25.96	7.51	28.70	21.62

Table 5-10 The Final design for the natural frequencies (Hz) for different frequency constraints (Hz) for the 10-bar planar truss.

Freq. No.	Initial Design	DM			FM		
		ω_1=14	ω_2=25	ω_1=7 $\omega_2\geq$15 $\omega_3\geq$20	ω_1=14	ω_2=25	ω_1=7 $\omega_2\geq$15 $\omega_3\geq$20
1	11.23	14.00	8.01	7.00	14.00	8.01	7.00
2	33.05	18.01	25.00	17.62	18.01	25.00	17.62
3	36.85	29.40	25.00	20.00	29.40	25.00	20.00
4	68.26	34.55	26.68	20.00	34.55	26.68	20.00
5	75.86	49.36	32.83	28.20	49.36	32.83	28.21
6	85.18	53.11	40.92	31.07	53.11	40.94	31.07
7	85.74	85.10	62.52	47.68	85.10	62.52	47.68
8	103.10	90.41	64.79	52.35	90.41	64.78	52.35

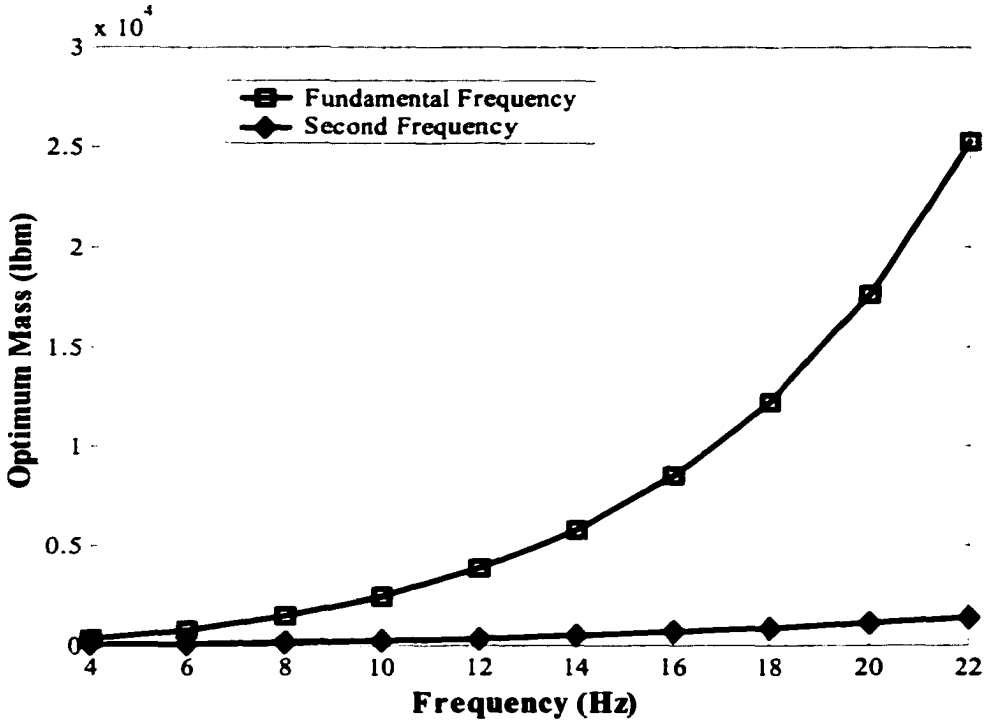

Figure 5-14 History of the optimum mass with respect to fundamental and second frequencies for the10-bar planar truss.

5.3.2 The 72-Bar Space Truss

This is a structure similar to the example discussed in sub-section 5.2.3. The material properties, element size and limits, and linking scheme are exactly the same. At the nodes 1-4, a nonstructural lumped mass of 5000 lbm (12.94 lb-s^2/in) is added. At the initial design stage, all the cross-sectional areas are 1 in^2 and the initial mass is 853.09 lbm. This problem has also been investigated by Tabarrok and Konzelman [172] using dual methods based on approximation concepts for optimization and the finite element approach based on displacement method for structural analysis. The structure was designed for a fundamental frequency of 4 Hz alone, using both the displacement and the force methods. A minimum mass of 632.361 lbm was obtained. It is noted that for this particular case, the number of iterations required by the DM is greater than that of FM. However, the computational time required by the DM is lower than that used by the FM. Therefore, it is inferred that when considering frequency constraints, the analysis of low

redundant structures using the FM is not necessarily more efficient than that of DM. Final results for frequencies and cross-sectional areas are given in Tables 5-11 and 5-12. For comparison with the literature, Ref. [172] reports a minimum mass of 632.36 lbm. Due to the symmetry imposed by the structural geometry and the linking scheme, the eigenvalue corresponding to the fundamental mode of vibration is a repeated eigenvalue of multiciplity two. This means that in the initial and optimum design, the first and second modes of vibration have the same natural frequencies. Thus a small change or deviation in the geometry of the structure can switch the mode of vibration from first to second mode, which may be undesirable in some design cases. Because of the intrinsic symmetry in the structure, any attempt to separate the fundamental and second natural frequencies during the optimization process failed.

Finally, to demonstrate the performance of the algorithm under multiple frequency constraints, the structure was designed for $\omega_1=4$ and $\omega_3\geq 6$. Using both the FM and the FM methods, a minimum weight of 721.597 lbm was obtained. The DM again performed better than the FM. The results are tabulated in Tables 5-11 and 5-12.

Table 5-11 The final results for the natural frequencies (Hz) for different frequency constraints for the 72-bar space truss structure

Freq. No.	Initial Design	DM		FM	
		$\omega_1=4$	$\omega_1=4$ $\omega_3\geq 6$	$\omega_1=4$	$\omega_1=4$ $\omega_3\geq 6$
1	3.113	4.000	4.000	4.000	4.000
2	3.113	4.000	4.000	4.000	4.000
3	5.374	5.001	6.000	5.001	6.000
4	9.425	6.505	6.247	6.505	6.247
5	13.189	8.595	9.074	8.595	9.074

Table 5-12 The final design for the cross-sectional areas (in^2) for different frequency constraints (Hz) for the 72-bar space truss structure

Element No.	DM		FM	
	ω_1=4	ω_1=4 $\omega_3\geq6$	ω_1=4	ω_1=4 $\omega_3\geq6$
1-4	0.7312	0.5423	0.7312	0.5423
5-12	0.8547	1.2295	0.8547	1.2295
13-16	0.1000	0.1000	0.1000	0.1000
17-18	0.1000	0.1000	0.1000	0.1000
19-22	1.8212	1.2487	1.8212	1.2487
23-30	0.8638	1.2417	0.8638	1.2417
31-34	0.1000	0.1000	0.1000	0.1000
35-36	0.1000	0.1000	0.1000	0.1000
37-40	2.9373	1.9858	2.9373	1.9858
41-48	0.8691	1.2494	0.8691	1.2494
49-52	0.1000	0.1000	0.1000	0.1000
53-54	0.1000	0.1000	0.1000	0.1000
55-58	4.0199	2.6782	4.0198	2.6782
59-66	0.8723	1.2537	0.8723	1.2537
67-70	0.1000	0.1000	0.1000	0.1000
71-72	0.1000	0.1000	0.1000	0.1000
Mass (lbm)	632.361	721.597	632.361	721.597
No. of Iterations	544	379	510	379
No. of A.C.	9	10	9	10
CPU time (sec)	283.78	200.37	302.96	227.62

5.3.3 The 6-Member Frame (Two-Story and One-Bay)

The 6-member frame is illustrated in Figure 5-15. This problem has been studied by Khan and Willmert [173] and MacGee and Phan [174] using the optimality criterion method as an optimizer and the finite element based on the displacement method as an analyzer. A uniformly distributed nonstructural mass of 10 lbm/in was added on the horizontal members of the frame. The density and Young's modulus are 0.28 lbm/in^3 and 30,000,000 psi, respectively. Each member is a WF steel section, according to the AISC code. The moment of inertia, I is empirically related to area, A, by the following expressions as given in Ref. [173,174].

$$I = 4.6248\,A^2\,, \quad 0 \le A \le 44 \qquad \text{and} \qquad I = 256\,A - 2300\,, \quad 44 < A \le 88.2813$$

where A has a dimension of in^2. A minimum constraint on the design variables (cross-sectional area of the members) was specified at 7.9187 in^2 and a maximum was set at 88.28 in^2. At the initial design stage, all the cross-sectional areas are equal to 30 in^2 with an initial mass of 11088 lbm.

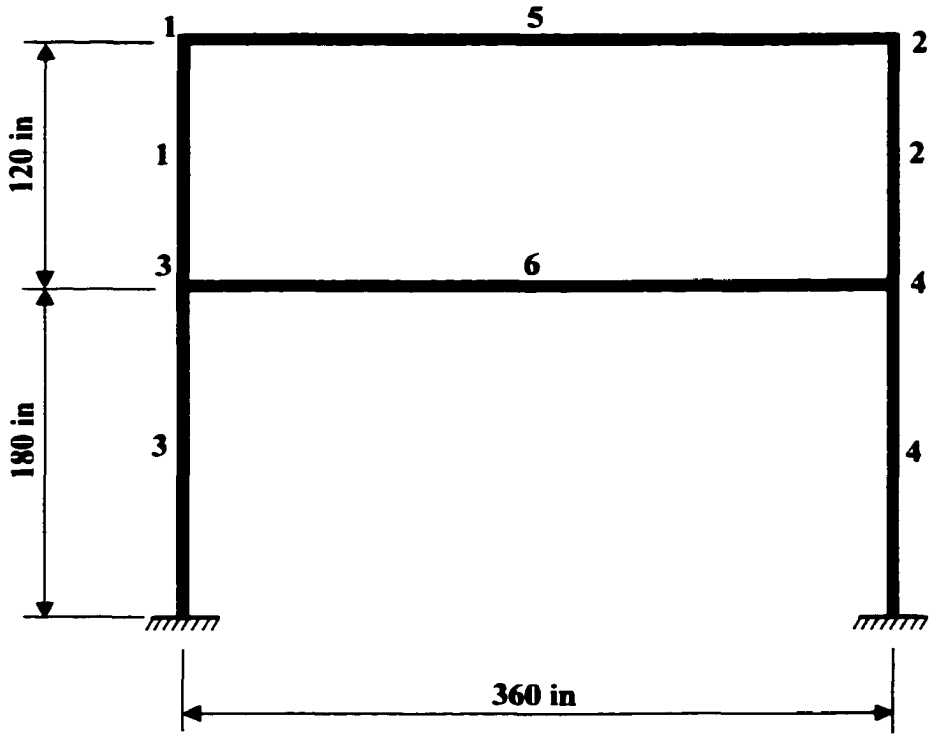

Figure 5-15 The 6-member frame structure.

First, the structure was designed for a fundamental natural frequency of 78.5 rad/sec. A minimum mass of 9410.39 lbm was obtained using both the FM and the DM. It is noted that the final design variables (cross-sectional areas) are different between the DM and FM solutions, pointing out optimum solution is not unique. However, the final natural frequencies are the same. The reason for this difference between the optimum results using the DM and the FM is that the final design depends on the path taken over the process of optimization. Depend on the problem, optimizer may be very sensitive to the output results from the analyzer so that even slightly difference may cause difference

path. It should be emphasized that although optimum results obtained through FM and DM are different, they resulted to the same optimum mass and same final natural frequencies. Therefore both are optimum solutions. The number of iterations and CPU time in DM are slightly greater than that of FM. The results are given in the Tables 5-13 and 5-14. Ref. [173] and Ref. [174] report a minimum weight of 9561 lbm and 9815 lbm, respectively. To check for the possibility that the optimality criterion employed by Refs. [173,174] produced a local minimum, another run is performed, starting with the solution from Refs. [173,174]. This run has resulted in a design change and has converged to the lighter solution of 9410.39 lbm previously obtained. Hence the solution in Refs. [173,174] does not represent a local minimum.

The structure was again designed using multiple natural frequencies of ω_1=78.5 and $\omega_2 \geq 180$. Surprisingly, the optimum mass of 9615.78 lbm using FM and 9732.3 lbm using DM was obtained. As explained before, this specific problem is path dependent and slightly difference in output results from analyzers (FM and DM) may cause different optimum solution. Investigating the final natural frequencies for DM and FM reveal that the in FM the inequality constraint is active in the optimum solution, but this is not the case for DM and that is the reason for lighter mass obtained using FM. For this case, it is interesting to note that the number of iteration and CPU time in FM is lower than that of DM. It can be said that for the frequency constraints, the CPU time totally depends on the iteration number, however this was not the case for the stress-displacement constraints.

Table 5-13 Final design of natural frequencies (rad/sec) in different frequency constraints for the 6-member frame structure.

Freq. No.	Initial Design	DM		FM	
		ω_1=78.5	ω_1=78.5, $\omega_2 \geq 180$	ω_1=4	ω_1=78.5, $\omega_2 \geq 180$
1	69.044	78.500	78.500	78.500	78.500
2	286.840	146.670	220.806	146.668	180.000
3	380.324	268.399	436.420	268.350	371.289
4	476.168	350.723	486.975	350.667	418.804
5	499.720	465.900	540.125	465.780	485.897

Table 5-14 The final design for the cross-sectional areas (in^2) for different frequency constraints (rad/sec) for the 6-memeber frame structure.

Element No.	DM		FM	
	ω_1=78.5	ω_1=78.5, $\omega_2 \geq 180$	ω_1=78.5	ω_1=78.5, $\omega_2 \geq 180$
1	33.4594	18.6862	7.9187	31.9749
2	7.9187	21.9793	33.4105	9.7256
3	7.9187	44.0000	56.7273	21.5089
4	56.9166	35.3030	7.9187	46.1708
5	7.9187	7.9187	7.9187	7.9187
6	39.2286	35.4252	39.3389	39.7360
Mass (lbm)	9410.46	9732.3	9410.39	9615.78
No. of Iterations	320	726	258	246
No. of A.C.	4	2	4	3
CPU time (sec)	15.31	34.29	11.76	11.21

5.4 Size Optimization - System Stability Constraints

In all the test cases presented in this section, unless otherwise stated, the material is aluminum with Young's modulus E =10^7 psi and material density ρ=0.1 lbm/in^3. The optimality criterion algorithm based on the potential energy (algorithm I) and the optimality criterion algorithm based on the sensitivity analysis of the limit load (algorithm II) have been used to optimize the structure and the displacement control technique has been used for analysis. As mentioned in Chapter 3, using either the $\boldsymbol{K}_\sigma$ or the $\boldsymbol{K}_{DI}$ as the geometric stiffness matrix does not have any significant difference in the geometric nonlinear analysis. Here, the geometric nonlinear matrix used for the nonlinear buckling analysis is based on the $\boldsymbol{K}_\sigma$. However, for linear buckling all the three matrices $\boldsymbol{K}_{\sigma c}$, $\boldsymbol{K}_\sigma$ and $\boldsymbol{K}_{DI}$ are used during the analysis and optimization and their effect are appropriately discussed.

The step size parameter in algorithm I was set initially equal to 4 and whenever the mass of the structure increased, the parameter was doubled to reduce the numerical oscillation induced by the algorithm. The minimum area for all elements was set at 0.1 in^2. The

minimum size constraint was treated as a passive constraint. If the recurrence relation reduced the area of any element to a value smaller than the minimum specified, then the cross-sectional area of that element was set to the minimum size.

The test cases considered here are shallow structures. These structures present excellent insight into the study of stability constraint problems as the stresses in the elements do not exceed the allowable stress limits before the structure reaches its critical system buckling load. Thus, the stress constraints do not control the design of the problem. For perfect elements, it is assumed that the individual elements are not buckled and the element formulation does not account for the instability at the element level. However, the imperfect element formulation, described in Appendix A, considers the buckling of the elements and as the individual elements attains the buckling load, the load response behavior of the system changes significantly, providing erroneous results. To guard against element buckling in the imperfect structure, a simple strategy is implemented. If the force in the individual elements goes beyond the element buckling load during the optimization process, the cross-sectional areas of the relevant elements are updated to avoid element force beyond the element buckling load.

5.4.1 The Symmetric 2-Bar Truss

A symmetric two-bar truss illustrated in Figure 5-16 is considered. The structure was designed for a specified limit load of 200 lbf applied at node 1 in the negative Y direction.

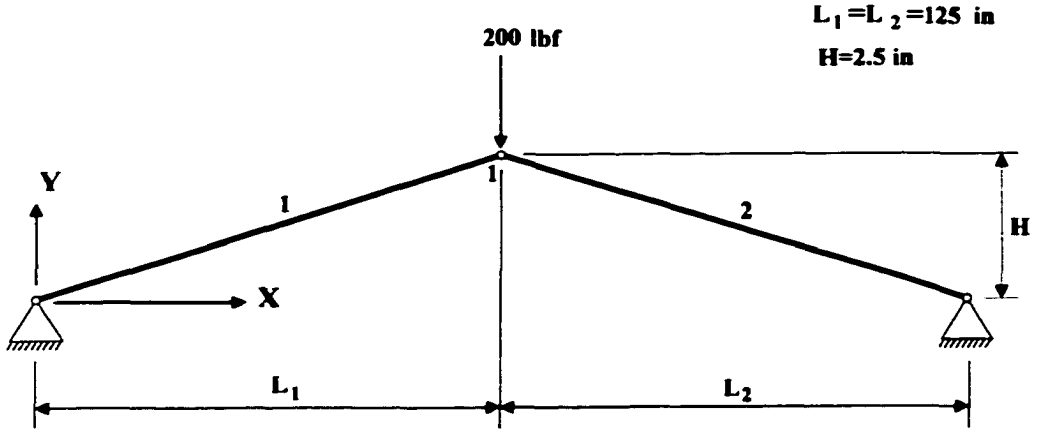

Figure 5-16 The symmetric 2-bar truss structure.

The downward vertical displacement at this node (V) is taken as the controlling displacement in the displacement control method. The displacement is applied at a rate of 0.05 inch at each time step. The optimization has been carried out using the optimality criterion algorithm based on the potential energy The initial cross sectional area of A=20 in^2 is considered for both elements and the initial mass is 500.100 lbm. The problem has been solved for both perfect and imperfect elements. The elements are tubular with solid circular cross-section. An imperfection amplitude of 0.5 in is assumed for all elements. A nonlinear buckling analysis has been done until limit load for both the perfect and imperfect structure, and the results are shown in Figure 5-17. It is observed that the effect of imperfection becomes more significant as the load approaches the limit load. For perfect elements, simulations with A=20 in^2 and A=5 in^2 produced a limit load of 615.594 lbf and 153.899 lbf, respectively. For the structure with imperfections, the limit loads were reduced to 561.955 lbf and 97.690 lbf, respectively. The decrease in the limit load shows that element imperfections can have a significant influence on the design of the structure.

When carrying out a nonlinear buckling analysis, a minimum mass of 162.4555 lbm was obtained after 3 iterations for the perfect structure and a minimum mass of 209.131 lbm was obtained after 12 iterations for the imperfect structure. The final results for the cross-sectional areas are shown in Table 5-15. The results reveal that by neglecting the effect of imperfection, the minimum mass was underestimated by 28.7 %. When optimizing the imperfect structure, the optimizer uniformizes the strain energy in the elements on the base of maximum stress in the elements, which are the axial and bending stresses. Using the final cross-sectional areas, a nonlinear buckling analysis was performed, and an exactly limit load of 200.00 was obtained for both the perfect and the imperfect structures, pointing out that the final design is on the constraint's boundary. This implies that the design is driven by the critical buckling mode, which is found to be axisymmetric. The final stresses in both members for the perfect and imperfect structures were found to be –1334.1 psi and –2613.5 psi, respectively, which are well below the buckling stress of the individual elements. The relative final strain energy density is 1.000 for the members in both the perfect and the imperfect structures.

The results for the perfect structure are in excellent agreement with the results reported by Khot and Kamat [111]. Although the initial cross sectional areas considered here are not in the feasible region (the initial limit load is not equal to the design load), the problem converges to the optimum solution in just 3 iterations for the perfect structure in comparison to the 10 iterations required for the solution in Ref. [111]. Here, the initial cross-sectional areas were set in the feasible region. More precisely, the present solution process obtains the optimum design with one analysis, and the other two analyses were needed to establish the convergence.

Next, the effect of geometric nonlinearity in buckling analysis was considered. A linear buckling analysis was performed on the perfect structure. It was found that the linear buckling analysis highly underestimates the minimum mass, which may lead to structural failure. The final results are given in Table 5-15. A closer inspection of the results reveals that using either $\boldsymbol{K}_{\sigma c}$ or $\boldsymbol{K}_{\sigma}$ as the geometric stiffness matrix does not result in a significant change in the final cross-sectional areas and minimum mass. However, using the $\boldsymbol{K}_{DI}$ geometric stiffness matrix produces more conservative results. The reason may be attributed to the nature of the $\boldsymbol{K}_{\sigma}$ and $\boldsymbol{K}_{DI}$ matrices. When computing a linear buckling load, the use of $\boldsymbol{K}_{\sigma}$ implies that pre-buckling rotations are zero, whereas the use of $\boldsymbol{K}_{DI}$ implies that pre-buckling rotations are small. For linear problems, the two matrices yield the same buckling load, but for problems with geometric nonlinearity where pre-buckling rotations are not negligible, the use of $\boldsymbol{K}_{DI}$ yields a smaller buckling load and larger optimum mass. Figure 5-18 shows the iteration history for all cases.

The optimum results for different heights H, for a perfect structure with L_1=L_2=100 in and its comparison to the exact solution are given in Table 5-16. It is noted that when the height reaches H=20 in and beyond, the stresses in the elements exceed the allowable stress so these situations will not arise in reality, however are mentioned here for comparison purposes to show the validity of the present solution. The comparison of linear and nonlinear buckling analysis for different initial angles of inclination is shown in Figure 5-19.

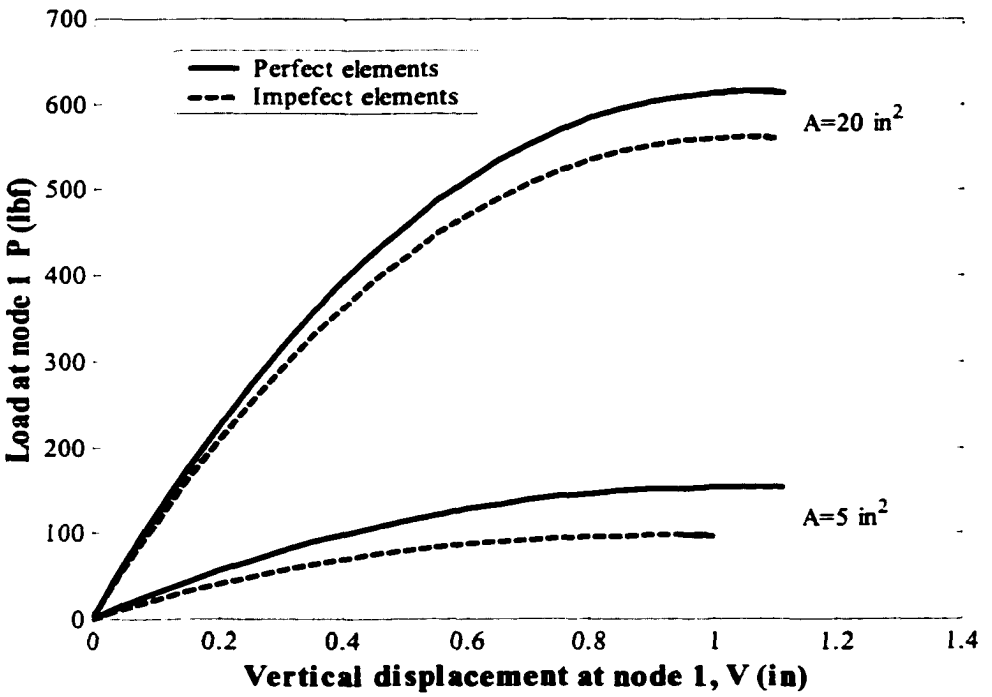

Figure 5-17 Load-deflection curve up to the limit load for the symmetric 2-bar truss for the perfect and the imperfect structure.

Table 5-15 Final designs for the cross-sectional areas (in^2) for the symmetric 2-bar truss structure.

Element No.	Linear ($K_{\sigma c}$)	Linear (K_{σ})	Linear (K_{DI})	Nonlinear (Perfect)	Nonlinear (Imperfect)
1	1.2502	1.2508	3.7523	6.4978	8.3647
2	1.2502	1.2508	3.7523	6.4978	8.3647
Mass (lbm)	31.2625	31.275	93.825	162.456	209.106
Iteration	3	3	3	3	8

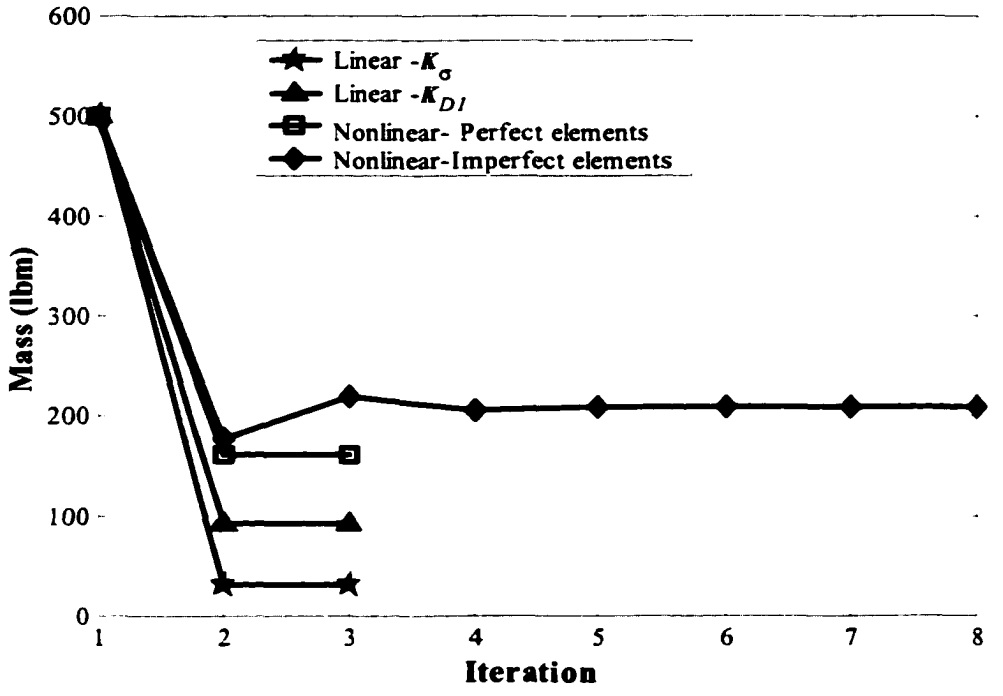

Figure 5-18 Iteration history for the perfect and imperfect symmetric 2-bar truss.

Table 5-16 Optimal designs for different H (in) for the symmetric 2-bar truss.

H	Present work				Exact	
	A_1/A_2	V (in)	Lf*	Max stress (psi)	V (in)	Lf
10	1.0	4.2289	5.20	-8319.5	4.23	5.19
20	1.0	8.4721	5.22	-33113	8.47	5.22
50	1.0	21.4247	5.36	-200050	21.42	5.36
75	1.0	32.6515	5.55	-429110	32.65	5.56
100	1.0	44.4240	5.83	-716820	44.42	5.83
125	1.0	56.8278	6.16	-1040900	56.83	6.17
150	1.0	69.9007	6.57	-1382300	69.90	6.57
175	1.0	83.6442	7.03	-1726300	83.64	7.03
200	1.0	98.0351	7.55	-2063000	98.04	7.55

* Lf=Load factor=(Nonlinear Optimum Volume)/(Linear Optimum Volume), for a specified limit load.

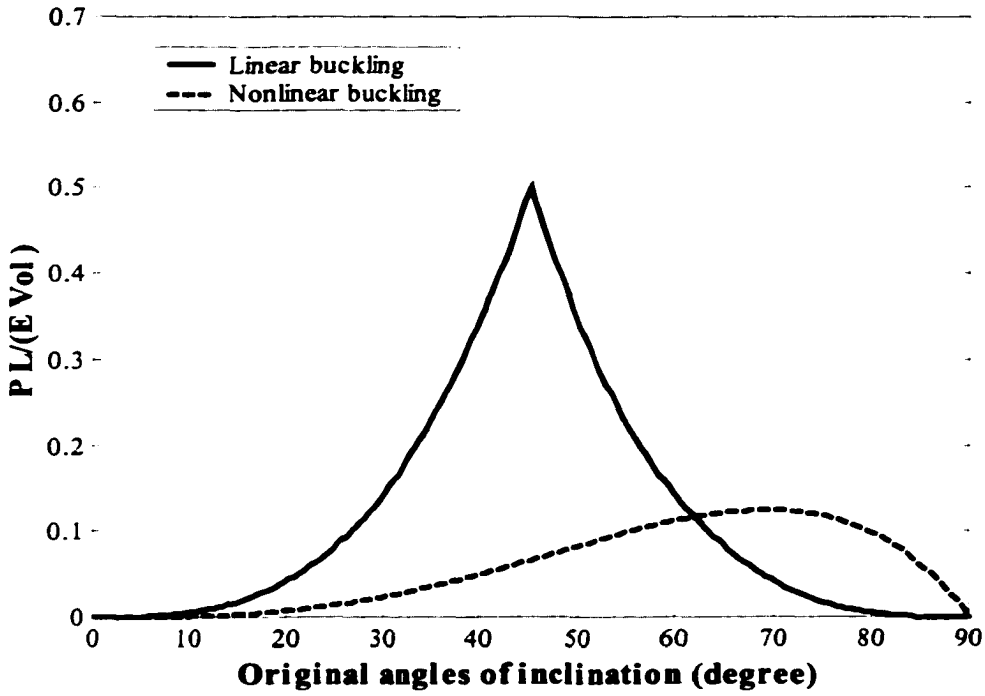

Figure 5-19 Comparison of linear and nonlinear buckling of the symmetric 2-bar truss structure.

5.4.2 The Asymmetric 2-Bar Truss

The asymmetric two-bar truss structure shown in Fig. 5-20 was optimized for a design limit load of 200 lbf applied at node 1 in the negative Y direction.

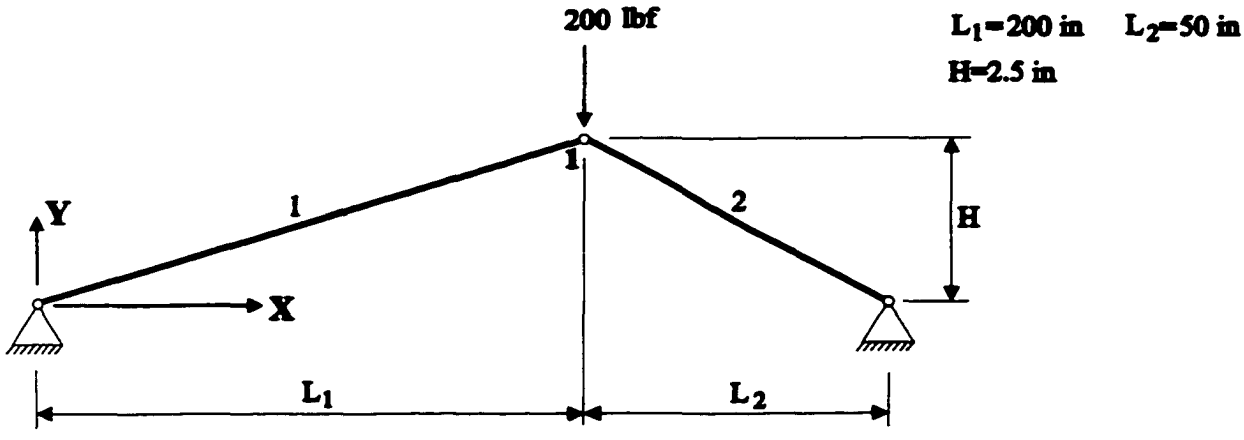

Figure 5-20 The asymmetric 2-bar truss structure.

The downward vertical displacement at this node (V) is taken as the controlling displacement in the displacement control method. The displacement is applied at a rate of 0.05 inch at each time step. The optimization has been carried out using the optimality criterion algorithm based on the potential energy. The initial cross sectional area of A=20 in^2 is considered for both elements and the initial mass is 500.156 lbm. The elements are tubular with solid circular cross-section. The problem has been solved for both perfect and imperfect elements with imperfection amplitude of 0.5 in. Figure 5-21 shows the effect of the element imperfection where a nonlinear buckling analysis has been carried out up to limit load for both the perfect and imperfect structure. This asymmetric structure demonstrates that the effect of imperfections are significant also for loads far below the limit load. For perfect elements, with A=20 in^2 and 5 in^2, the limit load of 1501.523 lbf and 375.381 lbf was obtained, respectively. These limit loads were reduced to 1280.335 lbf and 142.050 lbf, respectively for the imperfect structure. It is noted that the further the cross-sectional areas are decreased, the effect of the imperfections becomes more pronounced. Comparing these limit loads with those of the symmetric two-bar truss, it is clear that the load carrying capacity of the asymmetric truss is significantly greater than that of the symmetric one.

Next, let us consider nonlinear buckling. Here, a minimum mass of 66.607 lbm was obtained after three iterations for the perfect structure and 144.468 lbm after 27 iterations for the imperfect structure. The final results for the cross-sectional areas are shown in Table 5-17. It is noted that the optimum design of the structure with perfect elements is nearly symmetric, however this is not the case for the imperfect structure. Comparing the results of the symmetric and asymmetric two-bar truss structures, it can be concluded that the weight of the symmetric structure is greater than that of the asymmetric structure for the same specified design load. The effect of imperfection is quite severe for this structure so that neglecting this effect underestimates the minimum mass by 116.9 %. The solution history for the imperfect asymmetric structure exhibits high oscillatory convergence in comparison to the comparable symmetric structure. It may be inferred that the asymmetric structure is more imperfection sensitive than the symmetric

counterpart. Also, a nonlinear buckling analysis was performed using the final design cross-sectional areas. Here, an exact limit load of 200.00 was obtained for both the perfect and the imperfect structures, implying that the final design is in the elastic stability boundary. In other words, the design is driven by the critical buckling mode. The final stress in members 1 and 2 are found to be –2080.94 psi and –2081.34 psi for the perfect structure and –3306.65 psi and –3093.99 psi for the imperfect structure. These are well below the buckling stress of the individual elements. The relative final strain energy densities for the perfect structure are 0.9996 and 1.000 for members 1 and 2, respectively and for the imperfect structure are 1.000 and 0.9994.

The results for the perfect structure are in excellent agreement with the results reported by Khot and Kamat [111]. Although the initial cross sectional areas considered here are not in the feasible region, the problem converges to the optimum solution in just 3 iterations for perfect structure in comparison to the 10 iterations in Ref. [111] where the initial cross-sectional areas were taken in the feasible region.

Next, the effect of geometric nonlinearity in buckling analysis was considered. The problem was solved for the perfect structure using a linear buckling analysis. It was again observed that the linear buckling analysis highly underestimates the minimum mass. The final results are given in Table 5-17. As expected, using either $\boldsymbol{K}_{\sigma c}$ or $\boldsymbol{K}_{\sigma}$ as the geometric stiffness matrix does not result in any significant improvement in the final cross-sectional areas and minimum mass. However, using the $\boldsymbol{K}_{DI}$ matrix results in a more conservative design. Figure 5-22 illustrates the iteration history for all cases.

Finally, the optimum results, for different values of the height H, for the perfect structure are tabulated in Table 5-18. Here, U and V are the horizontal and vertical displacement at node 1 for the optimum design. The results are in good agreement with those obtained by Levy [127] who analyzed the problem analytically and used the generalized reduced algorithm of nonlinear programming as the optimizer.

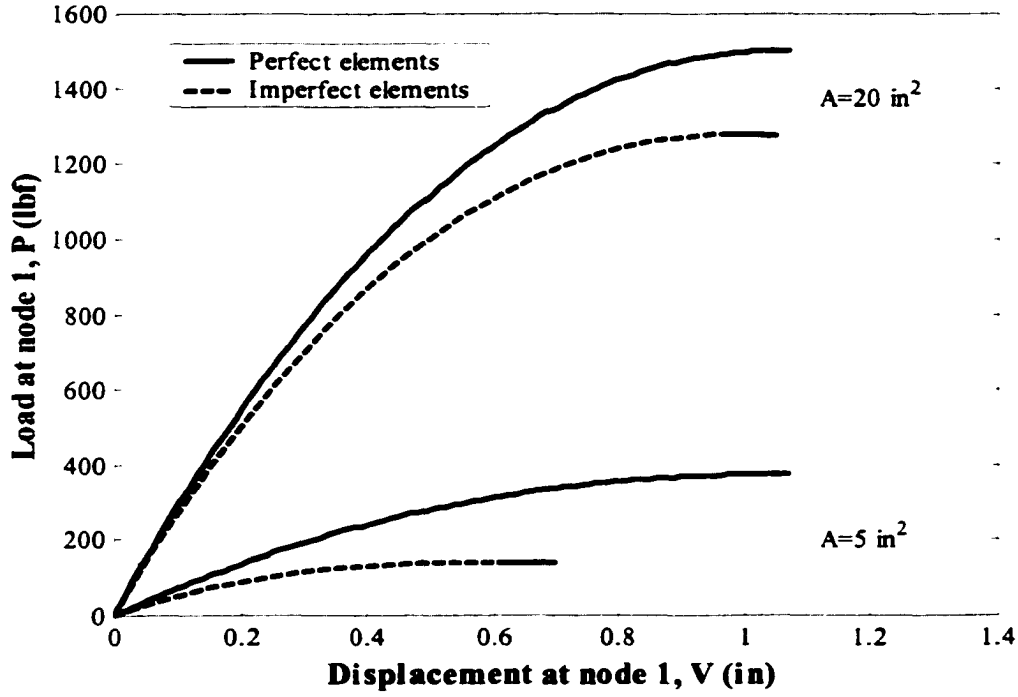

Figure 5-21 Load-deflection curve until limit load for the asymmetric 2-bar truss using perfect and imperfect elements.

Table 5-17 Final designs for the cross-sectional areas (in^2) for the asymmetric 2-bar truss structure

Element No.	Linear ($K_{\sigma c}$)	Linear (K_{σ})	Linear (K_{DI})	Nonlinear (Perfect)	Nonlinear (Imperfect)
1	0.5128	0.5131	1.8565	2.6638	6.1765
2	0.5133	0.5136	1.8581	2.6646	4.1850
Mass (lbm)	12.827	12.835	46.434	66.607	144.468
Iteration	3	3	3	3	27

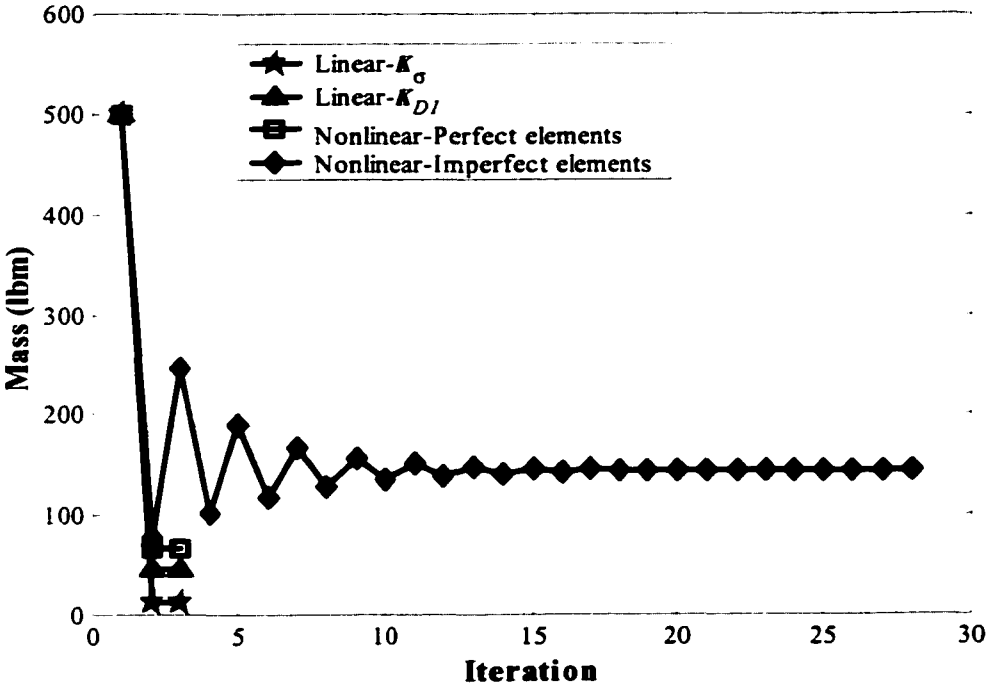

Figure 5-22 Iteration history for perfect and imperfect asymmetric 2-bar truss.

Table 5-18 Optimal designs for different H (in) – The asymmetric 2-bar truss.

H	A_1/A_2	V/V_0^*	U (in)	Lf
1.0	1.00	1.00	-0.0050	5.20
1.5	1.00	1.50	-0.0112	5.20
2.0	1.00	2.00	-0.0200	5.20
2.5	1.00	2.50	-0.0312	5.20
5.0	1.00	4.99	-0.1245	5.19
7.5	1.00	7.49	-0.2790	5.19
10.0	0.99	9.98	-0.4926	5.18
20.0	0.98	19.80	-1.8835	5.12
50.0	0.91	48.71	-9.2912	4.65
75.0	0.87	74.16	-16.3942	3.96
100.0	0.83	102.10	-23.3163	3.15
125.0	0.82	132.99	-29.3365	2.43
150.0	0.81	166.40	-34.5307	1.86

* V_0=0.4230 in

5.4.3 The 4-Bar Space Truss

The four-bar truss shown in Figure 5-23 was designed for a specified limit load of 200 lbf applied at node 1 in the negative Z direction. The downward vertical displacement at this node (W) is taken as the controlling displacement for the displacement control method. The displacement is applied at a rate of 0.1 inch in each time step. The optimization has been carried out using the optimality criterion algorithm based on the potential energy. An initial cross sectional area of A=4 in^2 is considered for all elements and the initial mass is 230.585 lbm. The problem has been solved for both perfect and imperfect elements. The elements are tubular with solid circular cross-section. An imperfection amplitude of 0.1 inch is assumed for all elements. With the assumed initial cross-sectional areas, a limit load of 382.231 lbf and 294.307 lbf was obtained for the perfect and the imperfect structures, respectively. The imperfection has a significant effect on the design of the structure. It is also noted that the initial limit loads is not equal to the specified limit load, implying that the initial design is not a feasible one.

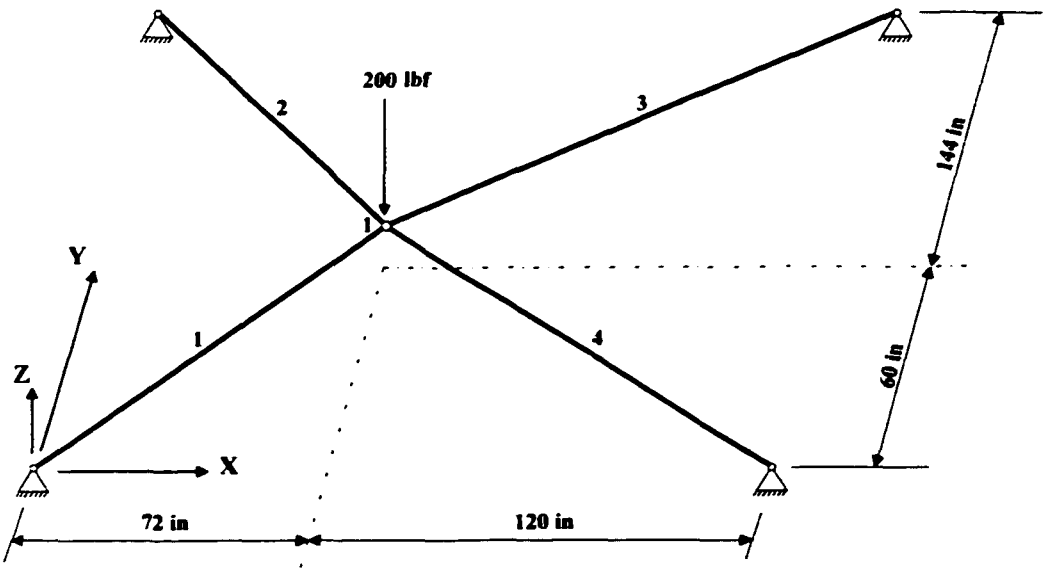

Figure 5-23 The 4-bar space truss structure.

Next, consider nonlinear buckling. Here, a minimum mass of 115.026 lbm was obtained after 10 iterations for the perfect structure. The imperfect structure solution required 26 iterations and resulted in a minimum mass of 184.06 lbm. The final results for the cross-sectional areas of the elements are tabulated in Table 5-19. The results for the perfect structure are in excellent agreement with the results reported by Khot and Kamat [111], where a feasible initial design was selected. Using the final design cross-sectional areas, a nonlinear buckling analysis was performed. A limit load of 200.00 lbf was obtained for both the perfect and imperfect structures, again implying that the final design is in the elastic stability boundary, with the design being driven by the critical buckling mode. The relative strain energy and stresses in the elements in the initial and optimum designs for both the perfect and the imperfect structures is given in Table 5-20. The elements stresses were found to be uniform and far below the element buckling stresses.

Finally, to consider the effect of geometric nonlinearity in buckling analysis, the problem was solved again considering the linear buckling analysis for the perfect structure. The final results are given in Table 5-17. The geometry matrix $\boldsymbol{K}_{DI}$ gives more efficient and conservative results. Also, it was observed that the linear buckling analysis highly underestimates the optimum mass. Figure 5-24 shows the iteration history for all cases.

Table 5-19 Final designs for the cross-sections (in^2)- The 4-bar space truss structure.

Element No.	Linear ($\boldsymbol{K}_{\sigma c}$)	Linear ($\boldsymbol{K}_{\sigma}$)	Linear ($\boldsymbol{K}_{DI}$)	Nonlinear (Perfect)	Nonlinear (Imperfect)
1	0.5575	0.5577	1.7284	2.8962	3.4262
2	0.3311	0.3313	1.0283	1.7210	3.1713
3	0.3206	0.3208	0.9958	1.6666	3.1154
4	0.4149	0.4151	1.2875	2.15560	3.1655
Mass (lbm)	22.138	22.150	68.710	115.026	184.060
Iteration	10	10	8	10	26

Table 5-20 The final relative strain energy and element stresses (psi) for the nonlinear buckling solution of the 4-bar space truss structure.

Element No.	Perfect		Imperfect	
	Initial	Final	Initial	Final
1	1.0000	1.0000	1.0000	1.000
2	0.3565	0.9979	0.6183	0.9558
3	0.3285	0.9979	0.5926	0.9537
4	0.5582	0.9988	0.7372	0.9732

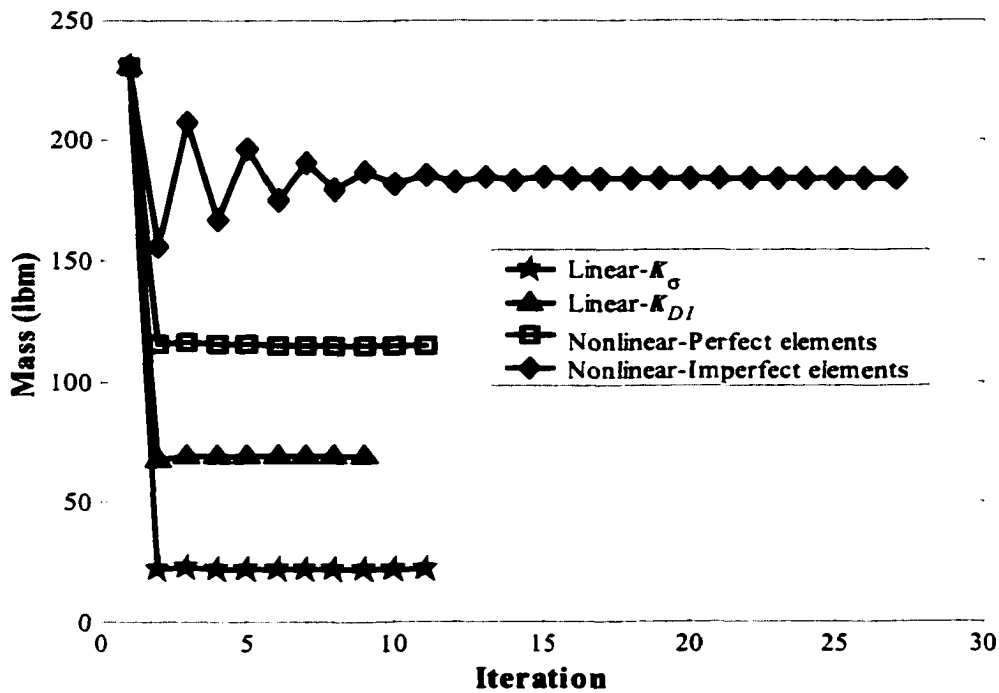

Figure 5-24 Iteration history for the perfect and the imperfect 4-bar truss structure.

5.4.4 The 46-Bar Planar Truss

The 46-element shallow truss structure is shown in Figure 5-25. This structure represents a typical crane or robotic manipulator. The nodal coordinates are given in Table 5-21. The structure is to be designed for loads of 300, 1200, 300 lbf applied in the negative Z direction at nodes 7, 13 and 19, respectively. The downward vertical displacement at node 1 is taken as the controlling displacement. The displacement is applied at a rate of

0.1 inch at each time step. An infeasible initial design with cross-sectional areas of 4 in^2 for all elements has been considered. Although the structure has symmetry with respect to the plane through node 13 and perpendicular to the X-Y plane, no variable linking has been used. The initial mass is 626.095 lbm. The members are tubular with annular cross-sections such that the wall thickness is equal to one tenth of the diameter. An imperfection amplitude of 0.1 inch is assumed for elements 5,9,13,17,30,34,38 and 42 (upper elements). A limit load of 22168.849 lbf and 20972.245 lbf was obtained for the perfect and the imperfect structures, respectively. Considering imperfection in all elements results in a limit load of 20957.848 lbf, confirming that imperfections in the lower and diagonal elements do not significantly affect the limit load of the structure.

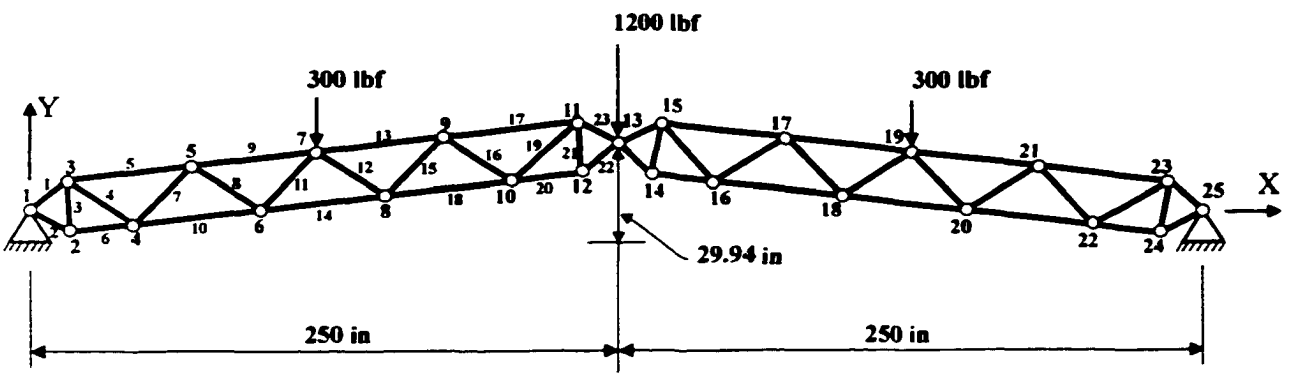

Figure 5-25 The 46-bar planar truss structure.

Table 5-21 Nodal coordinates of the 46-bar planar truss structure.

Node*	X	Y	Node*	X	Y
1	0.00	0.00	8	154.24	9.39
2	10.94	-4.94	9	181.74	24.20
3	9.75	7.00	10	211.64	15.13
4	39.60	-2.07	11	239.04	29.93
5	67.08	12.73	12	240.24	17.99
6	96.93	3.65	13	250.04	25
7	124.44	18.47			

* Coordinates of other nodes can be found by symmetry

When using a nonlinear buckling analysis, a minimum mass of 233.643 lbm was obtained after 14 iterations for the perfect structure. The final results are given in Table 5-22 and are in good agreement with the results reported by Khot and Kamat [111], where a feasible initial design was considered and the number of iteration was 17. Even without linking the design variables, the optimum design was found to be completely symmetric with respect to the plane passing through node 13. The relative strain energy density results are given in Table 5-23. The uniformity of the strain energy and stress in the final design is found to be better than that of Ref. [111], pointing out the current design is closer to the optimum design. Upon closer inspection, the results reveal that in the optimum design the forces in elements 5,7,9, 10-14, 16-18, 29-31, 33-38, 40 and 42 are considerably beyond the buckling load in the individual elements. This result is expected since both the optimality criteria algorithms are based on the system stability constraints. Next, to prevent the structure from buckling locally, the local buckling was treated as a passive constraint. A simple strategy similar to the stress-ratio technique was used. During the design iteration, if the force in the individual element reaches beyond the element-buckling load, the cross-section areas of the relevant elements are updated to guard against element forces beyond the buckling load. The above strategy was implemented successfully for both the perfect and the imperfect structures. This is particularly important for imperfect structures since the buckling of the element are integrated into the formulation of the imperfect elements. Thus, an optimum mass of 241.971 lbm and 270.470 lbm was obtained for perfect and imperfect structures, respectively. The final cross-sectional areas are given in Table 5-22. Note that while the increase in the mass is not particularly significant, all the element forces were found to be below the element buckling load.

Next, a nonlinear buckling analysis was performed using the optimum cross-sectional areas. A limit load of 300, 1200 and 300 was found at nodes 7, 13, 19 for both the perfect and imperfect structures, confirming that the final design is in the elastic stability boundary. Again, this means that the design is driven by the critical buckling mode.

Stability eigenanalyses performed for each solution show that this buckling mode is axisymmetric.

Finally, the effect of geometric nonlinearity was studied and similar conclusions are drawn as in the previous test cases presented. The results are summarized in Table 5-22. As expected, the linear buckling analysis underestimates the optimum mass significantly. The geometric stiffness matrix $\boldsymbol{K}_{DI}$ provides a better solution in comparison to the other two geometric matrices. The difference in optimum solution using $\boldsymbol{K}_{\sigma c}$ and $\boldsymbol{K}_{\sigma}$ is negligible. Figure 5-26 shows the iteration history for all cases.

Table 5-22 Final designs for the cross-sectional areas*(in^2) for the 46-bar truss.

Element No.	Linear ($\boldsymbol{K}_{\sigma c}$)	Linear ($\boldsymbol{K}_{\sigma}$)	Linear ($\boldsymbol{K}_{DI}$)	Nonlinear Perfect†	Nonlinear Perfect‡	Nonlinear (Imperfect)
1	1.4764	1.4788	1.8944	2.4832	1.7729	2.4435
2	1.3763	1.3785	1.7659	2.3789	1.6763	2.2894
3	0.6886	0.6897	0.8835	1.1744	0.8688	1.2224
4	0.1273	0.1276	0.1634	0.2522	0.2449	0.3499
5	1.3964	1.3987	1.7918	2.3756	2.6305	2.6531
6	1.19197	1.1939	1.5294	2.0585	1.4650	2.0111
7	0.1284	0.1286	0.1648	0.2206	0.4762	0.4620
8	0.1278	0.1280	0.1639	0.2199	0.1883	0.2787
9	1.6329	1.6355	2.0952	2.7716	2.8774	2.9663
10	0.9559	0.9574	1.2265	1.6310	2.0561	2.0873
11	0.1271	0.1273	0.1630	0.1904	0.4139	0.4275
12	0.1267	0.1269	0.1625	0.1914	0.4144	0.4215
13	1.6235	1.6262	2.0832	2.7651	2.8738	2.9588
14	0.7206	0.7218	0.9247	1.2601	1.7535	1.9887
15	0.1267	0.1269	0.1626	0.2197	0.1882	0.2782
16	0.1268	0.1270	0.1626	0.2191	0.4769	0.4602
17	1.3895	1.3918	1.7829	2.3706	2.6271	2.6477
18	0.9545	0.9561	1.2248	1.6317	2.0613	2.0924
19	0.1263	0.1265	0.1621	0.2515	0.2441	0.3486
20	1.1882	1.1900	1.5245	2.0570	1.4639	2.0088
21	0.6821	0.6832	0.8752	1.1662	0.8631	1.2141
22	1.3697	1.3719	1.7575	2.3734	1.6726	2.2835
23	1.4680	1.4704	1.8837	2.4757	1.7680	2.4359
Mass (lbm)	136.966	137.190	175.746	233.643	247.971	270.470
Iteration	14	14	14	14	20	9

* The area of the members on other half of the structure can be found by symmetry.
† Without considering local buckling.
‡ With considering the local buckling.

Table 5-23 Final results for the relative strain energy density distribution (Nonlinear buckling-Perfect structure) for the 46-bar planar truss.

Element No.	Initial Design	Final Design	Element No.	Initial Design	Final Design
1	0.7243	0.9957	13	0.9954	1.0000
2	0.5903	0.9982	14	0.1189	0.9852
3	0.1456	0.9861	15	0.0055	0.9815
4	0.0133	0.9734	16	0.0094	0.9744
5	0.7089	0.9956	17	0.7058	0.9956
6	0.4412	0.9960	18	0.2202	0.9921
7	0.0095	0.9743	19	0.0131	0.9734
8	0.0055	0.9814	20	0.4405	0.9960
9	1.0000	1.0000	21	0.1435	0.9860
10	0.2197	0.9921	22	0.5875	0.9982
11	0.0037	0.9759	23	0.7201	0.9956
12	0.0037	0.9757			

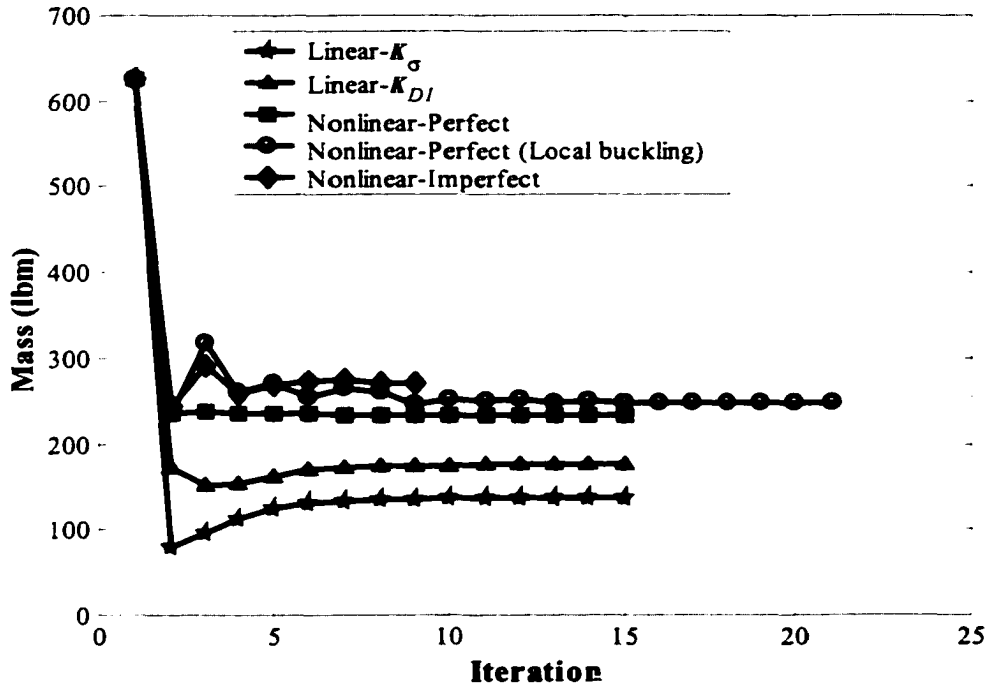

Figure 5-26 Iteration history for the perfect and imperfect 46-bar truss structures.

5.4.5 The 30-Bar Dome Space Truss

The 30-bar dome space truss is shown in Figure 5-27. This structure represents a typical space antenna. The structure was projected for a specified limit load of 200 lbf applied at node 1 in the negative Z direction. The downward vertical displacement at node 1 is taken as the controlling displacement. The displacement is applied at a rate of 1 inch at each time step. The members are tubular with annular cross-sections such that the wall thickness is equal to one tenth of the diameter. The structure has symmetry about X-Z and Y-Z planes, however, no variable linking strategy is implemented to check if the final optimum solution is symmetry or not. Two case studies have been investigated. During the optimization step, first the optimality criterion algorithm based on the potential energy has been implemented and applied and next, the optimality criterion algorithm based on the sensitivity analysis of the limit load has been used to optimize the structure.

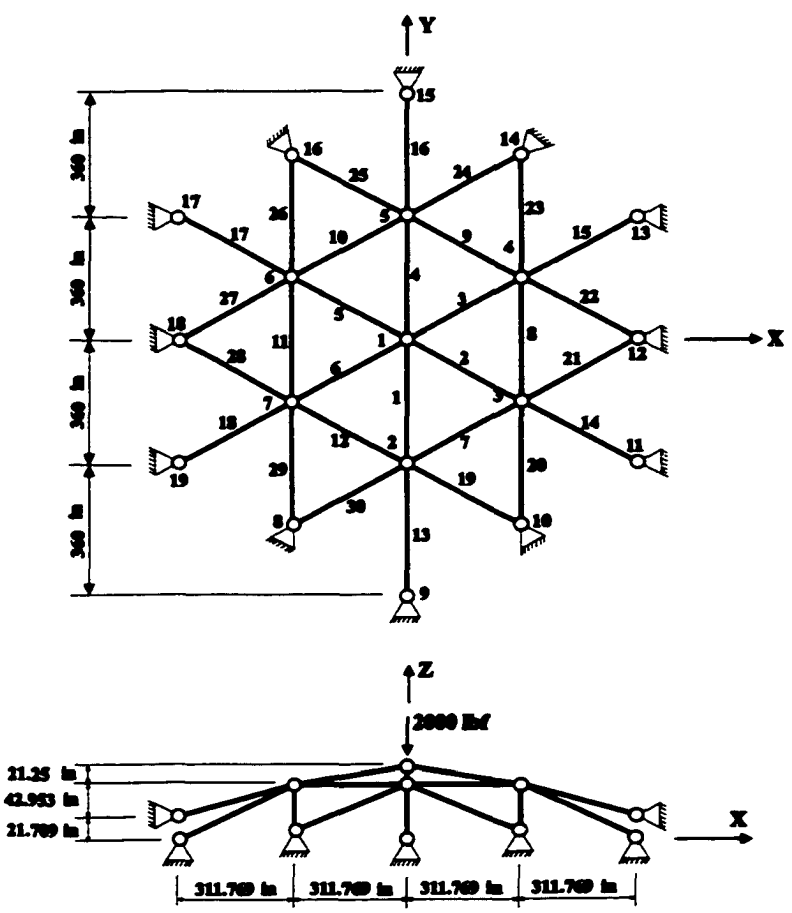

Figure 5-27 The 30-bar dome space truss structure.

(i) Case study I

The design was started with all the cross-sectional areas equal to 2 in^2 (infeasible design). A final mass of 778.470 lbm was obtained after 20 iterations. The same final mass result was obtained when starting the optimization process with other uniform initial areas. By starting the design with the cross-sectional areas of 2 in^2, 2 in^2, 0.1 in^2, 0.1 in^2 for elements 1-6, 7-12, 13-18 and 19-30, respectively (infeasible design) a final mass of 762.169 lbm was obtained after 14 iterations. The same problem was investigated by Khot and Kamat [111], where it was assumed that the Lagrange multiplier is equal to unity. The reported final mass was equal to 766.188 after 30 iterations. The final cross-sectional areas are given in Table 5-24. The results exhibited exact symmetry, as expected. The limit load for the initial design was found to be 2599.00 lbf. When using the final cross-sectional areas, a limit load of 2000.89 lbf was obtained, confirming that the optimum structure is at the elastic stability boundary corresponding to the fundamental buckling mode. Recalling Chapter 3, the limit load can be calculated with the desired accuracy and it is not sensitive to the displacement increment. To demonstrate this argument, the analysis was performed on the optimum structure using various displacement increments at node 1, as shown in Figure 5-28. In all analysis, the same limit point of 2000.89 was obtained. An eigenvalue analysis of the optimum results reveals that the fundamental buckling mode is axisymmetric (node 1 is moving down while nodes 2-7 are moving up uniformly) as expected due to the structural symmetry. However, real structures are always contaminated by non-axisymmetric imperfections in nodal coordinates, which may induce non-axisymmetric response. In order to allow the algorithm to recognize non-axisymmetric modes, a random perturbation in the nodal coordinates was artificially introduced. The perturbations were generated using a pseudo-random number generator whose elements are normally distributed with mean 0 and normalized to within the range of +1 and –1 in. Using the initial design, three nonlinear buckling analysis simulations were performed, where the coordinates of the internal nodes (1-7) were perturbed randomly. Surprisingly, the limit load of 2599.00 was again obtained in all three cases, confirming that the non-axisymmetric mode cannot be sensed by the presence of the nodal imperfections and that the axisymmetric mode is dominating the response of the structure. The problem was further probed. To confirm this

observation during the optimization iteration, that axisymmetry is the dominant mode, two optimization runs were performed and the optimum weight of 762.120 lbm and 762.039 lbm were obtained, confirming that system imperfections do not have any effect on the optimum solution of this symmetric structure. The optimum results for these two simulations are given in Table 5-24. A stability eigenanalysis of the optimum design shows that, for both runs, the critical mode, which drives the design, remains essentially axisymmetric.

The effect of geometric nonlinearity was studied next. The problem was solved using the linear buckling analysis with $\boldsymbol{K}_{\sigma}$ and $\boldsymbol{K}_{DI}$ as the geometric stiffness matrices. The final results are given in Table 5-24. The linear buckling using $\boldsymbol{K}_{\sigma}$ as the geometric stiffness matrix underestimates the optimum mass significantly. It is noted that for this structure, the geometric stiffness matrix $\boldsymbol{K}_{DI}$ provides an optimum solution relatively close to the real nonlinear solution. The difference in optimum solution using $\boldsymbol{K}_{\sigma c}$ and $\boldsymbol{K}_{\sigma}$ is negligible, as expected. Figure 5-29 shows the iteration history for all cases.

It was found that the relative strain energy density is nearly 1 for members 1-18, however it is far from 1 in members 19-30 for both the linear and nonlinear cases, indicating that the optimum solution may have not been reached. In order to check whether an optimum solution has been obtained, the algorithm II (please refer to chapter 4) was employed. The algorithm II is numerically much more expensive than the algorithm I, due to the computing sensitivity derivatives of the critical load with respect to the design variables. However, the sensitivity analysis may provide an improved solution.

(ii) Case study II

The results tabulated in Table 5-25 reveal that the final solution obtained using algorithm I is not an optimum solution. Using algorithm II, an optimum weight of 730.151 lbm was obtained for nonlinear buckling compared to 762.04 lbm obtained using algorithm I as shown in Table 5-24. Algorithm II is not designed to handle linear buckling. The computational resources required when carrying out a linear buckling analysis is much

less than when obtaining a nonlinear buckling solution. Therefore, the optimization for the linear buckling cases is performed using SQP, which is a computationally more intensive approach. For linear buckling analysis using the geometric stiffness matrix $\boldsymbol{K}_{\sigma}$, there is no significant difference in the optimum solutions between the algorithms I and SQP. However, the difference is significant when $\boldsymbol{K}_{DI}$ is used as the geometric stiffness matrix. Using Algorithm II, the members 13-18 reach their minimum. However, this is not the case for the algorithm I. Although the solutions obtained when using algorithm 1 does not produce the uniform strain energy density in all members, the final solutions obtained are close to the optimum solution. If the final strain energy obtained when using algorithm I is not uniform in the final design, one should exercise caution and check the design with other appropriate optimization methods. The iteration history for the optimization is given in Figure 5-30. The solution obtained for nonlinear buckling is in good agreement with the result reported by Smaui and Schmit [115], who solved the problem using an integrated approach employing the generalized reduced gradient technique.

Table 5-24 Final designs for the cross-sectional areas (in^2) for the 30-bar dome space truss structure (Algorithm I).

Element No.	Linear ($\boldsymbol{K}_{\sigma c}$)	Linear ($\boldsymbol{K}_{\sigma}$)	Linear ($\boldsymbol{K}_{DI}$)	Nonlinear	Nonlinear Perturbed nodes	
1-6	0.3976	0.3975	1.1865	1.6911	1.6910	1.6911
7-12	0.2814	0.2814	0.8129	1.3836	1.3835	1.3845
13-18	0.1000	0.1000	0.3240	0.2459	0.2459	0.2446
19-30	0.1000	0.1000	0.1000	0.10000	0.1000	0.1000
Mass (lbm)	212.267	212.231	546.926	762.169	762.120	762.04
Iteration	13	13	43	14	14	14

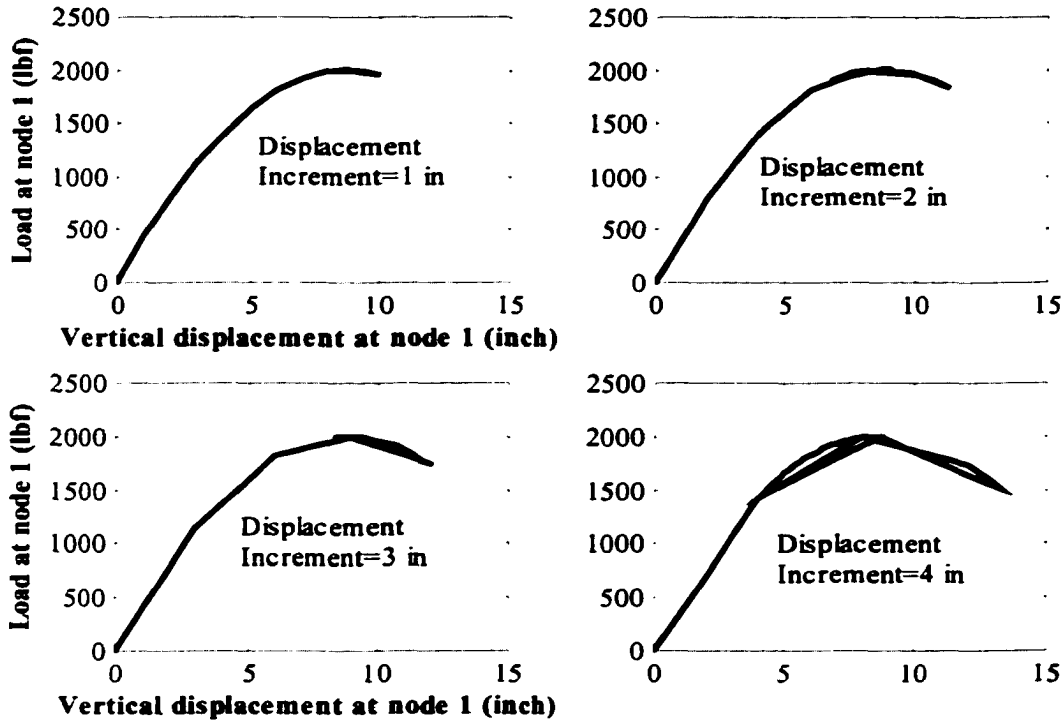

Figure 5-28 Load-displacement curve for the optimum solution using various displacement increments at node 1 for the 30-bar dome space truss.

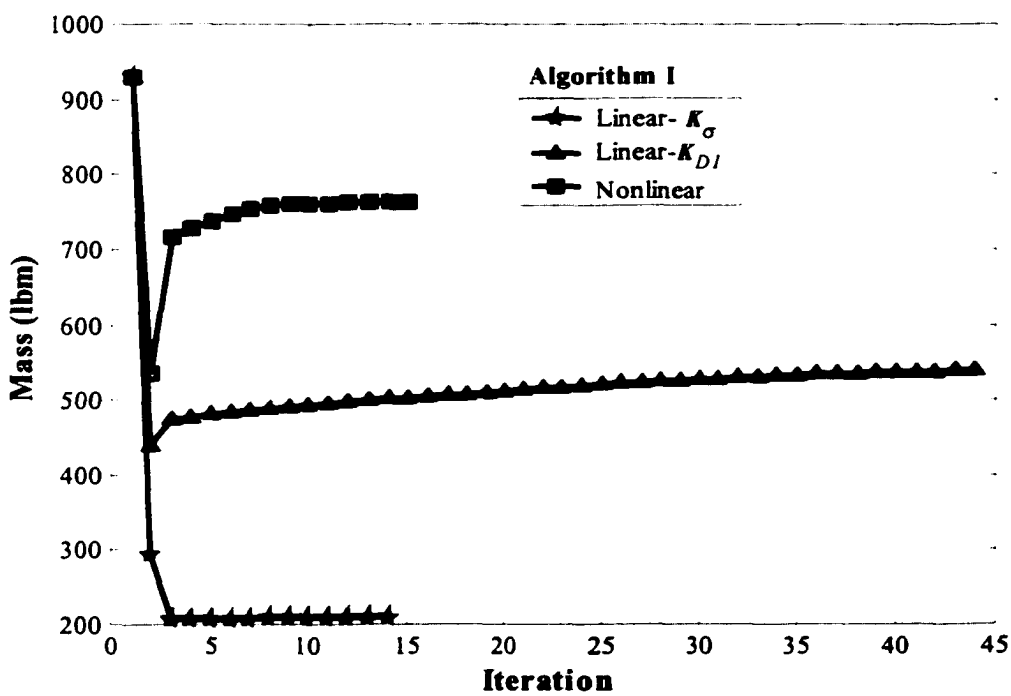

Figure 5-29 Iteration history for the 30-bar dome space truss structure (Algorithm I).

Table 5-25 Final designs for the area of cross-sections (in^2)- The 30-bar dome space truss structure (Algorithm II).

Element No.	Linear ($K_{\sigma c}$)	Linear (K_{σ})	Linear (K_{DI})	Nonlinear
1-6	0.3248	0.3253	0.9453	1.6150
7-12	0.3283	0.3279	0.9767	1.4595
13-18	0.1000	0.1000	0.1000	0.1000
19-30	0.1000	0.1000	0.1000	0.1000
Mass (lbm)	206.63	206.667	480.957	730.151
Iteration	9	9	9	11

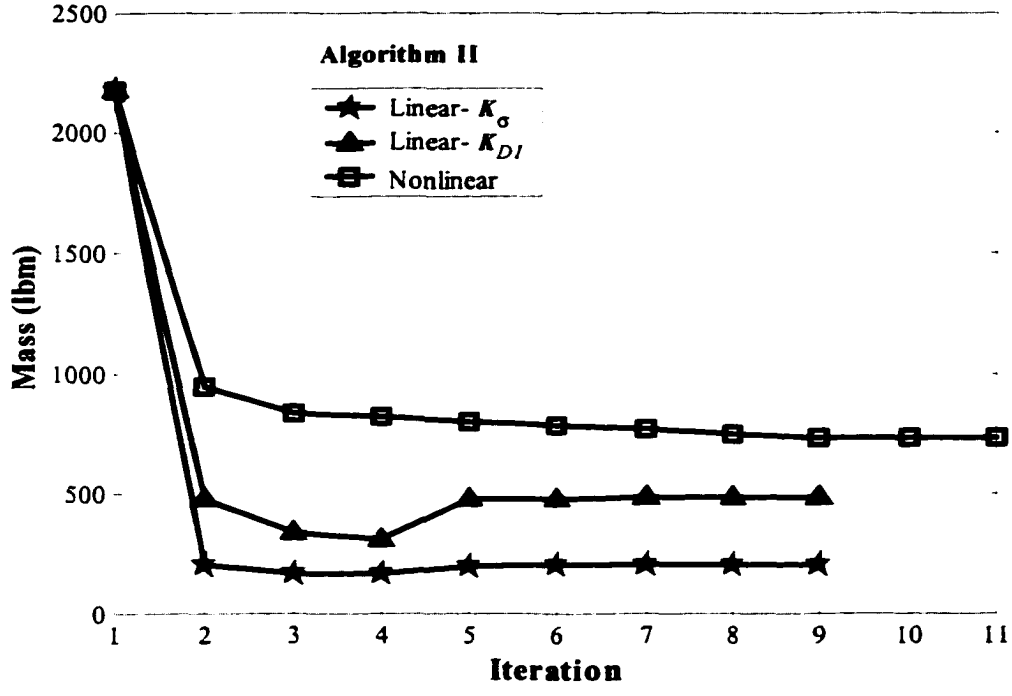

Figure 5-30 Iteration history for the 30-bar dome space truss structure (Algorithm II).

5.4.6 The 24-Bar Dome Space Truss

The 24-bar dome space structure is shown in Figure 3-27. This example is similar to the previous one, except that the elements 13-18 are eliminated. This test case has also been analyzed in chapter 3 to demonstrate the application of the group theoretic approach

(GTA). The purpose here is twofold: first, to show that it is possible to reach to uniform strain energy density in space dome structures; and second, to demonstrate clearly the application of the GTA in structural optimization with system stability constraints. To the author's knowledge, this particular problem has not been addressed in the literature.

The optimization of the structure has been carried out using the optimality criterion algorithm I. The material is assumed to be aluminum with Young's modulus $E=73\times10^{11}$ N/m^2 and material density $\rho=2770$ kg/m^3. The minimum area for all elements was set at 0.5 cm^2. The structure was designed for a specified limit load of 50000 N applied downward at node 4. The downward vertical displacement at this node is taken as the controlling displacement (displacement control method), and it is incremented in steps of 0.01 m per time step. The Group Theoretic Approach (GTA) is used to show its application in structural optimization of highly nonlinear problems. The GTA takes advantage of all possible symmetries in structure to reduce the number of degrees of freedom of the system model. In order to maintain the symmetry during the optimization as well, the elements have been linked into three groups as shown in the Table 5-26.

An initial cross-sectional area of 5 cm^2 was selected for all elements. The initial mass is 302.255 kg. With the given initial area, the limit point load obtained was 111729.2 N in both full and reduced subspace. Therefore the initial design is not in a feasible region (limit load is not equal to the design critical load of 50000 N). Considering an accuracy of 0.001% or less for the relative change in the mass, and considering nonlinear buckling, an optimum weight of 93.774 kg and 93.784 kg was obtained in full space and reduced subspace after 19 and 17 iterations, respectively. The final design for all cross-sectional areas using both the full space and the reduced subspace is shown in Table 5-27. It is noted that there is excellent agreement between the final designs in full space and reduced subspace. The little difference between the final solutions between the full space and reduced subspace can be attributed to round-off errors during analysis. Also, the basis vectors or projection matrix can cause a very small error when finding the limit point. The computational time decreased considerably when solving in the reduced subspace thus confirming that optimization using the GTA for a structure with symmetry is more efficient than the full space.

Table 5-28 shows the relative strain energy distribution in the initial design and final design for both the full space and the reduced subspace. Figure 5-31 shows the iteration history in both full space and reduced subspace. It is noted that in the initial design the strain energy is not uniform for all the elements. However, following optimization, the strain energy becomes exactly uniform in all elements when using the full space confirming that the optimum point has been reached. The reduced subspace, on the other hand, provides a solution where the strain energy is also fairly uniform in all elements, however not exactly equal, due to the approximate nature of the solution.

Table 5-29 shows the optimization results when the system stability constraint is considered as a linear buckling analysis using two different geometry matrices. It is noted that when using $\boldsymbol{K}_{DI}$ as the geometric stiffness matrix results in an optimum mass of 78.679 lbm, which is quite close to the optimum mass solution obtained using nonlinear buckling analysis. However, an analysis using $\boldsymbol{K}_{\sigma}$ as the geometric stiffness matrix highly underestimates the true solution, possibly leading to structural failure. It was observed that in the final design for linear analysis, the strain energy is not uniform in all elements, thus indicating that the optimum solution may have not been reached. In order to find out the possible optimum solution, the problem with linear buckling constraint was solved again using the Sequential Quadratic Programming (SQP) method, with the same initial areas. The weight was reduced to 31.725 kg and 60.986 kg when using the geometric stiffness matrices $\boldsymbol{K}_{\sigma}$ and $\boldsymbol{K}_{DI}$, respectively. This confirms that the optimum solution obtained using the optimality algorithm is not an optimal, however close to the optimum solution. It is noted in Table 5-30 that there is a significant difference in the number iteration and computational time between the optimality criterion and the SQP method, confirming that the optimality criterion is more efficient than the SQP.

Table 5-26 Variable linking groups for the 24-bar dome space truss.

Group	Elements
1	1-6
2	7-12
3	13-24

Table 5-27 Final designs for the area of cross-section (cm^2) for the nonlinear buckling solution for the 24-bar dome space truss.

Group No.	Nonlinear Buckling (Full Space)	Nonlinear Buckling Reduced Subspace
1	2.6544	2.6548
2	1.7481	1.7484
3	0.9082	0.9083
Mass (kg)	93.774	93.784
Iteration No.	19	17

Table 5-28 Initial and final relative energy density distribution (Nonlinear buckling)- The 24-bar dome space truss structure

Group No.	Initial Design	Final Design (Full Space)	Final Design (Reduced Subspace)
1	1	1.0000	0.9994
2	0.4841	1.0000	1.0000
3	0.0930	1.0000	0.9981

Table 5-29 Final designs for the area of cross-section (cm^2) for the linear buckling solution for the 24-bar dome space truss structure.

Group No.	Linear-Algorithm I		Linear -SQP Method	
	(K_σ)	(K_{DI})	(K_σ)	(K_{DI})
1	0.7407	2.0735	0.5069	1.4048
2	0.5000	1.0336	0.5932	1.4114
3	0.5000	1.0477	0.5000	0.6123
Mass (kg)	33.874	78.679	31.725	60.986
Iteration No.	17	23	47	128

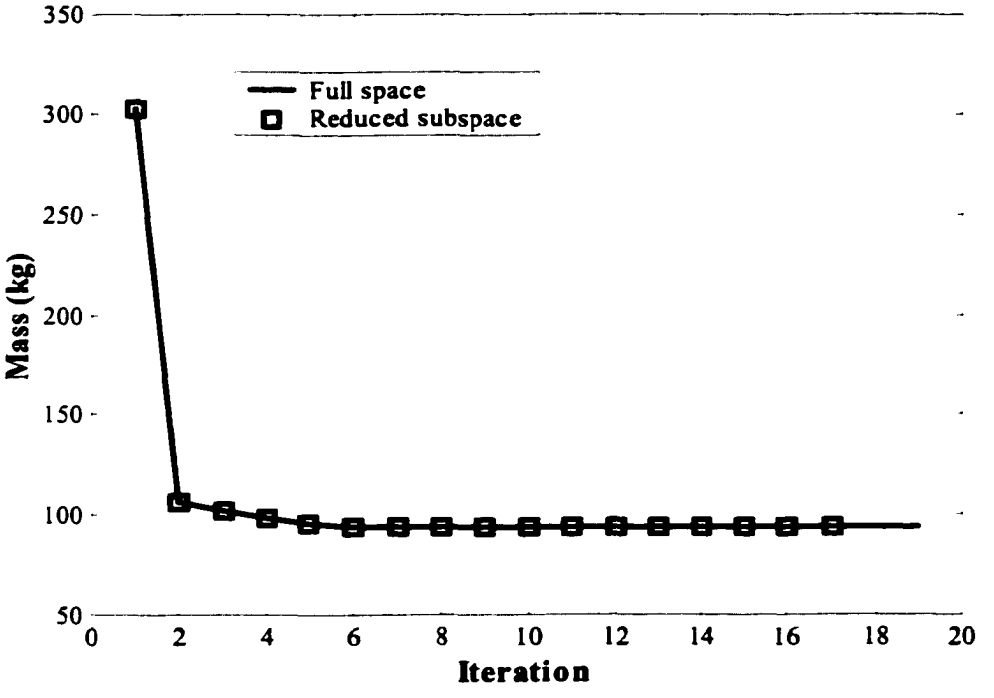

Figure 5-31 Iteration history through full space and reduced subspace using nonlinear buckling analysis- The 24-bar dome space truss.

5.4.7 The Shallow Frame Arch

A simply supported sinusoidal arch and its finite element model are shown in Figure 5-32.

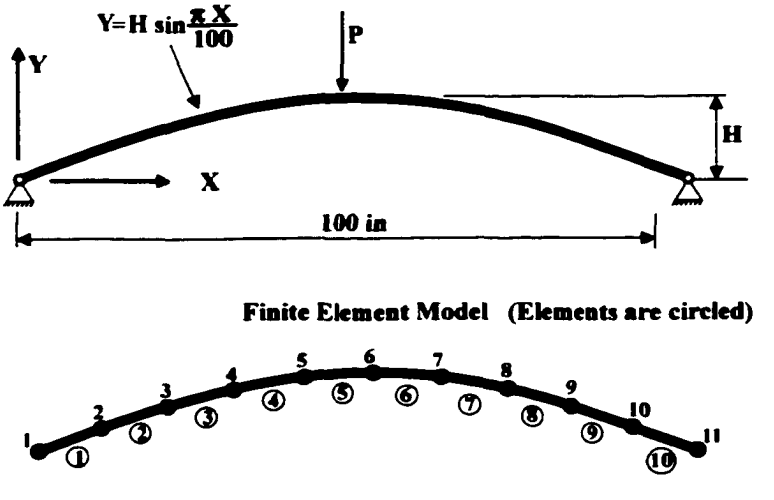

Figure 5-32 The sinusoidal shallow frame arch and its finite element model.

The arch is modeled using 10 plane beam elements, with equal projections in the X-axis. The Young's modulus is assumed to be $E=10^8$. The cross-sectional area, A, and the moment of inertia, I, of the arch obey the relationship $I=aA^b$, where b=1,2,3 and a is a specified constant. For b=1 and b=3 the rectangular cross-section with unit constant depth-variable width and variable depth-unit constant width have been considered, respectively. For b=2, the solid circular cross-section is selected. The analysis of the arch for its limit load calculation was carried out using nonlinear buckling analysis. Similar to the truss elements, the nonlinear buckling analysis based on the displacement control method was implemented successfully to capture the limit load as accurately as desired. The downward vertical displacement at node 6 is taken as the controlling displacement (displacement control method). The displacement is applied at a rate of 0.1 inch per time step. Due to the nonlinear coupling between stretching and bending actions, the design variables cannot be scaled to achieve a prescribe limit load by a simple linear scaling and it requires an iterative process. The dual problem, the maximization of the critical load under specified volume, has been addressed. The recurrence relation in algorithm I was used for the dual problem because it is a general relation which results in a uniform strain energy density.

Two arches with different rise have been investigated. For rise H=5 (low rise arch), the limit load is maximized under specified volume of 40 in^3 while for H=10 (intermediate rise arch) a specified volume of 35 in^3 is considered. The feasible initial design with cross-sectional area of 0.397579 in^2 for the arch with H=5 in and 0.341784 in^2 for the arch with H=10 in has been selected. The objective is to investigate the percentage increase in the limit load to be gained by redistributing the area. The final results are given in Table 5-30. Although no linking design variables strategy was used, the final cross-sectional areas were found to be exactly symmetric. Both the fully geometrical nonlinear buckling analysis and the linear analysis (stability eigenanalyses) are performed. In linear analysis, the effect of three different geometric stiffness matrices namely the stress stiffness matrix $(\boldsymbol{K}_\sigma)_E$ obtained by energy approach, the stress stiffness matrix $(\boldsymbol{K}_\sigma)_p$ obtained by perturbation method and the stiffness matrix based on the displacement $\boldsymbol{K}_{DI}$ have been investigated. The results reveal that when using a nonlinear

buckling analysis, an increase in limit load was observed. For the arch with b=3 this increase was the largest. For the arch with b=3 (H=5 in or H=10 in), the limit load for the optimal design was increased by approximately 1.314 times that for the initial design. The linear analysis resulted in erroneous results. Here, the limit load in the final design was decreased. However, the ratio of the final limit load to the initial limit load when using $\boldsymbol{K}_{DI}$ is greater than that of when using the other two geometric stiffness matrices. The ratios for $(\boldsymbol{K}_\sigma)_E$ and $(\boldsymbol{K}_\sigma)_p$ are in good agreement in all cases. It is noted that the final distribution of the area when using a linear analysis with different geometric stiffness matrices are exactly the same. When scaling the design, the volume of the arch is kept constant during the optimization process. Thus, in linear analysis, the distribution of the areas is the same using the three different geometric stiffness matrices. The final relative strain energy using the nonlinear buckling analysis is given in Table 5-31. The relative strain energy is nearly uniform in all cases. For the b=3 case, for both H=5 in and H=10 in, the exact uniform strain energy has been obtained, confirming that the optimum solution has been obtained. For the case b=1, for both H=5 inch and 10 in, an approximate uniform strain energy has been obtained. In order to improve the uniformity of the strain energy, the number of the elements was doubled to 20 elements. As expected, the nonlinear buckling analysis for a mesh with 20 elements was found to be computationally much more expensive than that for a mesh with 10 elements. The results are tabulated in Table 5-32. A fairly uniform strain energy was obtained for the arch modeled with 20 elements. For the arch with b=1 and H=5 in, modeled with 10 and 20 elements, the ratio of the final limit load to the initial limit load was increased from 1.136 to 1.219, respectively. Similarly, for the arch with b=1 and H=10 in, modeled with 10 and 20 elements, the ratio of the final limit load to the initial limit load was increased from 1.136 to 1.230, respectively. Thus, when the uniformity of the strain energy is not acceptable, increasing the number of the elements may help to increase the uniformity of the strain energy and in turn result in a more accurate optimum solution. The iteration history for the arch with b=1 and H=5 in and 10 in modeled with 10 and 20 elements, and using nonlinear buckling analysis is shown in Figure 5-33.

In all cases, the volume of the arch in the optimum design was found to be 40 in^3 for H=5 in, and 35 in^3 for H=10 in. For example, for H=5 in and b=1, the final volume was

40.000095 in^3, and for H=10 in and b=3, the final volume was found to be 35.0000028 in^3. This confirms that the fixed constraint was totally satisfied.

The initial and final configuration of the arch for b=1 with both H=5 in and 10 in is shown in Figure 5-34. It is clear that the symmetry of the arch is held in the final optimum design, pointing out that the design is driven by the axisymmetric mode. The eigenanalysis of the optimum design of the nonlinear buckling analysis confirms that the fundamental buckling mode is symmetric.

To confirm the duality, the problem was converted to the minimization of the volume under limit load constrained for the arch with b=1. This problem is computationally much more expensive than that of its dual problem, because scaling the design variable itself requires an iteration process. For arch with b=1, two to three iterations are usually needed to scale the design variable to the feasible design. The final results are shown in Table 5-33. When maximizing the limit load, for the arch with H=5 in, the volume is constrained at 40 in^3 and the initial limit load is 4145.505 lbf. In the optimum design, the limit load was increased to 4710.576 lbf while the volume was kept constant. When minimizing the volume, the limit load was specified as 4710.576 lbf and the initial volume was 201.218 in^3. In the optimum design, the volume was decreased to 39.999972 in^3 while the limit load was kept constant. The distribution of the area was found to be in excellent agreement for both cases. Therefore, excellent duality exists between the two problems. The same duality exists for the arch with H=10 in.

Finally to check the accuracy of the results obtained using the optimality algorithm I, the problem was solved again using mathematical programming method based on SQP. This method is computationally much more expensive than the algorithm I. Moreover the possibility that the design can be cast into a region where no limit load could be determined is relatively high. The results are shown in Table 5-34. Although it was expected to obtain a more accurate optimum solution, this turned out to be not the case for the arch with b=1. The limit load ratio of 1.136 was obtained using algorithm I and a limit load ratio of 1.018 was obtained using SQP. For b=1 and b=2, improvement in the limit load ratio is negligible confirming that the results obtained using algorithm I are accurate. The problem was also tried with different initial guesses, however in all cases

the optimum solution was the same. The lower limit load ratio in the SQP for b=I can be attributed to the premature termination during the optimization process. The SQP method complained that no limit load can be found in some iterations for arch with b=1. Considering that the shallow arch may exhibit no distinct limit load for some area distributions, this may be interpreted that during the iteration process, the design variables were updated in such a way that no limit load exists in the following iteration. For these kinds of situations, the optimization process will fail or terminate prematurely. The iteration history using algorithm I and the SQP method for the arch with H=5 in and H=10 in using a nonlinear buckling analysis are shown in Figures 5-35 and 5-36, respectively.

This problem has been reported by Kamat [110]. The approach here was based on the nonlinear analysis using the force control method. Both VMCON [175], which is based on the gradient search techniques, and an algorithm based on the maximum potential energy in optimum design were used. Here, the problem was addressed for just H=10 in and it is mentioned that for H=5, the optimization failed because no limit load was determined. For H=10 in, the limit load ratio for the arch with b=1 (1.033 and 1.047 using VMCON and an algorithm based on the maximization of the potential energy, respectively) was lower than that found in this research. For b=2, the limit load ratio of 1.064 and 1.092 was obtained through maximization of the potential energy, which is much lower than the results presented in this thesis. Because the algorithm based on the maximum potential energy in the optimum design is naturally the same as the algorithm based on the uniform strain energy in the optimum design, the lower limit load ratio obtained in Ref. [110] may be attributed to an inaccurate limit load calculation during the course of the optimization or inappropriate Lagrange multiplier formulae were used in the algorithm as it was reported that no limit load was determined for the case of H=5 in.

Table 5-30 Final designs for the area of cross-sections (in^2) – The shallow frame arch (Algorithm I)

Element No.		1	2	3	4	5	$(P_{cr})_o/(P_{cr})_i$	Iteration
b=1 H=5 in	Linear $(K_\sigma)_p$	0.2219	0.2723	0.2723	0.3293	0.8961	0.7690	22
	Linear $(K_\sigma)_E$	0.2219	0.2723	0.2723	0.3293	0.8961	0.7681	22
	Linear (K_{DI})	0.2219	0.2723	0.2723	0.3293	0.8961	0.8961	22
	Nonlinear	0.2936	0.3167	0.3165	0.3746	0.6900	1.136	11
b=1 H=10 in	Linear $(K_\sigma)_p$	0.1751	0.2257	0.2257	0.2729	0.8247	0.7366	25
	Linear $(K_\sigma)_E$	0.1751	0.2257	0.2257	0.2729	0.8247	0.7356	25
	Linear (K_{DI})	0.1751	0.2257	0.2257	0.2729	0.8247	0.9607	25
	Nonlinear	0.2570	0.2775	0.2771	0.3140	0.5922	1.136	7
b=2 H=5 in	Linear $(K_\sigma)_p$	0.2120	0.2290	0.2290	0.4711	0.8512	0.4601	35
	Linear $(K_\sigma)_E$	0.2120	0.2290	0.2290	0.4711	0.8512	0.4569	35
	Linear (K_{DI})	0.2120	0.2290	0.2290	0.4711	0.8512	0.6617	34
	Nonlinear	0.3102	0.3103	0.2892	0.4499	0.6311	1.235	16
b=2 H=10 in	Linear $(K_\sigma)_p$	0.1681	0.1776	0.1776	0.4283	0.7742	0.3798	35
	Linear $(K_\sigma)_E$	0.1681	0.1776	0.1776	0.4283	0.7742	0.3767	35
	Linear (K_{DI})	0.1681	0.1776	0.1776	0.4283	0.7742	0.6587	34
	Nonlinear	0.2685	0.2687	0.2466	0.3881	0.5451	1.236	18
b=3 H=5 in	Linear $(K_\sigma)_p$	0.2308	0.2308	0.2335	0.5157	0.7812	0.2974	17
	Linear $(K_\sigma)_E$	0.2308	0.2308	0.2335	0.5157	0.7812	0.2946	17
	Linear (K_{DI})	0.2308	0.2308	0.2335	0.5157	0.7812	0.5269	14
	Nonlinear	0.3296	0.3297	0.2980	0.4546	0.5781	1.315	13
b=3 H=10 in	Linear $(K_\sigma)_p$	0.1886	0.1886	0.2060	0.4527	0.6876	0.2801	16
	Linear $(K_\sigma)_E$	0.1886	0.1886	0.2060	0.4527	0.6876	0.2772	16
	Linear (K_{DI})	0.1886	0.1886	0.2060	0.4527	0.6876	0.5596	19
	Nonlinear	0.2853	0.2854	0.2552	0.3913	0.4980	1.314	12

$(P_{cr})_o$ = Optimum critical load $(P_{cr})_i$ = Initial critical load

Table 5-31 Final relative strain energy density for the shallow frame arch for the nonlinear buckling analysis

Element No.		1	2	3	4	5
b=1	H=5 in	0.9726	0.9621	0.9621	1.0000	0.9878
	H=10 in	0.9435	0.9237	0.9236	1.0000	0.9782
b=2	H=5 in	1.0000	1.0000	0.9976	1.0000	0.9973
	H=10 in	0.9999	0.9999	1.0000	0.9999	0.9999
b=3	H=5 in	1.0000	1.0000	1.0000	1.0000	1.0000
	H=10 in	1.0000	1.0000	1.0000	1.0000	1.0000

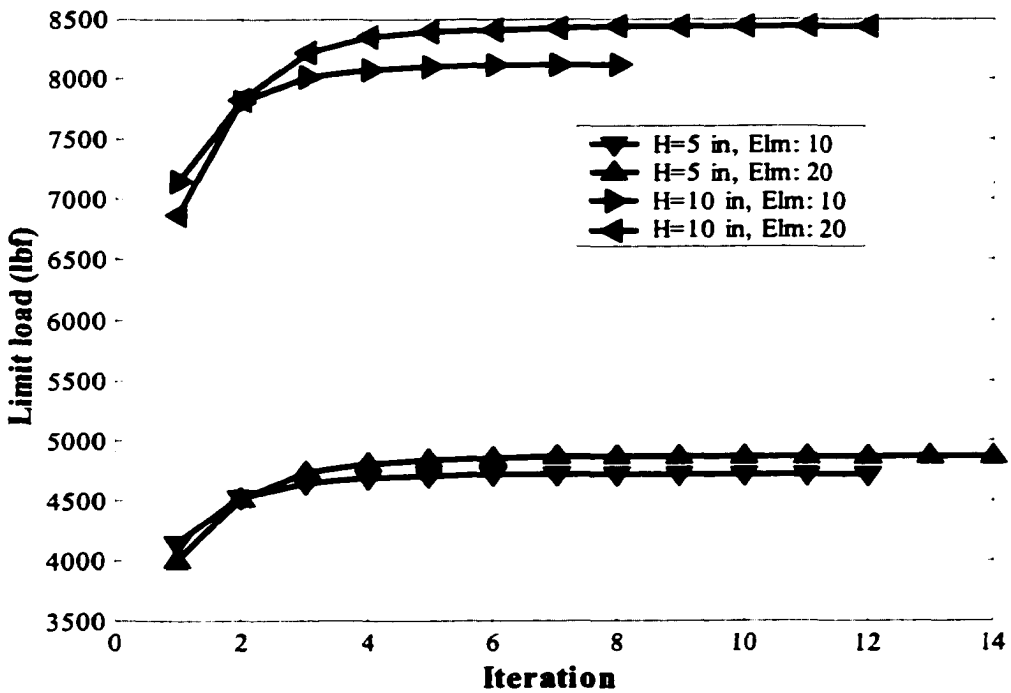

Figure 5-33 Iteration history for the arch with b=1 modeled with 10 and 20 elements.

Table 5-32 Final designs using 20 elements for the shallow frame arch with b=1 (Algorithm I – Nonlinear buckling).

Element No	Cross-sectional area		Relative Strain Energy	
	H=5 in	H=10 in	H=5 in	H=10 in
1	0.21244	0.1775	0.9978	0.9942
2	0.3291	0.2881	0.9979	0.9940
3	0.3809	0.3358	0.9975	0.9941
4	0.3810	0.3359	0.9975	0.9941
5	0.3567	0.3110	0.9967	0.9943
6	0.2548	0.2135	0.9950	0.9947
7	0.2252	0.1816	1.0000	0.9973
8	0.4300	0.3664	0.9978	0.9976
9	0.6204	0.5364	0.9966	0.9987
10	0.7922	0.6888	0.9956	1.0000
$(P_{cr})_o/(P_{cr})_i$	1.219	1.230		
Iteration No.	13	11		

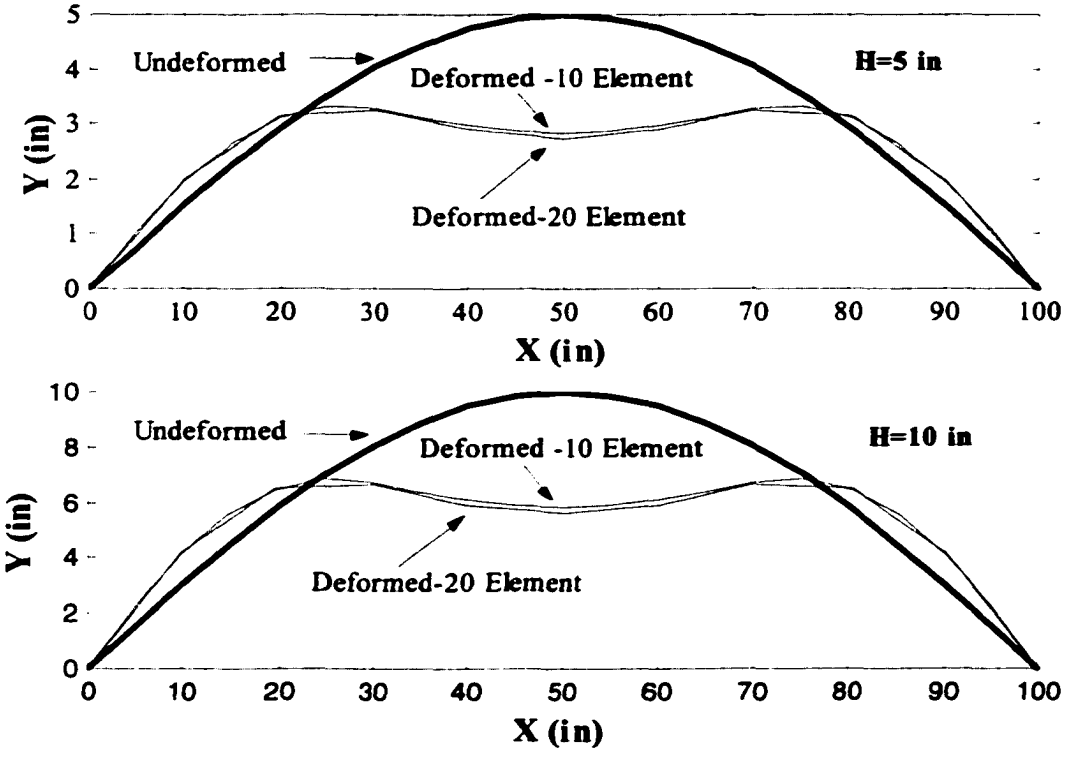

Figure 5-34 Undeformed and deformed configuration in the final design for the shallow frame arch with b=1.

Table 5-33 Verification of duality between maximum limit load and minimum volume designs - The Shallow frame arch with b=1.

Maximum Limit Load Design	Minimum Volume Design
H=5 in	H=5 in
Vol_s=40 in^3 $(P_{cr})_i$= 4145.505 lbf	$(P_{cr})_s$=4710.576 lbf Vol_i= 201.218 in^3
$(P_{cr})_o$=4710.576 lbf Vol_o=40.000095 in^3	Vol_o= 39.999972 in^3 $(P_{cr})_o$ =4710.576 lbf
H=10 in	H=10 in
Vol_s=35 in^3 $(P_{cr})_i$= 7144.674 lbf	$(P_{cr})_s$ =8111.754 lbf Vol_i= 81.923 in^3
$(P_{cr})_o$= 8111.754 lbf Vol_o= 35.0000673 in^3	Vol_o= 35.00779 in^3 $(P_{cr})_o$ =8111.754 lbf

Vol_s , Vol_i and Vol_o = Specified, initial and optimum volume.
$(P_{cr})_s$,$(P_{cr})_i$ and $(P_{cr})_o$ = Specified, initial and optimum critical load.

Table 5-34 Final designs for the area of cross-sections (in^2) –The shallow frame arch (SQP -Nonlinear buckling).

Element No.		1	2	3	4	5	$(P_{cr})_o/(P_{cr})_i$	Iteration
H=5 in	b=1	0.3712	0.3813	0.3976	0.4139	0.4243	1.018	13
	b=2	0.3161	0.4354	0.3580	0.3037	0.5757	1.222	31
	b=3	0.3087	0.3838	0.2562	0.4516	0.5894	1.379	138
H=10 in	b=1	0.3187	0.3498	0.3283	0.3557	0.3573	1.018	13
	b=2	0.2415	0.3255	0.1867	0.3943	0.5691	1.303	262
	b=3	0.2692	0.3319	0.2200	0.3879	0.5061	1.376	272

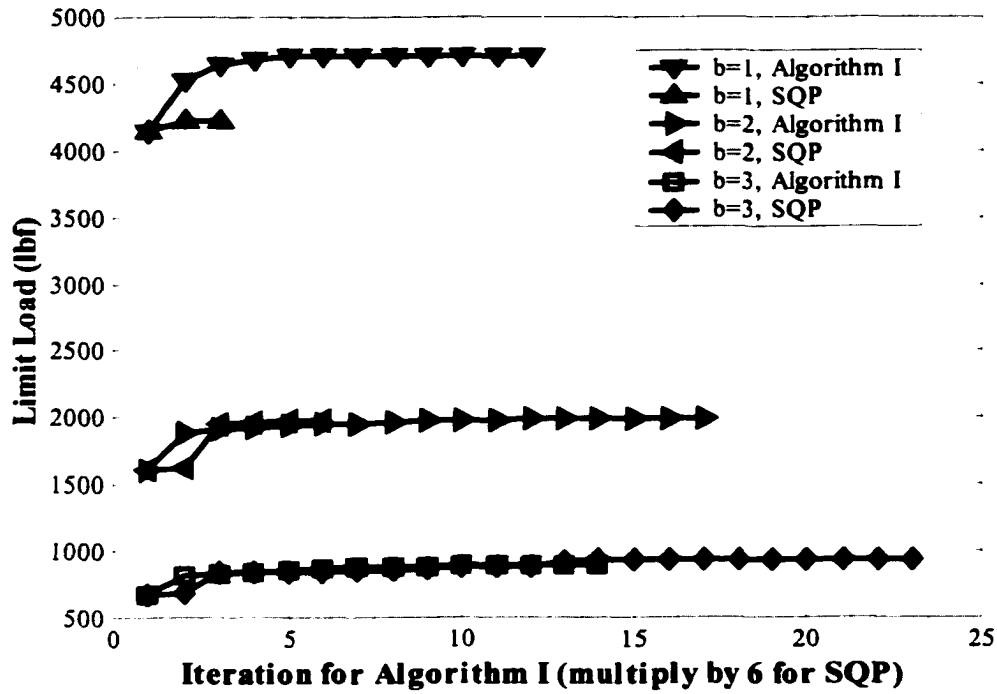

Figure 5-35 The iteration history for the shallow frame arch with H=5 in using algorithm I and SQP.

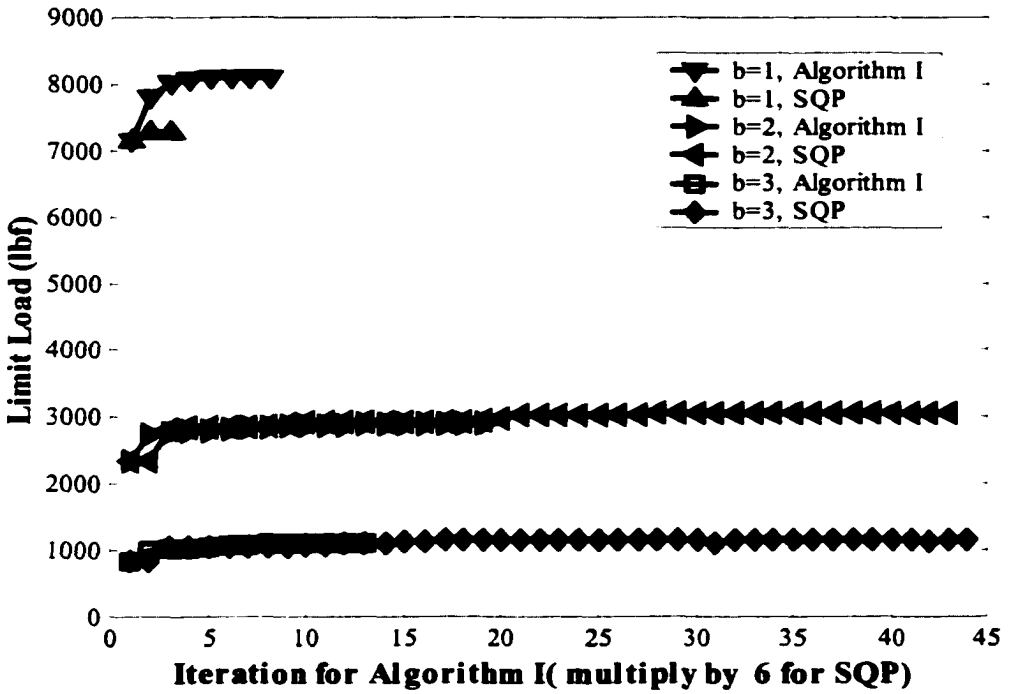

Figure 5-36 The iteration history for the shallow frame arch with H=10 in using algorithm I and SQP.

5.4.8 Williams Toggle Frame

The Williams toggle frame was analyzed in Chapter 3 using nonlinear buckling analysis. Here the same frame with similar geometry configuration and material properties is optimized to improve its limit load capacity. The frame with its finite element model is shown in Figure 5-37. The problem can be cast as a dual form as was done in the previous example in which the limit load is maximized with constant volume constraint.

The frame is modeled using 16 plane beam elements with equal length. The Young's modulus of $E=10.3\times10^6$ is assumed. Again, the cross-sectional area, A, and the moment of inertia, I, of the frame follow the relationship $I=aA^b$. Because the frame has basically a rectangular cross-section, b has been considered to be 1 and 3. For b=1, the depth of the cross-section is kept constant (0.243) while the width is allowed to be varied. Similarly for b=3, the width of the cross-section is kept constant (0.753) while the depth is allowed to be varied. A displacement control based nonlinear buckling analysis is used. The

displacement is applied at a rate of 0.1 inch in each time step. Both the optimality criterion algorithm I and the SQP method are used for optimization.

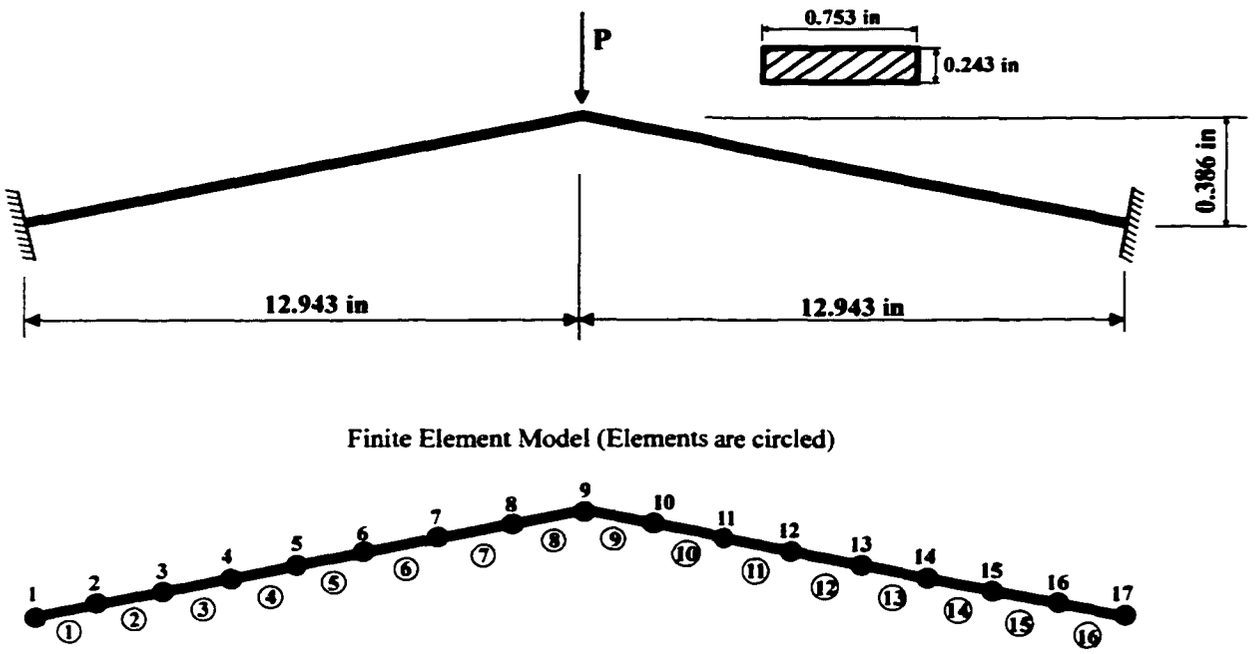

Figure 5-37 The Williams Toggle frame and its finite element model.

The limit load of the Williams toggle frame is maximized while its volume ($4.7387 in^3$) is kept constant. A feasible initial design with a cross-sectional area of 0.182979 in^2 is selected where the depth and width are 0.243 in^2 and 0.753 in^2, respectively. The objective is to probe for the possible optimum configurations for the Williams toggle frame. The final results for b=1 are given in Table 5-35. The design variables have not been linked. Nevertheless, the final cross-sectional areas were found to be exactly symmetric. Both a geometrical nonlinear buckling analysis and a linear analysis (stability eigenanalysis) using the geometric stiffness matrices $(\boldsymbol{K}_\sigma)_p$, $(\boldsymbol{K}_\sigma)_E$ and $\boldsymbol{K}_{DI}$ are performed. The results reveal that when using a nonlinear buckling analysis, a limit load ratio (ratio of the limit load in the optimum design to the initial limit load) of 1.0846 is achieved. The initial and final optimum limit loads were found to be 34.3203 lbf and 37.2224 lbf, respectively. The increase in the limit load is not significant thus confirming that the original configuration is close to the optimal configuration. The results for the stability

eigenanalysis using $(\boldsymbol{K}_\sigma)_p$ and $(\boldsymbol{K}_\sigma)_E$ shows that the limit load in the final design decreased and the limit load ratio are in good agreement between the two solutions. However, when using a linear analysis with $\boldsymbol{K}_{DI}$ as the geometric stiffness matrix, an increase in the limit load was observed and the limit ratio of 1.06556 was obtained which is close to that obtained using a nonlinear buckling analysis. To summarize the results, for linear analysis, the initial and final optimum limit loads were found to be 49.3439 lbf and 52.5790 lbf using $\boldsymbol{K}_{DI}$, 95.4082 lbf and 94.8305 lbf using $(\boldsymbol{K}_\sigma)_p$ and 92.9585 lbf and 92.2768 lbf using $(\boldsymbol{K}_\sigma)_E$, respectively. The relative strain energy density for initial and final design is given in Table 5-36. A fairly uniform strain energy distribution is obtained in the final optimum design. The iteration history for both the linear and nonlinear buckling analyses are shown in Figure 5-38.

To confirm the duality of the problem, the problem was now converted to the minimization of the volume under limit load constrained for the frame with b=1. The final results are shown in Table 5-37. When minimizing the volume, the limit load was specified as 37.2224lbf, which is the optimum limit load obtained in the dual problem and the initial volume is 25.8975 in^3. In the optimum design, the volume was decreased to 4.738692 in^3, which is exactly the constrained volume in the dual problem, while the limit load was kept constant. The distribution of the area was found to be in excellent agreement for both cases as shown in Table 5-37. Thus it is confirmed that an excellent duality exists between the two problem statements.

The initial and final configuration of the frame with b=1 is shown in Figure 5-39. It is clear that the symmetry of the arch is held in the final optimum design, pointing out that the design is driven by the axisymmetric mode. The eigenanalysis of the optimum design of the nonlinear buckling analysis confirms that the fundamental buckling mode is indeed symmetric.

Any attempt to optimize the frame for b=3 was failed because no limit load was found during the optimization process. This may be because the algorithm cast the design in a region where no limit load exists. This implies that the William's toggle frame for b=3 is very sensitive to the change in the design variables and even for a small changes in the

cross-sectional areas the limit load may not be found. Another attempt to optimize the frame using the SQP approach failed not only for b=3 but also for b=1. The SQP method complained that no limit load can be found in some iterations for frame with b=1. This may be interpreted that during the iteration process using the SQP approach, the design variables were updated in such a way that no limit load exists in some iterations.

Table 5-35 Final designs for the cross-sectional areas (in^2) for the Williams Frame.

Element No.	Linear $(K_\sigma)_P$	Linear $(K_\sigma)_E$	Linear (K_{DI})	Nonlinear
1	0.249276	0.249276	0.249271	0.224042
2	0.205078	0.205078	0.205076	0.211968
3	0.160880	0.160881	0.160882	0.176286
4	0.116682	0.116682	0.116687	0.120018
5	0.116682	0.116682	0.116687	0.119958
6	0.160880	0.160880	0.160882	0.176246
7	0.205078	0.205078	0.205076	0.211871
8	0.249276	0.249276	0.249271	0.223930
$(P_{cr})_o/(P_{cr})_i$	0.99394	0.99267	1.06556	1.08456
Iteration No.	10	10	7	15

Table 5-36 Relative strain energy density (Nonlinear buckling)–Williams Frame

Element No.	Initial Relative Strain Energy	Final Relative Strain energy
1	1.0000	0.9986
2	0.9443	0.9993
3	0.6798	0.9996
4	0.3411	0.9993
5	0.3411	0.9995
6	0.6798	0.9997
7	0.9443	1.0000
8	1.0000	0.9994

Table 5-37 Verification of duality between maximum limit load and minimum volume designs for the Williams Toggle Frame

Maximum Limit Load Design				**Minimum Volume Design**			
Vol_s= 4.7387 in^3 , $(P_{cr})_i$= 34.3204 lbf				$(P_{cr})_s$=37.2224 lbf , Vol_i= 25.8975 in^3			
$(P_{cr})_o$= 37.2224 lbf, Vol_o= 4.738700 in^3				Vol_o = 4.73869 in^3 , $(P_{cr})_o$ =37.2224 lbf			
Final cross-sectional areas (in^2)				**Final cross-sectional areas (in^2)**			
El. 1	El. 2	El. 3	El. 4	El. 1	El. 2	El. 3	El. 4
0.224040	0.211967	0.176286	0.120018	0.224042	0.211968	0.176286	0.120018
El. 5	El. 6	El. 7	El. 8	El. 5	El. 6	El. 7	El. 8
0.119958	0.176246	0.211871	0.223930	0.119958	0.176246	0.211871	0.223930

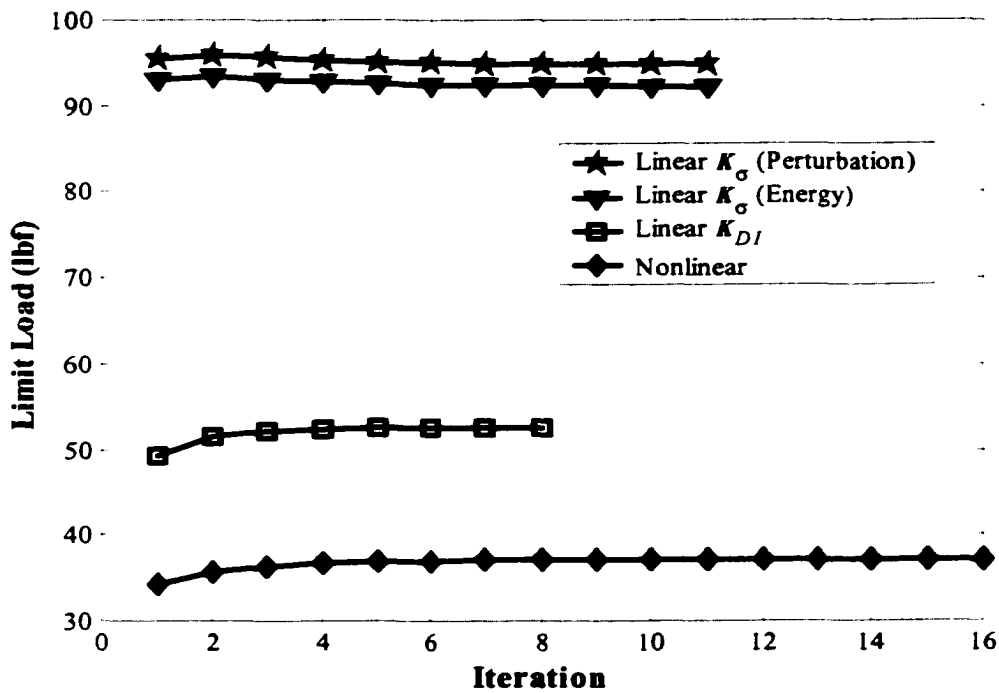

Figure 5-38 Iteration history-The Williams Toggle Frame

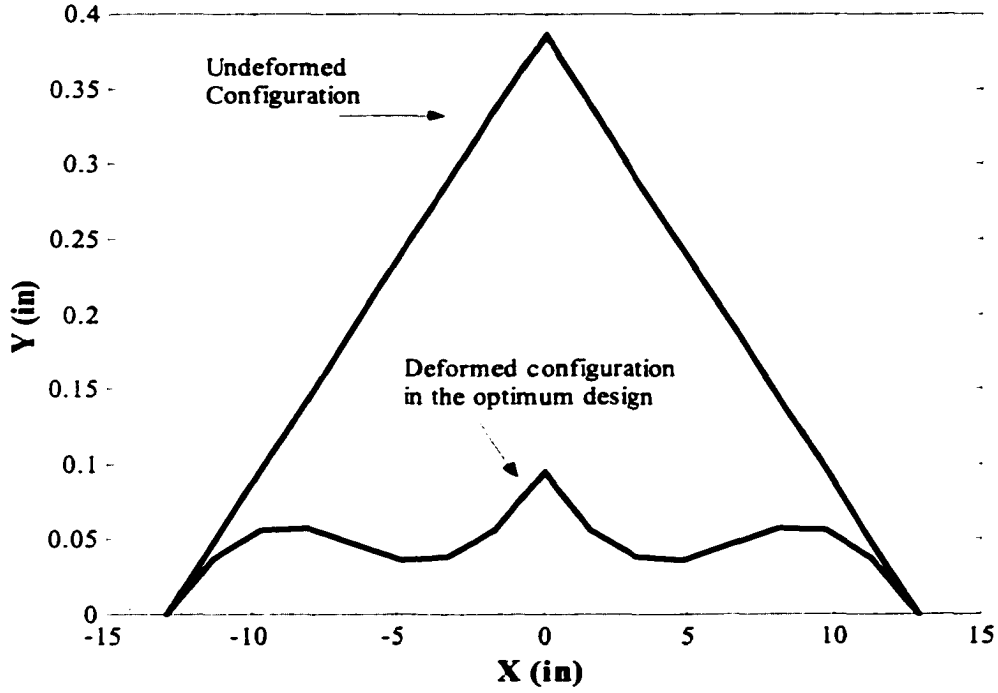

Figure 5-39 Undeformed and deformed configuration in the final design – The Williams toggle Frame

5.5 Geometry Optimization – Adaptive Structures

5.5.1 The 24-bar Truss – Static Analysis

The twenty-four-bar adaptive truss shown in Figure 5-40 (with $L = 2$ m) was topologically optimized to maintain the maximum structural strength in the presence of a varying loading condition. The truss structure has four bays and every bay contains one active member. Also, at the bottom of the structure there is an active member (member 18) that can rotate the whole structure. The truss consists of 24 members where members 5, 9, 13, 17, and 20 are active. Angles φ_1, φ_2, φ_3, φ_4, and φ_5 are taken as geometrical design variables, and these are related to each active member length. The range for the angles are $0^\circ \le \varphi_1, \varphi_2, \varphi_3, \varphi_4 \le 90^\circ$ and $0^\circ \le \varphi_5 \le 180^\circ$. The absolute maximum allowable force for all members is assumed to be 1000 N.

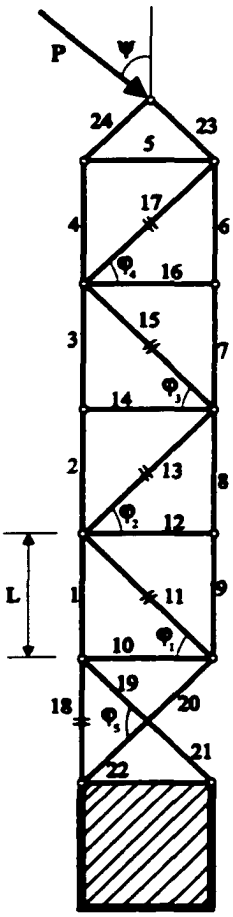

Figure 5-40 The 24-bar plane adaptive truss structure with elements 11, 13, 15 ,17 and 18 as active members.

First, the four angles $\varphi_1, \varphi_2, \varphi_3$ and φ_4 are taken as the geometrical design variables with φ_5 being fixed at 90° (base fixed). The structural strength (allowable applied force) for the fixed configuration ($\varphi_1 = \varphi_2 = \varphi_3 = \varphi_4 = 45°, \varphi_5 = 90°$) is plotted as a solid line in Figure 5-41. The structural strength for the optimal adaptive shape is plotted as the dashed curve. It can be observed that the structure becomes very rapidly weak for the loads applied in directions other than $\psi = 0°$. The direction of the applied load is varied between $-90^0 \leq \psi \leq 90^0$ and the structural strength decreases considerably from 1414.2 N to 208.3 N. The rapid decrease in structural strength demonstrates the weakness of the structure for transverse loads. The optimal geometries of the adaptive structure as the load is changing direction are shown in Figure 5-42. As expected, the structure aligns

itself toward the direction of the applied load in order to maximize its structural strength. The optimal results for the various values of the direction of applied load, ψ, are given in Table 5-38. The computational time required by the force and the displacement methods is also tabulated. The force method clearly provides a computationally more efficient and faster solution.

Next, the four variables of $\varphi_1, \varphi_2, \varphi_3$ and φ_4 are considered as design variables together with $\varphi_5 = 90^\circ - \psi$ (base moveable). The structural strength for the configuration ($\varphi_1 = \varphi_2 = \varphi_3 = \varphi_4 = 45^\circ$, $\varphi_5 = 90^\circ - \psi$) is plotted as the solid curve in Figure 5-43. The structural strength for the optimal adaptive geometries is plotted as the dashed curve. The optimal geometries of the adaptive structure are shown in Figure 5-44. The optimization results for the varying load direction ψ are shown in Table 5-39. The results indicate that the adaptive truss structure maintains a constant and high structural strength (1414.2 N) by making the structure align itself with the external applied load direction. In comparison to the conventional structure, the structural strength can be maintained constant for varying loading directions by adaptively optimizing the geometry of the structure.

This problem was also addressed by Murotsu and Shao [152] using the linear analysis based on the displacement method as the analysis and the conjugate gradient method as the optimization. The results obtained in this research are in good agreements with those in Ref. [152].

Table 5-38 Optimal values of φ_1, φ_2, φ_3, φ_4, optimum structural strength (N) and critical members in the optimal adaptive shapes for $\varphi_5 = 90^\circ$ (Static load).

ψ°	Design variables				CPU time (Sec)		Structural Strength	Critical Members
	φ_1°	φ_2°	φ_3°	φ_4°	FM	DM		
-90	78.89	8.54	83.82	4.66	1.62	8.68	244.1	1, 18 both C
-80	80.70	6.81	83.16	6.02	2.38	10.96	346.7	2 C
-70	80.90	9.16	80.71	9.71	1.88	11.97	518.7	2, 4 both C
-60	76.98	13.43	76.76	14.82	2.20	11.63	724.2	3, 4 both C
-50	71.72	18.60	71.72	19.15	1.45	8.94	880	4, 18 both C
-40	66.79	23.21	66.79	23.32	3.28	8.79	1003.8	24 T
-30	63.36	26.64	63.36	26.64	0.32	1.61	1035.3	24 T
-20	55.03	34.97	55.03	34.97	0.32	1.61	1103.4	24 T
-10	48.75	41.24	48.76	41.24	0.32	1.61	1220.8	24 T
0	45	45	45	45	0.17	0.81	1414.2	23, 24 both C
10	38.31	51.69	38.31	51.69	0.34	1.69	1220.8	23 C
20	32.30	57.70	32.30	57.70	0.25	1.22	1103.2	23 C
30	25.96	64.10	25.90	64.10	0.54	2.58	1035.3	23 C
40	25.49	71.57	18.43	71.57	1.04	6.97	1003.8	23 C
50	20.66	77.60	13.48	77.91	1.93	12.03	948.5	6 C
60	11.89	80.02	11.49	78.62	2.23	9.11	694.6	6, 19, 21 all C
70	9.12	82.83	9.07	80.84	2.40	14.69	508.9	7, 19, 21 all C
80	10.23	84.74	5.14	83.10	2.70	17.56	276.7	7, 8 both C, 10 T
90	20.43	83.33	7.11	86.22	2.21	11.70	208.3	6,8 both C, 10 T

C = Compression; T = Tension

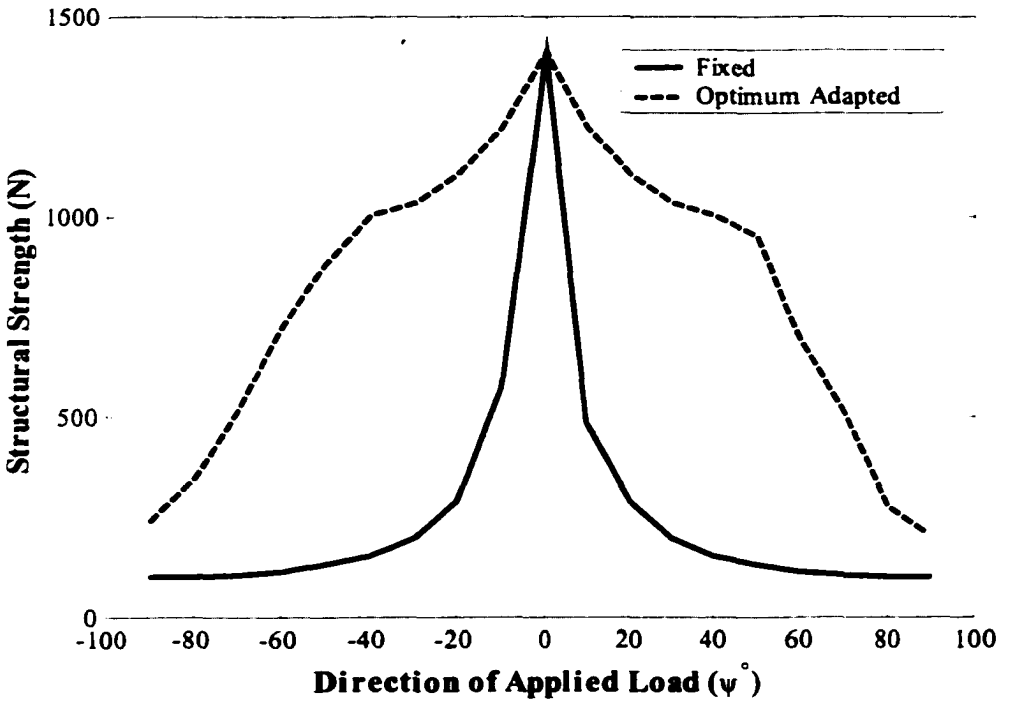

Figure 5-41 Structural strength versus the direction of the applied load for the fixed and optimized adapted structure with fixed base (Static load).

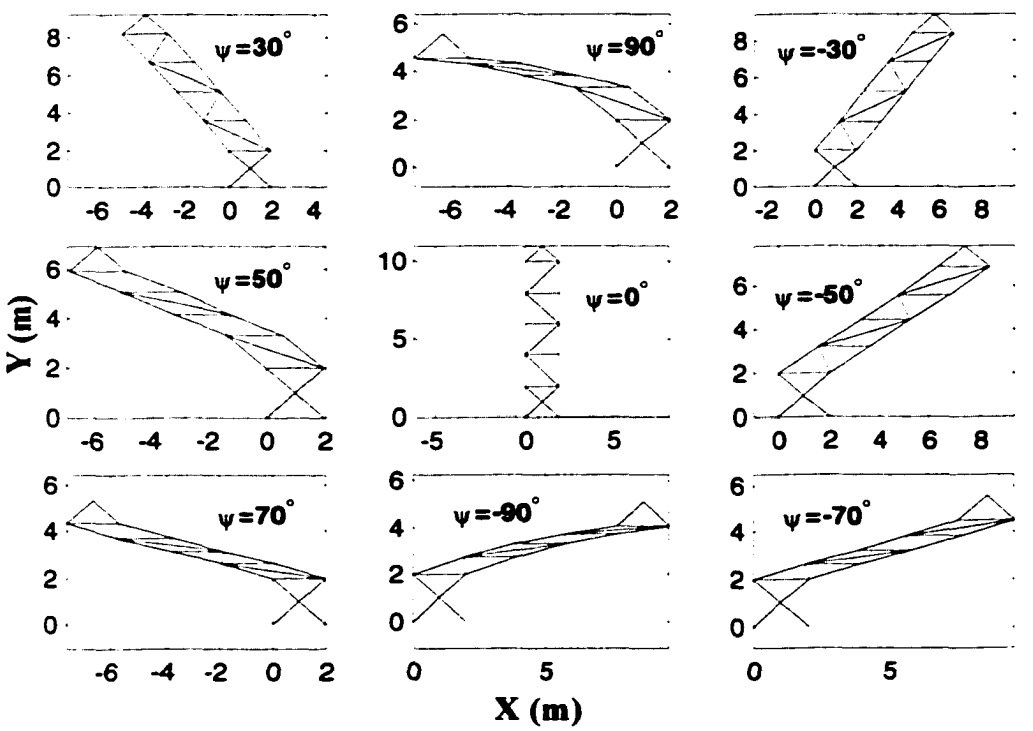

Figure 5-42 Optimal adaptive shapes of the truss structure with fixed base(Static load).

Table 5-39 Optimal values of φ_1, φ_2, φ_3, φ_4, structural strength (N) and critical members in the optimal adaptive shapes for $\varphi_5 = 90^\circ - \psi^\circ$ (Static load).

ψ°	Design variables				CPU time (Sec)		Structural Strength	Critical Members
	φ_1°	φ_2°	φ_3°	φ_4°	FM	DM		
-90	45	45	45	45	2.44	3.62	1414.2	20, 23, 24 all C and 21 T
-80	44.77	45.23	44.77	45.23	0.23	1.06	1414.2	23, 24 both C
-70	44.54	45.46	44.54	45.46	0.19	0.92	1414.2	23, 24 both C
-60	44.40	45.60	44.40	45.60	0.19	0.85	1414.2	23, 24 both C
-50	43.86	46.14	43.86	46.14	0.36	1.69	1414.2	23, 24 both C
-40	43.99	46.01	43.99	46.01	0.42	2.01	1414.2	23, 24 both C
-30	43.73	46.27	43.73	46.27	0.42	2.01	1414.2	23, 24 both C
-20	43.84	46.16	43.84	46.16	0.42	2.01	1414.2	23, 24 both C
-10	43.93	46.07	43.93	46.07	0.42	2.01	1414.2	23, 24 both C
0	45	45	45	45	0.20	0.87	1414.2	23, 24 both C
10	44.02	45.98	44.02	45.98	0.42	2.07	1414.2	23, 24 both C
20	43.68	46.32	43.68	46.32	0.50	2.45	1414.2	23, 24 both C
30	43.58	46.42	43.58	46.42	0.60	2.96	1414.2	23,24 both C
40	43.53	46.48	43.52	46.48	1.11	5.26	1414.2	1, 23, 24 all C
50	43.53	46.48	43.52	46.48	1.11	5.26	1414.2	1, 23, 24 all C
60	43.58	46.42	43.58	46.42	0.60	2.85	1414.2	23, 24 both C
70	43.68	46.32	43.68	46.32	0.50	2.36	1414.2	23, 24 both C
80	44.02	45.98	44.02	45.98	0.42	2.00	1414.2	23, 24 both C
90	45	45	45	45	0.18	1.92	1414.2	23, 24 both C

C = Compression; T =Tension

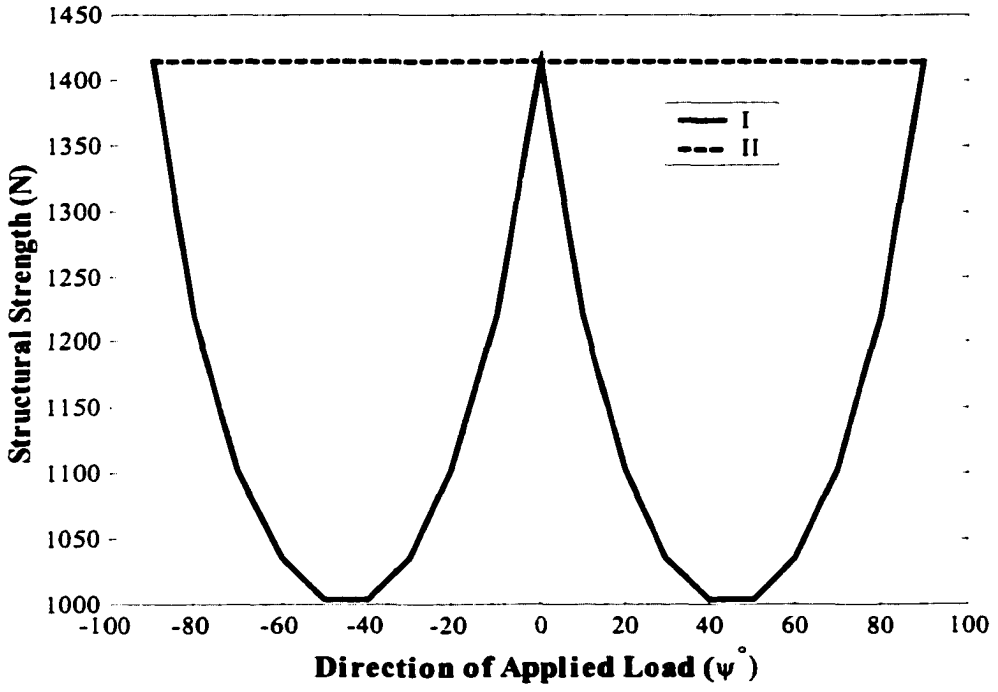

Figure 5-43 Structural strength versus the direction of the applied load for the fixed, I, and optimized adapted structure, II, with movable base (Static load).

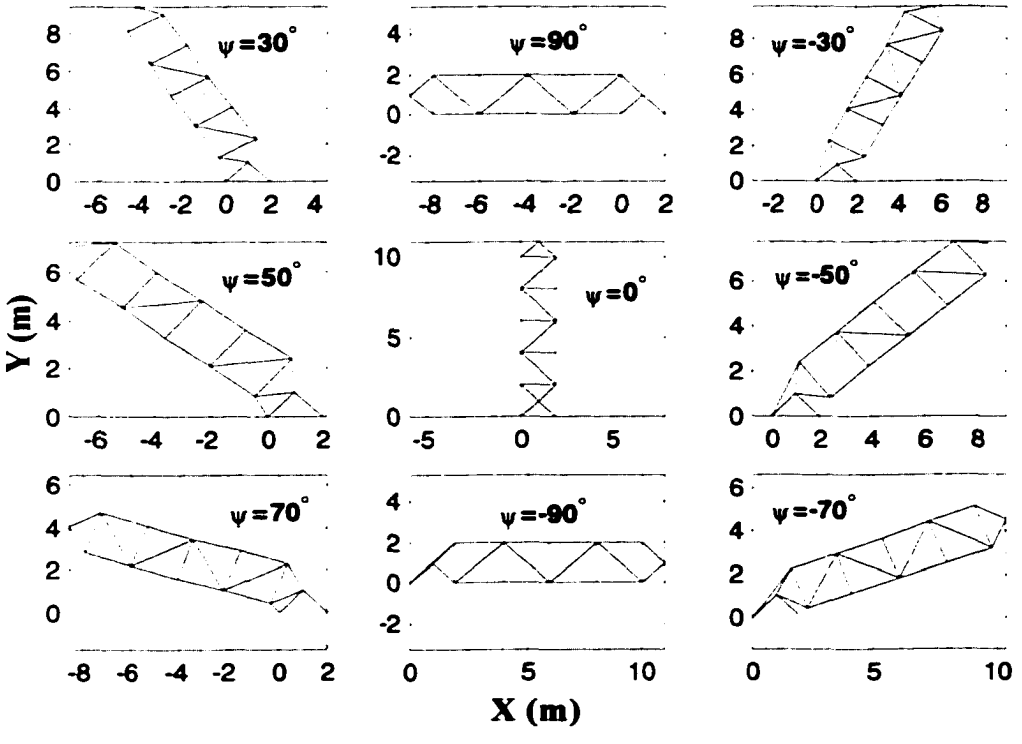

Figure 5-44 Optimal adaptive shapes with movable base (Static load).

5.5.2 The 24-Bar Truss – Dynamic Analysis

Let us consider the same adaptive truss structure as shown in Figure 5-40. The angles $\varphi_1, \varphi_2, \varphi_3$ and φ_4 are taken as the geometrical design variables. The material properties are: Young's modulus=7×10^{10} N/m^2 , Yield stress $\sigma=10^8$ N/m^2. The geometrical parameters are: cross-sectional area A=10^{-4} m^2 and length L=2 m. The Newmark direct integration method [133] has been used for time integration.

The minimum and maximum natural frequency of the structure are $\omega_{min} = 8.2815$ Hz and $\omega_{max} = 1026.5$ Hz, respectively. An external impact load P(t) is applied at node 1, and the following two cases are considered.

$$\text{Case I :} \qquad P(t) = \begin{cases} I_{mp}/h \ \ (\text{N}) & 0 \le t \le h \\ 0 & t > h \end{cases}$$

$$\text{Case II:} \qquad P(t) = \begin{cases} I_{mp}/(100h) \ \ (\text{N}) & 0 \le t \le 100\,h \\ 0 & t > 100\,h \end{cases}$$

where, $I_{mp} = \sum P(t)\,\Delta t$ is applied impact for each case. In each case the time increment h=1.3×10^{-4} Sec and total numerical time of 1000×h=0.13 Sec are considered.

In case I, the impact load acts on the structure for a very short time. It has been observed that either member 23 or member 24 have always the largest element force, irrespective of the direction of the impact load P (t). However, note that from the static case, the member 18 at the bottom of the structure is the most critical. Members 23 and 24 are at the top of the structure in the vicinity of the direct impact load. Figure 5-45 shows the time- history of the element forces in members 24 and 18 for an impact impulse of $I_{mp} = 1$ N - Sec and direction of $\psi = 90°$. It can be observed that, for stability parameters $\beta = 0.25$ and $\gamma = 0.5$, the numerical solution display spurious "beating" where the amplitude of response repeatedly grows and decays. For the above numerical integration parameters, the average results are good. However, the spurious oscillations and noise exhibited by the numerical integration algorithm are severe. The Newmark method [133]

, with these numerical stability parameters, is termed 'average acceleration' algorithm with accuracy of order two (trapezoidal rule), and is unconditionally stable. Considering γ >0.5 introduces artificial damping, which automatically dissipates the high-frequencies noises, but also reduces the accuracy of the Newmark method to first order. In order to maximize the high-frequency dissipation for a given value of γ>0.5, as recommended by Hughes [176], $\beta = 0.25(\gamma + 0.5)^2$ was considered. Thus, using γ =0.67 and $\beta = 0.25(\gamma + 0.5)^2$=0.34, the high-frequency noise can be eliminated. No optimal geometries were obtained for case I loading, because the largest internal force always exists in member 23 and 24. This implies that for impact load acting for a short time, the structural strength is not affected by the geometry of the structure. It is necessary to make the structure in the vicinity of the impact loading structurally much stronger than the other parts in the structure.

For case II loading, the duration of the impact load on the structure is relatively large. Figure 5-46 shows the time history of the element forces in members 24 and 18 for the impact impulse $I_{mp} = 1$ N-Sec and load direction $\psi = 90°$. Once more, the solution exhibits high-frequency noise for the selected stability parameters $\gamma = 0.5$ and $\beta = 0.25$. The effect of high-frequency noise is not as pronounced as for Case I, especially for member 18. Nevertheless, the solution was improved when selecting $\gamma > 0.5$ and $\beta > 0.25$. The structural strength for the fixed configuration ($\varphi_1 = \varphi_2 = \varphi_3 = \varphi_4$) using both the displacement and the force methods for analysis are shown in Figure 5-47. The results using both methods of analysis totally match. However, the computational time required by the force and displacement methods were 34 Sec and 738 Sec, respectively. There is a considerable savings in computational effort when using the force method of analysis. The structure becomes very rapidly weak when the direction of the impact load is other than $\psi = 0°$. The optimal results for the various values of the external impact load direction ψ are given in Table 5-40. Figure 5-48 illustrates the marked improvement in load carrying capability in terms of the structural strength for the adaptive truss structure in comparison to the fixed structure. The optimal geometries of the adaptive structure are shown in the Figure 5-49, corresponding to the varying load directions

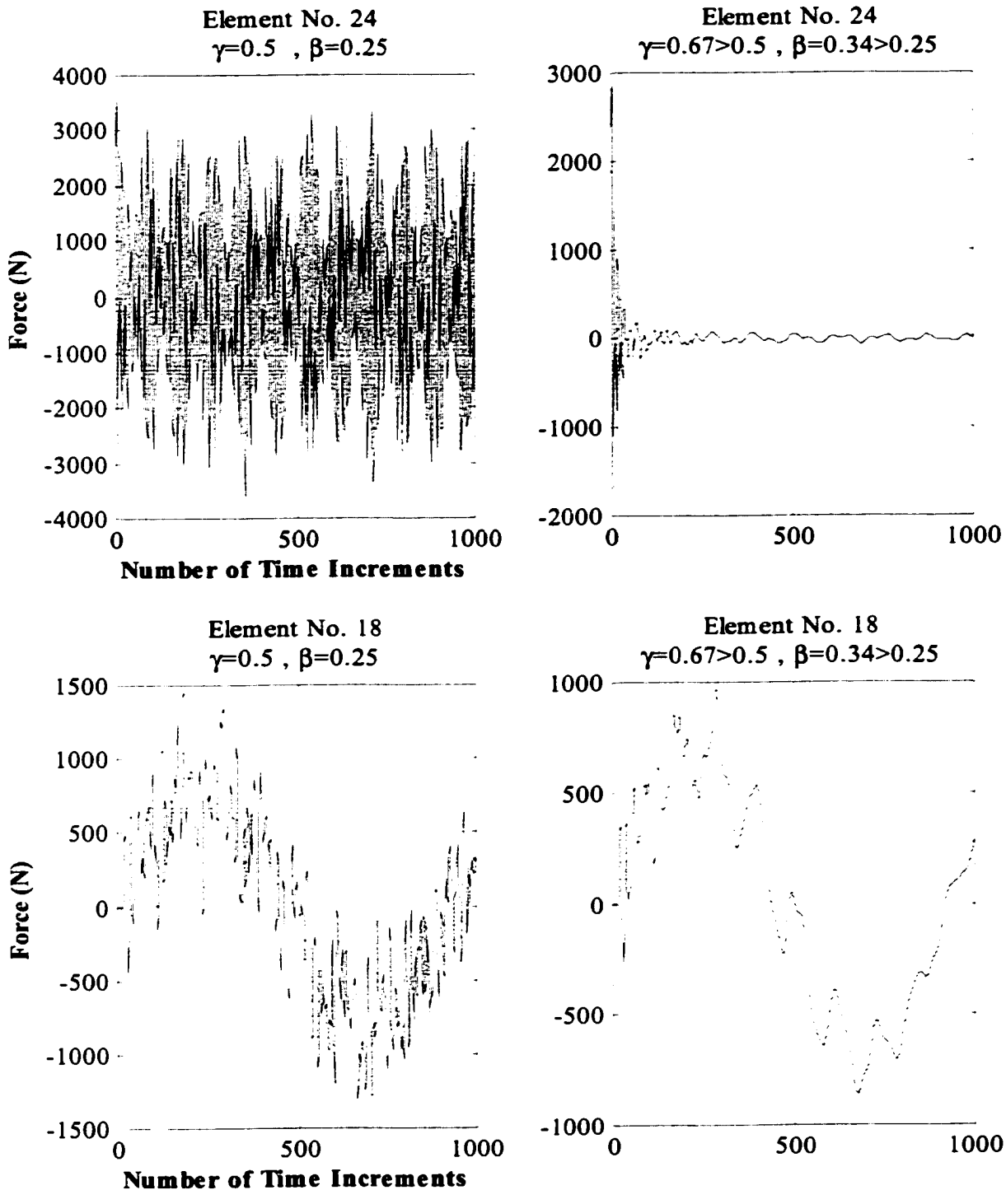

Figure 5-45 Time history of the element forces for case I and impact $I_{mp} = 1$ N - Sec.

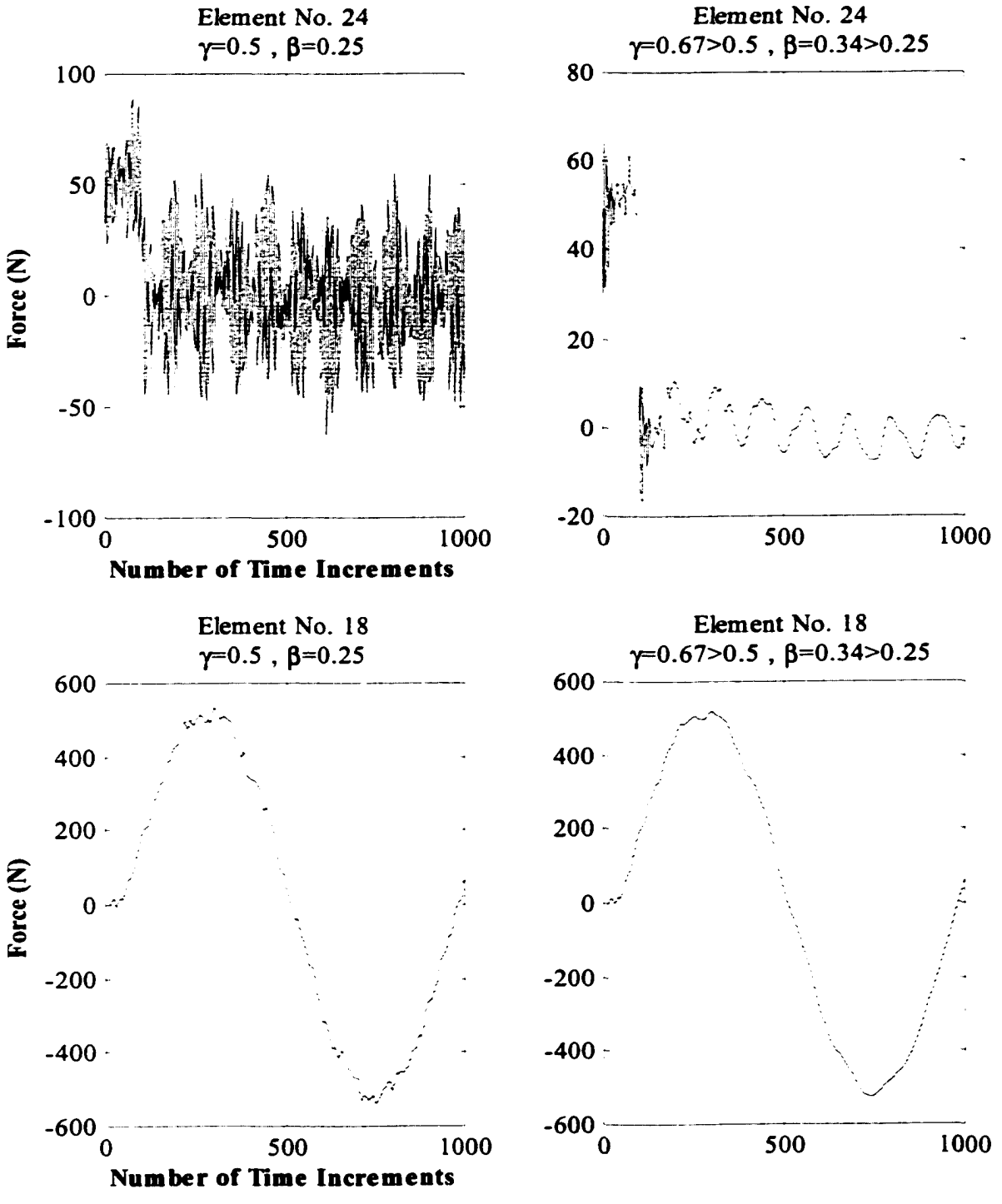

Figure 5-46 Time history of the element forces for case II and impact $I_{mp} = 1$ N - Sec.

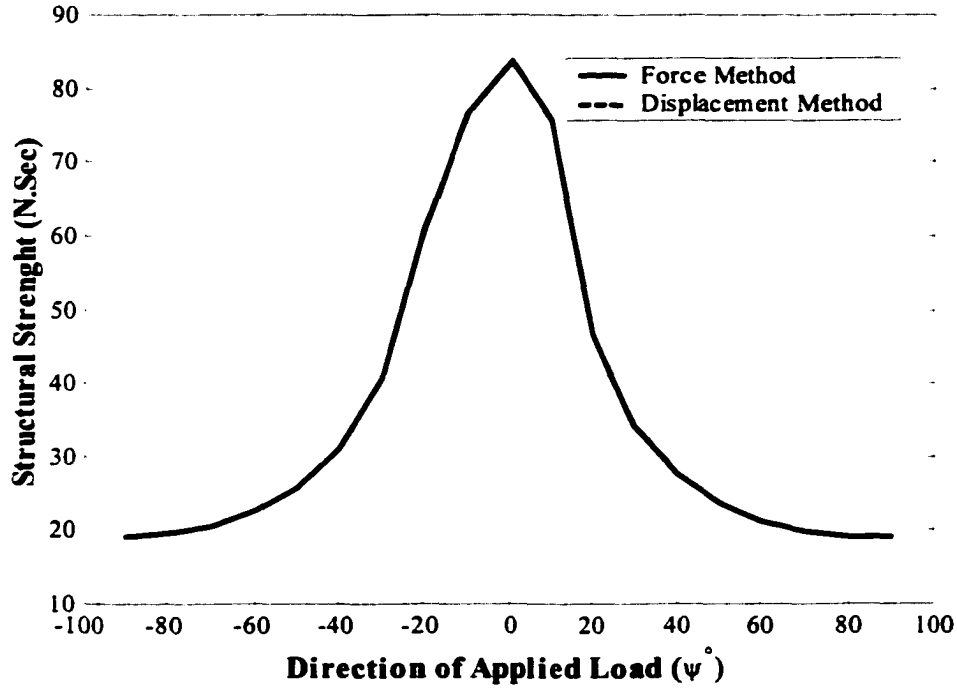

Figure 5-47 Structural strength versus the direction of the applied load (Fixed structure-Dynamic load).

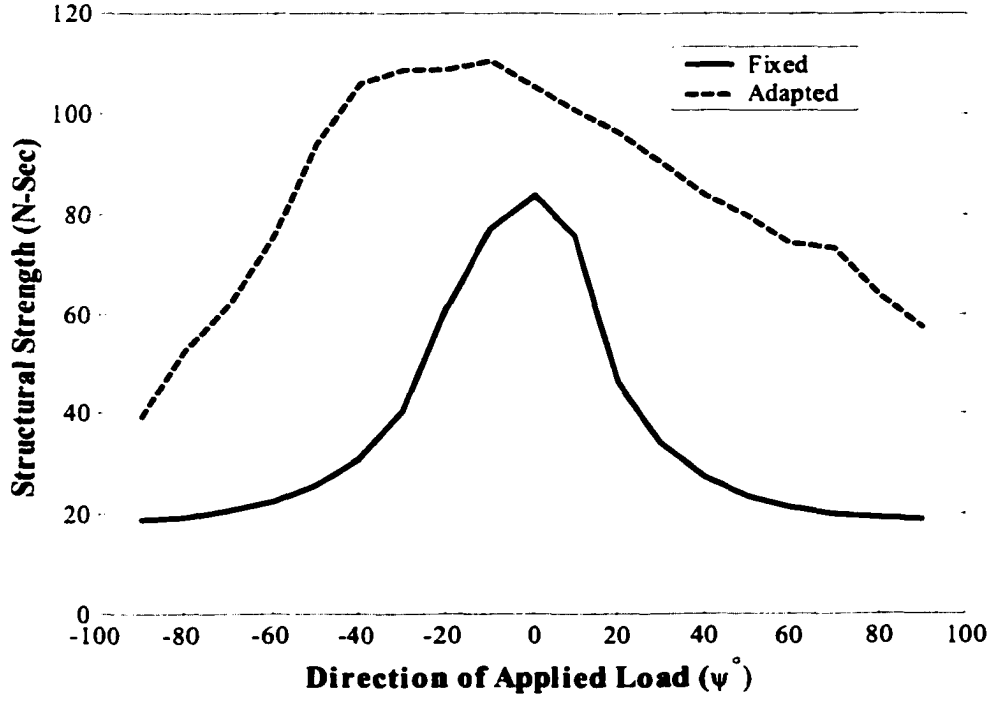

Figure 5-48 Optimal adaptive and fixed structural strength versus the direction of the applied load (Dynamic load).

Table 5-40 Optimal values of φ_1, φ_2, φ_3, φ_4 and structural strength in the optimal adaptive shapes (Dynamic load).

ψ°	Design Variables				Structural Strength (N-Sec)
	φ_1°	φ_2°	φ_3°	φ_4°	
-90	78.70	17.98	83.12	11.19	39.29
-80	77.69	20.03	82.40	11.64	52.29
-70	79.45	21.11	76.91	15.42	61.96
-60	77.68	23.84	72.37	19.50	75.78
-50	63.95	25.72	79.94	22.82	93.82
-40	57.32	30.08	70.55	24.94	105.83
-30	56.50	33.59	68.29	24.96	108.94
-20	51.85	37.10	60.03	29.97	108.69
-10	51.11	47.18	65.37	34.59	110.63
0	53.59	47.46	51.86	41.01	105.33
10	49.39	53.55	42.68	50.56	100.62
20	44.79	65.53	39.67	60.78	96.31
30	39.22	66.83	43.08	80.67	90.45
30	39.22	66.83	43.08	80.67	90.45
40	31.96	81.75	25.62	69.83	83.85
50	29.44	85.05	22.35	72.90	79.66
60	36.12	89.50	39.82	80.69	74.20
70	35.37	89.50	26.88	71.58	73.18
80	30.79	89.49	24.13	74.57	63.80
90	29.65	89.50	19.62	75.44	57.18

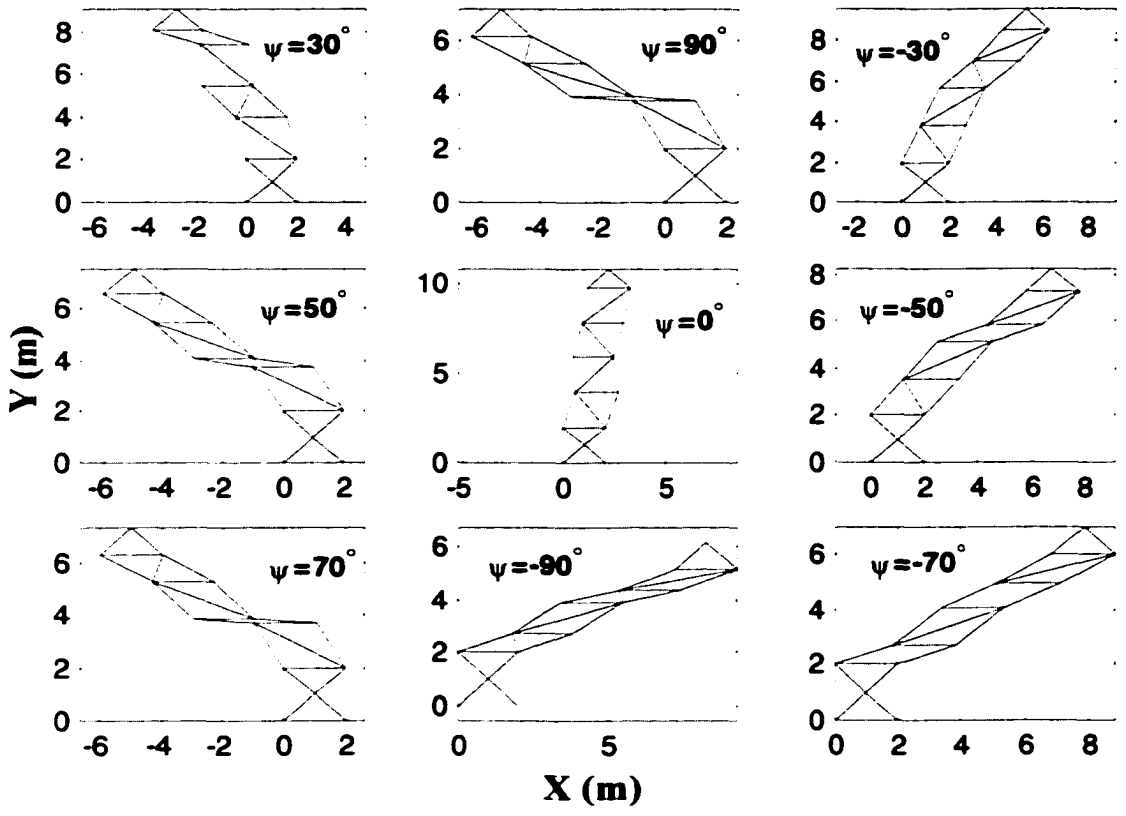

Figure 5-49 Optimal adaptive shapes of the truss structure with φ_1, φ_2, φ_3 and φ_4 as design variables (Dynamic load)

Chapter 6

CONCLUSIONS AND RECOMMENDATIONS

6.1 Conclusions

The development of new analysis methods, optimization algorithms and their integration into a structural analysis and optimization tool to study linear and nonlinear structural problems has been presented.

From the structural analysis perspective, a technique using the force method based on complementary strain energy has been introduced. In the proposed force method, the compatibility conditions are satisfied through the complementary energy. Automatic generation of a basis structure and redundant members using the gauss elimination technique has been successfully demonstrated for truss and beam-type structures. In the integrated force method, an efficient method based on single-value-decomposition technique has been developed to generate the compatibility conditions directly for truss and beam-type structures. The application of the force method to structures with small redundancies has proved to be computationally more efficient than the displacement method. Also, a new finite element impulse method based on the complementary Hamilton equation has been developed. However, the computer implementation and automation of this technique was found to be difficult to implement computationally

A nonlinear finite element method based on the force and displacement control techniques has been used to analyze nonlinear problems under stress, displacement and system stability constraints. Nonlinearity due to initial geometric imperfections has been addressed, as well. However, in nonlinear problems under stress and displacement constraints, the effect of nonlinearity was found to be insignificant in most practical problems.

In optimization, the most important contributions are the development of new and improved optimization algorithms based on the optimality criterion techniques. Their performance has been compared with the SQP technique. The structural optimization of truss and beam-type structures undergoing large rotations and small strains (geometrically nonlinear analysis) has been investigated and the effect of structural nonlinearity has been quantified in the presence of various constraints such as stress, displacement and system buckling.

The nonlinear analysis and optimization method has been applied to snap-through problems under limit load constraint. The methodology combines the nonlinear buckling analysis based on the displacement control and the optimality criterion techniques.

A thorough investigation has been done in linear and nonlinear stability using various types of geometric stability constraints. The effect of nonlinearity was found to be significant in nonlinear stability problems. It was found that the optimum results obtained using the linear stability with displacement dependent geometric stiffness is more conservative and closer to the nonlinear results compared to the stress geometric stiffness matrix. The effect of imperfections was found to be significant in most problems.

The application of the Group Theoretic Approach was introduced and applied to the optimum design of symmetric structures with high geometric nonlinearity. The analysis was transformed from full space to the reduced subspace by the GTA. The optimum design by the GTA using the reduced subspace was in excellent agreement with that using the full space. Design optimization using the GTA reduced subspace is computationally more efficient than that of the full space. Furthermore application of the GTA in post-buckling problems was addressed and it was shown that the agreement between full space and subspace was valid in post-buckling as well.

Finally, the finite element force method using the complementary strain energy was applied to topology optimization of adaptive structures. The optimization procedure was based on the Sequential Quadratic Programming method. The proposed method has performed well and it is extremely efficient in geometry optimization of adaptive truss structures where the primary design variables are the active member forces.

The proposed methods and tools offer an effective array of solutions to the analysis, design and optimization of nonlinear structures.

6.2 Contributions to the State of the Art

The present monogram constitutes a comprehensive study in the area of structural optimization. The development of finite element methods, optimization algorithms and their integration to study linear and nonlinear structural problems offer an effective analysis and optimization computational tool. The following points summarize the most important contributions of this thesis to the state of the art in the field of structural analysis and optimization:

- A new methodology based on the force formulation using the complementary energy approach has been formulated and implemented.
- The application of the force method based on the complementary energy to structural analysis and optimization and a comparison with the more popular and conventional displacement method has been carried out.
- A technique to directly derive the compatibility matrix in the integrated force method has been proposed and implemented.
- Efficient strategy has been implemented to generate the consistent redundant members and basis determinate structures.
- The integrated force method has been applied to truss and beam type structures requiring size and topology optimization in the presence of static and dynamic loads.
- The application of the finite element force method to linear structural optimization problems with stress, displacement and frequency constraints has been illustrated with numerous examples.

- A methodology based on the nonlinear finite element analysis using displacement control technique has been developed to catch the limit load in snap-through problems accurately.

- Optimization algorithms have been developed based on the optimality criterion technique for optimization of nonlinear problem with stability constraints.

- The nonlinear finite element optimization based on the displacement control technique and optimality criterion techniques has been applied to truss and beam structures.

- An efficient approach to incorporate element imperfections in structural optimization of nonlinear problems has been carried out.

- The effect of imperfections and geometric nonlinearity in structural optimization problems have been quantified and compared to the linear analysis results.

- An efficient method has been implemented to calculate the sensitivity of the load factor using adjoint method and information obtained from nonlinear buckling analysis based on the displacement control technique.

- The accuracy and efficiency of the optimization algorithms based on the developed optimality criterion techniques and mathematical programming technique using the Sequential Quadratic Programming Technique have been studied and applied to structural optimization of nonlinear problems.

- The effect of different geometric stiffness matrices (displacement and stress stiffness matrices) on nonlinear structural analysis and optimization has based studied. The derivations of the geometric nonlinear matrices are based on the energy and perturbation approaches.

- A methodology based on the Group Theoretic Approach has been studied and applied to nonlinear symmetric structures for buckling analysis. The post-buckling path has been traced using the Group Theoretic Approach in conjunction with the nonlinear finite element using the displacement control technique.

Summarizing, the depth and detail of the present investigation has allowed an appreciation and understanding of the foundations of structural optimization and has brought to light new developments that have furthered and enriched the field of nonlinear structural analysis, design and optimization.

6.3 Recommendations for Further Work

The methodologies developed and presented in this investigation have been successfully applied to a significant class of structures, exhibiting linear and nonlinear response subject to stress, displacement, frequency and stability constraints. Although this thesis has taken an important step towards the understanding of structural optimization, other numerous and interesting aspects are identified to improve the efficiency of the developed algorithms. These thoughts for future work are summarized as follows:

- This thesis has focused on truss and frame structures; however the analysis and optimization methods and tools should be extended to plate and shell elements.

- The force method formulation was developed for the optimum analysis and design of linear problems. Extending this methodology to the nonlinear problems presents a challenging task.

- In nonlinear problems under stress and displacement constraints, the method needs to be extended to the dynamic loads.

- In nonlinear problems under system stability constraints, the optimality criterion was developed based on the system stability constraint, causing local buckling in some members. To prevent against the local buckling, the cross-sectional areas were updated when the load was beyond the element-buckling load. However, a more accurate procedure would be to consider the local buckling as the constraint in the Kuhn-Tucker condition in the optimality criteria technique.

- The finite element formulation is general and was intended to account for geometric nonlinearity where strain was assumed to be small. Further work is required to account for nonlinear elastic materials.

REFERENCES

[1]. Sheu, C. Y., and Prager, W., " Recent Developments in Optimum Structural Design,"Applied Mechanic Review, Vol. 21, pp. 985-992, Oct. 1968.

[2]. Pierson, B. L., " A Survey of Optimal Structural design Under Dynamic Coinstraints," International Journal for Numerical Methods in Engineering, Vol. 4, pp. 491-499, 1972.

[3]. Venkayya, V. B., "Structural Optimization: A Review and Some Recommendations," International Journal for Numerical Methods in Engineering, Vol. 13, pp. 203-228, 1978

[4]. Krishnamoorthy, C. S. and Mosi, D. R., " A Survey on Optimal Design of Civil Engineering Structural Systems," Engineering Optimization, Vol. 4, pp. 73-88, 1979.

[5]. Haftka, R. T. and Prasad, B., " Optimum Structural Design with Plate Bending Elements- A Survey," AIAA Journal, Vol. 19, pp. 517-522, 1981.

[6]. Schmit, L. A., "Structural Synthesis- Its Genesis and Development," AIAA Journal, Vol. 19, pp. 1249-1263, 1981.

[7]. Schmit, L. A., " Structural Synthesis 1959-1969: A Decade of Progress," in Recent Advances in Matrix Methods of Structural analysis and Design, University of Alabama Press, Huntsville, pp. 565-634, 1971.

[8]. Vanderplaats, G. N., " Structural Optimization- Past, Present, and Future," AIAA Journal, Vol. 20, pp. 992-999, 1982.

[9]. Grandhi, R., " Structural Optimization with Frequency Constraints- A Review," AIAA Journal, Vol. 31, pp. 2296-2303, 1993.

[10]. Cox, H. L., *The Design of Structures of Least Weight, Pregamon Press*, New-York, 1965.

[11]. Michell, M. C. E., " The limits of Economy of Material in Frame-structures," Philosophical Magazine, Vol. 8, pp. 589-597, 1904.

[12]. Luenberger, D. G., *Linear and Nonlinear Programming*, Addison Wesley, 1984.

[13]. Schmit, L. A., " Structural Design by Systematic Synthesis," Proceedings, 2nd Conference on Electronic Computation, ASCE, New York, pp. 105-122, 1960.

[14]. Sander, G., and Flury, C., " A Mixed Method in Structural Optimization," International Journal for Numerical Methods in Engineering, Vol. 13, pp. 385-404, 1978.

[15]. Frind, E. O., and Wright, P. M., " Gradient Methods in Optimum Structural Design," Journal of the Structural Division, ASCE, Vol. 101, pp. 939-956, 1975.

[16]. Pappas, M., " Improved Methods for Large-Scale Structural Synthesis," AIAA Journal, Vol. 19, pp. 1227-1233, 1981.

[17]. Fleury, C., " An Efficient Optimality Criteria Approach to the Minimum Weight Design of Elastic Structures," Computers and Structures, Vol. 11, pp.163-173, 1980.

[18]. Wright, P. M., and Feng, C. C., " Optimum Design of Plane Frames Using a Multi-Mode Scheme," The Engineering Journal, Transactions of the Engineering Institute of Canada, Vol. 14, pp. 1-6, 1971.

[19]. Tabak, E. I., and Wright, P. M., " Optimality Criteria Method for Building Frames," Journal of the Structural Division, ASCE, Vol. 107, pp. 1327-1342, 1981.

[20]. Wright, P. M., and Hakim, H. F., " Automated Design of Rigid Steel Frames Including Member Selection," Canadian Journal of Civil Engineering, Vol. 5, pp. 114-125, 1978.

[21]. Iserb, M., " Three-Dimensional Beam Elements Synthesis Applications with Stress Constraints, Nonlinear size-Stiffness Relationships, and Various Size-Inertia Powers," Computers and Structures, Vol. 7, pp. 565-569, 1977.

[22]. Svanberg, K., "Weight Optimization of Beam Structures," Optimization Methods in Structural Design, Eschenauer, H. and Olhoff, N. (Editors), Bibliographisches Institut, pp. 403-408, 1982.

[23]. Khot, N. S., " Algorithms Based on Optimality Criteria to Design Minimum Weight Structures," Engineering Optimization, Vol. 5, pp. 73-90, 1981.

[24]. Dobbs, M. W., and Nelson, R. B., " Application of Optimality Criteria to automated Structural Design," AIAA Journal, Vol. 14, pp. 1436-1443, 1976.

[25]. Khan, M. R., Willmert, K. D., and Thornton, W. A., " A New Optimality Criterion Method for Large Scale Structures," Proceedings, AIAA/ASME 19th SDM Conference, Bethesda, Maryland, pp. 47-58, 1978.

[26]. Khot, N. S., Berke, L., and Venkayya, V. B., " Comparison of Optimality Criteria Algorithms for Minimum Weight Design of Structures," AIAA Journal, Vol. 17, pp. 182-190, 1979.

[27]. Allwood, R. J., and Chung, Y. S., " Minimum-Weight Design of Trusses by an Optimality Criteria Method," International Journal for Numerical Methods in Engineering, Vol. 20, pp. 697-713, 1984.

[28]. Templeman, A. B., " A Dual Approach to Optimum Truss Design," Journal of Structural Mechanics, Vol. 4, pp. 235-255, 1976.

[29]. Schmit, L. A., and Farshi, B., " Some Approximation Concepts for Structural Synthesis," AIAA Journal, Vol. 12, pp. 692-699, 1974.

[30]. Schmit, L. A., and Miura, H., " A New Structural Analysis / Synthesis Capability-ACCESS 1," AIAA Journal, Vol. 14, pp. 661-671, 1976.

[31]. Schmit, L. A., and Miura, H., " An Advanced Structural Analysis / Synthesis Capability – ACSESS 2," International Journal for Numerical Methods in Engineering, Vol. 12, pp. 353-377, 1978.

[32]. Schmit, L. A., and Miura, H., " Approximation Concepts for Efficient Structural Synthesis," NASA CR2552, 1976.

[33]. Miura, H., and Schmit, L. A., " Second Order Approximation of Natural Frequency Constraints in Structural Synthesis," International Journal for Numerical Methods in Engineering, Vol. 13, pp. 337-351, 1978.

[34]. Storaasli, O. O., and Sobieszczanski, J., " On the Accuracy of the Taylor Approximation for Structure Resizng," AIAA Journal, Vol. 12, pp. 233, 1974.

[35]. Noor, A. K., and Lowder, H. E., " Structural Reanalysis via a Mixed Method," Computers and Structures, Vol. 5, pp. 9-12, 1975.

[36]. Laarhoven, P. J. M. van., and Aarts, E., *Simulated annealing: Theory and Applications*, D. Reidel Publishing, Dordrecht, The Netherlands, 1987.

[37]. Goldberg, D. E., *Genetic Algorithms in Search, Optimization, and Machine Learning*, Addison-Wesley Publishing Co. Inc., Reading, Massachusetts, 1989.

[38]. Elperin, T, " Monte Carlo Structural Optimization in Discrete Variables with Annealing Algorithms," International Journal for Numerical Methods in Engineering, Vol. 26, pp. 815-821, 1988.

[39]. Kincaid, R. K., and Padula, S. L., " Minimizing Distortion and Internal Forces in Truss Structures by Simulated Annealing," Proceedings of the AIAA/ ASME/ ASCE/AHS/ASC 31st Structures, Structural Dynamics, and Materials Conference, Long Beach, CA., part 1, pp. 327-333, 1990.

[40]. Balling, R. J., and May, S. A., " Large-Scale Discrete Structural Optimization: Simulated Annealing, Branch-and-Bound, and Other Techniques," Presented at the AIAA/ASME/ASCE/AHS/ASC 32nd Structures, Structural Dynamics, and Material Conference, Long Beach, CA., 1990.

[41]. Chen, G.S., Bruno, R. J., and Salama, M., " Optimal Placement of Active/Passive Members in Structures Using Simulated Annealing," AIAA Journal, Vol. 29, pp. 1327-1334, August 1991.

[42]. Goldberg, D. E., and Samtani, M. P., " Engineering Optimization via Genetic Algorithm," Proceedings of the Ninth Conference on Electronic Computation, ASCE, pp. 471-482, February 1986.

[43]. Hajela, P., " Genetic Search- An Approach to the Nonconvex Optimization Problem," AIAA Journal, Vol. 28, pp. 1205-1210, 1990.

[44]. Rao, S. S., Pan, T. S., and Venkayya, V. B., " Optimal Placement of Actuators in Actively Controlled Structures Using Genetic Algorithms," AIAA Journal, Vol. 29, PP. 942-943, June 1991.

[45]. Bendsoe, M. P., *Optimization of Structural Topology, Shape, and Material*, Springer Heidelberg.

[46]. Xie, Y. M., and Steven, G. P., *Evolutionary Structural Optimization*, Springer-Verlag, London, 1997.

[47]. Przemieniecki, J. S., *Theory of Matrix Structural Analysis*, McGraw-Hill, New York, 1968.

[48]. McGuire, W., and Gallagher, R. H., *Matrix Structural Analysis*, John Wiley, New York, 1979.

[49]. Robinson, J., *Integrated Theory of Finite Element Methods*, John Wiley, New York, 1973.

[50]. Timoshenko, S., History of Strength of Material, McGraw-Hill, New York, 1953.

[51]. Przemieniecki, J. S., " Joining of Complex Structures by Matrix Force Method," Journal of Aircraft, Vol. 3, pp. 236-243, 1966.

[52]. Robinson, J., and Haggenmacher, G. W., *Recent Advances in Matrix Methods of Structural Aanalysis and Design*, The University of Alabama Press, Huntsville, 1971.

[53]. Robinson, J., *Structural Analysis for Engineers*, John Wiley, New York, 1966.

[54]. Robinson, J., " Automatic Selection of Redundancies in the Matrix Force Method, the Rank Technique," Canadian Aeronautics and Space Journal, Vol. 11, pp. 9-12, 1965.

[55]. Tapcu, A., " A Contribution to the Systematic Analysis of Finite Element Structures Using Force Method," Doctoral Dissertation, University of Essen, Germany, 1979.

[56]. Kaneko, L., Lawo, M., and Thierauf, G., " On Computational Procedures for the Force Method," International Journal for Numerical Methods in Engineering, Vol. 18, pp. 1469-1495, 1982.

[57]. Patnaik S. N., " An Integrated Force Method for Discrete Analysis," International Journal for Numerical Methods in Engineering, Vol. 16, pp. 237-251, 1973.

[58]. Patnaik S. N., and Yadagiri, S., "Design for Frequency by the Integrated Force Method," Computer Methods in Applied Mechanics and Engineering, Vol.16, pp. 213-230, 1978.

[59]. Patnaik S. N., and Yadagiri, S., " Frequency Analysis of Structures by Integrated Force Method", Journal of Sound and Vibration, Vol. 83, No. 1, pp. 93-109, 1982.

[60]. Patnaik, S. N., " The Integrated Force Method Verses the Standard Force Method", Computers and Structures, Vol. 22, No. 2, pp. 151-163, 1986.

[61]. Patnaik, S. N., " The Variational Energy Formulation for the Integrated Force Method", AIAA Journal, Vol. 24, No. 1, Jan. 1986.

[62]. Patnaik. S. N., and Nagaraj, M. S., " Analysis of Continuum by the Integrated Force Method," Computer and Structures, Vol. 26, pp. 899-905, 1987.

[63]. Vijayakumar, K., Krishna Marty., and Patnaik, S. N., " A Basis for the Analysis of Solid Continua Using the Integrated Force Method," AIAA Journal, Vol. 26, pp. 628-629, 1988.

[64]. Patnaik S. N., and Berke, L.,and Gallagher, R. H., " Integrated Force Method Versus Displacement Method for Finite Element Analysis", Computers and Structures, Vol. 38, No. 4, pp. 377-407, 1991.

[65]. Patnaik, S. N.; Joseph, K. T., " Compatibility Conditions from Deformation Displacement Relationship", AIAA Journal, Vol .23, No. 8, pp. 1291-1293, 1985.

[66]. Patnaik, S. N.; Joseph, K. T., " Generation of the Compatibility Matrix in the Integrated Force Method", Computer Methods in Applied Mechanics and Engineering, Vol. 55, pp. 239-257, 1986.

[67]. Nagabhusanam, J.; Patnaik, S. N., " General Purpose Program to Generate Compatibility Matrix for the Integrated Force Method", AIAA Journal, Vol. 28, No. 10, pp. 1838-1842, Oct. 1990.

[68]. Sokolnikoff, I. S., *Mathematical Theory of Elasticity*, McGraw-Hill, New York, 1956.

[69]. Patnaik, S. N., and Dayaratnam, P., " Behavior and Design of Pin Connected Structures," International Journal for Numerical Methods in Engineering, Vol. 2, pp. 579-595, 1970.

[70]. Patnaik, S. N., Guptill, J. D., and Berke, L., " Merits and Limitations of Optimality Criteria Methods for Structural Optimization," International Journal for Numerical Methods in Engineering, Vol. 38, pp. 3087-3120, 1995.

[71]. Patnaik, S. N., Gendy, A. S., Berke, L., and Hopkins, D. A., " Modified Fully Utilized Design (MFUD) Method for Stress and Displacement Constraints," International Journal for Numerical Methods in Engineering, Vol. 41, pp. 1171-1194, 1998.

[72]. Patnaik. S. N., and Gallagher, R. H., " Gradients of Behavior Constraints and Reanalysis via the Integrated Force Method", International Journal for Numerical Methods in Engineering, Vol. 23, pp. 2205-2212, 1986.

[73]. Zienkiewicz, O. C., *The Finite Element Method*, 3rd edition, McGraw-Hill, London, 1977.

[74]. Cook, R. D., Malkus, D. S., and Plesha, M. E., *Concepts and Applications of Finite Element Analysis*, 3rd edition, John Wiley & Sons, 1989.

[75]. Bathe, K. J., *Finite Element Procedures*, Prentice Hall, 1996.

[76]. Crisfield, M. A., *Non-Linear Finite Element Analysis of Solids and Strutures, John* Wiley & Sons, 1991.

[77]. Levy, R., and Spillers, W. R., *Analysis of Geometrically Nonlinear Structures,* Chapman & Hall, 1995.

[78]. Bathe, K. J., and Bolourchi, S., "Large Displacement Analysis of Three-Dimensional Beam Structures," International Journal for Numerical Methods in Engineering, Vol. 14, pp. 961-986, 1979

[79]. Bathe, K. J., Wilsob, E. L., and Iding, R. H., " NONSAP- A Structural Analysis Program for Static and Dynamic Response of Nonlinear Systems," UCSESM 74-3, University of California, Berkeley, 1974.

[80]. Belytschko T., and Hseih, J, " Nonlinear transient finite element analysis with convected co-ordinates," International Journal for Numerical Methods in Engineering, Vol. 7, pp. 255-271, 1973.

[81]. Rankin, C. C, and Brogan, F. A., "An Element Independent Corotational Procedure for the Treatment of Large Rotations," Journal of Pressure Vessel Technology, vol. 108, pp. 165-174, 1986.

[82]. Crisfield, M. A., "A Consistent Corotational Formulation for Nonlinear, Three-Dimensional, Beam elements," Computer Methods in Applied Mechanics and Enginnering, Vol. 81, pp. 131-150, 1990.

[83]. Turner, M. J., Dill, E. H., Martin, H. C., and Melosh, R. J., " Large Deflection of Structures Subject to Heating and External Load," Journal of Aeronautical. Sciences, Vol. 27, pp. 97-106, 1960.

[84]. Argyris, J. H., Recent Advances in Matrix Methods of Structural Analysis, Pergamon Press, 1964.

[85]. Argyris, J. H., " Continua and Discontinua," Proceedings Conference in Matrix Methods in Structural Mechanics., Air Force Institute of Technology, Wright Patterson Air Force Base, Ohio, 1965.

[86]. Mallet, R. H., and Marcel, P. V., " Finite Element analysis of Non-linear Structures," Proceedings of ASCE, Journal of Structural Division, Vol. 94, ST, pp. 2081-2105, 1968.

[87]. Marcel, P. V., " Finite Element Analysis of Combined Problems of Nonlinear Material and Geometric Behavior," Proceedings of American Society of Mechanics, Conference on Computational Approaches in Applied Mechanics, June 1969.

[88]. Oden., J. T., " Numerical Formulation of Nonlinear Elasticity Problems," Proceedings of ASCE, Journal of Structural Division, Vol. 93, ST3, paper 5290, 1967.

[89]. Oden, J. T., " Finite Element Applications in Non-linear Structural Analysis," Proceedings Conference On Finite Element Method., Vanderbilt University Tennessee, Nov. 1969.

[90]. Haisler, W. E., Stricklin, J. E., and Stebbins, F. J., " Development and Evaluation of Solution Procedures for Geometrically Non-linear Structural Analysis by the Discrete Stiffness Method," AIAA/ASME 12th Structure, Structural Dynamics & Materials Conf., Anaheim, California, April 1971.

[91]. Nayak, G. C., and Zienkiewicz, O. C., " Note on the 'alfa-constant' stiffness method of the analysis of non-linear problems," International Journal for Numerical Methods in Engineering, Vol. 4, pp. 579-582, 1972.

[92]. Brebbia, C., and Connor, J., " Geometrically Non-linear Finite Element Analysis," Proceedings of ASCE, Journal of Engineering Mechanical Division, Paper 6516, 1969.

[93]. Murray, D. W., and Wilson, E. L., " Finite Element Post Buckling Analysis of Thin Elastic Plates," Proceedings ASCE, Journal of Engineering Mechanical Division, Vol. 95, EM1, pp. 143-165, 1969.

[94]. Bergen, P. G., Horrigmoe, G., Krakeland, B., and Soreida, T. H., " Solution Techniques for Nonlinear Finite Element Problems," International Journal for Numerical Methods in Engineering, Vol. 12, pp. 1677-1696, 1978.

[95]. Shariffi, P., and Popov, E. P., " Nonlinear Buckling Analysis of Sandwich Arches," ASCE Journal, Engineering Division, Vol. 97, pp. 1397-1412, 1971.

[96]. Zienkiewicz, O. C., " Incremental Displacements in Nonlinear Problems", International Journal for Numerical Methods in Engineering, Vol. 3, pp. 587-592, 1971.

[97]. Haisler, W. E., Stricklin, J. A., and Key, J. E., " Incrementation in Nonlinear Structural Analysis by Self-Correcting Method", International Journal for Numerical Methods in Engineering , Vol. 11, pp. 3-10, 1977.

[98]. Batoz, J. L., Dhatt, G., " Incremental Displacement Algorithms for Nonlinear Problems", International Journal for Numerical Methods in Engineering, Vol. 14, pp. 1262-1267, 1979.

[99]. Ricks, E., " An Incremental approach to the solution of Snapping and Buckling Problems", International Journal for Solids and Structures, Vol. 15, pp. 529-551, 1979.

[100]. Wempner, G. A., " Discrete Approximation Related to Nonlinear Theories of Solids", International Journal for Solids and Structures, Vol. 7, pp. 1581-1599, 1971

[101]. Crisfield, M. A., " A Fast Incremental /Iterative Procedure that handles Snap-Through", Computers and Structures, Vol. 13, pp. 55-62, 1981.

[102]. Padovan, J., and Tovichakchaikul, S., " Self Adaptive Predicator-Corrector Algorithms for Static Nonlinear Structural Analysis", Computers and Structures, Vol. 17, pp. 871-879, 1983.

[103]. Bathe, K. J., and Dvorkin, E. N., " On the Automatic Solution of Nonlinear Finite Element Equations", Computers and Structures, Vol. 17, pp. 871-879, 1983.

[104]. Rosen, A., and Schmit, L. A. Jr., "Design Oriented Analysis of Imperfect Truss Structures. Part II- Approximate Analysis", International Journal for Numerical Methods in Engineering, Vol. 15, pp. 483-494, 1980.

[105]. Rosen, A., and Schmit, L. A. Jr., " Optimization of Truss Structures Having Local and System Stability", AIAA Journal, Vol. 21, pp. 1181-1186, 1983.

[106]. Tiexeira de Freitas, J. A., and Moitinho de Almeida, J. P. B., " Elastic Synthesis for Large Displacements," Proceedings of International Symposium on Optimal Structural Design, University of Arizona, Tucson, Arizona, pp. 13.35-13.41, 1981.

[107]. Khot, N. S., " Nonlinear Analysis of Optimized Structure with Constraints on System Stability", AIAA Journal, Vol. 21, pp. 1181-1186, 1983.

[108]. Kamat, M. P., Khot, N. S., and Venkayya, V. B., " Optimization of Shallow Trusses against Limit Point Instability", AIAA Journal, Vol. 22, pp. 403-408, 1984.

[109]. Kamat, M. P., Khot, N. S., and Watson, L. T., " On Optimizing Frame Type Structures in Nonlinear Response", Computer Methods for Nonlinear Solids and Structural Mechanics, Vol. 54, pp. 111-119, 1983.

[110]. Kamat, M. P., "Optimization of Shallow Arches Against Instability Using Sensitivity Derivatives," Finite Elements in Analysis and Design, Vol.3, pp. 277-284, 1987.

[111]. Khot, N. S., and Kamat, M. P., " Minimum Weight Design of Truss Structures with Geometric Nonlinear Behavior", AIAA Journal, Vol. 23, No. 1,pp. 139-144, 1985.

[112]. Kamat, M. P., and Raungasilasingha, P., " Optimization of Space Truss Against Instability Using Design Sensitivity Derivatives", Engineering Optimization, Vol. 8, pp. 177-188, 1985.

[113]. Levy, R, and Perng, H. S., " Optimization for Nonlinear Stability", Computer and Structures, Vol. 30, pp. 529-535, 1988.

[114]. Smaui, H., "An Integrated Approach to the Synthesis of Geometrically Nonlinear Structures," Master's Thesis, University of California, Los Angeles, 1985.

[115]. Smaui, H., and Schmit, L. A., " An Integrated Approach to the Synthesis of Geometrically Nonlinear Structures," International Journal for Numerical Methods in Engineering, Vol. 26, pp. 555-570, 1988.

[116]. Wu, C. C., and Arora, J. S., " Simultaneous Analysis and Design of Nonlinear Response", Engineering with Computers, Vol. 2, pp. 53-63, 1987.

[117]. Wu, C. C., and Arora, J. S., " Design Sensitivity Analysis of Non-Linear Buckling Load," Computational Mechanics, Vol. 3, pp. 129-140, 1988.

[118]. Cardoso, J. B. , and Arora, J. S., " Variational Method for Design Sensitivity Analysis in Nonlinear Structural Mechanics", AIAA Journal, Vol. 26, No. 5, 1988.

[119]. Arora, J. S., and Cardoso, J. B., " A Design Sensitivity Analysis Principle and its Implementation into ADINA", Computers and Structures, Vol. 32, pp. 691-705, 1989.

[120]. Choi, K. K., and Santos, J. L. T., " Design Sensitivity Analysis of Nonlinear Structural Systems. Part I: Theory", International Journal for Numerical Methods in Engineering, Vol. 24, pp. 2039-2055, 1987.

[121]. Santos, J. L. T., and Choi, K. K., " Sizing Design Sensitivity Analysis of Nonlinear Structural Systems. Part II: Numerical Method", International Journal for Numerical Methods in Engineering , Vol. 26, pp. 2039-2055, 1988.

[122]. Haftka, R. T., " Integrated Nonlinear Structural Analysis and Design", AIAA Journal, Vol. 27, pp. 1622-1627, 1989.

[123]. Orozco, C. E., and Ghattas, O. N., " Sparse Approach to Simultaneous Analysis and Design of Geometrically Nonlinear Structures", AIAA Journal, Vol. 30, pp. 1877-1885, 1992.

[124]. Saka, M. P., " Optimum Design of Nonlinear Space Trusses", Computers and Structures, vol. 30, pp. 545-551, 1988.

[125]. Saka, M. P., and Ulker, M., " Optimum Design of Geometrically Nonlinear Space Trusses", Computers and Structures, Vol. 42, pp. 289-299, 1992.

[126]. Lin, Y. t., Chung, T. t., and Sun, T. C., " Weight Optimization of Nonlinear Truss Structures with Static Response", Journal of Chinese Society of Mechanical Engineers (CSME), Vol. 13, pp. 317-326, 1992.

[127]. Levy, R., " Optimization for Buckling with Exact Geometries", Computers and Structures, Vol. 53, pp. 1139-1144, 1994.

[128]. Levy, R. " Optimal Design of Trusses for Overall Stability", Computers and Structures, Vol. 53, No. 5, pp. 1133-1138, 1994.

[129]. Orozco, C. E., and Ghattas, O. N., " A Reduced SAND Method for Optimal Design of Nonlinear Structures", International Journal for Numerical Methods in Engineering, Vol. 40, pp. 2759-2774, 1997.

[130]. Tabarrok, B., Rimrott, F. P. J., *Variational Methods and Complementary Formulations in Dynamics,* Kluwer Academic Publishers, 1994.

[131]. McGuire W., and Gallagher, *R. H .,Matrix Structural Analysis,* John Wiley, New York, 1979.

[132]. Golub, G. H., and Van Loan, *Matrix Computations,* third edition, the Johns HopkinsPress, Baltimore, 1996.

[133]. N. M. Newmark, "A method of Computation for Structural Dynamics," Journal of Engineering Mechanics Division, Proc. ASCE, Vol. 85, No. EM3, pp. 67-94, 1959.

[134]. Tabarrok, B. , *Finite Element Methods-Course Notes*, Revised April 1999, University of Victoria.

[135]. Chang, S.-C., and Chen, J.-J., "Effectiveness of Linear Bifurcation Analysis for Predicting the Nonlinear Stability Limits of Structures," International Journal for Numerical Methods in Engineering, Vol. 23, pp. 831-846, 1986.

[136]. Green, A. E., Knops, R. J. and Laws, N., "Large Deformations, Superimposed Small Deformations and Stability of Elastic Rods," International Journal of Solids and Structures, Vol. 4, pp. 555-577, 1968.

[137]. Oran, C., "Tangent Stiffness in Plane Frames," ASCE Journal of Structural Division 99 (ST6), pp. 973-985, 1973.

[138]. Spillers, W. R., "Geometric Stiffness Matrix for Space Frames," Computers and Structures, Vol. 36, pp. 29-37, 1990.

[139]. Bathe, K. J., and Cimento, A. P., "Some Practical Procedures for the Solution of Nonlinear Finite Element Equations," Computational Methods in Applied Mechanics and Engineering, Vol. 22, pp. 59-85, 1980.

[140]. Brockman, R. A., "Economical Stiffness Formulations for Nonlinear Finite Element," Computers and Structures, Vol. 18, pp. 15-22, 1984.

[141]. Boyle, F. F., and Jennings, A., "Accelerating the Convergence of Elastic-Plastic Stress Analysis," International Journal for Numerical Methods in Engineering, Vol. 7, pp. 232-235, 1975.

[142]. Williams, F. w., "Approach to the Nonlinear Behavior of the Members of a Rigid Jointed Plane Framework with Finite Deflections," Quarterly Journal of Mechanics and Applied Mathematics, Vol. 17, pp. 451-469, 1964.

[143]. Meek, J. L., and Loganathan, "Geometrically Nonlinear Behavior of Space Frame Structures," Computer and Structures, Vol. 31, pp. 35-45, 1989.

[144]. Healey, T. J., *Symmetry, Bifurcation and Computational Methods in Nonlinear Structural Mechanics*, Ph. D thesis, University of Illinois, Champaign, IL, 1985.

[145]. Healey, T. J., "Symmetry and Equivariance in Nonlinear Elastostatics, Part I," Archive for Rational Mechanics and Analysis, Vol. 105, pp. 205-228, 1989.

[146]. Healey, T. J., " A Group Theoretic Approach to Computational Bifurcation Problems with Symmetry," Computer Methods in Applied Mechanics and Engineering, Vol. 67, pp. 257-297, 1988.

[147]. Miller, Willard Jr. , *Symmetric Groups and Their Applications,* Academic Press, New York, 1972.

[148]. Chang. P., and Healey, T. J., "Computation of Symmetry Modes and Exact Reduction in Nonlinear Structural Analysis," Computer and Structures, Vol. 28, pp. 135-142, 1988.

[149]. Li, L. ,*Computational Nonlinear Static and Dynamic Analysis of Symmetric Structures by Using the Group Theoretic Approach,* Ph. D thesis, The University of Western Ontario, 1999.

[150]. Wood, E., *Crystals and Light*, 2nd Edn. Dover, New York, 1977.

[151]. Wada, B. K., Fanson, J. L., Garba, J. A., and Chen, G-S., "Adaptive Structures to Meet Requirements for Future Space Missions," AIAA-88-2481, 1988.

[152]. Murotsu, Y. and Shao, S., " Some Approaches to the Optimal Adaptive Geometries of Intelligent Truss Structures,", First Joint US/Japan Conference on Adaptive Structures, Hawaii US, pp. 743-771, Nov. 13-15 1990.

[153]. Murotsu, Y. and Shao, S., "Optimum Adaptation of Intelligent Truss Structures.", Journal of Intelligent Material Systems and Structures, Vol. 1, No. 2, April 1990, pp. 175-199.

[154]. Murotsu, Y. and Shao, S., "Optimal Adaptive Geometry of an Intelligent Truss Structure", AIAA-90-1093.

[155]. Lu, W. S., *The Lecture Notes,* University of Victoria.

[156]. Gallagher, R. H., 'Fully Stressed Designs', in Gallagher, R. H., and Zienkiewicz (eds.), *Optimum Structural Design*, Wiley, New York, pp. 19-32, 1973.

[157]. Coleman, T., Branch, M. A. and Grace, A., *Optimization Toolbox-For Use with Matlab*, The MathWorks Inc., User's Guides, Version 2, 1999.

[158]. Biggs, M. C., " Constrained Minimization Using Recursive Quadratic Programming," Towards Global Optimization (L.C.W.Dixon and G.P.Szergo, eds), North-Holland, pp. 341-349, 1975.

[159]. Han, S. P., " A Globally Convergent Method for Nonlinear Programming," Journal of Optimization Theory and Applications, Vol. 22, pp. 297-309, 1977.

[160]. Powell, M.J.D., "Algorithms for Nonlinear Constraints that use Lagrangian Functions," Mathematical Programming, Vol. 14, pp. 224-248, 1978.

[161]. Powell, M.J.D., " A Fast Algorithm for Nonlinearly Constrained Optimization Calculations," Proceedings of the Dundee Conference on Numerical Analysis, Lecture Notes in Mathematics, Vol. 630, pp. 144-157, Berlin, 1978.

[162]. Fletcher, R., *Practical Methods of Optimization*," 2nd edition, John Wiley and Sons, New York, 1987.

[163]. Gill, P. E., Murray, W. and Wright, M. H., *Practical Optimization*, Academic Press, London, 1981.

[164]. Haftka, T. H., and Zafar, G.,*Elements of Structural Optimization*, Kluwer-Academic Publishers, 3rd edition, 1992.

[165]. Fleury, C., and Schmit, L. A. Jr., "Dual Methods and Approximation Concepts in Structural Synthesis," NASA CR-3226, December 1980.

[166]. Saka, M. P., "Optimum Design of Space Trusses with Buckling Constraints," Proceeding of the Third International Conference on Space Structures, University of Surrey, Guildford, 1984.

[167]. AISC, Specification for the design, fabrications and erection of structural steel for buildings, American Institute of Steel Constructions, Chicago IL, 1978.

[168]. Khan, M. R., " Optimality Criterion Techniques Applied to Frames Having General Cross-Sectional Relationships," AIAA Journal, Vol. 22, No. 5, pp. 669-676, 1984.

[169]. Vanderplaats, G. N., "CONMIN- A Fortran Program for Constrained Function Minimization, User's Manual," NASA TMX-G2, 1973.

[170]. Venkayya V. B., and Tischler "Optimization of Structures with Frequency Constraints," Computers Methods for Nonlinear Solids and Mechanics, Vol.54, pp. 239-59, 1983.

[171]. Grandhi, R. V., and Venkayya, V. B. "Structural Optimization with Frequency Constraints," AIAA Journal, Vol. 26, pp. 858-866, 1988.

[172]. Konzelman, C. J., *Dual Methods and Approximation Concepts for Structural Optimization*, M.A.Sc thesis, Department of Mechanical engineering, University of Toronto, 1986.

[173]. Khan, M. R., and Willmert, K. D., "An Efficient Optimality Criterion Method for Natural Frequency Constrained Structures," Computers and Structures, Vol. 14, No. 5-6, pp. 501-507, 1981.

[174]. McGee, O. G., and Phan, K. F., "A Robust Optimality Criteria Procedure for Cross-Sectional Optimization of Frame Structures with Multiple Frequency Limits," Computers and Structures, Vol. 38, No. 5/6, pp. 485-500, 1991.

[175]. Crane, R. L., Hillstrom, K. E., and Minkoff, M., "Solution of the General Nonlinear Programming Problem with Subroutine VMCON," Argonne National Laboratory, Argonne, IL, ANL-80-64, July 1980.

[176]. Hughes, T. J. R., *The Finite Element Method: Linear Static and Dynamic Finite Element Analysis*, Prentice-Hall, Englewood Cliffs, NJ, 1987.

[177]. Rosen, A.; Schmit, L. A. Jr, "Design-Oriented Analysis of Imperfect Truss Structures. Part I- Accurate Analysis", International Journal of Numerical. Methods in Engineering, Vol. 14, 1309-1821, 1979.

[178]. Timoshenko, S. P., and Gere, J. M., *Theory of Elastic Stability,* McGraw-Hill Book Co., New York, 1961.

[179]. Korn, G. A., and Korn, T. M., *Mathematical Handbook for Scientists and Engineers*, MacGraw Hill, 1968.

Appendix A

AN IMPERFECT TRUSS ELEMENT

A.1 Introduction

Modeling the truss structures with imperfect elements is very important, especially for structures that are sensitive to the imperfections. In perfect truss structures, the initial geometry of each element is straight and remains straight during deformation. However, in reality a truss element is not perfectly straight. For structures with imperfect elements, the load-deformation behavior changes considerably due to the initial curvature and in most structures imperfection in the elements is primarily responsible for reduced load carrying capacity of the structural system.

A.2 Analysis of an Imperfect Truss Element

The finite element formulation for a truss element was carried out under the assumption that the element is straight or perfect. However, if the element is imperfect, a model that accounts for the imperfections is required and appropriate changes need to be incorporated in the perfect element finite element matrices derived in chapter 3.

Consider an initial imperfection of a truss element represented by a sinusoidal shape [177] as shown in Figure A-1. Thus

$$y_0 = b_0 \sin\left(\frac{\pi x}{L}\right) \qquad \textbf{(A-1)}$$

where b_0 is the midspan amplitude and L is the initial length defined as the distance ij. The ratio b_0/L is assumed small.

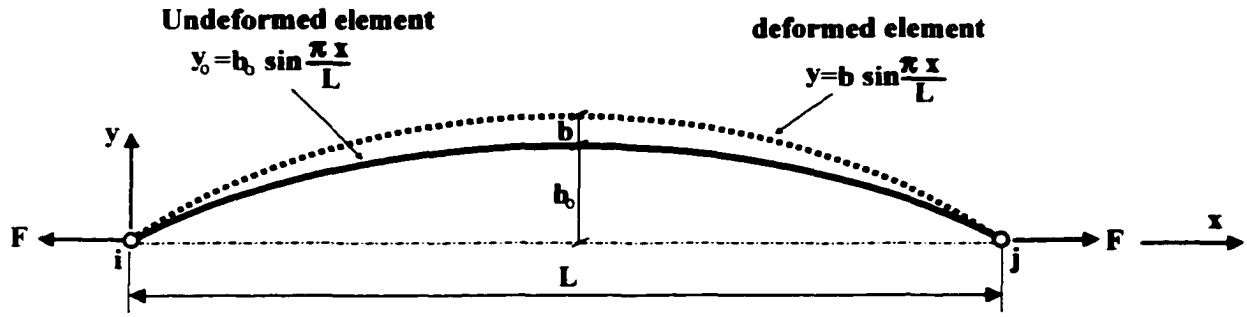

Figure A-1 Truss element with initial imperfection.

Owing to its initial curvature, an axial force F (positive in tension) applied at nodes i and j produces both bending and pure axial deformation. The pure axial deformation (u_a) is that of the straight element due to the action of the end force F and can be represented as

$$u_a = \frac{FL}{AE} \tag{A-2}$$

where A and E are the cross-sectional area and modulus of elasticity of the element, respectively. In the case of an initially curved element the force F also causes bending of the truss. This bending is accompanied by additional transverse deflection y, as shown in Figure A-1. The basic moment-curvature relation for an axially loaded imperfect truss element is

$$EI\frac{d^2}{dx^2}(y) - F(y + y_0) = 0 \tag{A-3}$$

where I is the moment of inertia of the truss element cross-section. Let us assume a solution of Eq. (A-3) in the form

$$y = b\sin\left(\frac{\pi x}{L}\right) \tag{A-4}$$

Substitution of Eqs. (A-1) and (A-4) into Eq. (A-3) gives

$$b = -\frac{b_0 F}{F + p_{cr}} = -\frac{b_0}{1+\alpha} \tag{A-5}$$

where $\alpha = p_{cr}/F$ is critical load factor and p_{cr} is the Euler-buckling load of the truss element given by

$$p_{cr} = \frac{\pi^2 EI}{L^2} \tag{A-6}$$

The change in the distance between the points i and j due to bending, is given by [178]

$$u_b = \frac{1}{2}\int_0^L \left[\left(\frac{dy_0}{dx}\right)^2 - \left(\frac{d(y+y_0)}{dx}\right)^2 \right] dx \tag{A-7}$$

Substituting Eqs. (A-1) and (A-4) into Eq. (A-7), results in

$$u_b = -\left(b_0 + \frac{1}{2}b\right) b \frac{\pi^2}{2L} \tag{A-8}$$

Substitution of Eq. (A-5) into Eq. (A-8) yields

$$u_b = \frac{b_0^2 \pi^2}{4L} \frac{(1+2\alpha)}{(1+\alpha)^2} \tag{A-9}$$

Now the resultant change of distance between the end points of the truss (u) is the algebraic sum of the two contributions given by Eqs. (A-2) and (A-9). Thus

$$u = u_a + u_b = \frac{FL}{AE} + \frac{b_0^2 \pi^2}{4L} \frac{(1+2\alpha)}{(1+\alpha)^2} \tag{A-10}$$

Eq. (A-10) can be expressed as

$$u = \frac{F L}{A E_{ef}} \tag{A-11}$$

where

$$E_{ef} = \frac{E}{1+\gamma\alpha\dfrac{(1+2\alpha)}{(1+\alpha)^2}} \quad \text{and} \quad \gamma = \frac{b_0^2}{4(I/A)} \tag{A-12}$$

Eqs. (A-11) and (A-12) may be interpreted as follows. The initially imperfect truss element can be replaced by an equivalent straight truss element with the same length L and cross-section of area A, but with an effective modulus of elasticity E_{ef} characterized by a non-linear elastic material model.

The axial force F in Eq. (A-11) depends on E_{ef} which itself depends on F. In Ref. [104], the axial force F is calculated by employing an iterative procedure. However, it is possible to convert Eq. (A-11) to a cubic equation in terms of α for which closed form solutions are available. Eq. (A-11) can be written as

$$F = E_{ef} A \varepsilon \tag{A-13}$$

where $\varepsilon = u / L$ is the strain in the element. Considering that $\alpha = p_{cr}/F$ and substituting E_{ef} from Eq. (A-12) into (A-13) and rearranging the terms, gives

$$\alpha^3 + \left(2 - \frac{1+2\gamma}{EA\varepsilon} p_{cr}\right)\alpha^2 + \left(1 - \frac{2+\gamma}{EA\varepsilon} p_{cr}\right)\alpha + \frac{p_{cr}}{EA\varepsilon} = 0 \tag{A-14}$$

Closed form solutions for the roots of a cubic equation are well documented [179]. The above cubic equation can have three real roots. However, physically, there can be only one valid solution. From the physics of the problem, the range of possible values for α can be

$$\begin{aligned} &\alpha \in \left(0, \frac{p_{cr}}{EA\varepsilon}\right) \quad \text{if} \quad \frac{p_{cr}}{EA\varepsilon} > 0 \ \text{(element is under tension)} \\ &\alpha \in (-1, 0) \quad \text{if} \quad \frac{p_{cr}}{EA\varepsilon} < 0 \ \text{(element is under tension)} \end{aligned} \tag{A-15}$$

Having calculated α from Eq. (A-14), the axial force F can be easily obtained from $F = p_{cr} / \alpha$.

Appendix B

CONSTRAINT SENSITIVITY

B.1 Sensitivity of the Stress and Displacement Constraints using the Displacement Method-Explicit Part

B.1.1 Displacement Constraint

Consider the design variables to be the cross-sectional area of the elements, **X=A.** If the constraint **g** is a displacement constraint expressed as $\mathbf{g} = \mathbf{U} - \overline{\mathbf{U}}$, the explicit part and the adjoint vector become

$$\frac{\partial \mathbf{g}}{\partial \mathbf{A}} = [\nabla U_1 \quad \nabla U_2 \quad \cdots \quad \nabla U_m] = 0 \qquad \text{and}$$
$$\boldsymbol{Z} = \frac{\partial \mathbf{g}}{\partial \mathbf{U}} = \frac{\partial \mathbf{U}}{\partial \mathbf{U}} = [\mathbf{e}_1 \quad \mathbf{e}_2 \quad \cdots \quad \mathbf{e}_m], \tag{B-1}$$

where m is the number of displacement degrees of freedom and displacement constraints; $\mathbf{e}_j$ is a vector of length equal to the number of displacement degrees of freedom with all elements zero except for the j^{th} displacement degrees of freedom (dummy-load).

B.1.2 Stress Constraint

Now consider the constraint **g** as a stress constraint, $\mathbf{g} = \sigma - \overline{\sigma}$. For the truss element

$$\sigma_i = \frac{F_i}{A_i} \tag{B-2}$$

and for the plane beam element

$$\sigma_i = \sigma_{ai} + \sigma_{bi} = \frac{F_i}{A_i} \pm \frac{m_i h_i}{E_i I_i} \tag{B-3}$$

where σ_{ai} and σ_{bi} are axial and bending stress in the element i; h_i is the maximum height of the beam in the element axis; and $m_i = \max(m_i^-, m_i^+)$ is the maximum moment in the element axis. The minus/plus sign in Eq. (B-3) depends if the axial force is in tension or compression. The plus sign corresponds to axial tension. Here, let us assume that there is a relationship between the moment of inertia I_i and the cross-sectional area expressed as

$$I_i = a A_i^b \tag{B-4}$$

where a and b are constants. Considering Eq. (B-2), the explicit part for the truss element becomes

$$\begin{aligned} &\partial \mathbf{g}/\partial \mathbf{A} = \partial\sigma/\partial \mathbf{A} = [\nabla\sigma_1 \quad \nabla\sigma_2 \quad \cdots \quad \nabla\sigma_n] \quad \text{and} \\ &\nabla\sigma_1 = \left[-F_1/A_1^2 \quad 0 \quad \cdots \quad 0\right]^T, \quad \nabla\sigma_1 = \left[0 \quad -F_2/A_2^2 \quad \cdots \quad 0\right]^T, \quad \cdots \end{aligned} \tag{B-5}$$

Considering Eqs. (B-3) and (B-4), the explicit part for the beam element becomes

$$\begin{aligned} &\nabla \mathbf{g} = \nabla\sigma = [\nabla\sigma_1 \quad \nabla\sigma_2 \quad \cdots \quad \nabla\sigma_n] \qquad \text{and} \\ &\nabla\sigma_1 = \left[-\frac{F_1}{A_1^2} \pm \frac{m_1 h_1}{E_1 I_1}\frac{b}{A_1} \quad 0 \quad \cdots \quad 0\right]^T, \quad \nabla\sigma_1 = \left[0 \quad -\frac{F_2}{A_2^2} \pm \frac{m_2 h_2}{E_2 I_2}\frac{b}{A_2} \quad \cdots \quad 0\right]^T, \quad \cdots \end{aligned} \tag{B-6}$$

where n is the number of design variables and stress constraints.

In order to obtain the matrix $\boldsymbol{Z}$ for the stress constraints, the relationship between element forces and nodal displacements is considered. Recalling Eqs. (2-8) and (2-32) in Chapter 2, we obtain

$$\mathbf{F} = \boldsymbol{G}^{-1}\boldsymbol{Q}^T \mathbf{U}. \tag{B-7}$$

Differentiating Eq. (B-7), yields

$$\frac{\partial \mathbf{F}}{\partial \mathbf{U}} = \boldsymbol{G}^{-1}\boldsymbol{Q}^{T} \tag{B-8}$$

For The truss element:

$$\frac{\partial \mathbf{F}}{\partial \mathbf{U}} = \left[\frac{\partial F_1}{\partial \mathbf{U}} \quad \frac{\partial F_2}{\partial \mathbf{U}} \quad \cdots \quad \frac{\partial F_n}{\partial \mathbf{U}}\right] \tag{B-9}$$

and the corresponding flexibility matrix is

$$\boldsymbol{G}_i = \frac{L_i}{E_i A_i}. \tag{B-10}$$

For the beam element:

$$\frac{\partial \mathbf{F}}{\partial \mathbf{U}} = \left[\frac{\partial F_1}{\partial \mathbf{U}} \quad \frac{\partial m_1^+}{\partial \mathbf{U}} \quad \frac{\partial m_1^-}{\partial \mathbf{U}} \quad \frac{\partial F_2}{\partial \mathbf{U}} \quad \frac{\partial m_2^+}{\partial \mathbf{U}} \quad \frac{\partial m_2^-}{\partial \mathbf{U}} \quad \cdots \quad \frac{\partial F_n}{\partial \mathbf{U}} \quad \frac{\partial m_n^+}{\partial \mathbf{U}} \quad \frac{\partial m_n^-}{\partial \mathbf{U}}\right], \tag{B-11}$$

and the flexibility matrix is

$$\boldsymbol{G}_i = \begin{bmatrix} \dfrac{L_i}{E_i A_i} & 0 & 0 \\ 0 & \dfrac{L_i}{3E_i A_i} & -\dfrac{L_i}{6E_i A_i} \\ 0 & -\dfrac{L_i}{6E_i A_i} & \dfrac{L_i}{3E_i A_i} \end{bmatrix}. \tag{B-12}$$

The system flexibility matrix $\boldsymbol{G}$ for truss and beam elements can be obtained by assembling Eqs (B-10) and (B-12), respectively.

B.2 Sensitivity of the Stress and Displacement Constraints using the Force Method-Explicit Part

B.2.1 Displacement Constraint

Recalling Eq. (2-42) ($\mathbf{U} = \boldsymbol{J}\ \boldsymbol{G}\ \mathbf{F}$), the explicit part for displacement constraint becomes

$$\frac{\partial \mathbf{g}}{\partial \mathbf{A}} = [\nabla U_1 \quad \nabla U_2 \quad \cdots \quad \nabla U_m] = \boldsymbol{J} \frac{\partial \boldsymbol{G}}{\partial \mathbf{A}} \mathbf{F} \tag{B-13}$$

where $\partial \boldsymbol{G}/\partial \mathbf{A}$ may be obtained by assembling $\partial G_i/\partial A_i$ for each element according to Eqs. (B-10) and (B-12) for truss and beam elements, respectively. Considering **F** as a primary variable, the matrix $\boldsymbol{Z}$ in the force method for displacement constant is a null matrix.

B.2.2 Stress Constraint

The explicit part of the stress constraint in the force method is exactly similar to that in the displacement method mentioned in the section (B.1.2). The matrix $\boldsymbol{Z}$ can be easily constructed using Eqs. (B-2) and (B-3). For truss elements

$$\boldsymbol{Z} = \frac{\partial \mathbf{g}}{\partial \mathbf{F}} = \frac{\partial \boldsymbol{\sigma}}{\partial \mathbf{F}} = \begin{bmatrix} 1/A_1 & & & 0 \\ & 1/A_2 & & \\ & & \ddots & \\ 0 & & & 1/A_n \end{bmatrix}. \tag{B-14}$$

The matrix $\boldsymbol{Z}$ for the beam element may be written as

$$\boldsymbol{Z} = \frac{\partial \mathbf{g}}{\partial \mathbf{F}} = \frac{\partial \boldsymbol{\sigma}}{\partial \mathbf{F}} = \begin{bmatrix} 1/A_1 & & & & \\ 0 & 1/A_1 & & 0 & \\ \pm h_1/(E_1 I_1) & 0 & & & \\ & \pm h_2/(E_2 I_2) & \ddots & & 1/A_n \\ & & & \ddots & 0 \\ 0 & & & & \pm h_n/(E_n I_n) \end{bmatrix} \tag{B-15}$$

where it is assumed that m_i is less than the m_i^- for all elements.

B.3 Sensitivity of the Linear Stiffness and Mass Matrix

Using the linear stiffness matrix for the truss element, Eq. (3-30), yields

$$\frac{\partial \boldsymbol{k}_E}{\partial A_i} = \frac{E_i}{L_i}\begin{bmatrix} 1 & 0 & -1 & 0 \\ 0 & 0 & 0 & 0 \\ -1 & 0 & 1 & 0 \\ 0 & 0 & 0 & 0 \end{bmatrix}. \tag{B-16}$$

Using Eq. (B-4) and the local stiffness matrix for the plane beam element (Eq. 3-49), we have

$$\frac{\partial \boldsymbol{k}_E}{\partial A_i} = \frac{E_i}{L_i}\begin{bmatrix} 1 & & & & & \\ 0 & 0 & & & \text{SYM} & \\ 0 & 0 & 0 & & & \\ -1 & 0 & 0 & 1 & 0 & \\ 0 & 0 & 0 & 0 & 0 & \\ 0 & 0 & 0 & 0 & 0 & 0 \end{bmatrix} + \frac{E_i\, b}{A_i}\begin{bmatrix} 0 & & & & & \\ 0 & 12 & & & \text{SYM} & \\ 0 & 6L & 4L^2 & & & \\ 0 & -6 & 0 & 0 & & \\ 0 & -12 & -6 & 0 & 12 & \\ 0 & 6L & 2L^2 & 0 & -6L & 4L^2 \end{bmatrix}. \tag{B-17}$$

The sensitivity of the system linear stiffness matrix , $\partial \boldsymbol{K}_E / \partial A_i$, can be obtained by transforming Eq. (B-16) and (B-17) to the global coordinates using the rotation matrix and subsequently assembling for all the elements.

The consistent mass matrix for the truss element in two-dimension is

$$\boldsymbol{m} = \frac{\rho_i A_i L_i}{6}\begin{bmatrix} 2 & 0 & 1 & 0 \\ 0 & 2 & 0 & 1 \\ 1 & 0 & 2 & 0 \\ 0 & 1 & 0 & 2 \end{bmatrix}, \tag{B-18}$$

and the consistent mass matrix for the plane beam element is

$$\boldsymbol{m} = \frac{\rho_i A_i L_i}{420}\begin{bmatrix} 140 & & & & & \\ 0 & 156 & & & \text{SYM} & \\ 0 & 22L & 4L^2 & & & \\ 70 & 0 & 0 & 140 & & \\ 0 & 54 & 13L & 0 & 156 & \\ 0 & -13L & -13L^2 & 0 & -22L & 4L^2 \end{bmatrix}. \tag{B-19}$$

By inspection of Eqs. (B-18) and (B-19), the element mass matrices are linearly dependent on the cross-sectional areas; therefore they can be easily differentiated.

B.4 Sensitivity of the matrix *S* in the force method

Recalling that the matrix $\boldsymbol{S}$ is the combination of the equilibrium equation and the compatibility conditions, it can be expressed as

$$\boldsymbol{S} = \begin{bmatrix} \boldsymbol{Q} \\ \cdots\cdots \\ \boldsymbol{C}\ \boldsymbol{G} \end{bmatrix}. \tag{B-20}$$

Recalling that equilibrium matrix, $\boldsymbol{Q}$ and compatibility matrix $\boldsymbol{C}$ do not depend on the design variables (cross-sectional areas), we have

$$\frac{\partial \boldsymbol{S}}{\partial A_i} = \begin{bmatrix} \boldsymbol{0} \\ \cdots\cdots \\ \boldsymbol{C}\,\dfrac{\partial \boldsymbol{G}}{\partial A_i} \end{bmatrix} \tag{B-21}$$

where the sensitivity of the flexibility matrix, $\frac{\partial G}{\partial A_i}$, may be computed for truss and plane beam element using Eq. (B-10) and (B-12).